A Comprehensive Scaling Up Technique for Pneumatic Transport Systems

By

Chandana Ratnayake

Department of Technology
Telemark University College (HiT-TF)
Kjølnes Ring, N-3914 Porsgrunn
Norway

Thesis submitted to
The Norwegian University of Sceince and Technology (NTNU)
for the degree of Dr. Ing.

Porsgrunn, September 2005

ABSTRACT

The main objective of this investigation was to formulate a comprehensive scaling up technique for designing of pneumatic conveying systems by addressing the whole pipeline together with all accessories.

Five different bulk materials together with five qualities of one of these materials have been used for the tests. A large number of pneumatic conveying tests has been conducted for five different pipeline configurations.

In order to develop a model for pressure drop prediction in different sections of pipeline i.e., horizontal, vertical, bends, valves, etc, the gas-solid flow has been considered to be a mixture having its own flow characteristics. The classical Darcy-Weisbach's equation has been suitably modified and used for prediction of pressure drop of gas-solid mixture. The concept of suspension density and pressure drop coefficient has been introduced. Two separate models for pressure drop determination have been proposed. While one is used for both horizontal and vertical straight pipe sections, other is used for bends, valves or any other pipe section, which are considered as individual units. It has been shown that the proposed model performs much better than other scaling up techniques considered under the present study.

Using dimensional analysis, a model has been formulated to scale up the pressure drop incurred at the entry section of a top discharge blow tank. The proposed model predicts the entry pressure losses within a maximum error margin of ±15% of experimental measurements. Since no other model was found in the open literature for such prediction, the proposed model could not be compared with any other.

To determine the minimum conveying velocity, a scaling up model has been proposed using multivariate data analysis techniques and dimensional analysis. The proposed model gives resoably better predictions, especially in case of fine particles, than the other available models considered in this study. It also shows a good agreement with experimental measurements.

Combining the models proposed in current study for pressure drop determination, entry loss calculation and minimum conveying velocity estimation, one can reliably design a complete pneumatic conveying system.

Computational fluid dynamics (CFD) principles have been used to determine the pressure drop across a standard 90º bend and a straight pipe section. A commercial software code; Fluent® has been used for the investigation. Eulerian approach has been used for the simulation and the results show that the tested software can be used as an effective tool to determine the pressure drop in pneumatic conveying systems.

ACKNOWLEDGEMENT

The experimental investigation described in this thesis has become a reality with the help of many individuals and organisations. Although it is a hard task to list each and every one of them, the author is struggling here to acknowledge their support for carrying out this scientific study being a foreign student in Norway.

- Firstly, I would like to express my sincere gratitude to Dr. Biplab K. Datta and Prof. Morten C. Melaaen for their invaluable guidance, encouragement and interesting discussions through out the work, amidst their busy schedules.
- I am greatly indebted to late Prof. Sunil D. Silva who helped me to come to Norway as a graduate student. Even though, I unfortunately missed him in early stage of this study, his inspiration for such a comprehensive work is greatly acknowledged.
- All my colleagues in POSTEC group are highly appreciated for their technical support for the research study as well as their social support, which has made my stay in Norway enjoyable.
- Many thanks also go all staff members of Telemark University College, specially, Unni S. Kassin, Trine Ellefsen, Anne Solberg, Inger Kristiansen, Anne M. Blichfeldt, Marit Olsen, Jarle Teigen and Inger-Judith for their kindly help.
- All administrative staff of Telemark Technological Research and Development Centre (Tel-Tek), specially, Marit Larsen, Liv Axelsen, June Kvasnes and Anniken Augestad are commended for their support.
- The Norwegian state education loan fund (Lånekassen), Tel-Tek, MODPOWFLOW scheme funded by The Norwegian Research Council (NFR) and POSTEC members are acknowledged for their financial support.
- I acknowledge my gratitude tawards National Oilwell, Statoil, Hydro aluminium and Unitor ASA for permitting publication of the findings of the studies, funded by them.

- Finally, I express my heartiest appreciation to my beloved wife; Chamila and two kids; Kavindu and Kaveesha for their patience and moral support during this work. Very special thanks to my mother and two sisters for their continuous encouragement and moral support extended to me from my country Sri Lanka.

September, 2005 Chandana Ratnayake

CONTENT

NOMENCLATURE

A	pipe cross-sectional area	[m^2]
b	bend equivalent length	[m]
B	bend pressure loss coefficient	[-]
C	constant	[-]
C_μ	turbulence model constant (given in Table 9-2)	[-]
C_D	drag coefficient	[-]
C_i *(i:1…n)*	constants	[-]
$C_{i\varepsilon}$ *(i:1,2,3)*	turbulence model constant (given in Table 9-2)	[-]
C_{mk}	ratio between solids and air velocities	[-]
D	diameter	[m]
d_p	particle diameter	[m]
e_{ss}	coefficient of restitution	[-]
Eu	Euler number	[-]
f	friction factor	[-]
Fr	Froude number	[-]
Fr_{st}	Froude number related to starting velocity	[-]
g	acceleration of gravity	[m/s^2]
G	rate of production of turbulent kinetic energy	[-]
$g_{0,ss}$	radial distribution function [as given in Equation (9.8)]	[-]
K	pressure drop coefficient [as introduced in Equation (4.5)]	[-]
k	turbulent kinetic energy	[m^2/s^2]
k_b	bend pressure loss coefficient	[-]
$K_{i,j}$	inter-phase momentum exchange coefficient (from *i* to *j*)	[-]
k_w	coefficient of internal wall friction	[-]
L	length of pipe section	[m]
L_b	length of the bend	[m]
l_p	length of the plug	[m]

L_s	length of solid column [i.e., (total volume of moving solids)/ (tube area)]	[m]
m	mass flow rate	[kg/s]
M	molecular weight	[-]
p	pressure	[N/m^2]
P	local pressure	[N/m^2]
R, r	radius	[m]
Re	Reynolds number	[-]
T	absolute temperature	[K]
U	superficial velocity	[m/s]
U_f	actual fluid velocity	[m/s]
u_i	velocity of i phase	[m/s]
U_t	particle terminal velocity of a single particle	[m/s]
v	velocity	[m/s]
V	volumetric flow rate	[m^3/s]
v_{st}	starting velocity	[m/s]
w_s	slip velocity	[m/s]
x_i $(i:1…n)$	constant	[-]

Greek Symbols

α_i	volume fraction of i phase	[-]
β_0	coefficient of wall friction	[-]
δ_{ij}	Kroenecker delta	[-]
Δp	pressure drop	[N/m^2]
ε	pipe roughness	[m]
ε_s	volume fraction of solid	[-]
ζ	additional pressure loss factor	[-]
η	dimensionless number [as introduced in Equation (6.22)]	[-]
θ	angle of inclination of the pipe	[deg.]
θ_s	granular temperature	[m^2/s^2]

λ	friction factor	[-]
μ	solids loading ratio	[-]
μ_d	dynamic viscosity	[kg/ms]
$\mu_{eff,g}$	effective viscosity of gas	[kg/ms]
μ_i	viscosity of phase *i*	[kg/ms]
μ_t	turbulent viscosity	[kg/ms]
μ_w	$tan\ \phi_w$	[-]
Π_i	dimensionless number	[-]
ρ	density	[kg/m^3]
σ	standard deviation	[-]
σ_f	normal stress at front face of slug	[N/m^2]
$\sigma_{i,j}$	turbulence model constant (given in Table 9-2)	[-]
υ_s	solids bulk viscosity	[kg/ms]
$\tau_{ij,g}$	stress tensor gas phase	[kg/ms^2]
ϕ_w	angle of wall friction	[deg.]
Ψ_s	shape factor	[-]

Subscripts

a	parameter due to air
A	parameters relevant acceleration pressure drop
b	bend
c	choking condition
cal	calculated value
col	collisional
e	error
entry	entry conditions
eq	equivalent
exp	experimentally measured value
g	gas phase

h	horizontal
i	inlet section conditions
kin	kinetic
m	mean value
max	maximum
min	minimum
o	outlet section condition
s	solid phase
st	straight pipe section
start	condition at starting of pipeline
sus	suspension
t	parameter for total flow
T	parameters relevant particles terminal velocity
v	vertical

1 INTRODUCTION

1.1 Introduction of Pneumatics and its Applications

Being originated from a Greek word *'pneumatikos'*, which means coming from the wind, pneumatics means the use of pressurized air in science and technology. Its applications can be seen in various industries and domestic appliances as well. Easiness in controlling and flexibility in installations are some of the favourable features of pneumatics applications in many industrial and non-industrial fields. Pneumatic conveying of particulate material is another well known application of pneumatics in the field of handling of particulate materials. This chapter looks into the details of history, advantages, disadvantages and basic types of pneumatic conveying systems. The motivation of this experimental investigation is described in detail in a later section. An outline of the thesis structure is also provided at the end of this Chapter.

1.2 Definition of Pneumatic Conveying

Pneumatic conveying is a material transportation process, in which bulk particulate materials are moved over horizontal and vertical distances within a piping system with the help of a compressed air stream. Using either positive or negative pressure of air or other gases, the material to be transported is forced through pipes and finally separated from the carrier gas and deposited at the desired destination. A general setup of a pneumatic conveying system is shown in Figure 1-1.

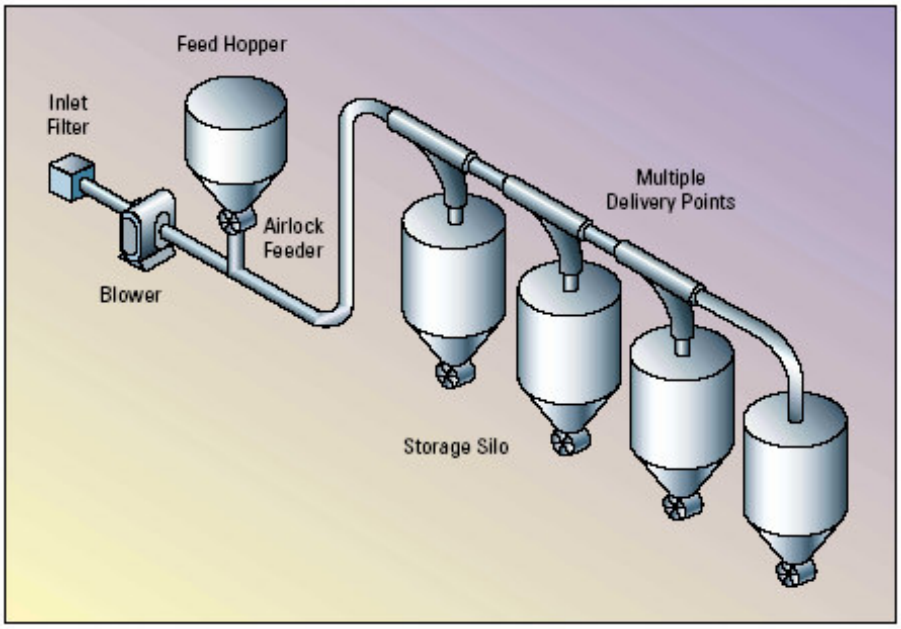

Figure 1-1: General setup of a pneumatic conveying plant [1].

This mode of bulk solid transportation holds an important position in the particulate material handling field, because of a series of advantages over other modes of transportation. It has a wide range of applications, with examples ranging from domestic vacuum cleaners to the transport of some powder materials over several kilometres. With a recorded history of more than a century, pneumatic conveying systems have been popularised in the bulk material handling field.

1.3 History of Pneumatic Conveying

Pneumatic tubes used for transporting physical objects have a long history. The basic principles of pneumatics were stated by the Greek Hero of Alexandria before 100 BC [2]. On the other hand, the concept of conveying materials in pipeline systems also goes back to pre-historical age with some evidence of that the Romans used lead pipes for water supply and sewage disposal and the Chinese used bamboo to convey natural gas [3].

Although there had been various applications of pneumatic conveying earlier in many civilisations, the first documented pipeline conveying of solid particles was

recorded in 1847 [4]. In Peugeot plant in France, the pneumatic conveying principle was used for the exhaust of dust from number of grindstones with the help of an exhaust fan, as shown in Figure 1-2.

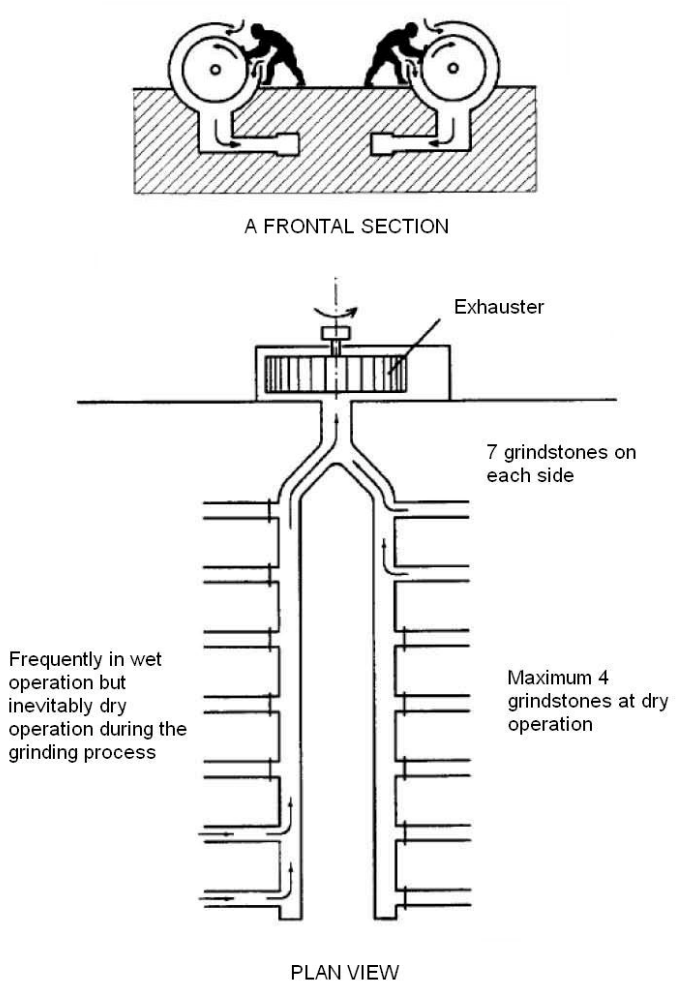

Figure 1-2: The first published pneumatic conveying system [4].

In 1864, an experimental pneumatic railway was built at Crystal palace with the intention of using the principle of vacuum applied to a railway tunnel to move a carriage, which had been fitted with a sealing diaphragm [5]. Another application of vacuum pneumatic transport was reported in ship unloading plant in London in 1890 [5]. A number of applications of operational principles of pneumatic transport could be seen in last decade of the 19th century at some places in Europe [4, 6] and especially, in the grain transport and handling field [5]. During this time period,

general break through events in the evolution of pneumatic conveying systems such as use of negative pressure systems, invention of auxiliary equipments like rotary feeders, screw feeders, valves, etc., could be emphasised.

During early decades of 20th century, it was common practice to use pneumatic conveying to transport grain [6]. Ref. [7] presented a chronology of pneumatic pipeline highlighting the innovatory individuals and companies, especially during early and middle era of 20th century. During the First World War, the development of pneumatic conveying was influenced by the high demand for foods, labour scarceness and risks of explosion. Since the pneumatic conveying systems were seen as the answer for those situations, a huge evolution of pneumatic transport was achieved during that time period. In the post-war period, pneumatic conveying systems were used for more industrial related materials like coal and cement. Beginning of theoretical approaches, invention of blowers, introduction of batch conveying blow tanks, etc., were among the highlighted milestones of the evolution of pneumatic transport systems during this era.

Nowadays, pneumatic transport is a popular technique in particulate material handling field. It has been reported that some plants have transport distance of more than 40 km [8], material flow rate of few hundreds tons per hour and solid loading ratio (the mass flow rate ratio between solid and air) of more than 500.

1.4 Applications of Pneumatic Conveying

The applications of pneumatic conveying systems can be seen in many industrial sectors. A list of industrial fields where it has extensively been used is given below;

- Chemical process industry
- Pharmaceutical industry
- Mining industry
- Agricultural industry
- Mineral industry
- Food processing industry

Virtually, all powders and granular materials can be transported using this method. In Ref. [9], a list of more than 380 different products, which have been successfully conveyed pneumatically is presented. It consists of very fine powders, as well as the big crystals such as quartz rock of size 80 mm. Even some strange products like prairie dogs [8], live chicken [3] and finished manufactured parts of irregular shapes have been successfully conveyed through pipeline systems. Recently, some speculations have arisen about a transport method for human beings with the help of pneumatic conveying principles [10]. This method is termed as capsule/tube transport, which has already been tested for lots of materials [11]. Pneumatic capsule pipeline (PCP) uses wheeled capsules (vehicles) to carry cargoes through a pipeline filled with air. The air is used to push the capsules through the pipeline. A proposed setup of a pneumatic conveying capsule, which could be used to transport human beings is shown in Figure 1-3.

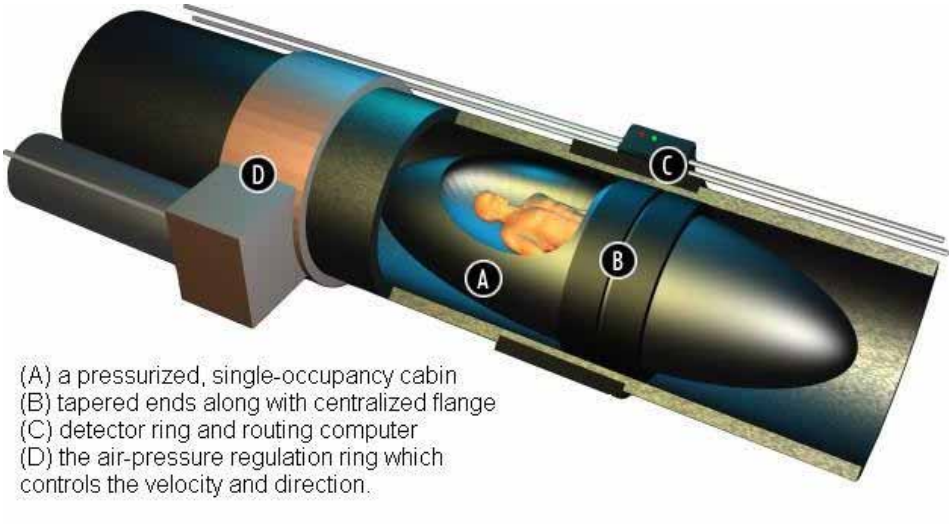

Figure 1-3: A proposed setup of a pneumatic conveying capsule line [10].

1.5 Advantages and Limitations of Pneumatic Conveying

In recent years, pneumatic transport systems are being used much more often, acquiring market sectors, in which other types of transport were typically used, especially in the field of bulk solids handling and processing. The reason is a series of advantages it has over the other methods of material conveying such as mechanical conveyers. Because of the flexibility of installation, this mode of bulk solids conveying is specially used to deliver dry, granular or powdered materials via pipelines to remote plant areas that would be hard to reach economically with mechanical conveyers. Since pneumatic systems are completely enclosed, product contamination, material loss and dust emission (thus, environment pollution) are reduced or eliminated. Particularly, to convey materials hazardous to health, a negative pressure (vacuum) pneumatic system is the best option. On the other hand, pneumatic conveying systems can be adopted to pick up the conveying bulk material from multiple sources and/or distribute them to many different destinations. In addition, reduced dimensions, progressive reduction of capital and installation costs, low maintenance costs (due to the small number of moving parts), repeated usage of conveying pipelines, easiness in control and automation are among the favourable advantages of pneumatic conveying over the other traditional methods of particulate material handling.

Although pneumatic conveying has seen increased use in many industrial sectors, there are still many major problems hampering its employment in a wider range of industrial conveying applications. Specially, in dilute-phase transport, high energy consumption, excessive product degradation and system erosion (pipelines, bends etc) are some of the major problems. In an alternative method, in dense-phase conveying also, unstable plugging phenomena, severe pipe vibration and repeated blockages are experienced frequently. Further, the lack of simple procedures for the selection of an optimal system is a major problem in pneumatic transport system design.

1.6 Major Components in a Typical Pneumatic Conveying System

There are a number of components in a pneumatic conveying plant, which are required to achieve the particular duty condition. Usually, a typical conveying system comprises different zones where distinct operations are carried out. In each of these zones, some specialised equipments are required for the successful operation of the plant. Any pneumatic conveying system usually consists of four major components;

1. **Conveying gas supply**-

   To provide the necessary energy to the conveying gas, various types of compressors, fans, blowers and vacuum pumps are used as the prime mover.

2. **Feeding mechanism**-

   To feed the solid to the conveying line, a feeding mechanism such as rotary valve, screw feeder, etc, is used.

3. **Conveying line**-

   This consists of all straight pipe lines of horizontal and/or vertical sections, bends and other auxiliary components such as valves.

4. **Separation equipment**-

   At the end of the conveying line, solid has to be separated from the gas stream in which it has been transported. For this purpose, cyclones, bag filters, electrostatic precipitators are usually used in the separation zone.

1.7 Classification of Pneumatic Conveying Systems

Pneumatic transport systems can be classified in a number of ways. Among them, the nature of system pressure and the mode of conveying are the two major aspects for the classification. So far as the system pressure is concerned, there are three major types of transport systems, which can briefly be explained in the following way:-

1. **Positive pressure systems** –

   In this type of pneumatic conveying system, the absolute pressure of conveying gas inside the piping system is always greater than atmospheric

pressure. This configuration is seen as the most famous type of pneumatic conveying system, especially in multiple discharge applications, in which the conveying material is picked up from a single point and delivered to several receiving stations. One typical arrangement of a positive pressure system is shown in Figure 1-4.

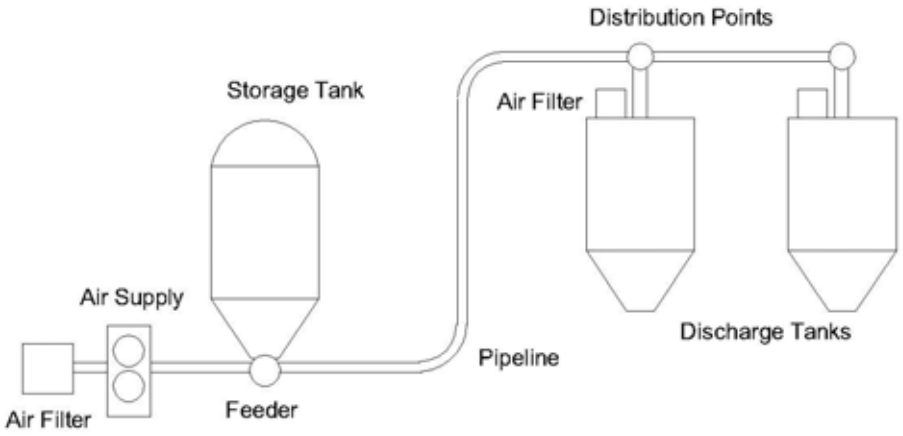

Figure 1-4: The line diagram of a positive pressure system.

2. **Negative pressure systems** –

   This type is also termed as vacuum/suction conveying where the absolute gas pressure inside the system is lower than atmospheric pressure. The simplest example for negative pressure pneumatic conveying may be the domestic vacuum cleaner and it varies from this application to heavy duty ship unloader. Especially in transport of toxic and hazardous materials, a negative pressure system may be the best choice since it allows dust free feeding and provides leak free material handling. This configuration is generally used for the transport of material from several feeding points to a common collection station. One such negative pressure system is schematically presented in Figure 1-5.

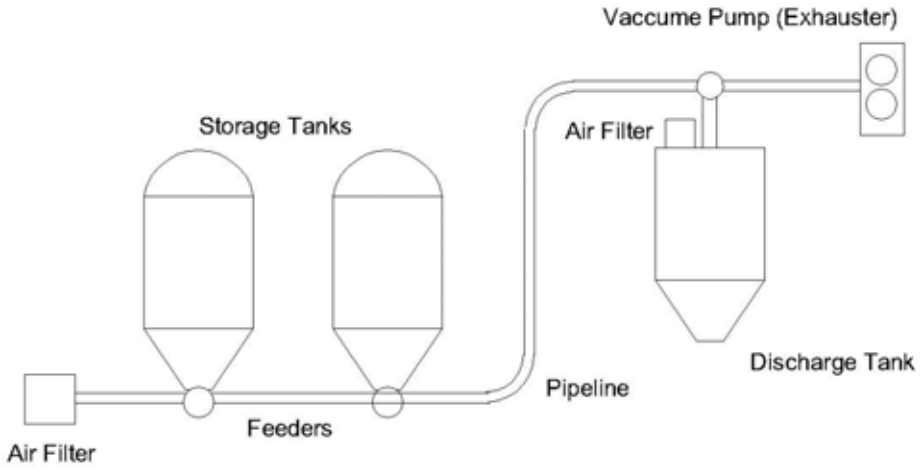

Figure 1-5: The line diagram of a negative pressure system.

3. **Combined negative-positive pressure systems –**

   To overcome the weaknesses and combine the advantages of positive and negative pressure systems, some plants can be seen in operation combining both these configurations together. This type is also termed as 'suck-blow' system where multiple feeding as well as multiple deliveries are easy to perform.

As mentioned earlier in this section, the other classification method of pneumatic conveying systems is based on the modes of transportation, which depends on air velocity and at the pipeline inlet. According to this aspect, pneumatic conveying systems can be classified into two different categories, which can be briefly described as below;

1. **Dilute phase conveying systems** -

   By employing large volumes of gas at high velocities, particulate material transportation in suspension mode is usually termed dilute phase conveying. In this mode, the bulk material is carried by an air stream of sufficient velocity to entrain and re-entrain it for a distance, which depends on the available pressure [12]. Figure 1-6 shows a schematic diagram of a typical dilute phase conveying system.

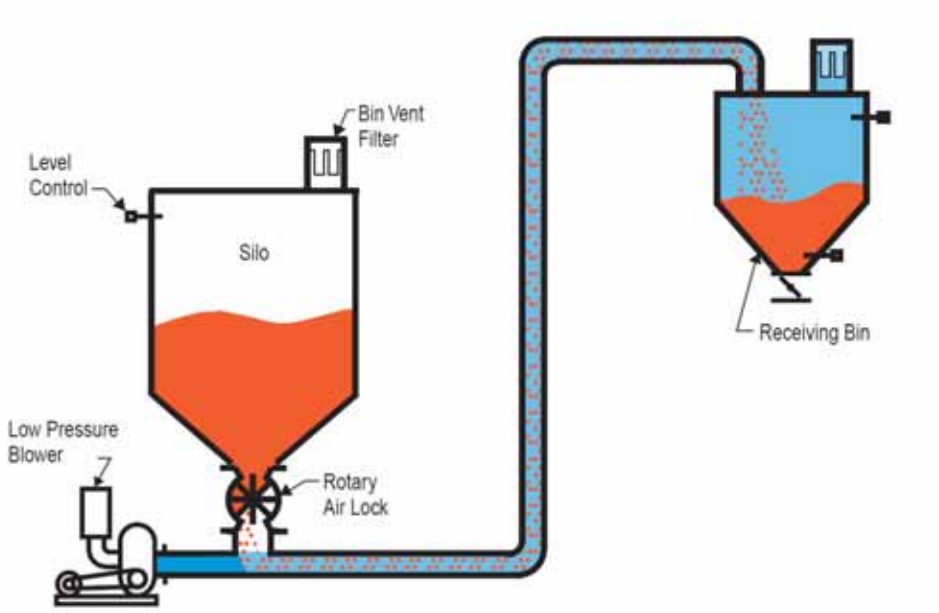

Figure 1-6: Schematic diagram of a typical dilute phase conveying system [13].

2. **Dense phase conveying systems** –

   By reducing the gas velocity, bulk materials can be transported in stratification mode with non-uniform concentration of solids over the pipe cross-section. The material is pushed through a pipeline as a plug, which occupies the whole cross section or as a moving bed for a pressure dependent distance [12]. Even though there are different terms to define the different conveying patterns under reduced gas velocity, such as plug flow, slug flow, strand flow, moving beds, etc, in general, they all come under dense phase conveying. One such dense phase system is shown in Figure 1-7.

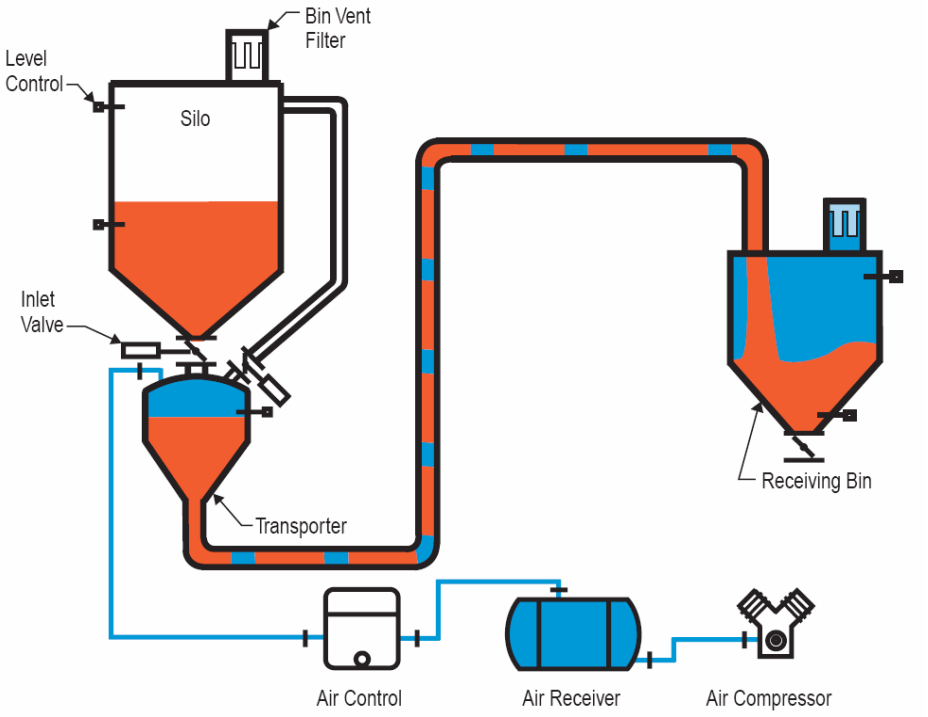

Figure 1-7: Schematic diagram of a typical dense phase conveying system [13].

The definition of the above two modes of transportation is controversial with the different views of different researchers regarding the setting up of boundary in between them. Some researchers use solid mass loading ratio, which is the ratio between the solid mass flow rate and the gas mass flow rate, to demarcate the boundary, while others use conveying air velocity. Even with those concepts, many discrepancies have been reported in literature in case of the definition of transport mode. All these different views and philosophies will be described in details under Chapter 2.

1.8 Operation of a Pneumatic Conveying System

Various flow regimes exist inside the pipeline in a pneumatic conveying system, straddling the entire range of conveying conditions from extrusion flow (packed bed) to fully dilute suspension flow. Through numerous experimental studies together with visual observations using glass tubes, etc, scientists have concluded these

varieties of flow regimes. It has been seen that these different flow regimes could be explained easily in terms of variations of gas velocity, solids mass flow rate and system pressure drop. This clarification also explains the general operation of a pneumatic conveying system.

Most of the research workers and industrial system designers have used a special graphical technique to explain the basic operation of a pneumatic conveying system. This technique utilises the interaction of gas-solid experienced inside the conveying pipeline in terms of gas velocity, solids mass flow rate and pressure gradient in pipe sections in a way of graphical presentation, which was initially introduced by Zenz [14, 15]. Some researchers [16-25] named this diagram as pneumatic conveying characteristics curves, while others [6, 26-28] used the name of state or phase diagram. The superficial air velocity and pressure gradient of the concerned pipe section are usually selected as the x and y axes of the diagram and number of different curves are produced on these set of axes in terms of different mass flow rates of solids.

There is a distinguishable difference between the relevant flow regimes for horizontal and vertical pipe sections. On the other hand, the particle size and particle size distribution also have influence on the flow patterns inside the pipelines. The general operation of horizontal and vertical pneumatic conveying systems are briefly explained in the following sections with the help of pneumatic conveying phase diagrams together with varieties of flow regimes.

1.8.1 Horizontal Conveying

One typical horizontal phase diagram is shown in Figure 1-8, together with various cross-sectional diagrams showing the state of possible flow patterns at different flow situations.

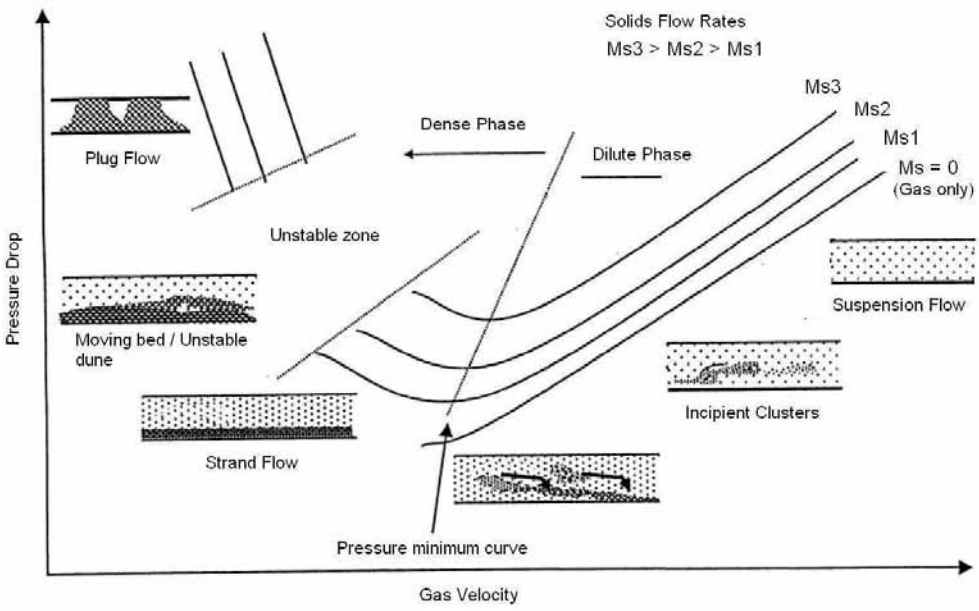

Figure 1-8: A typical conveying characteristic curves: horizontal flow.

The curves in Figure 1-8 show the variations of constant solids mass flow rate contours, when the conveying gas velocity and system pressure drop varies independently. The gas only line shows the pressure drop vs. gas velocity curve, which is characteristically a single phase flow. When the solids particles are introduced to the system with a particular solids mass flow value, the pressure drop increases to a higher value than in case of gas only transport even though the gas velocity is maintained constant. By keeping the solids flow rate constant and reducing the gas velocity further, pressure drop decreases down to a certain point where the minimum pressure drop is experienced. The pressure minimum curve connects such points for different solids flow rate values. Generally, the flow regimes up to this point from the right hand could be categorized as the dilute phase flow with low values of mass loading ratios. Further reduction of gas velocity leads to particle deposition in pipe bottom and then the flow mode is called dense phase conveying. Pressure drop can be seen increasing, when gas velocity is decreasing. After an unstable flow region, the conveying pattern shows a plug flow

characteristic, which will cause the pipeline to be totally blocked in attempts of further reduction of gas velocity.

Figure 1-8 shows the different boundaries of the conveying characteristic curves. One boundary is the extreme right hand side limitation, which depends on the air volume flow capacity of the prime mover. The upper limit of the solid flow rate is influenced by the allowable pressure value of compressed air supply. The left-hand side boundary is fixed by the minimum conveying velocity, which will be discussed in details in later chapter.

1.8.2 Vertical Conveying

The orientation of the pipe makes a considerable effect to the flow patterns and conveying regimes, because of the influence of gravity force. Consequently, the cross-sectional diagrams are totally different for the vertical pipe sections from those of horizontal sections, although the general appearance of the mass flow rate contours are similar to each other. Figure 1-9 shows a typical phase diagram of a vertical pipe section, together with various cross-sectional diagrams showing the representative state of possible flow patterns at different flow situations. Further details of the vertical flow of pneumatic conveying will be discussed under Section 2.5.

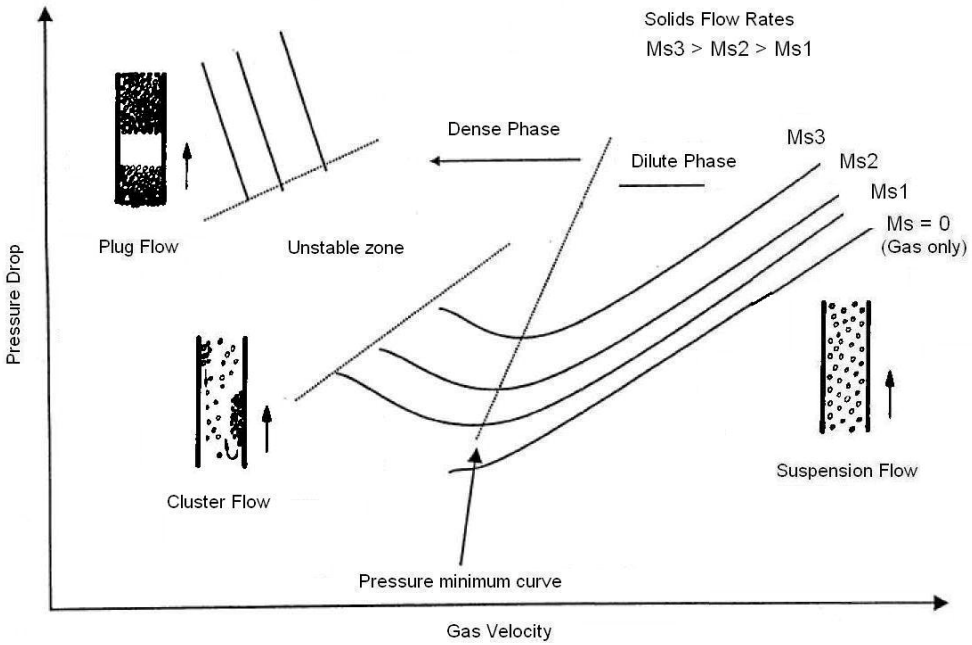

Figure 1-9: A typical conveying characteristic curves: vertical flow.

1.9 Motivation

Despite considerable study and research into various aspects of gas-solids flow, the subject remains very much an art, and the successful design and operation of pneumatic handling still depends to a great extent of practical experience. In order to design and construct an industrial installation that will be reliable and efficient, it is necessary to have some appreciation of the mechanism of flow of gas-solids suspensions in pipes.

Most of the problems in pneumatic conveying discussed under Section 1.5 are due to the inherent unpredictability of multiphase flow. Although models are now well established for single–phase flow, no such reliable theoretical descriptions are yet available for multiphase flow. The reliability and usability of existing mathematical models for gas-solids flow are very limited. The predictions based on these models change drastically with different conveying conditions and types of conveying materials.

To design a reliable pneumatic conveying system, basically two system parameters should be established precisely. These are;

a) the pressure drop across the total pipeline system and
b) the minimum conveying condition for reliable transportation.

The total pressure drop is utilised to overcome the friction between the pipeline wall and the gas-solids mixture, which can be considered as one of the flow properties of the conveyed material. To prevent pipeline blockage, with minimum system power consumption, the minimum conveying condition is employed. Since there are numerous influential parameters (e.g. particle size and size distribution, particle density, particle shape, etc.), empiricism has been used extensively, to establish the mathematical models using some of the above parameters. Thus, the applicability of these models to industry is very limited, and is reduced further for materials possessing small particle size, relatively wide particle distributions, and complex physical properties.

Therefore, designers are compelled to use experimentation in the design of industrial pneumatic conveying installations. In this approach, a sample of product, which is to be conveyed in the industrial plant, is tested in a laboratory pneumatic conveying test rig (pilot plant) over a wide range of operating conditions. The product and airflow rates and resulting pressure drops are measured as the test data. This approach has the advantage that real test data on the product to be conveyed in the proposed system are used for the design process. Thus, it gives a higher reliability level about the effects of product type. This is very important because it provides useful information on the conveyability of product and determination of minimum conveying limits as well.

However, it is not always feasible to use a pilot plant, which is of identical geometry (length, bore, number of bends, types of bends, etc.) to that of the required industrial installation. Therefore, it is required to scale up the conveying characteristics that are based on the pilot plant data, to predict the behaviour of the proposed industrial (full scale) plant, using some experimentally determined factors. Scaling up in terms of pipe line geometry needs to be carried out with respect to conveying distance, pipeline bore, the air supply pressure available, etc. Pipeline material, bend geometry

and stepped pipelines are other important parameters that are also needed to be considered.

The scaling up of pilot plant data is considered to be the most important stage of the design process, because it provides the required link between laboratory pilot plant test results and the full-scale industrial installation. Hence, accuracy and reliability of scaling methodology are vital. A considerable number of researches have been carried out to establish the mathematical models and relevant conditions of scaling up procedure.

Several relationships, based on different conditions have been proposed in the literature on scaling concepts, which will be discussed in details in Chapter 2. Although these theories have been established with a number of investigations with different materials and various pipeline configurations, there are still some doubts and uncertainties about their validity, according to a recent experimental investigation by the author [29]. The main objective of that investigation was to examine the scale up criteria with regard to the transport distance and pipeline diameter. As per the finding of the said investigation, it was clear that the predicted values of pressure dropare over-estimated (higher than the experimental values), in most of the cases. On the other hand, in case of scaling down, the available methods do not also give correct results [29].

One popular alternative to the above explained classical methods of pressure drop determination is the numerical simulation techniques using computational fluid dynamic (CFD) principles. This technique has been very precise for the single phase flow applications, but for multi phase flow situations like pneumatic transport it is still to have a reliable prediction of flow patterns and determination of flow parameter like pressure drop, solid velocity, etc. Recently, there has been a big forward leap in CFD techniques with the invention of high speed computers and innovative models to explain the flow phenomenon like turbulence, solid pressure etc. The granular kinetic theory is a popular example for this kind of innovatory models.

But until recently, a very few researches have tried to use CFD techniques to determine the pressure drop across the components of a pneumatic conveying

system. Since the CFD analysis are economically cheaper than the experimental investigation, it is worthwhile to find out whether the commercially available CFD software codes are provided with enough tools to predict the pressure drop of a pneumatic transport system reliably.

1.10 Aim of the Project

According to the conclusions and suggestions of the preliminary investigation [29] and the other factors discussed in the following sections, the current research project was planned to address the problems identified during the said experimental work. As discussed earlier, the scaling up techniques have been identified as the best approach in system design of pneumatic conveying. The investigation was planned to address the whole conveying system, i.e., from the feeding point to the receiving tank, including all typical components on it. Consequently, the final aim of the current investigation was to formulate a reliable design technique, which can be used in the design and scaling up of pneumatic conveying systems.

As an alternative approach, the available CFD techniques have also been examined for prediction of pressure drop across pipe components.

The main objectives of the subsections of the investigation can be listed as below;

a) To formulate a scaling up technique for the pressure drop determination of pipeline system of a pneumatic transport system.
b) To formulate a scaling up technique to determine the entry pressure loss of a blow tank feeding system with top discharge facility.
c) To formulate a technique for scaling up the minimum conveying conditions
d) To use Computational Fluid Dynamics (CFD) simulation techniques to determine the pressure drop across a short straight section and a standard 90º bend.

1.11 Outline of the Thesis

As an introductory part to the whole thesis, Chapter 1 looks into the details of historical developments, advantages, limitations and basic types of pneumatic

conveying systems. Additionally, the motivation as well as the basic objectives of this experimental investigation is described in detail under this Chapter.

Chapter 2 provides a detailed description about the available mathematical models and experimental explanations of pneumatic conveying systems. Simultaneously, the flow mechanisms of different sections and components of a typical pneumatic conveying plant are also explained in the light of published research works in open literature.

Experimental setup is described with all instruments on it, in Chapter 3. Brief explanation of operating principles, sensitivities and measurable ranges of each instrument used for the investigation are provided under this Chapter.

The experimental procedure and the formulation of scale up technique using 'Pressure Drop Coefficient' or 'K Factor' for dilute and dense phase pneumatic conveying is presented in details under the Chapter 4. The characteristic behaviour of 'K Factor' with the help of experimental data is also included. In addition, validation procedure of proposed model is discussed in Chapter 4.

A detailed comparison analysis of the proposed model with different scaling techniques proposed in literature is included in Chapter 5. Four different popular scaling techniques are compared with the proposed model under this investigation using graphical and statistical tools.

Theoretical approach to the proposed mathematical model, validation of the model with the help of experimental data of the investigation carried out with the aim of formulating a model to scaling up of the pressure drop of entry section of a high pressure pneumatic conveying system are described in Chapter 6.

Chapter 7 gives the experimental results, description and validation of the proposed model with respect to the investigation related to the scaling techniques of minimum conveying velocity. The prediction of proposed model is compared with that of available models with the help of experimental measurements.

Chapter 8 provides a detailed description about the computer based calculation programme, which comprises of all the scaling models proposed in the present study. As an application of the calculation programme, a case study is also described.

Chapter 9 looks in to the details of the CFD simulation, which has been carried out focussing on the flow across a short straight pipe section and a 90º standard bend with the help of the Fluent® software. The details of comparison of simulation results and experimental measurements are also presented.

The conclusion and the suggestions for the future improvements are given in Chapter 10.

The list of references sited in this thesis is given at the end before the Appendices, which contain additional figures and graphs. A list of published research papers in international journals and conferences during the course of this experimental study is also given.

2 BACKGROUND AND REVIEW OF LITERATURE

2.1 Introduction

As explained in Chapter 1, this experimental investigation addresses the whole conveying line by considering the individual components separately in order to formulate a detailed scaling up technique for the dilute and dense phase pneumatic conveying systems. In order to gain an understanding of the flow phenomenon in different sections of pneumatic conveying system and how different researches addressed these issues, a detailed literature survey was done on the available models and descriptions of the gas-solids flow in closed pipelines in laboratory scale and much longer pneumatic transport lines of industrial scale as well. To understand the current situation of the available theoretical descriptions, in the sense of how far they are tallying or contradicting each other was another objective of this literature review.

In this literature review, gas-solid flow in pipes is described with help of some suggested mechanisms that have been proposed in open literature. Simultaneously, the models available to explain the large scale pneumatic rigs were used to compare them with each other. To cover those models, in the first part of this section, the conveying line is virtually divided into different sections, such as;

a) feeding devices and entry section
b) horizontal pipes
c) pipe bends
d) vertical sections, etc, where distinguishably different flow behaviour could be expected and the available theoretical descriptions relevant to these sections are discussed. It starts from the beginning of the conveying line and proceeds along the pipeline upto the end of transport line, by considering different sections and components. After that, the models, which explain the whole conveying line as a

global one, are reviewed. Finally, the available scale-up procedures based on mathematical descriptions are also discussed in details.

In addition to the mathematical and stochastic models, numerical computational methods have also been extensively used to describe the flow phenomenon of gas-solids flow during the last decade. Under this literature survey, computational fluid dynamics models were also discussed.

2.2 Entry section

In the entry section, the flow behaviour and the pressure losses incurred basically depend on the feeding device. Usually, the feeding systems are classified on the basis of pressure limitations, since their function of the physical constructions are coupled with methods of sealing. In terms of commercially available feeding devices, it is convenient to classify feeders in three pressure ranges [6];

- Low pressure - maximum 100 kPa
- Medium pressure – maximum 300 kPa
- High pressure – maximum 1000 kPa

Commonly used feeding devices with their relevant pressure ranges can be listed as below;

1. Rotary valves (drop-through/blow-through) – low pressure
2. Screw feeders – medium pressure
3. Venturi feeder – low pressure (operate upto 20 kPa)
4. Vacuum nozzle – negative pressure
5. Blow tanks – high pressure

In the case of the first two devices, they are capable of feeding at a controlled rate and continuous operation and, they are especially suitable for low-pressure (up to 1.0 bar) systems, operating with fans or blowers [30]. The incorporation of a rotary valve at the bottom of a feeding tank is perhaps the more common technique of effecting solids flow control. It is common practice to fit a variable speed drive to the valve, thereby affecting the control. Where it is required to convey a product over long distances and/or in dense-phase, a high pressure system is used and feeding into

high-pressure systems almost always involves the use of blow tanks, which usually are capable of working pressures upto 7 ~ 10 bars.

2.3 Blow Tank

Blow tanks are very often used in pneumatic conveying systems, as they offer a wide range of conveying conditions, both in terms of pressure and flow rates. Basically, there are two modes, which are called discontinuous mode and continuous mode. These modes can respectively be achieved using single and twin blow tank systems. A single blow tank system is only capable of conveying single batches. In order to ensure continuous flow, it is accepted practice to use two blow tanks fitted to a common discharge line. The simplest type of dense phase pneumatic conveying feeder, a high pressure blow tank with a fluidising membrane at the bottom, is successfully being used for wide varieties of particulate materials.

2.3.1 Top Discharge and Bottom Discharge

Blow tanks are typically available in two different structures; 'Fluxo type' – top discharge and 'Cera type' – bottom discharge, which generally refers only to the direction, in which the contents of the vessel are discharged. In top discharge blow tanks, normally porous membrane is used to fluidise the material. For a given product, top- and bottom-discharge blow tanks will differ in their performance. Mills [31] studied this phenomena and recommended the top-discharge tanks for products to be conveyed in dense phase, as they provide better control for this mode of conveying. The top-discharge tanks seemed to achieve the highest feed rates, according to his findings. On the other hand, in the top discharge blow tank systems with fluidising membranes, the pressure drop across the membrane and the discharge pipe is comparatively high. If the fluidising air flow rate is high and/or the membrane area is small, the pressure drop further increases. However, he recommended bottom-discharge tanks for granular materials. In fact, top-discharge type may not be able to handle them at all, because the ease of air permeation through the mass of granules may prevent the build-up of enough lift. Marcus et al. [32] found that the discharge

performance from a blow tank can be significantly influenced by the method of introducing air into the blow tank. With some products, by adding air to the top of the material, the highest rate was obtained. Other materials performed better when the air was introduced into the material via a nozzle located at the discharge pipe. Jones et al. [33] compared the performance differences between top and bottom discharge blow tanks and found that there is no significant difference in the pressure, and thus the energy, required to convey a product through a pipeline at a given mass flow rate and loading condition in both configurations.

2.3.2 Velocity at Entry Section

Another important parameter at the entry section is the start gas velocity, which is also termed as pickup velocity, saltation velocity and critical velocity in some literatures. Due to the continuous expansion of the conveying gas over the conveying distance, the gas velocity at the start of the pipeline is the lowest gas velocity in the conveying system having a constant bore size. Nowadays, some industrial pneumatic conveying systems are using stepped pipelines to avoid the continuous increase of conveying velocity alone the conveying line. In those cases, there may be a possibility to have low conveying velocities at the pipe sections where the diameter enlargements are available.

To avoid pipeline blockages and to facilitate an efficient conveying without high particle degradation, an optimum value of the start gas velocity should be chosen at the entry section of the conveying line. The determination of minimum conveying velocity has been a topic for a vast number of researches [34-39], which will be addressed in section 2.8.1, in detail.

2.4 Horizontal Pipe Sections

Usually, horizontal sections are the most common pipe sections in industrial pneumatic conveying installations. The flow pattern existing in two-phase, gas-solid mixtures travelling along horizontal pipes have been studied by many researches using theoretical aspects and visual observations [3, 6, 16, 30, 40]. According to their

findings, these patterns are principally dependent upon the velocity of the gaseous phase, the ratio of the mass flow rate of solids to the mass flow rate of gas (i.e., the 'solids loading ratio/ phase density') and the nature of particulate solid material being conveyed.

These flow patterns have been discussed with several aspects, specially, in terms of modes of transportation, i.e., dilute and dense phase conveying. However, there is no uniformity in terminology, which adds the confusion of understanding the phenomena. Although it is difficult to define the boundaries between the dense phase and dilute phase flow modes, the conveying air velocity and the solids loading ratio have been used more frequently to categorise these flows. Many dilute-phase conveying systems are known to operate with solid loading ratio less than 15, whereas for dense phase that is greater than 15. In some research papers [24, 41], the flow is considered as dilute phase upto solids loading ratio of 30. In terms of air velocity, to have the dilute phase conveying it is necessary to maintain a minimum value of conveying air velocity is generally of the order of 13 to 15 m/s [16]. The flow is considered as medium phase when solids loading ratio is above 30, where the conveyance occurs with moving beds and dunes accompanied by more or less segregation. The flows with loading ratios of much larger values than 30 and with approximate inlet air velocity of 7 m/s, conveyance occurs as plugs with high pressure gradients but low velocities, which is called as dense phase transport.

2.4.1 Pressure Drop Determination

The usual assumption of pressure drop determination in gas-solid two-phase flow is to consider the total pressure drop as being comprised of two hypothetical pressure drop components, i.e., due to the flowing gas alone and the additional pressure drop attributable to the solid particles [6, 16, 22, 25, 27, 41-43]. In this classic approach, the pressure loss of air remains constant with respect to different loadings and qualities of the conveyed materials.

$$\Delta p_t = \Delta p_a + \Delta p_s \qquad (2.1)$$

2.4.1.1 'Air-Only' Pressure Drop

The procedure involved in the determination of the air only pressure drop component, is quite straightforward, since single-phase flow is well established with reliable mathematical models such as Darcy-Weisbach's [44]. It can be given by;

$$\Delta p_a = 4\frac{f\rho_a v^2 L}{2D} \tag{2.2}$$

Here, the friction coefficient for the gas, f can be determined according to Blausius equation, i.e,

$$f = \frac{0.316}{\mathrm{Re}^{0.25}} \tag{2.3}$$

where, Re is Reynolds number; $\mathrm{Re} = \frac{\rho v D}{\mu_d}$

Klinzing et al. [6] used Koo equation given in equation (2.4), for their calculations by emphasising it's applicability for the turbulent single phase flow.

$$f = 0.0014 + 0.125\frac{1}{\mathrm{Re}^{0.32}} \tag{2.4}$$

In addition, there are other semi-empirical correlations available [27] to determine f, especially for the calculation procedures using computers. Alternatively, it can be obtained graphically with the help of well-known Moody chart.

In fact, the equation (2.2) was developed from experiments, in which an incompressible fluid such as water was used.

Commonly used formulae for incompressible flow;

- Laminar flow (i.e., 0 < Re < 2300): $\Delta p_a = \lambda_a \rho_a v_a^2 \frac{\Delta L}{2D}$ (2.5)

  (Note that $\lambda_a = 4f$)

  where $\lambda_a = 64/Re$
- Turbulent flow (i.e., Re > 2300): Using dimensional analysis, same formula (i.e., equation (2.3)), as in laminar flow case can be obtained. But, λ_a is calculated by the following equations,

$$\lambda_a = \frac{1.325}{\left[\ln\left(\frac{\varepsilon}{3.7D} + \frac{5.74}{\mathrm{Re}^{0.9}}\right)\right]^2} \tag{2.6}$$

(for $10^{-6} \leq \varepsilon/D \leq 10^{-2}$ and $5*10^3 \leq Re \leq 10^8$) as presented by Swamee and Jain as cited by Streeter et. al. [45]

However, in pneumatic conveying, the compressibility effect of conveying gas may be significant. To modify the above equations (2.3) and (2.6) for compressible flow in conveying pipeline, Wypych et al. [46] proposed to replace the values of constants of equation (2.6) by number of coefficient (i.e., $x_1,\ldots x_5$), which could be determined by minimising the sum of squared errors of pressures at different points on conveying line.

$$\lambda_a = \frac{x_1}{\left[\ln\left(\frac{\varepsilon}{3.7D} + \frac{x_2}{\mathrm{Re}^{x_3}}\right)\right]^2} \tag{2.7}$$

$$\lambda_a = \frac{x_4}{\mathrm{Re}^{x_5}} \qquad (\text{for } Re \sim 10^5) \tag{2.8}$$

Based on an empirical relationship, Klinzing et al. [6] proposed the following equation to calculate the pressure drop in straight pipe for compressed air pipe works.

$$\Delta p_a = 1.6\times 10^3 \dot{V}^{1.85} \frac{L}{D^5 p_i} \tag{2.9}$$

To calculate the air only pressure drop in the pipeline, Wypych and Arnold [25] proposed the following empirical formula.

$$\Delta p_a = 0.5\left[\left(101^2 + 0.004567 m_a^{1.85} L D^{-5}\right)^{0.5} - 101\right] \tag{2.10}$$

2.4.1.2 Pressure Drop Due to Solid Particles

Although the possibility of the existence of a unique mathematical model to determine the pressure drop component due to the presence of dispersed solid particles is very low, because of the complex nature of two-phase gas solid flow in pipes, many correlating equations have been proposed by various authors in different

publications. Some of these methods, which show comparatively better agreements with experimental consequences, are briefly discussed below.

One of the simplest approaches is to consider the pressure drop due to solid particles in terms of the air-only pressure drop [16, 27, 40]. As an equation, this can be presented;

$$\Delta p_s = \zeta \times \Delta p_a \tag{2.11}$$

Here ζ is termed as the additional pressure loss factor that may be a function of a number of different variables. The dependence of the pressure loss factor ζ on the various system variables has been the subject of considerable research work. As per the findings of these efforts, it is clear that ζ is directly proportional to the solids loading ratio. Woodcock [27, 40] stated that the frictional pressure loss due to solid particles increases as solids loading ratio increases and also as the velocity is decreased. In addition, many other parameters involved in the flow within the pipe such as pipe diameter, free falling velocity, drag coefficient, etc and the physical characteristics of solid particles, such as size, density and shape were found to be important in the determination of ζ.

A useful comparison of published correlations for the determination ζ for dilute – phase suspensions has been given by Arastoopour et al. [47]. The correlations, which they considered and compared with each other, can be summarized in tabular form as follows.

Table 2.1: Available correlations to determine the additional pressure loss factor (ζ).

Equation	Remarks
$\zeta = \frac{\pi}{8}\frac{\lambda_s}{\lambda_a}\left(\frac{\rho_s}{\rho_a}\right)^{0.5}\mu$ [48]	λ_s is called as solid friction factor $\lambda_s = \frac{0.026}{\mathrm{Re}^{0.85}} + \frac{0.0034}{\mathrm{Re}^{0.6}}$
$\zeta = \frac{\lambda_s}{\lambda_a}\frac{v_s}{v_a}\mu$ [49]	v_s is solid velocity
$\zeta = \frac{C_1 m_s}{v_s^2 u_T}$ [50]	C_1 is a factor depend on D and u_T is the free falling terminal velocity of solids
$\zeta = C_2\frac{1}{\mathrm{Re}}\left(\frac{D}{d}\right)^2\frac{\rho_s}{\rho_a}\mu$ [51]	Re is gas phase Reynolds number and C_2 is a constant
$\zeta = \frac{C_3 m_s g}{\rho_a D v_s v_a u_T}$ [50]	A modification to the equation in 3rd row

2.4.1.3 Solid Friction Factor

Another popular technique in the pressure drop determination of horizontal pipe sections is 'the solid friction factor method', in which the pressure drop due to the presence of solid particles, is analysed in a form analogous to single phase flow. In this approach, the Darcy-Weisbach's equation is modified such that λ is considered either as the friction coefficient for the total flow or as a combination of friction coefficients for the solid flow and the gas flow separately. When the friction factor of gas-solid mixture is considered, the total pressure drop can be presented as below;

$$\Delta p_t = \frac{\lambda_t \rho L v^2}{2D} \qquad (2.12)$$

In one of the approaches to calculate λ_t, Yang [52] suggested to correlate two dimensionless groups called modified friction factor and modified Reynolds number and proposed the following correlation for λ_t for horizontal conveying.

$$\lambda_t = 0.117 \frac{1-\varepsilon_s}{\varepsilon_s^2} \left[\frac{(1-\varepsilon) v}{(gD)^{0.5}} \frac{\mathrm{Re}_T}{\mathrm{Re}_s} \right]^{-1.15} \tag{2.13}$$

Szikszay [53] proposed an empirical method to determine λ_t in terms of Froude number (Fr), solids loading ratio (μ), mean particle size (d_s) and pipe diameter (D).

$$\lambda_t = Fr^{x_1} \mu^{x_2} \left(\frac{d_s}{D} \right)^{x_3} \tag{2.14}$$

The coefficients (x_i) are to be found using empirical fitting.

In the other approach, the friction factor of the gas-solids mixture (λ_t) is considered as a combination of two hypothetical friction components as;

$$\lambda_t = \lambda_a + \mu \lambda_s \tag{2.15}$$

Here, λ_s means the pressure loss coefficient of the solids as already defined in Table 2.1 that comprises the influences due to friction and weight. Its value must be determined empirically and is valid only for one specific type of solid.

Weber [41, 43] proposed a method to determine the pressure drop due to solids particle in horizontal pipe sections, by comparing pneumatic and hydraulic conveying in pipelines. He proposed the following mathematical model for the solids pressure loss and claimed that the friction coefficient of air only (λ_a) remains constant with respect to different loading and qualities of the conveyed material.

$$\Delta p_s = \mu \lambda_s \rho_a v^2 \frac{L}{2D} \tag{2.16}$$

In this interpretation, λ_s means the pressure loss coefficient of the solids, which comprises the influences due to friction and weight. Weber [41, 43] proposed to determine it by the following equation.

$$\lambda_s = x_1 \mu^{-0.3} Fr_a^{-x_2} Fr_s^{0.25} \left(\frac{D}{d_s} \right)^{0.1} \tag{2.17}$$

The values of x_1 and x_2 are to be determined by empirical fittings of experimental data and should be valid only for one specific type of solid. However, the accuracy of this model seems to depend on the degree of confidence of fitting the experimental data to the correlation of equation (2.17).

In another investigation [43], same author claimed that the solids, depending on their loading and quality, influence the air part of the total pressure drop. According to the findings, air friction part decreases a lot with increasing solids loading ratio. This phenomenon is explained in terms of the strong interaction between the solids and the air during the transportation. Taking this in to consideration, Weber suggested following equations to calculate λ_a and λ_s.

$$\lambda_a = \frac{0.4}{\sqrt[4]{\mathrm{Re}}} \frac{1}{1+\mu^2} \tag{2.18}$$

$$\lambda_s = x_1 \mu^{x_2} Fr^{x_3} \tag{2.19}$$

Here, the coefficients (x_i) are to be determined by empirical fitting of experimental data and valid only for the specified material.

Pan et al. [54] proposed a model to predict the pressure drop in horizontal pipes using a semi-empirical correlation to determine λ_s. They considered a number of parameters, which can be regarded as the influential variables to pressure drop of a straight pipe section and used dimensional analysis to find out the dimensionless groups of most important factors as shown below.

$$\lambda_s = x_1 \mu^{x_2} Fr_m^{x_3} \rho_{am}^{x_4} \tag{2.20}$$

Based on the experimental data of pressures along a constant diameter straight section of pipe, exponent x_i is determined by minimising the sum of square errors of pressures. These exponents, as in the previous cases, are valid only for the given product.

Rizk [39] used equation (2.1) to calculate the total pressure drop in a horizontal pipeline and proposed a new model to calculate the pressure loss coefficient of the solids; λ_s. In this approach, the balance of energy in a control volume and the balance of power on a moving cloud are considered and λ_s is presented as a combination of

two terms; one due to the influence of impact and friction between particles and other due to the weight of solid particles or the influence of gravity.

In a review of published papers on dilute pneumatic transport, Duckworth [55] presented a comparison of earlier mathematical models to calculate solid pressure drop coefficient, λ_s, with respect to the present notation. According to his analysis, the most important variable is the solids loading ratio. Reynolds number, Froude number, diameter ratio (d_p/D) and solids velocity are among the other important variables to determine λ_s. It was found that λ_s decreased as the ratio (d_p/D) decreased. He proposed to consider the momentum transfer equation and dimensional analysis to identify some dimensionless group of variables. As the final step, Duckworth also choose the empirical method to find out the appropriate coefficients in those correlations, which are in turn valid for the specified materials only. The following relationship was proposed for fine particles.

$$\lambda_s = x_1 \left(\frac{d_p}{D} \right)^{x_2} \mu \tag{2.21}$$

where, x_1 and x_2 are constant, which depend on type of bulk solid, its particle size range and pipe material.

In another review publication on dilute transport, Klinzing et al. [26] claimed that the commonly used mathematical formula to calculate the solids particle contribution to the total pressure drop could be presented with the following equation.

$$\Delta p = 2\lambda_s \rho_s \left(1-\varepsilon_s\right) v_s{}^2 \frac{\Delta L}{D} \tag{2.22}$$

The available mathematical models to determine λ_s can be tabulated as shown in Table 2.2.

Table 2.2: Available correlations for solids friction factor.

Author	Solid Friction Factor, λ_s
Stemerding [56]	0.003
Redding & Pei [57]	$0.046v_s^{-1}$
Capes & Nakamura [58]	$0.048v_s^{-1.22}$
Konno & Saito [59]	$0.0285\sqrt{gD}v_s^{-1}$

Klinzing et al. [60], in a study on Yang's theory, proposed the following expression to calculate the pressure drop in horizontal gas-solid conveying systems.

$$\frac{\Delta p_s}{L} = \left(\frac{\Delta p_a}{L}\right) x_1 \mu \frac{gD}{v_a} \frac{1}{f} \tag{2.23}$$

where, f is the air friction factor explained in equation (2.3).

Molerus [4, 61] used a state diagram approach to relate the pressure drop due to solid particles and other relevant parameters. Here, the pressure gradient due to the solid particles was generally represented in dimensionless form as a function of a dimensionless fluid velocity. The proposed state diagram consists of the ordinate of the dimensionless pressure gradient, i.e., Euler number and the abscissa of a dimensionless gas velocity in the form of a friction number, which can be defined as follows.

$$Eu_p = \frac{2D\left(\frac{\Delta p_s}{\Delta L}\right)}{\rho_g v_a^2} \tag{2.24}$$

$$Fr_i \equiv \frac{v_g}{\left\{f_R \mu \left[1 - \left(\rho_a / \rho_s\right)\right] Dg\right\}^{0.5}} \tag{2.25}$$

where Eu_p is called Euler number and f_R is the friction factor. He claimed that this approach is very suitable for scaling up of laboratory pilot plant test data to the industrial scale designs.

In another extensive review, Arastoopour et al. [47] examined the published methods of pressure drop calculations for dilute phase conveying. They classified all the available correlations broadly in to two categorise. i.e.,

- Group 1, in which the ratio of total pressure drop to the pressure drop due to gas alone, $\frac{\Delta P_t}{\Delta p_a}$ is correlated (like in equation (2.11))
- Group 2, in which the total pressure drop is expressed as the summation of pressure drops due to acceleration, wall friction, and gas-solids friction.

Arastoopour et al. [47] criticized the group 1 approach, because using a pipe of different material and roughness, the total pressure drop will not change as much as that for the gas alone and recommended the group 2, even though that group has the similar problem with wall friction. They proposed the following model to determine λ_s;

$$\lambda_s = \frac{3}{8}\frac{\rho_a}{\rho_s} C_D \frac{D}{d_p}\left(\frac{v_a - v_s}{v_s}\right)^2 \tag{2.26}$$

In group 2 approach, the total conveying line pressure drop is divided into several components and focus on each of them separately, by considering their distinguishable features. The pressure drop incurred in horizontal sections can be determined by one of the analytical methods explain above. Another important concept highlighted with this approach is the pressure drop relevant to the acceleration region, which usually exists after some sudden change in flow direction or flow restriction.

2.4.2 Acceleration Length and Pressure Drop

When the pressures drop determination of straight pipe is concerned, another important aspect is the acceleration length and acceleration pressure drop. For any pneumatic conveying system the particles must be feeded into the gas stream and there exists a period over which the particles and gas are not at a steady state. During the transport of gas-solid mixture, the particles undergo deceleration and acceleration, whenever there is a direction change like bend or a flow restrictor like

valves. Researchers have found that this phenomenon contributes significantly to the overall system pressure drop.

Mills et al. [62] published a research paper with a detailed review of models available with regard to acceleration length. By monitoring the erosive wear of a number of bends, they presented a technique to establish acceleration lengths that showed a big influence of the conveying conditions and product characteristics, such as particle size distribution, density and shape.

In a simple model, Woodcock et al. [27] suggested to treat the whole length of the system as fully-accelerated flow and then to add on an appropriate extra pressure – drop for each obstruction, which causes the acceleration/deceleration. This extra pressure drop arises from the need to re-accelerate the solid particles after they have been slowed down by the obstruction. This additional pressure component was calculated by the following model.

$$\Delta p_A = \frac{m_s v_s}{A} \tag{2.27}$$

Duckworth [55] found the acceleration length/pressure drop an important parameter, particularly in the case of short pipelines. He proposed the following two equations to determine the acceleration length and pressure drop respectively, and claimed that they are best for uniformly sized coarse particles of spherical shape having diameter greater than about 600 μm.

$$\frac{L_A}{D} = 6\left[\left(\frac{m_s}{\rho_a g^{\frac{1}{2}} D^{\frac{5}{2}}}\right)\left(\frac{D}{d_p}\right)^{\frac{1}{2}}\left(\frac{\rho_s}{\rho}\right)^{\frac{1}{2}}\right]^{\frac{1}{3}} \tag{2.28}$$

$$\Delta p_A = \frac{m_s}{m_a}\frac{\rho v_a^2}{2}\phi_A\phi_B \tag{2.29}$$

where, ϕ_A and ϕ_B are dimensionless parameters relating $\left(\frac{v_a^2}{g d_p}\frac{\rho^2}{\rho_s^2}\right)$ and θ (angle of pipeline inclination) respectively.

By dividing the total pressure drop into several components, Marcus [63] proposed the following model to calculate the acceleration pressure drop.

$$\Delta p_A = \left(0.5 + \mu \frac{v_s}{v_a} \right) \rho v_a^2 \tag{2.30}$$

2.4.3 Dense Phase Transport

As discussed early in Chapter 1, the use of the term 'Dense Phase' is far from being precise. Some have used the word in pneumatic conveying to mean solid particles flowing at a velocity less than their saltation velocity. Some researchers have used the phase diagram to designate the region to the left of the minimum pressure drop curves as the dense phase region of flow. In spite of these discrepancies in definitions of the dense phase conveying, it has been the main subject of considerable number of theoretical and experimental research works over a substantial period of time. Because of the number of advantages over dilute phase transport, this has been acquiring more industrial applications during the past period of time. In particular, the low rates of pipe wear and particle attrition that are obtained with the low velocities involved and less air requirement thus the low power consumption are among the advantages of dense phase conveying. But, unfortunately, there are number of uncertainties, design difficulties and unforeseen pipe blockages, most of which arise from the fact that the precise mechanism by which the particles are conveyed has never been well understood.

Among the vast number of literatures on dense phase conveying, few of them, which show a comparatively good agreement with the experimental data and are well documented, has been selected for this study. In this section, the models on horizontal dense phase conveying are considered and the vertical sections and the velocity concepts will be discussed in their respective sections.

The work done by Konrad et al. [64] could be seen as one of the earliest and frequently cited publication by fellow reseachers. They developed a theoretical model to predict the pipeline pressure drop in horizontal dense phase plug conveying. They describe the flow mechanism with following phenomenal concepts.

- The material is conveyed only in the plugs and in the regions just in front and behind them.
- There is a layer of stationary material between the plugs.
- The flow pattern is similar to that of a gas-liquid system.

The proposed model for the pressure drop in horizontal pipe section can be presented in following equations;

$$\frac{\Delta p}{L_s \rho_s} = 2 g \mu_w + \frac{2.168 \mu_w K_w u_{sm}}{\left(D / g \right)^{0.5}} \tag{2.31}$$

Where, $u_{sm} = \overline{u}_s \left[\frac{1 - \frac{2m_s}{\left(\rho_s A \overline{u}_s \right)}}{1 - \frac{m_s}{\left(\rho_s A \overline{u}_s \right)}} \right]$; $\overline{u}_s$ is the mean particle velocity

Basically, this model predicts a linear pressure loss behaviour with the plug length. Konrad [65] stated that the overall conveying pressure difference increases exponentially with pipeline length and emphasized the significant contribution of the compressibility of the carrier gas. He described the expansion of gas inside the pipeline as an isothermal process. Konrad [65] proposed a modification to equation (2.31) by replacing its constants (i.e., 2 and 2.168) with the correlation coefficients, which have to be determined empirically. Similarly, he used an integration method to calculate the overall pressure drop in the pipeline.

For the plug flow conveying, Klinzing et al. [6] have used another form of an integration equation to calculate the pressure on the pipeline referring to a publication by Weber (published in German).

$$\frac{dp(x)}{dL} = \lambda_{sp} \frac{1 - \varepsilon_s}{\varepsilon_s} \frac{\rho(x)}{2} \left(v_a - v_s \right)^2 \frac{1}{d_p} \tag{2.32}$$

where $p(x)$ is the pressure and $\rho(x)$ is the relevant density of carrier fluid at $L=x$ and λ_{sp} is given in graphical form as a function of Re_p.

Legel et al. [66] investigated the plug conveying of cohesion less materials and introduced the transmission ratio of radial stress to axial stress, which is also called

the force (stress) transmission coefficient k_w. The following model has been proposed to calculate the pressure drop across a single plug.

$$\Delta p_p = (1 + 2.6 Fr_p^{0.2}) \tan \phi_w \rho_s g L_p \tag{2.33}$$

Here, the suffix '*p*' means the specified parameter related to the plug.

Mi and Wypych [67] proposed some modifications to Konrad's model, challenging the applicability of Ergun's equation in slug flow. It was observed that, although there is a relative motion between the slug and the pipeline wall, there is no relative motion between the particles within the slug. They emphasized that the slug flow situation is closer to a fluidised bed than a packed bed. Also, they used a well known theoretical approach called Mohr's circle analysis to determine k_w and developed a semi-empirical model to calculate the pressure drop, which can be used to optimise a pneumatic conveying system. They presented it to determine the pressure gradient in a single horizontal slug, as shown below.

$$\delta p_m = 2\rho_s g \mu_w + \frac{4\mu_w k_w}{D} \sigma_f \tag{2.34}$$

where, σ_f is given by;

$$\sigma_f = A_c \rho_s v_s^2 \tag{2.35}$$

where, A_c is the cross sectional area ratio of stationary bed to pipe and v_s is the slug velocity. To determine A_c, the procedure proposed by Konrad et al. [64] was used and where as an empirical method was used to determine v_s by correlating it with superficial air velocity and minimum air velocity for horizontal flow.

From a theoretical analysis, Mi et al. [67] suggested the following relationship for k_w.

$$k_w = \frac{\sigma_{rw}}{\sigma_x} = \frac{1 - \sin \phi_s \cos(\omega - \phi_w)}{1 + \sin \phi_s \cos(\omega - \phi_w)} \tag{2.36}$$

where $\sin \omega = \dfrac{\sin \phi_w}{\sin \phi_s}$ and ϕ_s is the static internal friction angle, which is defined by

$\phi_s = \dfrac{4}{3} \phi_w \gamma_b^{1/3}$; γ_b is the bulk specific gravity of solid.

They assumed that the sum of the pressure drop caused by the all slugs was equal to that caused by a single slug having a total length equal to all the small slugs, as long

as the mean condition (based on average air density) were used. With this basis, the following was used to determine total length of slugs in the pipeline.

$$L_s = \frac{m_s L}{A(1-A_c)\rho_s v_s} \tag{2.37}$$

Their final expression for the pressure drop of total pipeline length can be presented as below.

$$\Delta p = \left(1+1.084k_w Fr^{0.5} + 0.542Fr^{-0.5}\right)\frac{2g\mu_w m_s L}{Av_s} \tag{2.38}$$

An iterative procedure, by assuming a preliminary pipeline pressure drop and continuing until convergence is obtained was recommended for practical applications. Elsewhere, Mi et al. [68] and Pan et al. [69] have presented the applicability of this method for nine different materials.

Based on this investigation, Pan et al. [23] published another work on dense phase conveying. They modified equation (2.35) as shown below.

$$\sigma_f = \rho_s(U_s - U_p)U_p \tag{2.39}$$

where U_p is the average particle velocity in the slug.

The gas-liquid analogy was used to determine U_p and the resultant equation for the pressure drop in a single slug was presented as;

$$\delta p_m = 2.168\rho_s\mu_w k_w U_s\sqrt{\frac{g}{D}} + \rho_s g\mu_w(2-1.175k_w) \tag{2.40}$$

With the help of specific vertical test chamber and the packed bed model which relates the overall pressure drop to the slip between the gas and the particles, an empirical method was used to determine U_s. Then, the overall pressure drop is proposed below;

$$\Delta p = \delta p_m L_s \tag{2.41}$$

Here L_s is determined by the equation (2.37).

Matsuda et al. [70] proposed a model which is similar to the dilute phase approach i.e, by hypothetical splitting of total pressure drop into two components as air only and solid pressure drop. They found a direct relationship between Froude number and solids friction factor and suggested an empirical fitting method to determine it.

$$\lambda_s = \frac{x_1}{Fr^{x_2}} \tag{2.42}$$

Here, the values of x_1 and x_2 are to be determined by empirical method and valid only for the specified material.

Referring to the model proposed by Muschelknautz and Krambrock (published in German) considering the expansion of gas inside the pipeline as an isothermal process, Marcus [63] proposed a step wise trial and error method to calculate the pressure drop in plug flow dense phase transport. Here, the overall conveying pressure difference is assumed to be increased exponentially, thus the model can be presented as;

$$\frac{P_i}{P_e} = \exp\left(\frac{\mu g \tan\phi_w M L_a}{RTC_{mk}}\right) \tag{2.43}$$

where, $C_{mk} = \frac{U_s}{U_a}$

Finally, equation (2.44) can be used to determine the total pressure drop, provided the exit pipeline air pressure.

$$\Delta p = P_e\left(\frac{P_i}{P_e} - 1\right) \tag{2.44}$$

Although Marcus [63] considered C_{mk} as a constant, Konrad [65] described it as a strong function of $\mu(\rho/\rho_s)$ and it increased with both increasing μ and with decreasing particle size. Based on equation (2.43) and assuming the isothermal expansion of carrier gas, Konrad [65] proposed an integration method to determine pressure P at a distance l from the outlet of the pipe (where the pressure is atmospheric, P_a) as follows.

$$P - P_a = \int_{l=0}^{l} f(P)dl \tag{2.45}$$

By explaining the interaction mechanism between suspension and sliding bed, Hong et al. [71] carried out an experimental work. They considered the dilute phase suspension and sliding bed separately and presented a model to calculate total pressure gradient in stratified flow situations. They have used very simple pipeline

configuration with an 8m long pipe with a diameter of 20mm to transport sand and lime, under a wide range of solids loading from 30 to 200.

Woodcock and Mason [72] proposed a simple model for stratified flow conveying, referring to Muschelknautz and Krambrock (published in German).

$$\Delta p = (1 - A_c) L \rho_s g f_d \tag{2.46}$$

where, f_d is a friction coefficient for the sliding and rolling product.

Werner [73] found a direct influence of the size distribution of conveyed material to the pressure drop and suggested a different approach. He proposed the following equation to calculate the pressure drop in the pipeline, in general valid for the dense-phase, starting from a power balance for the complete air-solid flow.

$$\Delta p = \left(\frac{1}{1 + \frac{\rho_s C_{mk}}{\mu \rho}} \right) \rho_s g (\lambda + \sin\theta) L \tag{2.47}$$

Detecting an influence of particle size distribution, he used the following formulae to determine λ and C_{mk}, i.e., friction factor and velocity ratio;

$$\lambda \left(\frac{d_m}{D} \right)^{C_1} \left(\frac{d_m}{d_s} \right)^{C_2} = f(\mu, Fr_s) \tag{2.48}$$

$$C_{mk} \left(\frac{D}{d_m} \right)^{C_3} \left(\frac{d_s}{d_m} \right)^{C_4} = f(\mu, Fr_s) \tag{2.49}$$

where, d_m and d_s are mean particle diameters when arithmetically weighted and as reciprocal value of the surface respectively. He suggested an empirical fitting method to determine C_i.

For his data, the models for λ and C_{mk} are shown below;

$$\lambda = \left(0.25 + 7.82 \times 10^{-5} \mu Fr_s\right) \left(\frac{d_m}{D} \right)^{-0.3} \left(\frac{d_s}{d_m} \right)^{0.2} \tag{2.50}$$

$$C_{mk} = 921 \left(\mu Fr_s\right)^{-0.59} \left(\frac{d_m}{D} \right)^{0.3} \left(\frac{d_s}{d_m} \right)^{-0.2} \tag{2.51}$$

From the above equations, it is clear that the particle size distribution has a considerable effect on friction factor and velocity ratio of the phases.

Molerus [4, 61] proposed a state diagram aprroach for rather coarse-grained particles in strand flow. He defined the strand flow as a flow with rope-like clusters or aggregate of particles. Considering mass and momentum balances on a moving strand and assuming that the quality of material conveyed in the suspended phase is negligible in comparison with that conveyed in the strand, an equation for the additional pressure drop required to convey the strand was developed. This analysis leads to the realization that the volumetric loading and not the solids loading is the important factor in determining the stability of a system. Here, the pressure gradient due to the solid particle is generally represented in dimensionless form and is represented as a function of the volumetric flow ratio, voidage and the friction number which can be defined as flows;

$$\frac{\frac{\Delta p_s}{\Delta L}}{f_R(\rho_s-\rho_a)(1-\varepsilon_s)g} = f\left[Fri; \frac{\rho_g \mu}{\rho_s(1-\varepsilon_s)}; \varepsilon_s\right] \tag{2.52}$$

Where;

$$Fri \equiv \frac{U_g}{\left\{f_R\left[\left(\rho_s/\rho_a\right)-1\right][1-\varepsilon_s]Dg\right\}^{0.5}} \tag{2.53}$$

The proposed state diagram consists of friction number as the abscissa and dimensionless pressure gradient over the frictional resistance of the strand as the ordinate. The diagram contains two other additional parameters, the volumetric flow ratio, i.e., $\frac{\rho_g \mu}{\rho_s(1-\varepsilon_s)} = C$ and the ratio of the strand velocity w to the gas velocity U_g above the strand in the form of curved lines. In the state diagram, the regions of stable strand type conveying and the transition to plug flow can be clearly identified.

Klinzing et al. [6] used the frictional approach as discussed in dilute phase conveying and utilized the following equation to calculate the solid friction factor for dense phase conveying.

$$\lambda_s = 0.52\mu^{-0.3}\frac{Fr_s^{0.25}}{Fr_a}\left(\frac{d_p}{D}\right)^{-0.1} \tag{2.54}$$

2.5 Vertical Pipe Sections

Same as the horizontal sections, vertical sections are also very important in pneumatic conveying systems. Particularly, when there is a height difference between the sending source and the receiving station, at least one vertical section is inevitable. A quite large number of researches relavant vertical pipes can be seen in open literature. Recently, there has been a trend to use inclined pipe sections instead of vertical section. In the first section this chapter, the available models and theories related to the vertical section are discussed and in the second half the inclined sections will be focused on.

In contrast to horizontal gas-solid flow, vertical flow is very unstable, especially in the case of cohesionless particles. This is because the gravitational force essentially tends to collapse the plug, which makes the flow pattern very complicated. In addition, vertical gas-solid two-phase flow is heterogeneous in nature and always also locally unsteady. Particularly, when the solids volume fraction increases, particles no longer flow as individuals but form groups of particles. This behaviour has been detected by many researchers [6, 72, 74-76] and those loose particle groups are called, according to their shape, clusters, streamers or sheets. It differs from the horizontal pipe in that the complexity of stratification under gravity is replaced by the three-dimensional behaviour, including possible recirculation. In many cases, the particle groups are not all moving upwards, rather considerable downflow may be observed, especially near the wall.

In case of vertical sections, the different flow behaviours called lean or dilute- phase and dense-phase can be seen as in horizontal sections. The term ‘choking’ has generally been used to describe a particular change in the flow behaviours when a pneumatic conveying flow collapses into a relatively dense condition. At low pressure drops, the solid is conveyed in the form of strands and clusters whereas, at high pressure drops, the solid is transported as migrating fluidised bed that is in the

regime of the so-called fluidised bed conveying. A sudden increase in pressure drop produces an equally sudden change in flow pattern. The superficial gas velocity corresponding to this transition is referred to as the choking or critical velocity.

Consequently, the velocity determination plays a very important role in vertical section. In this section, mainly the available models for the pressure drop determination of verticle sections are addressed.

In a simple approach, Woodcock [40, 72] proposed to modify equation (2.11) to compensate a vertical section as follows;

$$\Delta p_s = \zeta \Delta p_a + \rho_g g \mu \left(\frac{u_a}{u_a - u_T} \right) L_v \qquad (2.55)$$

In one of the earliest approach to calculate the pressure drop in vertical lines, λ_t, Yang [77] recommended that the total pressure drop should be considered as a combination of different contributions due to acceleration, gravity and wall friction. To determine λ_s for a vertical flow, Yang [77] proposed the following models for different air velocity values.

$$\lambda_s = 0.0126 \frac{1-\varepsilon_s}{\varepsilon_s^3} \left[(1-\varepsilon_s) \frac{\mathrm{Re}_T}{\mathrm{Re}_p} \right]^{-0.979} \qquad \text{for } \frac{v_a}{v_T} \rangle 1.5 \qquad (2.56)$$

$$\lambda_s = 0.041 \frac{1-\varepsilon_s}{\varepsilon_s^3} \left[(1-\varepsilon_s) \frac{\mathrm{Re}_T}{\mathrm{Re}_p} \right]^{-1.021} \qquad \text{for } \frac{v_a}{v_T} \langle 1.5 \qquad (2.57)$$

Where $\mathrm{Re}_T = d v_T \rho \frac{1}{\mu}$ and $\mathrm{Re}_p = d(v_a - v_s) \rho \frac{1}{\mu}$

Based on the above approach, Rautiainen et al. [75] considered the frictional pressure drop by subtracting the static head and gas only frictional pressure from the total pressure drop. It was revealed that for a constant gas velocity, as the solids mass flow rate increases, then the friction pressure loss increases respectively at high gas velocities but at the low gas velocities the reverse applies. In some cases, the friction pressure loss is less than the friction pressure loss for gas only. It means that the solid friction factor becomes negative corresponding to the low values of gas and solid velocities. This phenomenon was supported by the visual observation, which showed

that at high gas velocities all the particles moved upward, but at low gas velocities some of the particles flowed down near the wall.

Weber [41], in a comparison study between hydraulic and pneumatic conveying, suggested the following relationship for vertical λ_s.

$$\lambda_s = \frac{v_a}{v_s}\left[\frac{1}{1200} + \frac{2}{Fr}\right] \tag{2.58}$$

Tsuji et al. [76] carried out an experiment to investigate the frictional characteristics of plug flow conveying in vertical pipe sections. They expressed their doubt about the applicability of packed bed models (such as Konrad's [64]) in vertical conveying, because of its high instability. They considered the total pressure drop across a plug as a summation of two components; Δp_1, which is due to the flow contraction at the end of the plug and Δp_2, which is the ordinary packed bed pressure drop. The following were proposed to determine these two components.

$$\Delta p_1 = 0.5\left(\frac{1}{\varepsilon_s^2} - 1\right)\rho v_s^2 \tag{2.59}$$

$$\Delta p_2 = 0.5 d_p \left(C_1 v_s + C_2 \rho_s v_s^2\right) \tag{2.60}$$

where constants C_1 and C_2 are given by;

$$C_1 = 150\frac{\left(1-\varepsilon_s\right)^2 \mu}{d_p^2 \varepsilon_s^3} \text{ and } C_2 = 1.75\frac{\left(1-\varepsilon_s\right)}{d_p \varepsilon_s^3}$$

2.6 Inclined Pipe Sections

To replace a combination of a vertical pipe section and a horizontal section, inclined pipe sections have often been used. This has been the topic of number of experimental investigations [6, 78-81]. One of the main advantages of these approaches is that these models have the potential to be used in both horizontal and vertical pipes as generalised approaches. Aziz et al. [82] proposed the frictional approach for the inclined sections as well and used the following equation to determine the friction factor.

$$\lambda_s = \frac{D}{2v_s^2}\left[\frac{3C_D\varepsilon_s^{-4.7}\rho\left(v_a - v_s\right)^2}{4\left(\rho_s - \rho_a\right)d_p} - g\sin\theta\right] \tag{2.61}$$

where θ is the angle of inclination of the pipe.

Hirota et al. [80] carried out an experimental investigation on inclined conveying of solids in high-dense and low-velocity. They found a linear relationship between Fr and friction factor of the gas-solid mixture, which can be presented in the following form.

$$\lambda_t = 2\left(\sin\theta + C_1\mu_{di}\cos\theta\right)\frac{1}{Fr} \tag{2.62}$$

where, μ_{di} is the dynamic internal friction factor and C_1 is a constant between 1 and 2 (1.5 is recommend). In addition, they found that the pressure drop is maximum between 30°-45° inclination angles.

2.7 Pipe Bends

Being certainly the most common pipe or tubing fitting, bends are a reality in all pneumatic conveying systems. There are two major effects of a bend in a pneumatic transport system, i.e;

a) bend causes a loss of energy, which results in an additional pressure drop
b) bend can cause product attrition and/or it can be subjected to wear, depending on the relative hardnesses of the product and pipe materials.

The problem of determining the pressure loss produced by a bend has been the subject of research for many years, because of its considerable importance in the design and analysis of pneumatic transport systems. However, no general consensus on how to analyse the two-phase flow across a bend has emerged, since the motion of particle around a bend and exact calculation of the pressure drop caused by a bend are highly complex. Especially, when gas-solid flows experience the centrifugal and secondary flows incited by the bends, all system parameters explained in the early sections come into play.

In a detailed investigation of bends of different included angles, Ito [83] recommended the following formulae to calculate the air only pressure drop of fully developed turbulent flow across a bend.

$$\Delta p_{b,a} = \frac{0.029 + 0.304\left[\mathrm{Re}\left(r/R_b\right)^2\right]^{-0.25}}{\left(R_b/r\right)^{0.5}} \frac{L_b \rho_a v_a^2}{2D} \tag{2.63}$$

The validity range of the equation is given by $300 > Re(r/R_b)^2 > 0.034$. He claimed when the parameter falls below its lower bound, i.e., 0.034, the bend can be considered as a straight pipe.

Wypych et al. [46] proposed a semi-empirical method to calculate the air only pressure drop across bends. They first considered the pressure drop formulae for incompressible flow situation, such as;

$$\Delta p_{b,a} = \frac{1}{2} \lambda_{b,a} \rho_a v_a^2 \tag{2.64}$$

where, $\lambda_{b,a} = \dfrac{0.217\phi}{\mathrm{Re}^{0.17}} \left(\dfrac{R_b}{r_o}\right)^{0.84}$ for $Re(r_o/R_b)^2 > 91$

$$\lambda_{b,a} = \frac{0.248\phi}{\mathrm{Re}^{0.2}} \left(\frac{R_b}{r_o}\right)^{0.9} \quad \text{for } Re(r_o/R_b)^2 < 91 \tag{2.65}$$

and $\phi = 0.95 + 17.2\left(\dfrac{R_b}{r_o}\right)^{-1.96}$ for $R_b/r_o < 19.7$

$$\phi = 1.0 \quad \text{for } R_b/r_o > 19.7 \tag{2.66}$$

To modify the above equation (2.64) for compressible flow in conveying pipeline, the values of constants have been replaced by number of coefficients (i.e., x_i; i = 1,….,6), which could be determined by minimising the sum of squared errors of pressures at different points on conveying line, as shown below.

$$\lambda_{b,a} = \frac{x_1\phi}{\mathrm{Re}^{x_2}} \left(\frac{R_b}{r_o}\right)^{x_3} \quad \text{for } Re(r_o/R_b)^2 > 91$$

$$\lambda_{b,a} = \frac{x_4\phi}{\mathrm{Re}^{x_5}} \left(\frac{R_b}{r_o}\right)^{x_6} \quad \text{for } Re(r_o/R_b)^2 < 91 \tag{2.67}$$

where ϕ is calculated using the equations (2.66)

Wypych et al. [46] concluded that the analysis of compressible flow through straight sections of pipe and bends can be represented adequately by an incompressible flow, as long as mean conditions for each straight section of pipe (based on average air density) and conditions at the outlet of each bend are used. In addition, it is revealed that for air only, acceleration length is very short.

The simplest approach proposed in the literature is the equivalent length method, in which the bend effect is replaced with a straight pipe of specific length [16, 72]. The following form can present this concept.

$$L_{b,eq} = \frac{k_b}{4}\frac{D}{f}(1+\mu) \tag{2.68}$$

where f is the Darcy's friction factor [see equation (2.2)] and k_b is called as the bend pressure drop factor given in tabulated form with respect to bend radius.

Then, the bend pressure drop is;

$$\Delta p_b = k_b \rho_s \frac{v_a^2}{2} \tag{2.69}$$

In an extensive experimental investigation programme, in which long radius bends, short radius bends tight elbows and blind tees were examined, Mills and Mason [84] considered the whole pipeline (including different types of bends) pressure drop in a wide range of conveying condition, such as dilute and dense phase. They found that there were very significant differences in pressure drop between the different bends over the entire range of conveying conditions. According to their findings with one conveying material (pulverised fuel ash), they concluded that the short radius bends with a bend diameter to pipe bore ratio of 6:1 provided the best performance over the widest range of conveying conditions. The long radius bends were marginally better at the highest values of the flow rates and the performance of the blind tees was significantly below that of the short radius bends.

In some published works [85-87], the pressure drop of the gas-solid across a bend has been split into two parts as gas only and solids contribution components. To determine the gas only pressure drop one can use the equations for single-phase flow

like equation (2.63). The interpretation of the pressure drop components due to the presence of solid particle is arguable same as in the case of straight pipe sections.

Pan et al. [86] carried out an experimental investigation with short radius bends, which are connected by short straight pipes and proposed an empirical method to determine the pressure drop in such cases. They in a different way, considered the bends' outlet conditions such as velocity, density, etc., for the calculation of bend pressure losses. Their model can be presented in the following form.

$$\Delta p_{b,s} = \mu \lambda_{b,s} \frac{\rho_{a,o} v_{a,o}^2}{2} \tag{2.70}$$

where $\rho_{a,o}$ and $v_{a,o}$ are the density and velocity of air at the bend outlet section.

$$\lambda_{b,s} = x_1 \mu^{x_2} Fr_o^{x_3} \rho_{a,o}^{x_4} \tag{2.71}$$

Here, the values are to be determined by an empirical fitting method and only valid for a given product and bend geometry.

Marcus et al. [88] used the following equation for the 90° bend.

$$\Delta p_{b,s} = 12 \left(\frac{\rho_s}{\rho_a} \right)^{0.7} \left(\frac{\rho_a v_a}{2} \right)^2 \frac{L}{D} C_t \tag{2.72}$$

where $L = \frac{\pi}{4} D$ and C_t is the ratio between solid and total volumetric flow rate.

After reviewing a few publications, Marcus et al. [88] proposed the following form of equation where the unknown coefficients, i.e., x_1, x_2 and x_3 have to be determined using an empirical method.

$$\frac{\Delta p_{b,s}}{\Delta p_s} = x_1 \left(\frac{2R_b}{D} \right)^{x_2} \left(\frac{d_p}{D} \right)^{x_3} \tag{2.73}$$

2.8 Velocity Consideration

Successful and optimal operations of pneumatic conveying systems depend upon the determination of minimum conveying velocity at which the solids may be conveyed steadily through pipeline. Consequently, this topic has been a major focus of many

research works, which have been produced a considerable number of publications in open literature.

2.8.1 Determination of Minimum Conveying Velocity

In general, minimum-conveying velocity can be defined as the lowest safe gas velocity for the horizontal transport of solids. If this gas velocity is set at the beginning of the pneumatic conveying system (at the feed point), the gas velocity will increase along the pipeline due to the compressibility effects, i.e. density decrease, so the rest of the pipeline should be operating well above this lower velocity bound. Keeping gas velocity above minimum conveying velocity in all horizontal sections of a pipeline ensures no deposition of solids in the system and a continuous and steady transport.

Over the years, many terms have been used to refer to minimum conveying velocity; saltation velocity, pickup velocity, suspension velocity, deposition velocity, critical velocity, velocity at the pressure minimum point of the general state diagram, etc. Definitions of these terms are based on visual observations and pressure drop measurements, and they are often applied to indicate some transition in the way in which the particles are moving or begin to move. Unfortunately, a controversy exists on how to define the minimum conveying velocity. The saltation velocity is usually defined as the gas velocity in horizontal pipeline, at which the particles start to drop out from suspension and settle on the bottom of the pipeline. The minimum gas velocity in a system containing a horizontal pipeline that will prevent solids deposition on the bottom of the pipeline is similar definition to the saltation velocity. Pickup velocity has been defined as the gas velocity required for resuspending a particle initially at rest on the bottom of a pipe or as the fluid velocity required to initiate sliding, rolling and suspension of particles.

Although a considerable number of research works have been carried out in this field, a general procedure to predict the minimum conveying velocity is not available. Since a thorough understanding of the pickup and saltation mechanism has not been possible yet, the theoretical predictions of pickup and saltation velocities

from the first principles have yet to be developed. However, some of the experimental works, which give some theoretical correlations showing good agreements with experimentally measured data, are discussed in subsequent chapters.

In one of the earliest addresses to the topic of saltation and minimum conveying velocity, Zenz [14] defined the saltation velocity as the minimum fluid velocity required to carry solids at a specified rate without allowing them to settle out in any horizontal pipe section and thereby partially obstruct the flow area. He used the dimensional analysis to correlate the saltation velocities of single particles in a horizontal pipe to the free fall velocities. When both the saltation velocity and terminal velocity are plotted, the difference is shown to be large at low Reynolds numbers. To identify the influence of size distribution, he used the minimum and maximum particle diameters of the size distribution and found an approximation to the functional relationship between single particle saltation velocity and particle diameter for the distribution. This is then incorporated into the correlation for saltation velocity and solids feed rate in the following form.

$$U_{gs} = \frac{WU_{gso}}{0.21\rho_s \left(S_\Delta\right)^{1.5}} + U_{gso} \tag{2.74}$$

where U_{gs} is the superficial air velocity at saltation, U_{gso} is the single-particle saltation velocity, W is the solid flux (solid mass flow rate per unit pipe cross section) and S_Δ is the particle size and size distribution characteristic, which represents the slope of a curve of single particle saltation velocity versus particle diameter between the extremes of the largest and smallest particle in the mixture.

Cabrejos and Klinzing [34] carried out a detailed investigation to determine minimum pickup velocity of different materials of different particle sizes (10 to 1000 μm) in a horizontal pipe, using visual observations. First they used a theoretical force balance analysis and proposed the following equations to determine minimum pickup velocity for large and small spherical single particles.

For a large single spherical particle;

$$U_{gpuo} = \left[1 - \left(\frac{d_p}{D}\right)^{1.5}\right]\left[\frac{4}{3}\frac{f_s g d}{C_D}\left(\frac{\rho_s - \rho_a}{\rho_a}\right)\right]^{0.5} \tag{2.75}$$

For a small single spherical particle;

$$1.54\times10^{-4}\left[1-\left(\frac{d_p}{D}\right)^{1.5}\right]^{-2} C_D\rho_a d_p^3\left(\frac{U_{gpuo}^7}{\upsilon^3 D}\right)^{0.5}$$
$$= f_s\left[\frac{\pi}{6}gd^3\left(\rho_s-\rho_a\right)+1.302\times10^{-6}d_p-6.35\times10^{-3}\rho_a d_p^3\left(\frac{U_{gpuo}^{21}}{\upsilon^5 D^3}\right)^{1/8}\right] \quad (2.76)$$

Here, f_s denote the coefficient of sliding friction. They proposed an iterative procedure for equation (2.76). Combining the single-particle model with the experimental results of a layer of particles, a general correlation was developed for the minimum pickup velocity.

$$U_{gpu}=\left(1.27Ar^{-1/3}+0.036Ar^{1/3}+0.45\right)\left(0.7Ar^{-1/5}+1\right)U_{gpuo} \quad (2.77)$$

where $Ar=\frac{g}{\upsilon^2}\frac{\rho_s-\rho_a}{\rho_a}d_p^3$, which is called as Archimedes number, υ denotes the carrier fluid kinematic viscosity.

The same authors elsewhere [35] proposed an empirically correlated equation to determine the pickup velocity of coarse particles (above 100 μm). They used dimensional analysis combined with their experimental findings, which show a strong relationship to pickup velocity of horizontal pipe with the particle and pipe diameters, and particle and carrier gas densities.

$$U_{gpu}=0.0428\left(gd_p\right)^{0.5}Re_s^{0.175}\left(\frac{D}{d_p}\right)^{0.25}\left(\frac{\rho_s}{\rho_a}\right)^{0.75} \quad (2.78)$$

They claimed the validity ranges of this relationship as; $25<Re_s<5000$, $8<(D/d_p)<1340$ and $700<(\rho_s/\rho_a)<4240$.

In a seperate investigation, Cabrejos and Klinzing [89] studied pickup, saltation and particle velocities in horizontal dilute-phase pneumatic transport. In the case of pickup velocity, they emphasized the applicability of equation (2.78) published elsewhere [35].

They proposed the following expression to predict the saltation velocity of coarse particles with help of dimensional analysis.

$$U_{gs} - U_{gso} = 0.00224\left(\frac{\rho_s}{\rho_a}\right)^{1.25} \mu^{0.5}\sqrt{gd_p} \tag{2.79}$$

where U_{gs} is the saltation velocity. In addition, they emphasized the influence of particle diameter to saltation velocity highlighting that adhesive and cohesive forces play a significant role in the case of fine particle, while friction and the particle weight are more important for coarse particles.

In the same article, Cabrejos and Klinzing [89] highlighted that the particle velocity increases as mean gas velocity increases, and particle velocity decreases as solids flow rate increases, showing the importance of solids loading ratio on particle velocity from the plots of particle velocity vs. velocity difference of saltation and mean gas velocities. They proposed the following relationship to determine the particle velocity.

$$U_s = x_1\left(U_g - U_{gs}\right)^{x_2} \tag{2.80}$$

The coefficients x_1 and x_2 best fitted the experimental results, were obtained using a least squares technique.

Hayden et al. [90] followed a similar procedure as Cabrejos and Klinzing to determine the pickup velocity for fine particles of size range 5-35 μm. According to their findings;

- Pickup velocity remains relatively constant at very small particle diameters, specially, less than 10 μm.
- Pickup velocities for non-spherical particles are higher due to particle interlocking.

Molerus [4, 91] suggested to predict the minimum conveying velocity using the following relationship;

$$\frac{\rho_g}{\rho_s\left(1-\varepsilon_s\right)}\mu = 0.018 Fri_{\min}^4 \tag{2.81}$$

where;

$$Fri_{\min} \equiv \frac{u_{g,\min}}{\left\{f_R\left[\left(\rho_s/\rho_a\right)-1\right]\left[1-\varepsilon_s\right]Dg\right\}^{0.5}} \tag{2.82}$$

Here f_R is the wall friction factor.

In a comparison study, Weber [92] tried to find out some hydraulic transport analogy to the pneumatic conveying. He proposed the following relationships to determine the minimum velocity for dilute suspension flow.

$$Fri_{\min} = \left(\frac{8}{3}u_{so} + 7\right)\mu^{0.25}\left(\frac{d_p}{D}\right)^{0.1} \qquad \text{for } u_{so} \le 3 \text{ m/s}$$

$$Fri_{\min} = 15\mu^{0.25}\left(\frac{d_p}{D}\right)^{0.1} \qquad \text{for } u_{so} > 3 \text{ m/s} \qquad (2.83)$$

where u_{so} is the free settling velocity of a single particle.

However, the great complexity of the above equations, coupled with the fact that it was developed from the data obtained in rather small-scale model tests, might well discourage the use of this correlation for the design purpose.

2.8.2 Choking Velocity in Vertical Flows

The above discussion is mainly focussed on flow of horizontal pipe sections. When the vertical sections are dealt with, the above mentioned models are no longer valid, since the flow behaviour in vertical pipe is totally different from that in horizontal sections, as discussed in section 2.5. In contrast to the term 'saltation' used in horizontal pipes, most of the researchers, the term 'choking' has generally been used to describe a particular change in the flow behaviour when a pneumatic conveying flow collapses into a relatively dense condition in vertical sections. But unfortunately, there is no clear-cut definition of choking available in the literature as yet. However, three different mechanisms that trigger the choking were distinguished in different investigations [93]. They can be detailed as follows;

a. Accumulative choking; which stresses the essence of solid accumulation at the bottom of a vertical conveying tube
b. Classical choking; the sudden formation of slugs or plugs when a steady operation ceases.
c. Pipe choking; due to the inappropriateness of the pipeline components.

Here, the types *a* and *b* are due to the inherent changes in gas-solid flow itself, while the type *c* choking actually stems from facility inefficiency.

Yang [94] published a paper describing the choking phenomena, with the aim to present a unique approach to calculating the choking velocity and choking voidage by using readily available properties of the transported materials and system characteristics. He expressed that the choking evolved as a result of range of instabilities and defined it as the point where internal solid circulation, with solids moving downward at the wall and moving upward in the core, began. Assuming that the slip velocity is equal to the free-fall velocity at choking, he proposed the following equation;

$$\frac{U_c}{u_t} = 1 + \frac{\frac{U_s}{u_t}}{1-\varepsilon_c} \tag{2.84}$$

where U_c is the choking velocity.

Then, he assumed a constant value, i.e., 0.01 for solid friction factor at the choking condition $\lambda_{s,c}$, and proposed the following equation;

$$\lambda_{s,c} = \frac{2gD\left(\varepsilon_c^{-4.7} - 1\right)}{\left[U_c - u_t\right]^2} = 0.01 \tag{2.85}$$

Since this assumption was arbitrary, later he proposed some modifications to equation (2.85) as shown below;

$$\frac{2gD\left(\varepsilon_c^{-4.7} - 1\right)}{\left[U_c - u_T\right]^2} = 6.81\times10^5 \left(\frac{\rho_a}{\rho_s}\right)^{2.2} \tag{2.86}$$

2.8.3 Determination of Average Particle Velocity

When the particle velocity is considered, the other terms that come into the picture are terminal velocity, slip velocity and voidage. Klinzing et al. [6] discussed these parameters in detail and recommended the following relationships.

The actual carrier fluid velocity can be given in the following form when the voidage is considered.

$$u_a = \frac{U_a}{\varepsilon_s} \tag{2.87}$$

Slip velocity is the resultant velocity between the fluid and solid caused by the particle-particle and particle-wall interactions and can be represented by the following equation;

$$w_s = u_a - u_s \tag{2.88}$$

Another important velocity parameter of a two-phase flow is the particle terminal velocity, which depends on the drag coefficient thus, on the Reynolds number as well. There are number of different correlations available for different *Re* regions as shown below.

$$v_T = \frac{d_p{}^2 (\rho_s - \rho_a) g}{18\eta} \qquad \text{for } Re_T < 2.0$$

$$v_T = \frac{0.153 d_p{}^{1.14} (\rho_s - \rho_a)^{0.71} g^{0.71}}{\rho_a^{0.29} \eta} \qquad \text{for } 0.5 < Re_T < 500$$

$$v_T = 1.74 \left[\frac{d_p (\rho_s - \rho_a) g}{\rho_a} \right]^{0.5} \qquad \text{for } 500 < Re_T < 2\times10^5$$

$$v_T = 3.65 \left[\frac{d_p (\rho_s - \rho_a) g}{\rho_a} \right]^{0.5} \qquad \text{for } 2\times10^5 < Re_T \tag{2.89}$$

where v_T is the terminal velocity and Re_T is the Reynolds number related to v_T.

To determine the solids velocity, Klinzing et al. [6] proposed the following equations, referring some earlier work by Hinkle.

$$v_s = v_a \left(1 - 0.68 d_p^{0.92} \rho_s^{0.5} \rho_a^{-0.2} D^{-0..54}\right) \tag{2.90}$$

They proposed another empirical correlations referring to Yang, as shown below.

$$v_s = \frac{v_a}{\varepsilon_s} - w_{fo} \left(1 + \frac{\lambda_s v_s^2}{2gD} \varepsilon_s^{4.7} \right)^{0.5} \tag{2.91}$$

where, λ_s is the solid friction factor discussed in details in Section 2.4.1.3.

2.9 Scale Up Techniques

One method that is used for predicting pressure drop involves testing a sample of the product to be conveyed in the final system in a pilot scale rig over a wide range of operating conditions, and measuring the product and air flow rates and resulting pressure drops. The obtained data are then scaled by experimentally determined factors to predict the pressure drop in the full scale system. This method has the advantage that real test data on the product to be conveyed in the projected system are used for the design work. This is important because it provides useful information about the conveyability of the product, as well as determining valuable data on the minimum conveying velocity etc.

The scaling of test data is considered to be one of the most important stages of the design process, in that it provides the link between laboratory-scale apparatus and full-scale industrial installations. Hence, accuracy and reliability of scale-up are essential.

Basically, there are two approaches in scaling up techniques available in literature; the global testing approach and the piecewise approach. Both approaches have their own advantages and undesirable characteristics as well.

2.9.1 Mills Scaling Technique

The basic condition of Mills' [16] technique is that conveying conditions, in terms of air velocities, should be identical for the pilot plant and full-scale plant. Since the air velocity depends on the pressure and the air mass flow rate, the scaling has been proposed to be carried out for the data points having the same conveying line pressure drop and inlet air velocity. Here, the total pressure drop is considered as a combination of pressure drop due to air alone and additional pressure drop caused by the presence of the solid particles. Throughout, the whole scaling procedure, the pressure drop due to solid particles is considered to be equal for the pilot plant and full-scale plant.

The entire scaling procedure is to carry out in two stages; first stage involves scaling to the required distance, with allowances for vertical sections and bends, while the

second stage scales the conveying characteristics in terms of the pipe diameter. The concept of equivalent length of a bend has been introduced to compensate for the different effects of bends in pilot plant and full-scaled plant.

2.9.1.1 Straight Horizontal Pipe Section

The horizontal pipe sections are considered to contribute directly to the equivalent length of the whole conveying line, having the same magnitude as their physical length.

For vertical sections, a scaling parameter is proposed in terms of length of straight horizontal pipe sections. Since the pressure drop in vertical conveying is approximately double of that in horizontal conveying, the equivalent length for the vertical section is considered as,

$$L_{ev} = 2L_v \tag{2.92}$$

2.9.1.2 Effect of Bends

The same concept of a hypothetical equivalent length has been proposed for bends. But, it is not an independent parameter as for the vertical sections. As a simplification, the variation of equivalent length with velocity should be found for the conveying material, using pilot plant.

$$L_{b,eq} = nb \tag{2.93}$$

2.9.1.3 Total Length

Considering the above relationships, the equivalent length of the whole conveying line can be calculated. A model based on a reciprocal law has been proposed for equivalent length of the pipeline as shown in equation (2.94).

$m_s \propto \left(\frac{1}{L_e}\right)$ for a constant Δp_s and v_a.

That is,

$$m_{s2} = m_{s1}\left(\frac{L_{e1}}{L_{e2}}\right) \tag{2.94}$$

Where, $L_e = L_h + L_{ev} + L_{eb}$, for a constant Δp_s and v_a.

2.9.1.4 Pipe Diameter

A scaling model for pipe diameter is proposed, on the basis of pipe cross-sectional area,

$m_s \propto A \propto D^2$ for a constant $m_a D^{-2}$ and Δp_s.

Alternatively,

$$m_{s2} = m_{s1}\left(\frac{D_2}{D_1}\right)^2 \tag{2.95}$$

and

$$m_{a2} = m_{a1}\left(\frac{D_2}{D_1}\right)^2 \tag{2.96}$$

Mills suggested an iterative `trial and error´ procedure to determine the minimum conveying limits, since conveying line inlet air velocity, pressure drop, airflow rate and phase density (= m_s/m_a) are interrelated.

2.9.2 Wypych & Arnold Scaling Method

Wypych and Arnold [25] examined the validity of the scale-up procedure proposed by Mills [16]. It has been revealed that the equations used in Mills scale-up technique are inadequate, especially when data are scaled-up with respect to pipeline diameter. They proposed following scale-up equation;

$$m_{s2} = m_{s1}\frac{L_1'}{L_2'}\left(\frac{D_2}{D_1}\right)^{2.8} \tag{2.97}$$

Here, L'_1 and L'_2 represent the adjusted values of lengths to allow for any differences between the number and type of bends used on the test rig and full-scale plant.

For the purposes of general design and feasibility studies, it is proposed to use generalised pneumatic conveying characteristics. Using the data of pilot plant, the co-ordinate system $m_f D^{-2}$ (abscissa) and Δp_s (ordinate) could be used to represent the parameter $m_s L D^{-2.8}$ for the purpose of generalising pipeline conveying characteristics. In this investigation, the effects of pipeline bends are not considered and no allowance has been made for the bends when pipeline lengths are calculated.

2.9.3 Keys and Chambers Scaling Technique

Keys and Chambers [95] proposed a scaling technique, based on empirical correlations. It combines a number of non-dimensional flow parameters to predict the pressure loss in the pipeline system.

$$\Delta p_b = nB\frac{\rho v_a^2}{2} \tag{2.98}$$

To calculate the air alone friction factor, the following relationship was used.

$$\lambda_a = 2D\frac{\left(\Delta p_t - \Delta p_b\right)}{\rho v_a^2 L} \tag{2.99}$$

An empirical correlation was obtained by plotting λ_a verses *Re*, in the form of the following equation.

$$\lambda_a = x_1 \mathrm{Re}^{x_2} \tag{2.100}$$

To calculate solids friction factor;

$$\lambda_s = 2D\frac{\left(\Delta p_t - \Delta p_b\right)}{\rho v_g^2 L\mu} - \frac{\lambda_a}{\mu} \tag{2.101}$$

Similar to the calculation of λ_a, the constants in the following equation should be found by fitting empirical curves.

$$\lambda_s \mu^{x_3} = x_4 . Fr^{x_5} \tag{2.102}$$

The pressure drop for the full-scale plant can be predicted with the following.

$$\Delta p_{predicted} = \left(\lambda_a + \lambda_s \mu\right)\frac{\rho v_g^2 L}{2D} \tag{2.103}$$

The authors emphasised that the effect of bends has to be considered when the solid friction factor is calculated.

2.9.4 Molerus Scaling Technique

Molerus [91] proposed to consider a relationship between two non-dimensional parameters given below;

$$\lambda_p \equiv \frac{2\left(\Delta p_s / \Delta L\right) D}{\mu \rho_a v_a^2} \tag{2.104}$$

$$Fr_a \equiv \frac{v_a}{\sqrt{Dg}} \tag{2.105}$$

where λ_p is called as the non-dimensional particle pressure drop and Δp_s is the pressure drop due to the solid particle. Molerus [91] stated that the combination of above two parameters defines fully suspended gas-solid pipe flow for given combination of gas and particulate material. Based on this assumption, he proposed to carry out pilot plant tests to get the data in terms of λ_p versus Fr_a and to use the resulting curve for the prediction of the pressure drop of the plant to be designed.

2.9.5 Bradley et al. Scaling Technique

In a series of publications, Bradley et al. [96-101] formulated a piecewise scaling technique for pneumatic conveying system designs. They use the concept of air only and solid contribution to total pressure gradient of straight pipe sections. The concept of suspension density also was used to categorise different flow conditions experienced during conveying process.

Bradley [96, 97, 101] found a relationship for a pressure drop across bends, which can be presented as shown below.

$$\Delta p_b = \frac{1}{2} k \rho_{sus} v_a^2 \tag{2.106}$$

Here 'k' is a dimensionless coefficient and ρ_{sus} is termed as suspension density which is considered as the mean density of the gas-solid mixture in the pipeline. The value of suspension density was simply calculated by dividing the solids flow rate by the air flowing. It could be presented as shown in equation (2.107).

$$\rho_{sus} = \mu \rho_a \tag{2.107}$$

He found that the variation of '*k*' with superficial air velocity was similar in shape for all of the radiused bends and could be represented by a single curve on a graph in each case.

Hettiaratchi et al. [98] used the concept of suspension density to formulated a scaling method for vertical pipe sections. They isolated the solid contribution to the total pressure and then the solid pressure per unit suspension density was plotted versus superficial air velocity. A constant trend was found between the above mentioned quantities in the non-suspension transport region.

In similar line, Hyder et al. [100] investigated the effect of particle size on straight-pipe pressure gradient in dilute-phase conveying. They used the relationship shown in equation (2.108) to model the pressure gradient along straight pipe sections.

$$\left(\frac{dp}{dl}\right)_s = k\rho_{sus} \tag{2.108}$$

The value of '*k*' was determined in terms of mean particle size.

2.10 Effects of Material Physical Characteristics

To describe a bulk material with the aim to understand its behaviour and performances in pneumatic conveying systems, there are basically two major levels;

a. With the use of features of the material in its bulk form (cumulative/bulk properties)
b. With the use of features of constituent particles (individual/singular properties)

There are many descriptive terms and numerical parameters, which can be used in the characterisation of conveying materials. The main properties that have been identified as the most influential parameters on transport performances are briefly listed below [72]:

- **Particle size and size distribution** – The natural force of attraction increases with the decreasing particle size. Mean diameter, volume diameter, surface diameter and Stokes diameter are few of the commonly used terms to define the particle size.

- **Particle shape** – Usually, the shape of the constituent particles in a bulk solid is an important characteristic as it has a significant influence on their packing and flowing behaviour. Highly irregular shaped and fibrous particle can interlock thereby increasing the resistance of a bulk solid to flow.
- **Cohesiveness** – This property gives a sort of an idea how strong the inter-particle attraction forces, which can cause some problems in hopper discharge, feeding and conveying as well.
- **Hardness** – The hardness is important when a pneumatic conveying installation is being designed since it will give an indication of the need to take steps to avoid undue erosive wear of the system components.
- **Electrostatic charging** – Due to some handling of bulk materials, constituent solid particles acquire electrostatic charges. With electrostatic charges, material may exhibit some cohesive properties.

As an early research on particle characterisation, Geldart [102] work, which has been used as a base for many other experiments later, is worthwhile to take into account. Based on experimental evidence, Getdart found that most products, when fluidised by a gas, are likely to behave in a manner similar to one of four recognisable groups and these groups of materials can be represented graphically as shown in Figure 2-1.

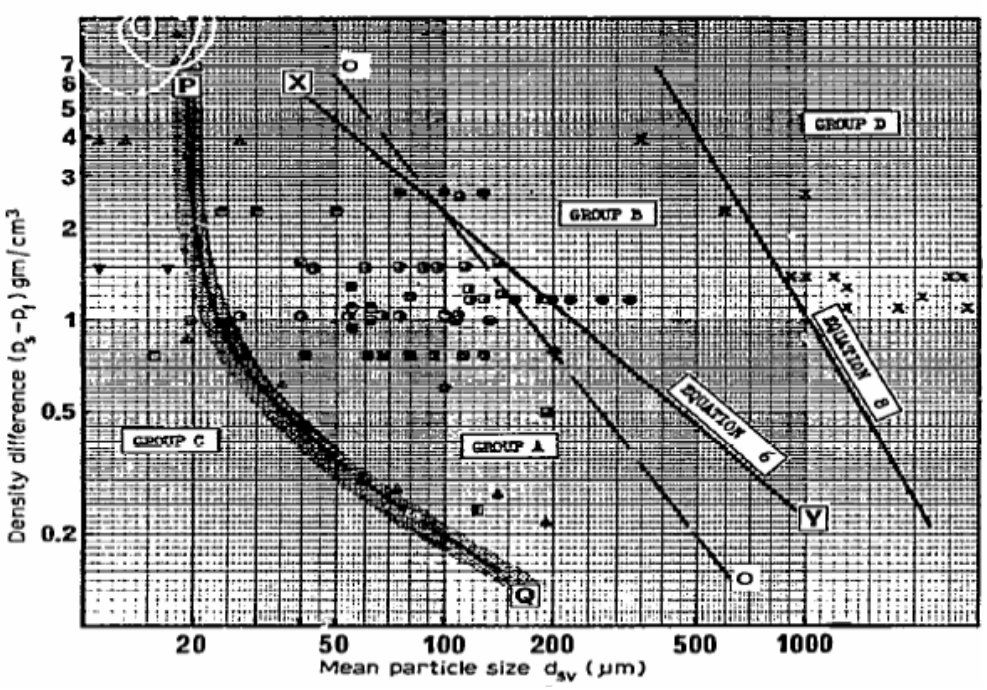

Figure 2-1: Powder classification diagram for fluidisation by air (as appeared in the original publication by Geldart [102]).

An abbreviated version of his description of the characteristics of these four groups is as follows;

1. **Group A**

   Materials having a small mean size and/or low particle density will generally exhibit considerable bed expansion before bubbling commences. When the gas supply is suddenly cut off, the bed collapses slowly.

2. **Group B**

   Naturally occurring bubbles start to form in this type of material at, or slightly above, the minimum fluidising velocity. Bed expansion is small and the bed collapses very rapidly when the gas supply is shut off.

3. **Group C**

   This group contains powders, which are of small particle size and cohesive in nature. Consequently, normal fluidisation is very difficult. The powder lifts as a plug in small diameter tubes or, preferentially channels.

4. **Group D**

This group contains large and/or high-density particles. It is belived that the bubble sizes may be similar to those in Group B and if gas is introduced only through a centrally located hole, this group can be made to spout.

In later investigations, Dixon [103, 104] recognised that the fluidisation properties of a product have significant implications with regard to its conveyability in dense phase. His theoretical description enabled boundaries between expected flow conditions to be drawn on the same axes as Geldart's classification. It can be seen that the boundaries between strong axisymmetric slugging, weak asymmetric slugging and no slugging relate well to Geldart's boundaries between groups D, B and A. Dixon concludes that group A products are the best candidates for dense phase conveying and, although not natural sluggers, can be made to slug using commercially available equipment or systems. Group D products are also good candidates because of their strong natural slugging behaviour. Group B products can cause problems if high solids loading ratios are used and group C products are possibly the least suitable materials for conveying in a dense phase mode.

Mainwaring and Reed [105, 106] found two parameters; permeability factor and de-aeration factor can be measured with the help of small laboratory test rig to understand the importance of the permeability and air retention characteristics of the conveying material. They proposed a graphical method to determine the suitable mode of conveying of particular material, by plotting the permeability factor, de-aeration factor and pressure gradient together with minimum fluidising velocity. The importance of above two factors were also empathised by Jones and Mills [107].

Goder et al. [108] examined the dependence of the transportability of a product in a dense phase on the particle size, size distribution, moisture content and bulk density. It was found that larger particles were less convenient for pneumatic conveying in dense phase and addition of small fraction of smaller particles could increase the transportability. Hyder et al. [100] reported the results of investigation whose aim was compare the materials of similar particle densities, chemical composition and shape. They found that as the particle size gets larger, the pressure losses along straight sections of pipelines increase.

Pan [109] developed a flow mode diagram characterised by loose-poured bulk density and mean particle diameter. The flow mode diagram classifies the bulk solid materials into three groups; materials which can be transported smoothly and gently from dilute to fluidised dense phase, materials that can be conveyed in dilute phase or slug flow and bulk solids which can be conveyed only in dilute phase.

2.11 Computational Models

In the first part of this section, the computational model technique is described in general and the multi-phase flow applications especially; pneumatic conveying systems are then focused in connection with special methodologies adopted and different applications.

The term CFD implies a computer-based simulation technology that enables one to study the dynamics of things that flow, with the ultimate goal to understand the physical events that occur in the flow of fluids around and within designated objects. Using CFD, a computational model that represents a system or device to be studied can be developed. Then, the fluid flow physics has to be applied to this virtual prototype. Finally, the CFD software outputs a prediction of the fluid dynamics. Being a sophisticated analysis technique, CFD not only predicts fluid flow behaviour, but also some other phenomena such as transferring of heat and/or mass (e.g.: dissolution, diffusion), changing phases (e.g.: freezing, boiling), chemical reaction (e.g.: combustion), mechanical movement (e.g.: an impeller turning), and stress or deformation of related solid structures (e.g.: wind loading). Hence, this technique is very powerful and spans a wide range of industrial and non-industrial application areas such as various engineering disciplines; mechanical, structural, electrical, environmental, etc, and biomedical and meteorology fields as well [110].

There are number of unique advantages of CFD, which are compelling reasons to use it against experiment-based approaches to fluid systems design. Those can be described with the following features of CFD:

1. **Insight** - There are many devices and systems that are very difficult to prototype, hence the controlled experiments are difficult or impossible to

perform. Often, CFD analysis shows parts of the system or phenomena happening within the system that would not otherwise be visible through any other means. CFD gives a means of visualizing and enhanced understanding of designs.

2. **Foresight** - CFD is a tool for predicting what will happen under a given set of circumstances, thus, it can answer many 'what if?' questions. With given variables, it gives relevant outcomes quickly. In a short time, one can predict how the design will perform, and test many variations until an optimal result is arrived. Even that can be done before physical prototyping and testing and gained practically unlimited level of detail results
3. **Efficiency** – There is a substantial reduction of lead times and costs of new designs. CFD is a tool for compressing the design and development cycle.

To deal with the fluid flow systems, usually the CFD simulation codes are structured around the numerical algorithms and comprise of basically three principal components; pre-processor, solver and post-processor. A user-friendly interface, which can be used to introduce the inputs of a flow problem to the solver algorithm is employed in the pre-processing stage. The demarcation of computational domain, grid generation, designation of fluid properties, boundary condition specifications and problem specifications are usually performed in pre-processing level. Usually, a solver uses one of the available streaming techniques: finite difference, finite element and spectral method. Generally, three basic operations of a solver can be listed as below:

a) Assume/approximate the unknown flow variable
b) Substitute the assumed variables in the governing flow equations and discretisation [111]
c) Solve the differential equations

Post-processor stage comprises of the various means of data visualization tools, like vector plots, contour plots, surface plots, particle tracking, animations, etc., to visualize the output results of the problem.

2.11.1 Applications of CFD in Gas-Solid Flows

As explained in the early section, CFD is increasingly used in all branches of engineering, including multi-phase flow applications like pneumatic conveying systems. In this section, the general use of CFD in gas-solid flow systems, especially in pneumatic transport, is described briefly.

CFD has proven to be extremely useful and accurate for a host of single-phase flows. Indeed, it is now possible to make numerical predictions for many single-phase flows that are more precise than the most accurate experimental local measurements that can be obtained in a physical apparatus of the same geometry. CFD originally applied to single phase flow problems, with advances in computer processing power and more powerful numerical methods it can now be applied to more complex situations. Multiphase flows involving a solids phase (or granular phases) have been studied using this technique. Although the behaviour of solids has not been always fully understood, attempts have been made to include granular phases into CFD packages, by using approximations to describe the particle phase [112].

The CFD models of multi-phase flow problems are basically built on the principles of the traditional way for modelling them, i.e., to use one-dimensional continuity and momentum equations for each of the phases. Firstly by adding gas phase and solids phase momentum equations together to obtain a mixture momentum equation, and then by integrating the mixture momentum equation over the computational domain, the differential equations reduce to a simple equation where the total pressure drop is the sum of the pressure drops due to acceleration, gravity, and friction. Usually to solve the equations, an iterative procedure is followed until a predefined residual of convergence is achieved.

There are two fundamentally different approaches in numerical modelling of gas-solid two phase flows according to the manner in which the particulate phase is treated; Euler-Lagrangian and Euler-Euler granular approaches. The Lagrangian model calculates the trajectories of individual or representative particles in the solids phase, considering the velocity, mass and temperature history of them. In this approach, for any interactions between the particles or with the boundaries of the

system, momentum is conserved and dissipation of energy is also possible. The Eulerian approach simulates the granular phase as a continuous second fluid, and solves a similar set of equations for the solids phase as for the fluid phase.

While CFD also holds great promise for gas-solid flows, obtaining accurate solutions is much more challenging especially in dense phase situations, not just because each of the phases must be treated separately, but, in addition, a number of new and difficult factors come into play. For any gas-solid flow problem where the concentration of dispersed phase is at least a few percent, the factors, such as; drag and lift forces, slip or relative motion between the phases, inter-particle forces, etc, have to be considered.

As a result, many different approaches, like; Eulerian, Lagrangian or combinations of the two; interpenetrating two-fluid approach or discrete particles, etc, have been used to model the multi-phase flow situations.. In addition, since the solids pressure generated in Eulerian approach is not as easy to calculate as the equivalent fluid pressure and a separate equation has to be used for closure in solution procedure. Turbulence too is a problem, which is only partially solved by the introduction of the concept of 'Granular Temperature'. The granular temperature is a function of the average difference between the individual particles velocity and the mean particle velocity and defined according to the kinetic theory approach for granular flow systems. The kinetic theory approach based on the oscillation of the particles uses a granular temperature equation to determine the turbulent kinetic energy of the particles, assumes either a Maxwellian or non-Maxwellian distribution for instantaneous particle velocity, and defines a constitutive equation based on particle collision and fluctuation. In fact, this approach allows the determination of solid pressure and viscosity in place of the empirical equations.

Methods based on both Eulerian and Lagrangian approaches have difficulties in accurately representing particle size distributions. To represent a full particle size distribution, it is necessary to have a number of different particle phases, with varying diameters and in similar proportions to the different sizes in the original distribution [113]. This is a particular problem for the Eulerian methods, as each extra phase requires that a new set of equations be solved.

2.11.2 CFD Applications in Pneumatic Conveying

A considerable number of publications on CFD applications on gas-solid systems can be seen in open literature [81, 113-130]. The simulation works that are directly related to pneumatic conveying systems are briefly described in this section.

One approach to simulate pneumatic transport system is the discrete element method (DEM) based on an equation of motion for each individual particle. Pioneering research in the development of the Lagrangian approach for the calculation of pneumatic conveying has been performed by the group of Tsuji et al., [131-134] especially with regard to modelling particle-wall collisions with wall roughness or for non-spherical particles. Thus, in principle, individual particle size, shape and density can be introduced directly into the equation. However this approach requires huge computational time when many particles exist in the considered system. Later, Tsuji [122] reported the developments of the discrete element method and suggested a method to deal with large number of particles efficiently. Levy et al. [81] uses a similar method to analyse the flow behaviours in vertical and inclined pipe sections, with the help of a commercial software. A two-dimensional DEM was used by Watano et al. [116] to analyse the particle movements, collision velocity, number of collision, etc, in a pneumatic conveying process in order to compute the electrification of particles during the transportation. A detailed summary of research related to pneumatic conveying of particles in pipes or channels was recently provided by Sommerfeld [135].

In another attempt to use a commercial software package for the prediction of pneumatic conveying flow phenomena, Bilirgen et al. [127] compared the simulation results with available experimental data from other sources. Levy [125] developed a two-layer model to simulate plug flow in horizontal pneumatic conveying pipeline and claimed that the model could be effectively used to predict the dense phase behaviour. Later, Mason and Levy [126] used the same model to simulate dense phase pneumatic transport of fine powders and claimed a good quantitative agreement with experimentally determined pressure profiles for fully developed flows in straight horizontal pipes. Pelegrina [124] used a one-dimensional steady-

state model for the simulation of pneumatic conveying of solid particles under different conditions and determine the effects of the pipe diameter, air temperature and inlet velocity on the pressure drop. A computational study of fully developed gas –solid flow in a vertical riser is carried out by Yasuna et al. [119] in order to assess qualitatively the predictive capacities of a computational model. Arastoopour et al. [136, 137] considered particles of each size as a separate phase, developed an experimentally verified particle-particle collision theory, introduced it in the one-dimensional equations, and compared the calculated flow parameters with experimental data for flow in dilute gas-solid systems. Mathiesen et al. [118] developed a multi-fluid Eulerian model to describe the turbulence in solid phase using the kinetic theory of granular flow. He proposed a model to enable a realistic description of the particle size distributions in gas-solid flow systems. The model is generalised for one gas phase and number of solid phases, characterising each solid phase by a diameter, density and restitution coefficient. Li and Tomita [117] carried out a numerical simulation for swirling and axial flow pneumatic conveying in a horizontal pipe with an Eulerian approach for the gas phase and a stochastic Lagrangian approach for particle phase, where particle-particle and particle-wall collisions were taken into consideration.

3 EXPERIMENTAL SETUP AND INSTRUMENTATIONS

For the experimental investigation, the pneumatic conveying test facilities available in powder research laboratory ('*Powder Hall*') of the department of Powder Science and Technology (***'POSTEC'***) of Telemark Technological Research and Development Centre (***'Tel-Tek'***) has been used with some additional components to accomplish the objectives of the work, since Telemark University College (***'HiT'***) has a close collaboration with *Tel-Tek*. *Tel-Tek* is a research foundation, which has been functioning as a national organisation for industrial research, development projects, technology transfer, academic research, etc.

This chapter gives a detailed description of the experimental setup used for the investigation. As described in early chapters, the whole investigation was carried out using different conveying pipeline configurations and instrumentations. The special features added and modifications done to cater to the particular requirements of individual sections of the investigation are described in relevant individual sections.

3.1 Available Pneumatic Transport Test Facilities at POSTEC Powder Hall

The test rig has been designed with the objective of handling the research activities of both the main transport modes, i.e., dilute and dense phase conveying. It mainly consists of a top/bottom discharge blow tank of 3.5 m^3, which can withstand a maximum pressure of 10 bar g, a receiving tank of 2.6 m^3 mounted on a special arrangement of load cells to monitor the weight accumulation during the experimentations, number of conveying pipes of different bore sizes and lengths, various type of bends of different radii and configurations and a combination of a screw type air compressor and a drier cum air cooler. The pipelines are laid out in such a way that it is possible to have any combination of horizontal, inclined and vertical sections depending upon requirements. The conveying line usually forms a

closed loop pneumatic transport circuit by placing the receiving tank on top of the blow tank so that the particulate material under testing can be repeatedly tested without taking it out of the test rig. In addition to these main items, number of different measuring instruments like pressure transducers, flow transducers, thermometers, humidity meters and an online sampler are also mounted on the transport line in order to achieve the desired measurements. The transport rig is equipped with facilities for continuous online data logging and visualising of data like air pressure at various locations, air temperature, humidity, material transport rate etc, on a real time basis. The data acquisition and analysis are undertaken with the help of a user friendly software program of the LabVIEW® package. The test rig facilitates with a control room where the operations of most of the valves, sampler and data acquisition can be controlled by one operator.

3.2 Air Compressor

A screw type air compressor is used to supply the air requirement of the transport rig. In this type of compressor, two helicoidal rotors, one with lobes and the other with flutes, turn into each other and the first one turns 50 % quicker than the latter. The inlet ends of the rotors are uncovered and the rotational motion of the rotor elements sucks air to the compartment formed by the male lobe and a female flute. As the rotors turn, the compartment becomes progressively smaller, thereby compressing the entrapped air between the rotors and their housing. After successive compression stages, air leaves at high pressure from the outlet port of the compressor [138] .

The technical data and specifications of the air compressor are given below.

- Production Company : Atlas Copco™
- Model : GA 1108
- Maximum working pressure : 8 bar
- Maximum air flow rate : 1000 Nm3/h
- Voltage/frequency : 380 V/50 Hz
- Maximum rotational speed : 1470 rpm
- Approximate thermal power : 106 kW

- Noise level : 66 dB

3.3 Dryer cum Cooler

The compressed air that goes into the dryer is pre-cooled in an air heat exchanger using its own outgoing air to recover some energy loss. Then, the pre-cooled air is directed to the evaporator where, by direct expansion of the refrigerant fluid, it is cooled down to the dew point. At the dew point temperature, the compressed air has the water condensates and oil, which exceed the corresponding saturation humidity. Therefore, it goes then through a high efficiency condensate separator, which eliminates them through an automatic drain system. The air cooled to its dew point, finally circulates through the air to air heat exchanger in order to pre-cool the compressed air coming in and at the same time acquire the final heating, which makes the compressed air usable for the conveying process [33].

The outlet air from the refrigerant dryer approximately has the following qualities;

- the dew point : +3°C
- relative humidity : 25%

3.4 Control Valves

After the treatment of air in the refrigerant dryer, compressed air is supplied to the main test rig through an array of valves, which controls and distributes the air supply according to the requirements of the experimentations. Figure 3-1 shows a schematic diagram of the air supply routes from the dryer to the main conveying line including blow tank and for the operation of other accessories like mechanical filter at the receiving tank and pneumatically driven valves.

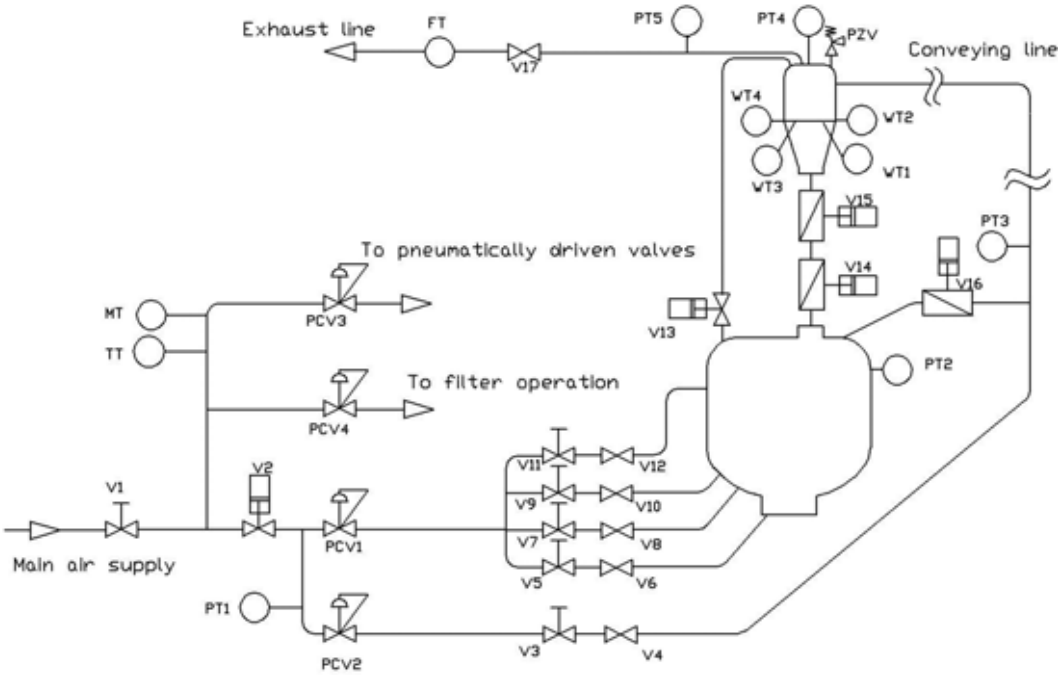

Figure 3-1: A line diagram of the array of valves used to distribute and control the compressed air supply to the test rig.

The valve *V1* is functioning as the main air supply switch and an emergency stop valve of the whole air supply to the pneumatic conveying rig. A thermometer, *TT* and a humidity meter, *MT* are placed on the main air supply to measure the temperature and the humidity of the supply air. Compressed air is supplied to the pneumatically driven valves and mechanical filter at the receiving tank by branching out from the main air supply.

The pressure of supply air to the blow tank is controlled by a pressure control valve, *PCV1*, which is an automatic control valve according a set value at the main control panel. *PCV 2* is used to control the pressure of direct supply air to the conveying pipe and usually termed as 'bypass air/supplementary air'. A bank of manually operated valves is used to control the air supply to the different regions of the blow tank to ensure an evenly distributed fluidization of bulk material. During the experimentations, different conveying air flow rates can be achieved with different combinations of settings of this bank of valves. The method of manipulation of valves during the experiments is given under Section 4.5.

V16 is the main supply valve to the conveying loop and the gas-solid mixture can be introduced to the transport line by opening this. Valve *V4* is used to supply or cut off the bypass air to the pipeline system. To release the pressure of blow tank after each conveying test, valve *V13*, which can be operated from the control panel is used. Two pneumatically driven valves, *V14* and *V15* are placed in between the receiving tank and the blow tank so that the material collected in the receiving tank after each test run can be redirected to the blow tank for the successive test runs.

The weigh cells to monitor the material collection rate at the receiving tank during the experimentations are denoted by *WT* in Figure 3-1. To measure the total air flow rate during the test, a flow transducer depicted by *FT* in Figure 3-1 is located on the exhaust line. *PT* depicts the pressure transducers fixed in various positions on blow tank and air supply circuit as well as at various locations on the pipeline depending on the test requirements.

3.5 Control Room

The operations of most of the valves mentioned under the section 3.4, the on line sampler, the mechanical filter and data acquisition can be controlled by one operator being in side the control room. The control panel is arranged in such a way that the operator can see the air volume flow rate through the pipeline system, the mass collection in the receiving tank, the available pressure in blow tank, positions of the control valves, etc. A personal computer facilitated with the data acquisition software is also available. The variations of the pressures on different locations, volume flow rate, mass accumulation rate can be observed and controlled from the control room. Figure 3-2 shows an inside view of the control room.

Figure 3-2: The arrangement of control panel and PC inside the control room.

3.6 Pressure Transducers

A comparatively large number of pressure transducers have been used in the experimentations to measure the pressure values at different points on the conveying line. The type of pressure transmitter used in this investigation is called Cerabar S and model PMC 731 manufactured by Endress+Hauser™. This type uses a rugged ceramic diaphragm as the sensor and the deflection of the ceramic sensor caused by the process pressure is transmitted to an electrode where the pressure-proportional change in the capacitance is measured. The measuring range is determined by the thickness of the ceramic diaphragm. The change in capacitance is then converted to an analogue current signal by a built-in universal communication protocol and power supply system called HART®. The technical details of the pressure transducers are given below [139];

- Manufacturing Company : Endress+Hauser ™

- Designation : Cerabar S PMC 731, standard
- Pressure range : -1…10 bar
- Minimum pressure : 500 mbar
- Maximum pressure : 40 bar
- Current output : 4…20 mA
- Accuracy : ± 0.1% of set span (0-10 bar)

Before fixing on the conveying line, each pressure transmitter was calibrated to ensure the accuracy of their reading. This was done with the help of a portable pressure calibrator (Manufacturer: Beamex, Model: PC 105). The pressure transducer is supplied with different known pressures by a hand operating pump and then, the readings were compared with actual values of supply pressures. The deviations of readings were recorded as percentage errors with respect to their actual values. To check how the errors are varying with supply pressures, the percentage error values were finally plotted against their corresponding supply pressures. All the calibration curves show almost the same trend and one typical calibration curve is shown in Figure 3-3.

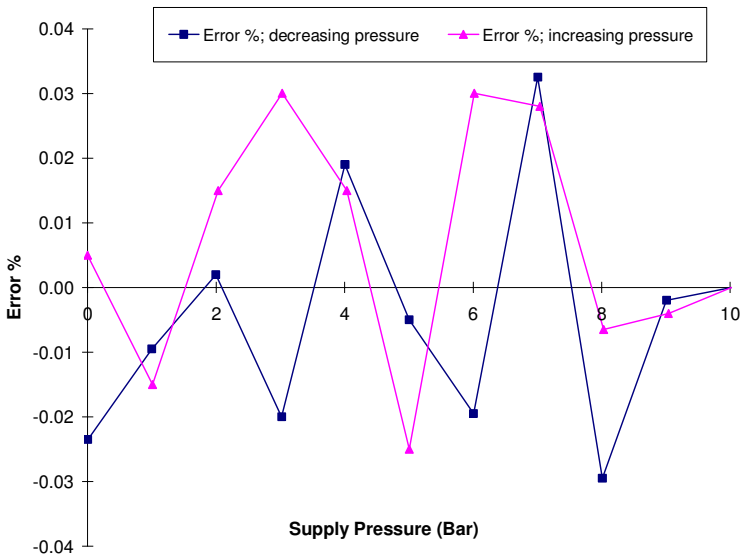

Figure 3-3: Typical calibration curve of pressure transmitter calibration.

According to the calibration curve, the percentage error is well within the accuracy margin given in pressure transmitters' specification.

3.7 Air Flow Meter

To measure the total air flow rate through the conveying line, a vortex flow meter (*FT*) is fixed on the exhaust line as shown in Figure 3-1. The operating principle of the flow meter is based on fluid mechanics phenomenon called 'Vortex Street', which is briefly described in Ref. [140].

The technical specifications of the vortex type flow meter used in the investigation are given below:

- Manufacturing Company : Yokogawa Electric™ (YEWFLOW)
- Model : YF108, Style E
- Capacity : 1000 Nm^3/h
- Allowable max./min flow rates : 1142.2/ 59.4 Nm^3/h
- Output current : 4…20 mA
- Supply voltage : 24 VDC
- Accuracy : ±1.0% of reading (for velocity ≤ 35 m/s)
  ±1.5% of reading (for 35 m/s <velocity ≤ 80 m/s)

3.8 Weigh Cells

During the pneumatic conveying experimentations, it is usually required to measure the solids transport rate. As explained earlier, the receiving tank where the solids are being collected after the transportation is mounted on four load cells as shown in Figure 3-1.

A load cell converts load acting on it into an analogue electrical signal. This conversion is achieved by the physical deformation of strain gauges bonded into four load cell springs made out of hardened, tempered steel.

The technical data of a load cell used in the investigation are given below [141]:

- Manufacturing Company : HBM (Hottinger Baldwin Messtechnik)

- Model : Z6 H3
- Nominal load : 1 t
- Sensitivity (output at nominal load) : 2 mV/V
- Accuracy : ±0.1%
- Nominal range of supply voltage : 0.5…12 V

3.9 Temperature and Humidity Transmitter

Since the performance of most of the conveying particulate materials is influenced by the humidity content of carrier gas, the temperature and humidity of the supply air to the rig are monitored for all the test runs. A combination of a thermometer and a hygrometer is located on the supply air line as shown in Figure 3-1.

The humidity sensor is a capacitor, of which a dielectric material uses a hygroscopic polymer. Because of its high dielectric constant, the water which penetrates into the polymer, as a function of the surrounding humidity, gives a very wide range of capacity between 0 and 100% of relative humidity. The technical details of the humidity transmitter are given below [142].

- Provider : Flow Teknikk AS
- Model : DGT-MARK 5
- Ranges : RH; 5% - 98% and 0C – 60C
- Resolution : 0.1% RH and 0.1C
- Accuracy : ±2% RH and ±0.4C
- Output current : 4…20 mA

3.10 Blow Tank

The blow tank used for the investigation is of $3m^3$ capacity and it can withstand a maximum pressure of 10 bar. It is provided with top discharge and bottom discharge facilities, but for this investigation, only the top discharge configuration was used. Inside the blow tank, there is a porous fluidizing membrane at the bottom portion to fluidise the conveying material when they are inside the blow tank. Four different

independent compressed air streams are provided to ensure an even fluidisation of bulk material in the blow tank. A riser tube was used to feed the transport line. There is a small gap between the fluidizing cloth and the riser tube. To accommodate different pipeline diameters, the riser tube can be changed according to the required conveying configuration. Figure 3-4 shows a view of the blow tank together with the receiving tank on top of it.

Figure 3-4: The blow tank and the receiving tank.

3.11 Pipelines

The test setup consists of a number of pipes of different diameters and lengths. The available pipe sizes are 38.5mm, 54mm, 76mm, 106mm and 125mm. The lengths of the conveying lines can be adjusted according to the requirements of the tests. The total lengths of available pipelines of different diameters are approximately 500m each. The experimental setup is also provided with some vertical pipe sections. Currently, a vertical riser of approximately 8m is possible. The pipelines are laid out in such a way that it is possible to have any combination of horizontal, inclined and vertical sections depending upon requirements.

In addition to the straight pipe sections, number of different bends is also available to use in the conveying loop to meet the objectives of the experiments. Bends of different radii and configurations like standard 90º, blind tee, etc., provides a great flexibility to the experimental setup. A part of the full scale pneumatic conveying pipeline, which lies along the wall of the POSTEC powder laboratory is shown in Figure 3-5.

Figure 3-5: A part of the conveying pipeline.

A schematic diagram, which is common for all pipeline configurations used in this investigation, is shown in Figure 3-6.

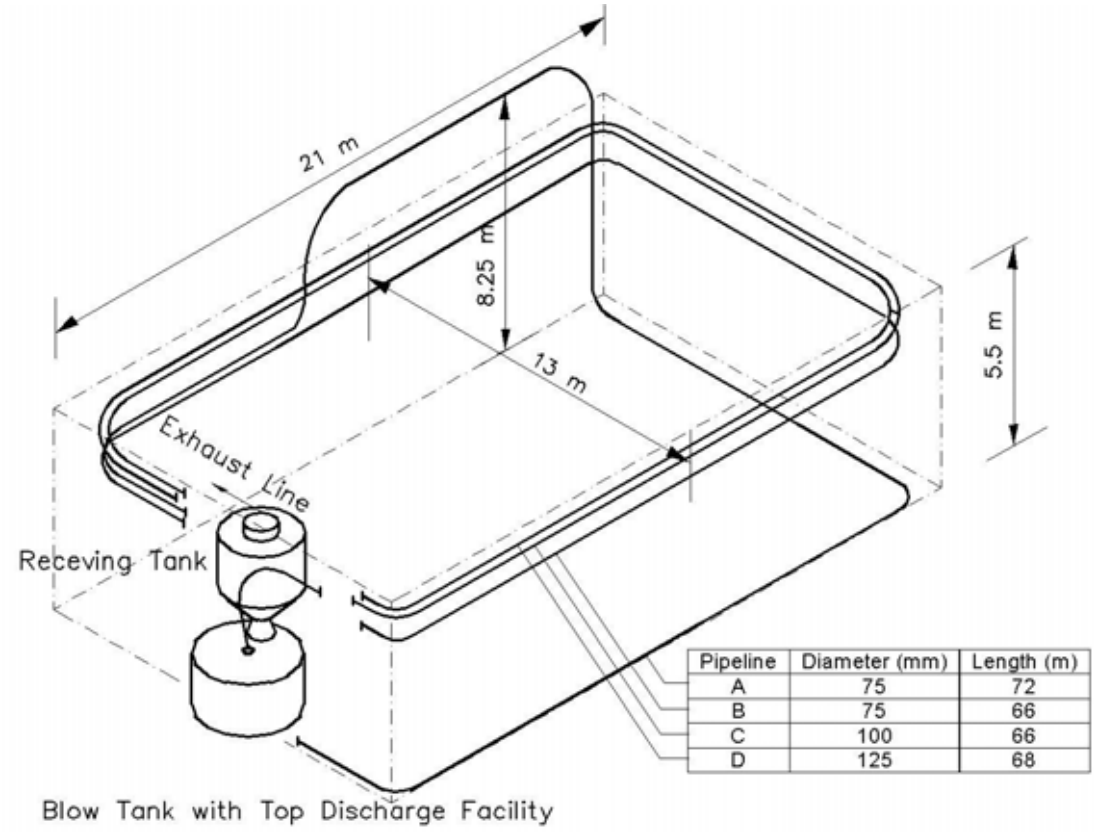

Figure 3-6: Schematic view of the experimental setup.

There are mainly two main configurations of the test pipeline. One starts from the ground level and goes up with a vertical section of approximately 8 m and the other has only horizontal sections in top loop. Combining test loops, longer transport line could be achieved.

3.12 Data Acquisition and Processing

According to previous discussions on different measuring instruments like pressure transmitters, flow meters, etc, it is clear that all these instruments create analogue electrical signals with different magnitudes compatible to their measuring quantities. To convert all these electrical signals into digital forms, an analogue-digital signal conversion (AD) card is used. The AD card used for data acquisition was a universal

screw-terminal board of PCLD-780 model, which has 40 terminal points for two 20-pin flat cable connector ports. Before feeding to the AD card, all signals are conditioned with the help of a signal conditioning circuit, which consists of a parallely connected resistance of 250 Ω to the relevant instrument, as shown in Figure 3-7 [143].

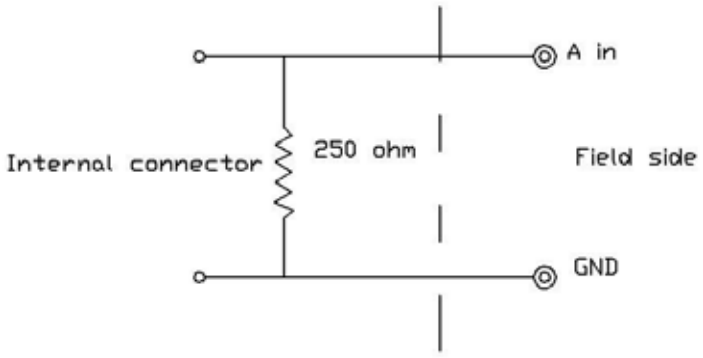

Figure 3-7: Signal conditioning circuit [143].

Then the digital signals corresponding to different qualities and quantities of measurements are fed to a desk top computer with an Intel®, Pentium III microprocessor, for the purpose of monitoring, storing and analysing the various system parameters. A user-friendly software programme written in LabVIEW® is used to handle the data in desired manner. This program facilitates the online visual observations of different signals from various measuring instruments, while the experimentations are being carried out. Under the configuration settings of program for individual testing, user has the liberty to choose the required signals to be shown during the experimentations among the signals that would be stored. On the other hand, user can select the signal to be shown in main display. The rest of the signals are displayed in the secondary frame. A screen shot of signal monitoring mode during a test is shown in Figure 3-8.

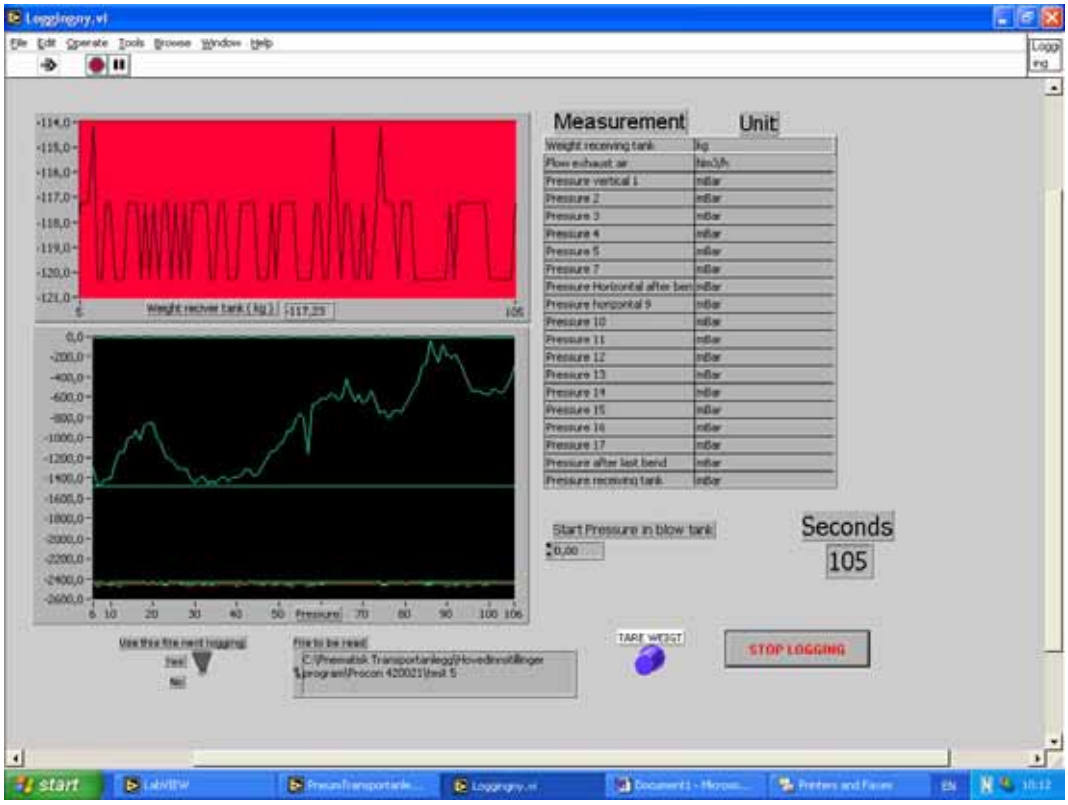

Figure 3-8: A screen shot of signal monitoring mode of the LabVIEW program.

Simultaneously, the data generated during the experiment is logged in the PC for the purpose of future analysis. The program has the facility to retrieve the saved data and analyse them by inspecting their behaviours with respect to the time span. The LabVIEW program is flexible enough to choose the steady conveying regions and specially, to obtain the average values of different quantities during the steady time span. Figure 3-9 shows a screen shot of the LabVIEW program operating in data analysing mode.

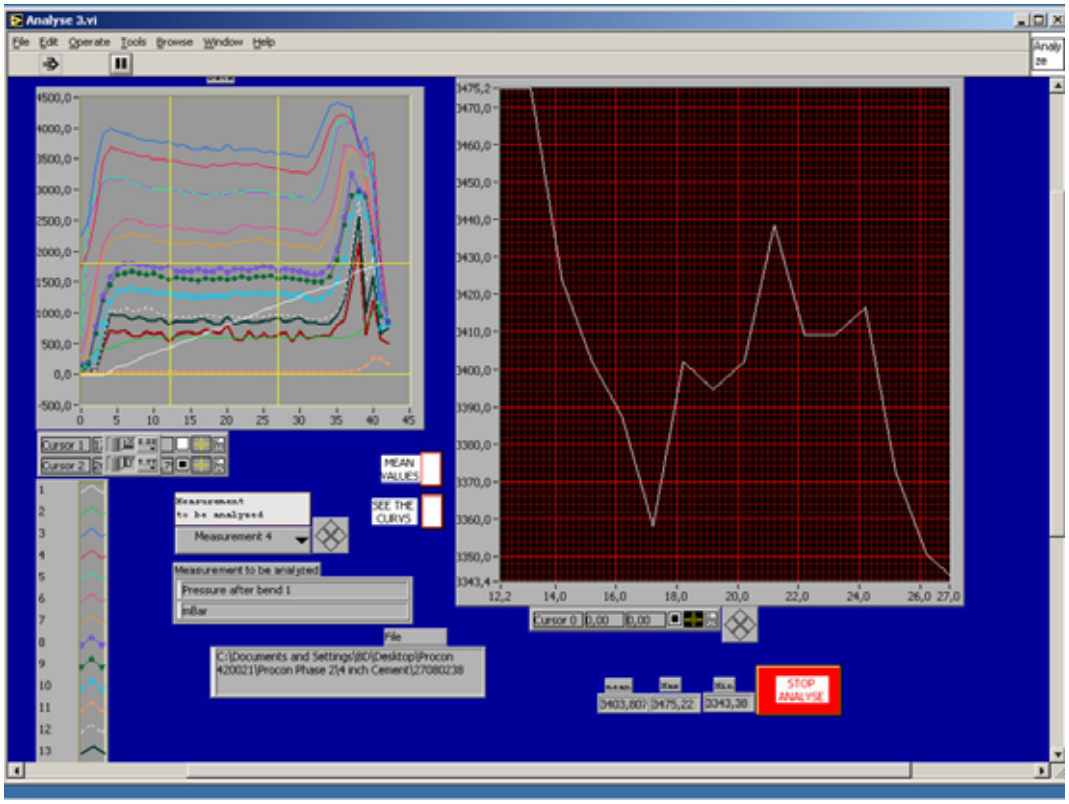

Figure 3-9: A screen shot of data analysing mode of the LabVIEW program.

In addition to the above discussed main facilities, an online sample taker is also available for the purpose of collecting the solid particles in order to monitor the change in particle size distribution, moisture content etc, during the experimentations.

3.13 Particle Size Analyser

The POSTEC laboratory is equipped with a particle size analyzer of the Sympatec Helos® model. The Sympatec Helos® system is based on an optical principle for the fast analysis of particle size distributions in suspensions, emulsions, aerosols and sprays covering a size range from 0.1 to 8750 microns [144]. This technique is termed as laser diffraction, which has lots of applications in size analysis and many other fields as well.

4 PRESSURE DROP DETERMINATION AND SCALE UP TECHNIQUE

4.1 Introduction

As discussed in the Chapter 1 and 2, pneumatic conveying has been identified as one of the efficient methods for transporting bulk particulate materials. To ensure reliable operation of a pneumatic conveying system, at least two parameters have to be determined accurately in its design stage. These are;

- the pressure head required to have a predetermined solid transport rate along a known pipeline length, and
- the optimised air velocity to have a safe transport without pipe blockages and undesirable product degradations/ pipe erosions.

Consequently, plant designers and researchers have been trying to figure out a straight forward, easy but reliable method to determine these parameters using physical and geometrical characteristics of the conveying pipeline and bulk material to be transported in it.

The strong dependence of the possible mode of pneumatic transport on the nature of the material to be conveyed plays a significant role in the design of a pneumatic conveying system. Unfortunately, there exists no reliable technique for characterisation of particulate materials, which can be readily used for the design of pneumatic conveying systems as available in the open literature. Consequently, the system designers are compelled to use experimentation based design strategies in the design of industrial pneumatic conveying installations.

In this approach, a representative sample of product, which is to be conveyed in the industrial plant, is tested in a laboratory pneumatic conveying test rig (pilot plant) over a wide range of operating conditions. The product and airflow rates and resulting pressure drops are measured. Additionally, the minimum conveying conditions and blocking limits are also observed. This approach has the advantage that real test data on the product to be conveyed in the proposed system are used for

the design process. Thus, it gives a high reliability level about the effects of product type. This is very important because it provides useful information on the conveyability of product. On the other hand, in determination of specified conveying limits like minimum conveying velocity, pressure minimum conveying, etc, this approach gives better results.

However, it is not always feasible to use a pilot plant, which is of identical geometry with respect to length, pipe bore, number of bends, types of bends, etc., to that of the required industrial installation. Therefore, it is required to scale up the conveying characteristics based on the pilot plant data, to predict the behaviour of the proposed industrial (full scale) plant, using some experimentally determined factors. Scaling up in terms of pipe line geometry needs to be carried out with respect to conveying distance, pipeline bore and the air supply pressure available. Pipeline material, bend geometry and stepped pipelines are other important parameters that need to be considered. The scaling up of pilot plant data is considered to be the most important stage of the design process, because it provides the required link between laboratory pilot plant apparatus and the full-scale industrial installation. Hence, accuracy and reliability of scaling methodology are vital.

The importance of scaling up methods in pneumatic conveying system designs has paved the way for quite a large number of research studies on the subject. Many researchers have been trying out to establish the mathematical models and relevant conditions of scaling up procedure [16, 22, 25, 42, 95, 97, 101, 145, 146], during the last two decades or so. In Chapter 2, their applicability and limitations were discussed in details. Although several relationships, based on different conditions have been proposed in the literature on scaling concepts, there are still some doubts and uncertainties about their validity. Under this chapter, the theoretical approach to the proposed model and the experimental measurements together with the procedure are discussed in details.

4.2 Theoretical Approach

4.2.1 Background

When the published scaling techniques are concerned, there can be seen two basic approaches:

1. the global testing approach [16, 95, 145]
2. the piecewise approach [22, 25, 42, 101]

In the first approach, the transport pipeline is considered as a whole unit with the different components like bends, vertical sections, etc, without taking into account their discrete positions on the pipeline. In most of the applications of this method, the equivalent length approach is used to address the different components despite their different position either in pilot plant or in projected plant. Alternatively, the individual features of the pipeline are treated separately in the piecewise approach. The different components on the transport line like bends, vertical sections, etc, of the pilot plant are considered separately and different models are formulated using the experimentally measured values of pressure drop across them. Then, in the second stage, those models are used to predict the pipeline pressure drop of the proposed plant, starting from a known flow condition at one end of the pipeline and estimating the pressure drop and change in flow conditions caused by each component and straight length in turn, processing right along the pipeline and thus finishing up with a value for the total pressure drop. These approaches have their own advantages and limitations, which were discussed in the Section 2.9.

The determination of the pressure drop in single-phase flow situation is well established with more reliable mathematical models such as French engineer Henry Darcy's [44]. There is a quite long history of Darcy's equation, which is also defined with different terminologies like Darcy-Weisbach's equation, Fanning's theory, etc. An excellent survey on the historical development of Darcy-Weisbach equation and the contributions made by other research workers and scientists to establish it as a universally acceptable theory, could be seen in Ref. [147] and [148].

However, Darcy's equation could be represented in the simplest way as shown in Equation (4.1).

$$\Delta P = 4\frac{f\rho_a v^2 L}{2D} \tag{4.1}$$

In later developments, some researchers tried to modify Darcy's theory to suit multiphase flow situations. The applications of such attempts could also be seen in research publications on pneumatic conveying. Some researchers [16, 22, 25, 42, 46, 95] have used this equation as a basis for models, which could be used to calculate the total pipeline pressure drop of pneumatic conveying systems. Most of them have tried to split the effect of friction caused by the gas-solid mixture into two components as air friction and solid contribution to it. This approach leads to create two hypothetical pressure drop components namely; air only pressure drop and pressure drop due to the presence of solid particles, as shown in equation (4.2), (4.3) and (4.4).

$$\Delta p_T = \Delta p_a + \Delta p_s \tag{4.2}$$

$$\Delta p_a = \lambda_a \rho_a v^2 \frac{L}{2D} \tag{4.3}$$

$$\Delta p_s = \mu\lambda_s \rho_a v^2 \frac{L}{2D} \tag{4.4}$$

In this approach, calculation of air only pressure drop using the Equation (4.3) gives quite a straightforward methodology, which is similar to the conventional single phase flow situation, where as some additional terms and modifications are introduced in case of solid pressure drop. One of the modifications is to replace the air friction factor with its counterpart relevant to solid particles, namely; solid friction factor (λ_s), as shown in the Equation (4.4). But, unfortunately, this concept of 'solid friction factor' has not yet been established as a universally accepted parameter and thus a lot of divergent opinions could be found in literature [22, 26, 41, 43, 53, 77, 78, 92, 149]. Under Chapter 2, Table 2.2 shows some of the available correlations for determining the solid friction factor. One can clearly see how they vary from one another. On the other hand, some models [41, 43, 77, 92] even require solid velocity, which would be rather difficult to determine in dense phase conveying

conditions. Hence, it is clear that the traditional way of considering the gas-solid mixture as two distinguished components is difficult to deal with and there exists a necessity for a scaling up technique, which is simple and straight forward and could be used for both dilute and dense phase.

4.2.2 Formulation of New Model

During the present investigation, it was examined whether the well-known Darcy's equation could be modified for the two phase flow, which is experienced in pneumatic conveying systems by considering the gas-solid as a mixture having its own flow characteristics, instead of recognizing the two components separately. Basically, the pressure drop coefficient; K, the solid suspension density; ρ_{sus} and the entry velocity; v_{entry} were introduced to equation (4.1), instead of $4f$, ρ_a and v respectively. The total pressure drop of the conveying line was addressed in discrete way by considering horizontal and vertical straight pipe sections, bends and other pipe accessories like valves separately.

Equation (4.1) is thus modified for the pressure drop of a straight pipe section as shown below;

$$\Delta p_{st} = \frac{1}{2} K_{st} \rho_{sus} v_{entry}^2 \frac{\Delta L}{D} \tag{4.5}$$

The equation (4.5) is directly applicable for the straight pipe sections irrespective of whether they are vertical or horizontal. For the pressure drop due to bends, the equation in a slightly different form has been used, which is similar in form to that used by some other researches [96, 97];

$$\Delta p_b = \frac{1}{2} K_b \rho_{sus} v_{entry}^2 \tag{4.6}$$

It should be highlighted that all v_{entry} value is the true gas velocity at the entry section of the concerned pipe section or pipe component.

The suspension density (ρ_{sus}) can be defined as the mixture density when a short pipe element is considered. As an equation, it can be presented in the following way.

$$\rho_{sus} = \frac{m_s + m_a}{V_s + V_a} \tag{4.7}$$

The concept of suspension density becomes more rational as the considered pipe section becomes shorter. Practically, it is difficult to measure the pressure difference between two points that are not at least one metre apart. Thus, the maximum allowable distance between the two consecutive pressure points to have a reliable K has been defined as two metres.

4.3 Material Data

Basically, five different bulk materials including one with five different qualities with respect to the mean particle diameter have been used for the testing. Under this section, brief descriptions of test materials together with their major properties are given.

4.3.1 Barytes

The quality of barytes used in the experiments was oil drilling grade barytes whose chemical formula is $BaSO_4$. Barytes is the most commonly used weighting agent in oil and natural gas drilling. In this process, barytes is crushed and mixed with water and other materials. It is then pumped into the drill hole. The weight of this mixture counteracts the force of the oil and gas when it is released from the ground. This allows the oil and gas rig operators to prevent the explosive release of the oil and gas from the ground. In natural form, barytes is of white colour and roughly uneven fractural (prismatic) in shape. The general shape of a barytes particle in an artist's view is shown in Figure 4-1.

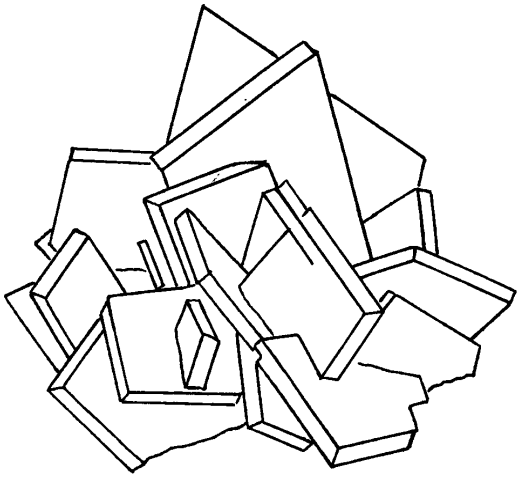

Figure 4-1: The shape of a barytes particle in an artist's view [150].

4.3.2 Bentonite

Bentonite is used in preparation of drilling mud and it is mainly used as circulation mud in rotary system of drilling for oil. The main purpose of bentonite is to lubricate and cool the rotary cutting bits, carry away rock cutting fragments and to act as a seal against the escape of gas from the bore hole and to improve and prevent the hole from blowing out. Another function of such bentonite based fluids is to condition the wall of the drill hole to prevent caving. The chemical formula of bentonite is generally given as $Al_2O_34SiO_2H_2O$ and bentonite particles are of light cream in colour.

4.3.3 Cement

The tested quality of cement is called as oil well cement because of it's usage in the oil and gas industry. It has the characteristics of high sulphate resistance and is usually used for the cementing operations related in oil drilling sites. Cementing is a very important phase of the well construction plan. Usually, an oil well is created by drilling a hole (5 to 30 inches wide) into the earth with an oil rig turning a drill bit. After the hole is drilled, a metal pipe called 'casing' is cemented into the hole. During

this process the casing is reciprocated or rotated to allow the scratches to work to remove excess wall cake to give the cement a better bond.

4.3.4 Ilmenite

This is also related to the oil well drilling. Ilmenite ($FeTiO_3$ –Iron Titanium Oxide) is also used as a weighting agent instead of barytes. In natural form ilmenite is of colour Iron black or black and conchoidal in shape as shown in Figure 4-2.

Figure 4-2: An ilmenite particle under microscope [151].

4.3.5 Alumina

Alumina has a chemical formula of Al_2O_3 and is a compound of aluminium and oxygen. Alumina qualities used for the testing are used in the aluminium industry. Usually, alumina is refined from the chemical breakdown of bauxite and it is the starting material for the extraction of aluminium by means of the electrolytic reduction process. Aluminium oxide, commonly referred to as alumina, possesses strong ionic inter-atomic bonding giving rise to its desirable material characteristics. It can exist in several crystalline phases, which all revert to the most stable hexagonal

alpha phase at elevated temperatures. Alumina is white when pure and usually exists in spherical or hexagonal crystals.

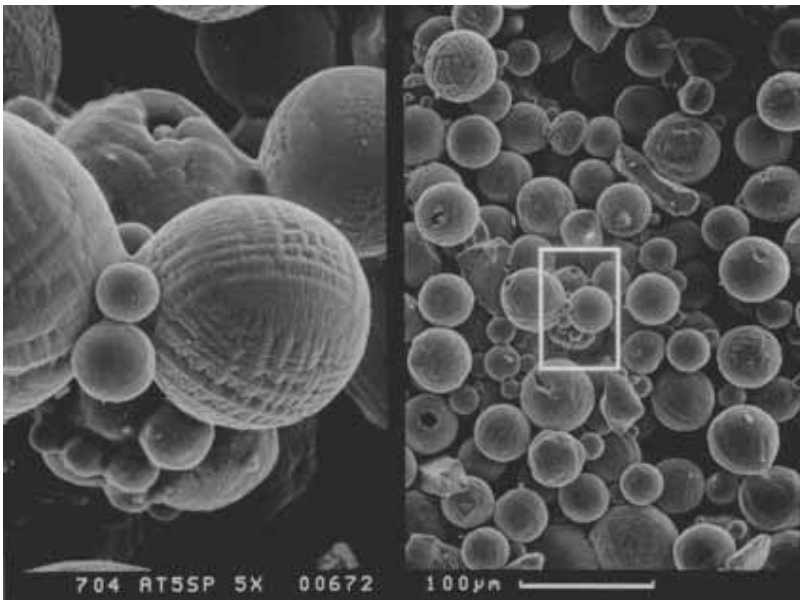

Figure 4-3: Alumina particles under microscope [152].

The five different qualities of alumina were prepared by mixing known quantities of fines and coarse fractions according to pre-determined volume fractions. Naturally, this procedure produced five different qualities of alumina with different mean particle sizes and their size distribution curves are given in Appendices.

In general, as their characteristic properties, particle densities and mean particle diameters of the test bulk materials are given in Table 4-1. Additionally, the Figure 4-4 shows the positions of the test materials in the well-known Geldart diagram [102], which has been referred by many researches to classify the powdered materials according their characteristic behaviours in fluidized beds, thus possible distinguished transport modes in pneumatic conveying systems.

Table 4-1: Data for test material.

Test Material	Mean Particle Size (μm)	Particle Density (kg/m^3)
Barytes	12.0	4200
Bentonite	25	2500
Cement	15.5	3100
Ilmenite	9.5	4600
Alumina 1	59.2	2800
Alumina 2	72.0	2800
Alumina 3	79.3	2800
Alumina 4	86.7	2800
Alumina 5	90.5	2800

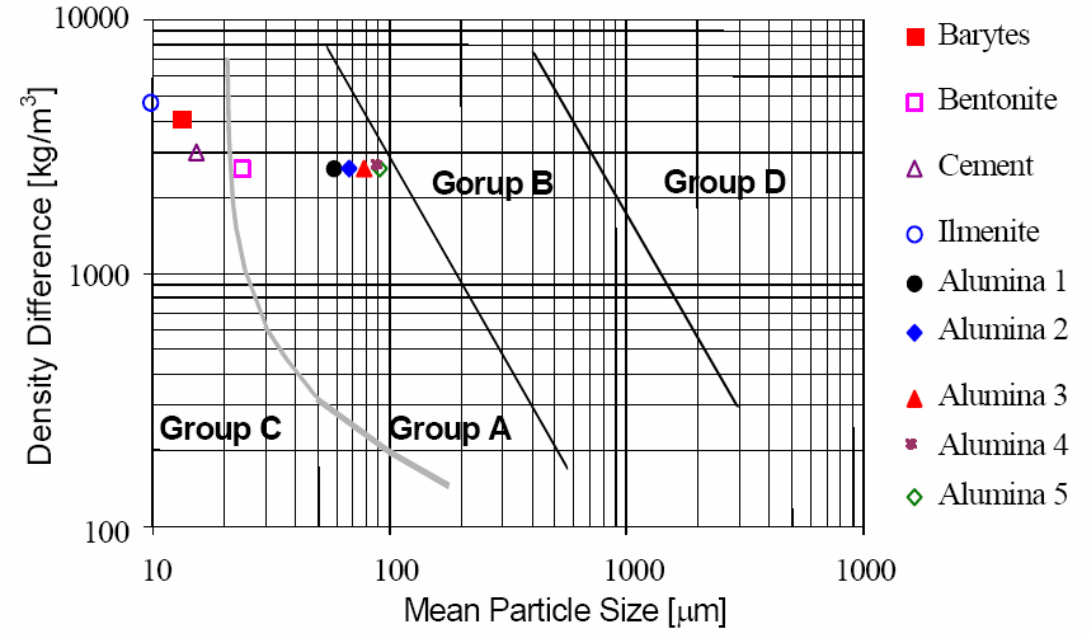

Figure 4-4: The locations of the test materials on Geldart's classification diagram [102].

4.4 Experimental Set-up

The test set-up mainly consists of a blow tank, feeding system, four different pipeline loops and a gas solid separation system consisting of a cyclone type receiving tank. The main features and different accessories of the experimental setup were described in details under Chapter 3. Under this section, the special components used to meet the requirements of the experiments are discussed.

For the series of tests, four different pipeline configurations as shown in Figure 3-6 have been used. In case of barytes, cement, bentonite and ilmenite conveying, the pipeline configurations labelled as A, B, C and D were used while pipelines A and B were connected together to form a single continuous loop for alumina conveying that is named as pipeline E.

In addition to the general features of the test setup described under Chapter 3, number of butterfly type valves was set on pipelines as per one on each, since it is a very common accessory of most of the industrial plants.

A special attention was given for mounting the pressure transmitters in order to isolate the effect of each of the pipeline accessories. In case of bends, two pressure transmitters were fixed just before and after the bend. Similarly, the pressure drop effects caused by other components like valves, flexible hoses, etc, were isolated by properly fixing the pressure transducers just before and after the concerned component.

As described under the Section 4.2.2, the suspension density has to be defined for comparatively short pipe sections having a maximum length of 2 m. In order to isolate the effects of other pipe components on the straight pipe sections, the pressure tappings on straight sections, for both vertical and horizontal pipes, were always set as far away as possible from bends, valves, etc.

According to the above discussed conditions, the pressure transducers were placed on the conveying lines as shown in Figure 4-5. It has to be noted that only the general positions of the pressure transducers are shown in Figure 4-5, while the pressure transducers were placed before and after all the bends and other special pipe

elements on individual pipelines to isolate their pressure drop effects in actual arrangement. The details of the distinct pipelines are given in the Table 4-2.

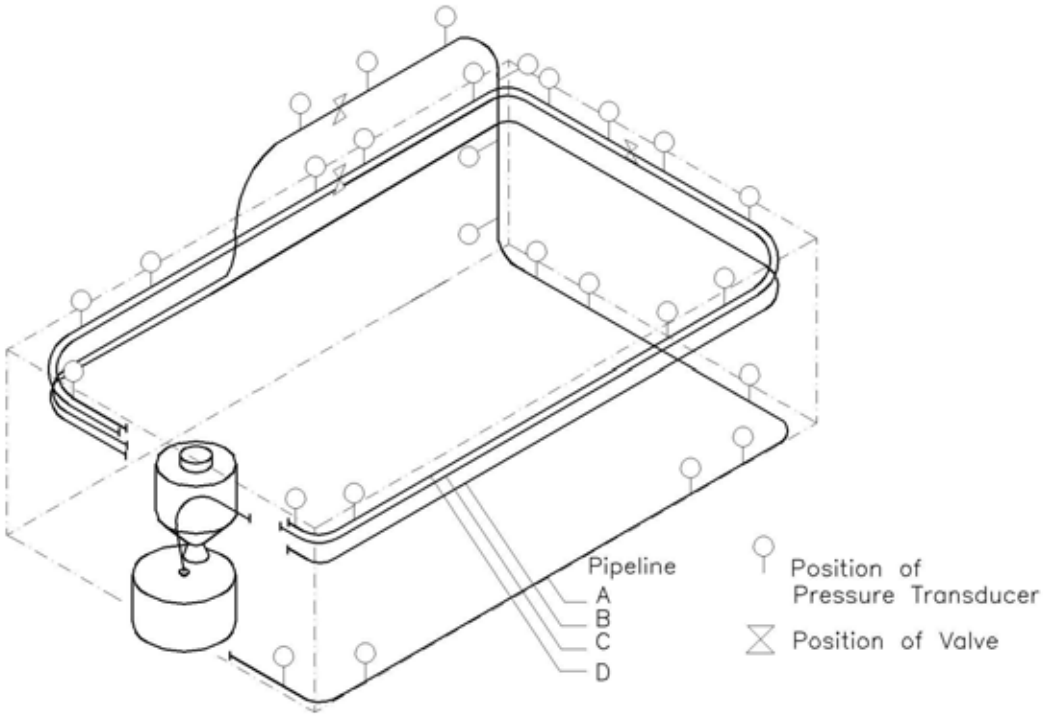

Figure 4-5: Schematic diagram of the test set-up showing the position of pressure transducers and valve.

Table 4-2: Details of the pipelines.

Pipeline	Length (m)		Diameter (mm)	Number of Bends
	Horizontal	Vertical		
A	64	8	75	5
B	66	-	75	4
C	66	-	100	4
D	68	-	125	4
E (=A+B)	130	8	75	9

4.5 Experimental Procedure

For the investigation, five different materials including one with five different qualities (Table 4-1) have been used to test with five different pipeline configurations (Figure 4-5 and Table 4-2). For each material, the number of test runs has been carried out by varying the start pressure (set pressure of blow tank) and the volumetric flow rate of conveying air. The test procedures adopted for the different bulk materials and pipeline configurations were similar to each other. The whole experimental procedure can be described by dividing it basically into three main sections; i.e., pre-test arrangements, testing procedure and post-test analysis. Setting up of test rig, programming of data acquisition software, etc, come under the pre-test arrangements, while post-test analysis comprises of test data averaging and relevant analysis. The general procedure of experiments is explained in detail in the following section while the special conditions for particular materials are indicated in case by case basis.

For each test, approximately 0.5 - 1.0 m^3 of bulk material was used for testing. Before testing in the pneumatic conveying rig, a representative sample of each material was tested in the laboratory for the size distribution. During testing samples were collected from time to time using an online sampler and size analysis was carried out in order to check if there were any size degradation during transportation.

The first step of testing was filling up the blow tank with the test material. Before pressurising the blow tank, the pressure control valve on the main air supply line (PCV1 in Figure 3-1) was regulated by setting the pre-determined pressure value on the pressure control unit. Generally, the pre-set pressure values were ranging from 2 bar to 5.5 bar in 0.5 bar intervals. For higher pipe sizes (e.g. 125 mm), this value has to be lowered to 1.75 bar. By opening the main air supply valve, the blow tank was allowed to pressurise gradually. In this stage, the valves on the fluidising air supply side (V6, V8, V10 and V12 in Figure 3-1) were partially opened to make sure of even fluidisation.

After the pressure in the blow tank reached to the desired value, the conveying of material was started by opening the main supply valve on conveying line (V16 in

Figure 3-1) and the data acquisition programme was simultaneously started. The recording of all signals were inspected during the test run. During the comparatively long conveying cycles, the settings of the fluidisation air supply valves were changed in order to get different air volume flow rate values within one cycle. In case of smaller pipe sizes, it could be possible to obtain 3-4 different stable conveying regions with respect to the air volume flow rate, depending on the cycle time. The samples were taken using online sampler at regular intervals of approximately 15 runs and were tested in the laboratory for particle size distribution in order to check if any size degradation had occurred.

The end of the conveying cycle could be determined by checking the amount of material collected in the receiving tank that was digitally displayed on an LCD panel in main control panel. Then, the main supply valve of material was closed and the data logging programme was also stopped at the same time. The pipeline was then supplied some additional compressed air through the by-pass line to clean any residual materials deposited inside the pipeline. After that, the blow tank was let to depressurise through the ventilation line provided in between the blow and the receiving tank. Then, the materials were taken down to the blow tank for the next test run.

The different signals recorded during the test were then analysed and the stable conveying regions were identified by inspecting the signal curves with respect to time scale. One typical set of signal curves are shown in Figure 4-6.

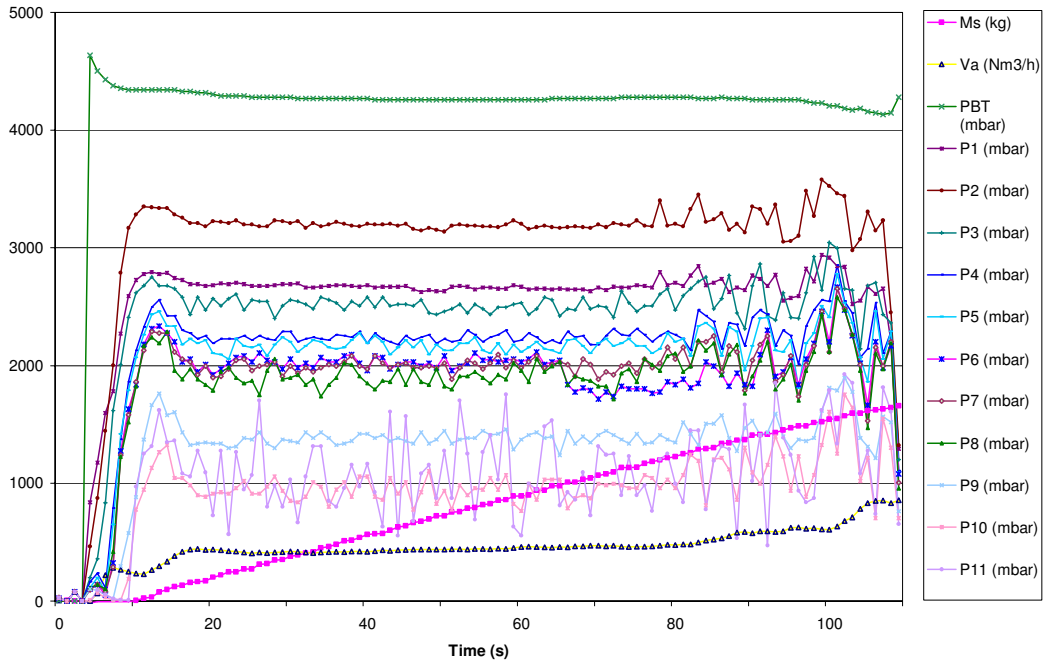

Figure 4-6: Typical curves of signals recorded during a test run (Material: barytes, Pipeline: A).

The stable conveying regions were chosen by considering the behaviour of the air volume flow rate curve. It was noticed that when the air volume flow rate remains stable during a considerably long time interval, the pressure signals also show a quite stable behaviour. The data analysis software package was programmed so that all the signals could be displayed in one set of axes as shown in Figure 4-6 and the time interval during, which the stable conveying conditions prevailed, could be isolated. Time averaged values of different signals were also recorded with the help of the data analysis software package. Basically, the set pressure of blow tank, the air volume flow rate, solid flow rate and pressure values at discrete positions of the conveying line were recorded as the output results of the experiments.

This general procedure was followed for all bulk materials to generate the conveying data. While performing the tests, especial effort was made to cover the whole conveying range of a particular bulk material. Different conveying modes, i.e., from dilute phase to dense phase, could be achieved by controlling the air volume flow rate values. This could be done by adjusting the air supply valves to the blow tank

manually. From an intermediate value, the air flow rate was increased gradually to very high values where very dilute phase conveying prevailed. On the other hand, the air flow was gradually decreased until it reached to the total pipeline blockage. This procedure was repeated until it generated a large number of data points, which were satisfactorily enough to generate the pneumatic conveying characteristic curves. The conveying characteristics curves in terms of air volume flow rate, solid mass flow rate and pipeline pressure drop were generated at the same time as the tests proceeded.

4.6 Experimental Results

The results of the experimentations are discussed in a few stages. Initially, the conveying characteristics curves of different materials will be discussed. The special behaviours of different materials were analysed next and the results relevant to the scaling model will be discussed at the end.

4.6.1 Pneumatic Conveying Characteristics Curves

Under the Section 1.8, the concept and the importance of pneumatic conveying characteristics of a bulk material in a system design was explained in details. With the test results, pneumatic conveying characteristics curves were developed for the various combinations of different materials and different pipeline configurations. In this section, some of those characteristics curves, which represent the all test materials and pipeline configurations, are presented and their special features are discussed. The rest of the conveying characteristics are given in Appendices. The nomenclatures indicated in the Figures are as depicted in Figure 3-6.

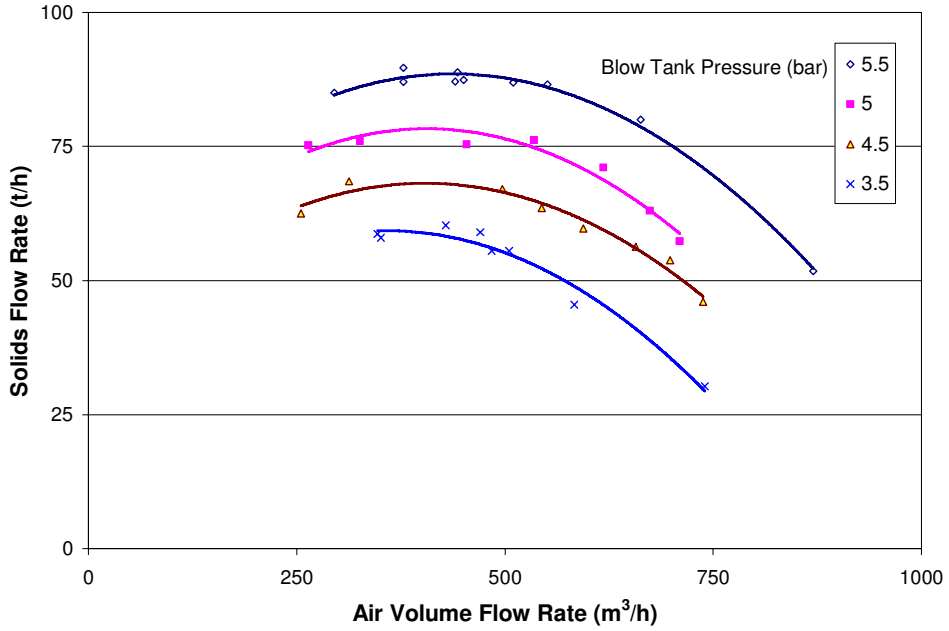

Figure 4-7: Pneumatic conveying characteristics for bentonite conveying in pipeline A.

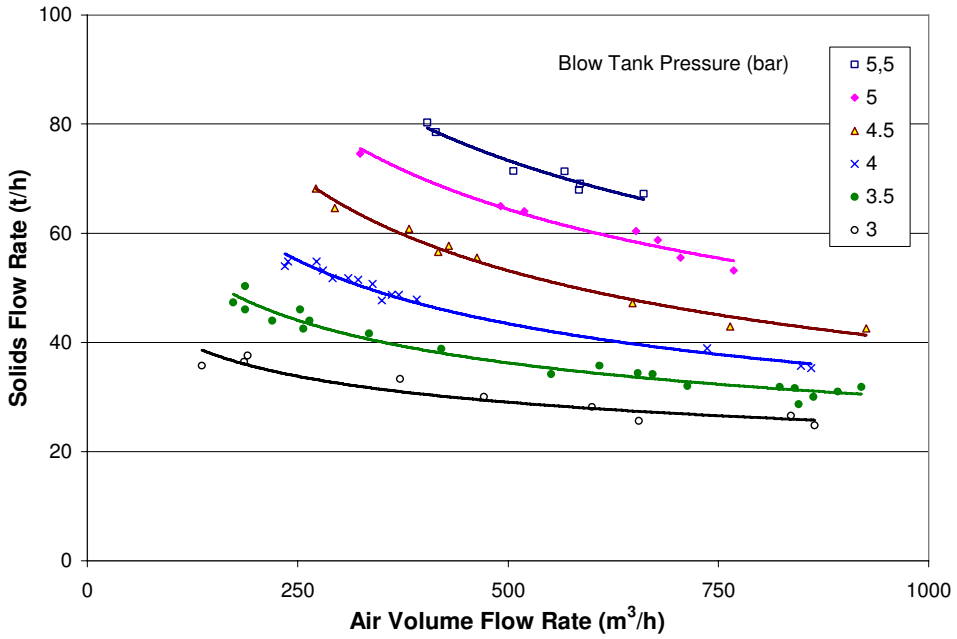

Figure 4-8: Pneumatic conveying characteristics for barytes conveying in pipeline B.

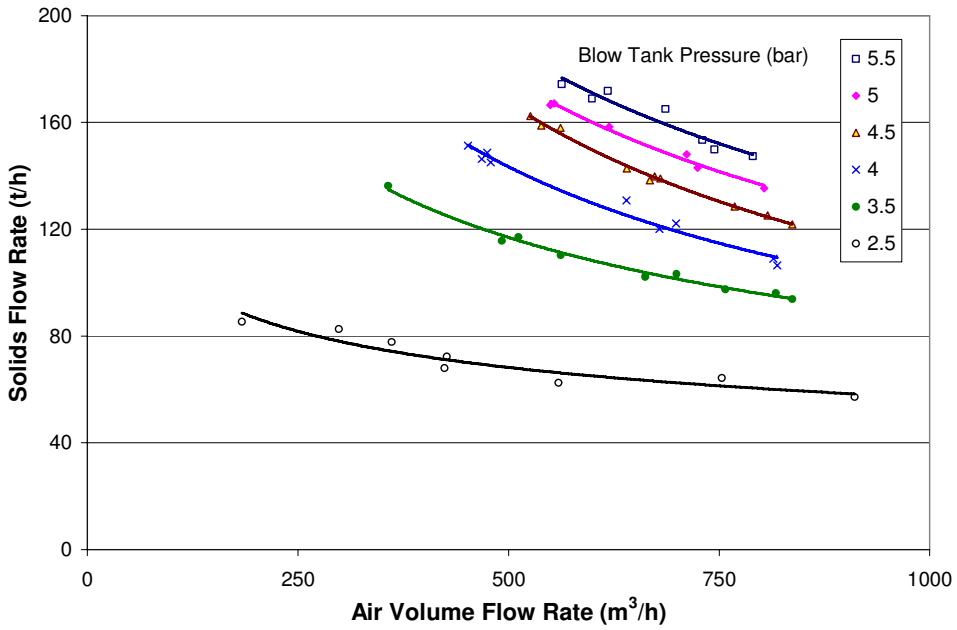

Figure 4-9: Pneumatic conveying characteristics for cement conveying in pipeline C.

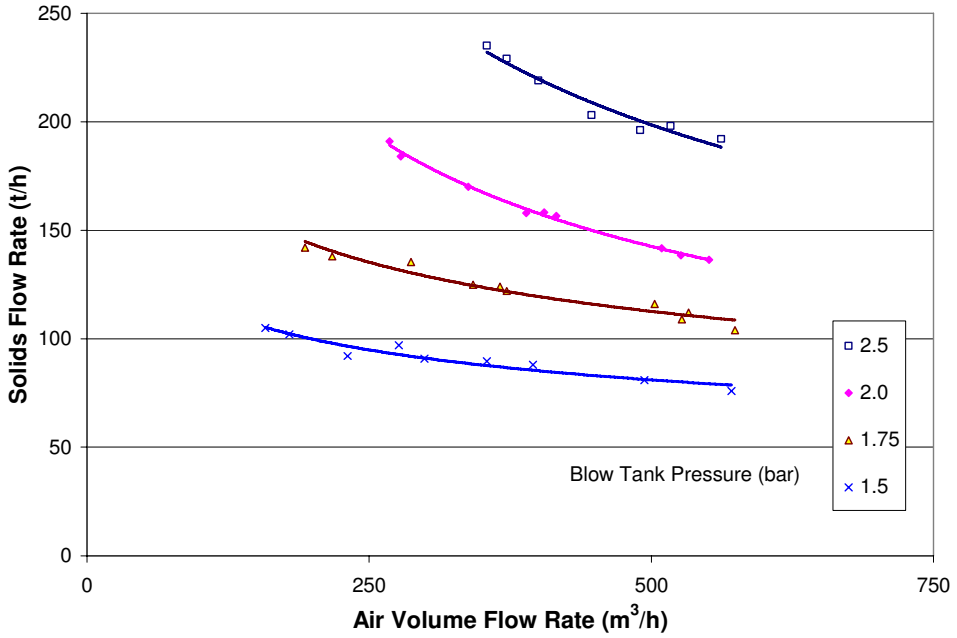

Figure 4-10: Pneumatic conveying characteristics for ilmenite conveying in pipeline D.

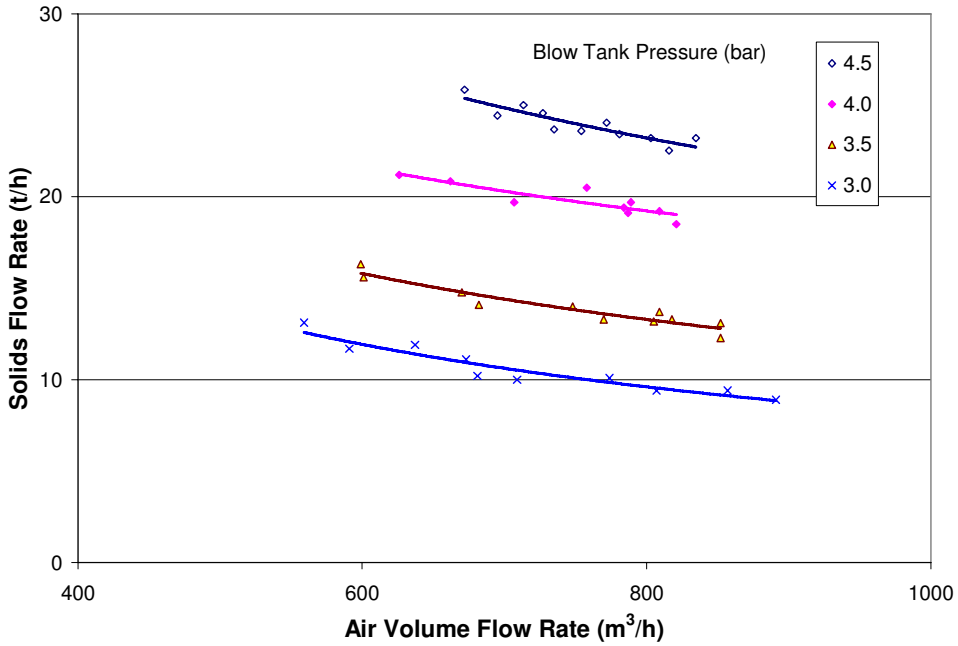

Figure 4-11: Pneumatic conveying characteristics for alumina 4 conveying in pipeline E.

As discussed in Section 1.8, some boundaries of pneumatic conveying characteristic curves are determined by the geometrical properties of the conveying line and the capacity of the prime mover (in this case, the compressor). The right hand side boundary, which depends on the air flow rate capacity of the compressor, is one example. According to the ratings of the compressor, 1000 m^3/h was the maximum value of air volume flow rate, which has been the right hand side boundary of the characteristics curves, in most of the cases. Although it was bit difficult to obtain this value for higher pipe sizes such as 100 mm and 125 mm, the maximum air volume flow rate values were close to 1000 m^3/h for the test with 75 mm line.

For all bulk materials, the blow tank pressure could be increased up to 5.5 bar for 75 mm line, even though that was not possible for 100 mm and 125 mm lines. Specially, in case of 125 mm line, the blow tank set pressure could not be increased beyond 4 bar except for barytes. For ilmenite, the maximum blow tank pressure for 125 mm line had to limit at 2.5 bar, since the whole loop was experiencing high vibrations in the attempts of higher pressure values. In case of bigger pipe sizes, the conveying cycle time was so short that the stable conveying conditions were difficult to obtain.

4.6.2 Loading and Conveying Velocities

Table 4-3**:** Maximum and minimum solids loading ratios and inlet velocities.

Material	Pipeline	Solids Loading Ratio		Inlet Velocity of Pipeline (m/s)	
		Max.	Min.	Max.	Min.
Baryte	A	277.8	19.2	12.2	2.1
	B	222.8	27.7	12.6	2.4
	C	455.9	68.3	6.3	1.1
	D	339.3	121.3	4.2	2.0
Cement	A	274.1	38.0	10.3	2.3
	B	252.2	24.4	12.2	2.7
	C	379.1	51.2	9.0	1.8
	D	389.5	130.5	4.5	1.7
Ilmenite	B	455.1	25.2	12.6	2.3
	C	520.1	47.1	8.0	1.6
	D	600.6	108.6	5.0	1.4
Bentonite	A	235.2	33.4	10.1	2.7
Alumina 1	E	50.9	11.8	14.0	6.9
Alumina 2	E	50.1	12.7	13.3	5.8
Alumina 3	E	39.9	7.9	16.1	5.7
Alumina 4	E	31.4	8.2	13.7	7.5
Alumina 5	E	23.7	8.2	13.3	8.3

Table 4-3 shows the maximum and minimum values of solids loading ratios and conveying velocities achieved for different combinations of conveying bulk material and pipeline configurations. Accordingly, the maximum loading ratios of all materials except alumina were in the range of 200-600, while that of alumina qualities were in range of 30-50. Another feature was the comparatively high values of conveying velocity processed by alumina. In most of the cases, barytes, cement, bentonite and ilmenite could convey with the minimum velocity of 2 m/s approximately, whereas the minimum velocity was approximately 7 m/s for alumina. The clear difference of the conveying figures in terms of loadings and velocities can be explained with the help of conveying distances. As shown in Figure 4-5 and Table 4-2, it is clear that conveying distance of barytes, cement, bentonite and ilmenite was shorter than that of alumina. The conveying distance of alumina qualities was approximately double of the other cases. According to findings of many researchers [6, 16, 20, 27], there is a reciprocal relationship between the solid mass flow rate and the conveying distance. This may be one of the reasons for the differences in solid loadings and velocities revealed in the testing.

4.7 Variations of 'K' Curves

After obtaining the required data, the pressure drop values across the vertical and horizontal straight sections and bends were considered and relevant *K* values were calculated according to the conditions discussed under Section 4.2.2. Under this sub-section, the procedure followed to obtain the *K* curves and the individual characteristic features of *K* curves of different materials and of different pipeline components are discussed in detail. The effect of the orientation of pipe section is also discussed with respect to the different conveying material. At the end, the characteristic features of combined *K* curves are analysed.

4.7.1 Method of 'K' Calculation

As discussed under the Section 4.2.2, the K values for different pipe sections were calculated with the help of Equations (4.5) and (4.6). The experimental pressure

readings of pressure transducers fixed before and after the concerned section were used to determine the pressure drop of the same. To calculate the air velocity and volume flow rate at the entry section, the effect of compressibility had to be considered. The true values of above parameters were determined by adjusting the experimentally measured air volume flow rate according to the true pressure value prevailing at the entrance of the pipe section. In the same line, the mass flow rate of air was also determined. The time averaged value of solids mass flow rate, during which the stable conveying conditions were prevailed was used to determine the mass and volume flow rate of solids within the concerned section. Using Equation (4.7), the suspension densities of considered sections were calculated. Finally, the value of K was calculated using Equation (4.5) or Equation (4.6). Figure 4-12 shows a general procedure adopted to calculate K for different section as a flow chart.

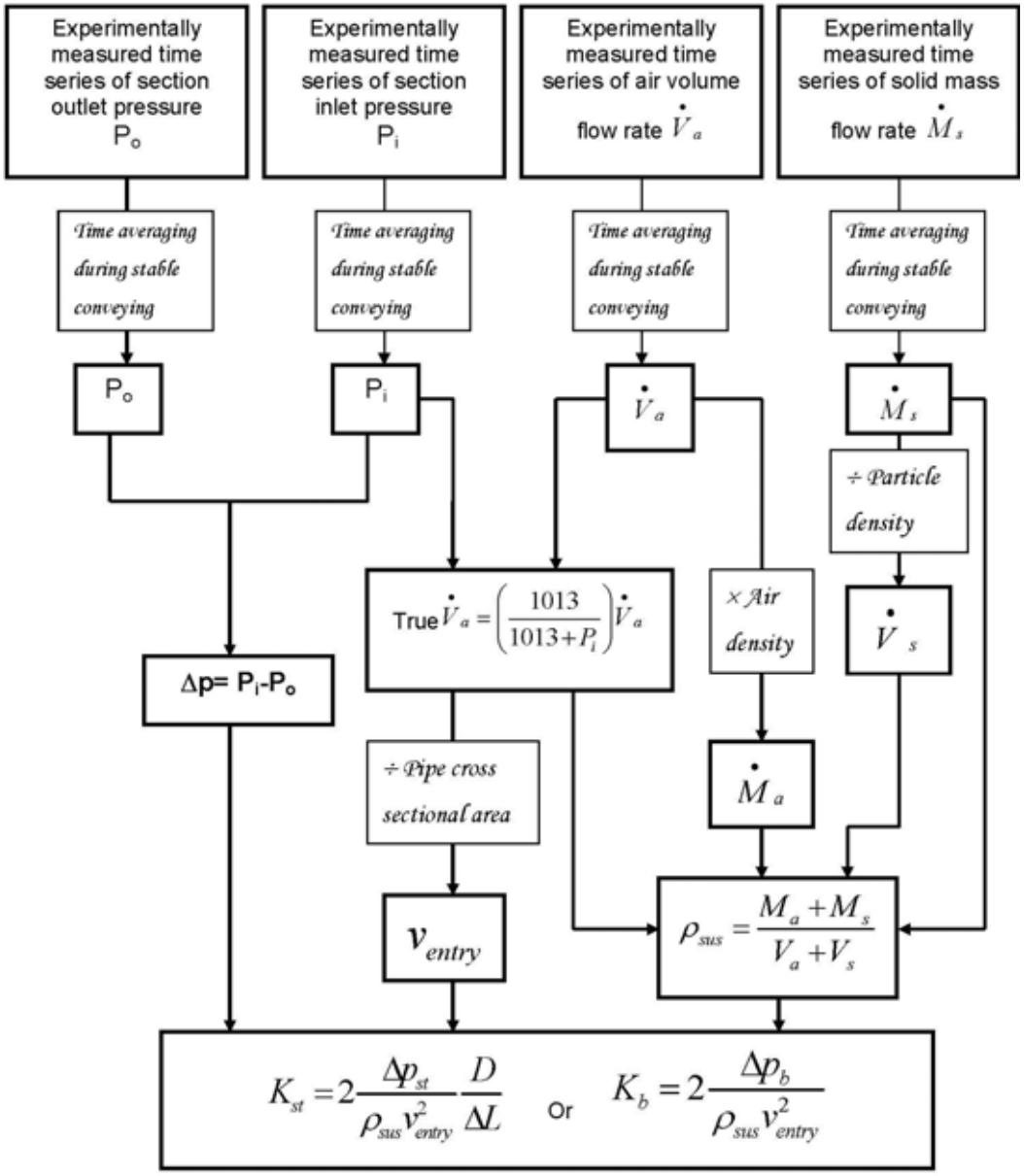

Figure 4-12: Flow chart of the general *K* calculation procedure.

4.7.2 'K' vs. V^2_{entry} Curves

After calculating the *K* values for different features like horizontal and vertical straight sections, bends and valves, those were then plotted against the square values of the entry velocities of each individual component. As described in Section 4.2.2, the *K* values show a good proportional relationship with the square value of the entry

velocity of the relevant features. In this section, the behaviour of K vs. V_{entry}^2 curves for different pipe components are discussed in details.

4.7.2.1 Straight Pipe Sections (Horizontal and Vertical)

Figure 4-13 to Figure 4-15 show the behaviour of K vs. V_{entry}^2 curves of straight pipe sections for barytes conveying in different pipeline configurations. These curves were generated for the experimental data using the tool of best fitted power curve available in MS Excel® software package.

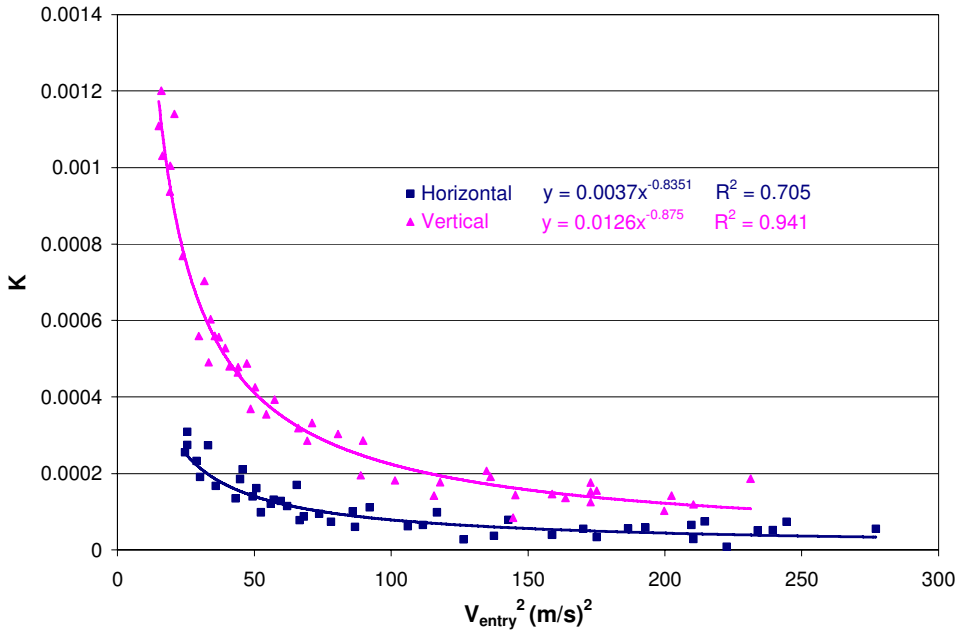

Figure 4-13: K vs. V_{entry}^2 for straight pipe sections for barytes conveying in pipeline A and B.

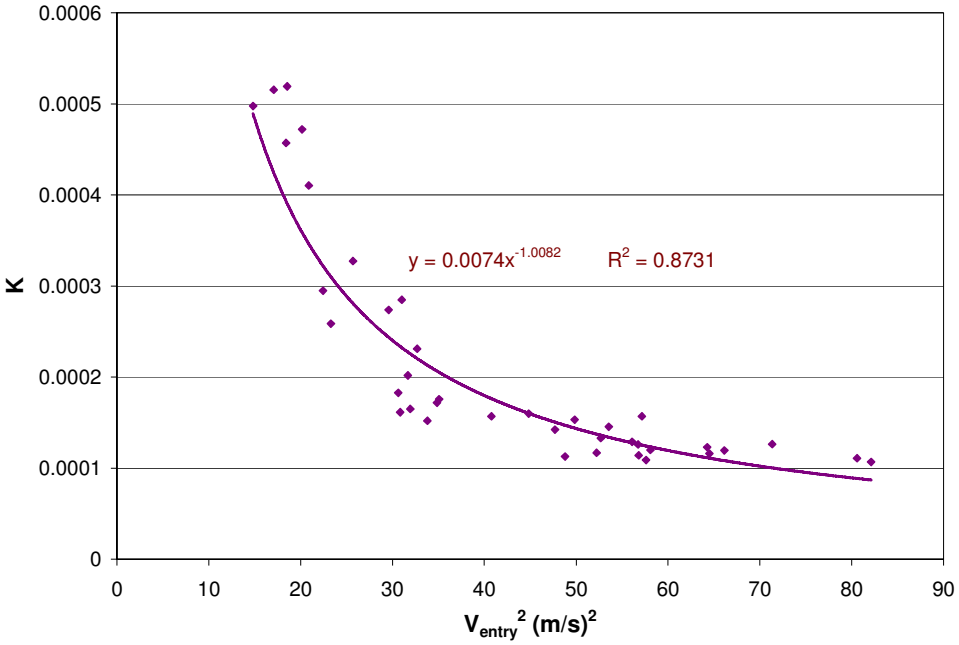

Figure 4-14: K vs. V_{entry}^{2} for straight pipe sections for barytes conveying in pipeline C (horizontal).

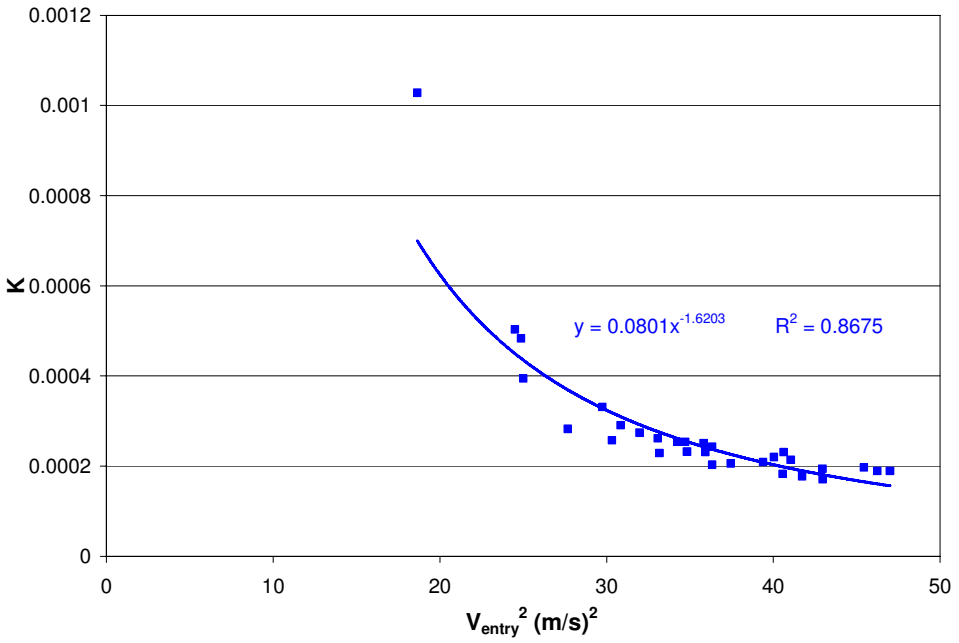

Figure 4-15: K vs. V_{entry}^{2} for straight pipe sections for barytes conveying in pipeline D (horizontal).

As one can see, K data of vertical section is only available in 75 mm pipeline ('A'), while all pipe diameters have the data relevant to horizontal sections. It was clear that all K vs. V_{entry}^2 curves describe similar trends, which show power-law relationship of K with the square value of entry velocity. In the low velocity regions, K values were very high and as the entry velocity increases, K value decreases gradually. It seemed that K reached a constant value in the high velocity regions. Both the horizontal and vertical sections showed similar trends, although the K values for the vertical section were always higher than those for horizontal sections as shown in Figure 4-13.

The general appearance of the K curves gives some information about the behaviour of the gas solid mixture within the pipeline system. In low velocity conveying, which is usually termed as dense phase flow, there a strong dependence of K on the conveying velocity. On the contrary, K becomes independent of conveying velocity in dilute phase conveying conditions.

In the similar lines, the curves of K vs. V_{entry}^2 curves for straight pipe sections were generated for conveying of the other materials also. They showed quite similar behaviours as in the case of barytes.

When all the four curves of K vs. V_{entry}^2 for barytes for straight horizontal pipe sections were drawn for four different pipe configurations representing data from three different pipe dimensions, it was found that all the four curves got superimposed on each other resulting in one curve only as shown in Figure 4-16.

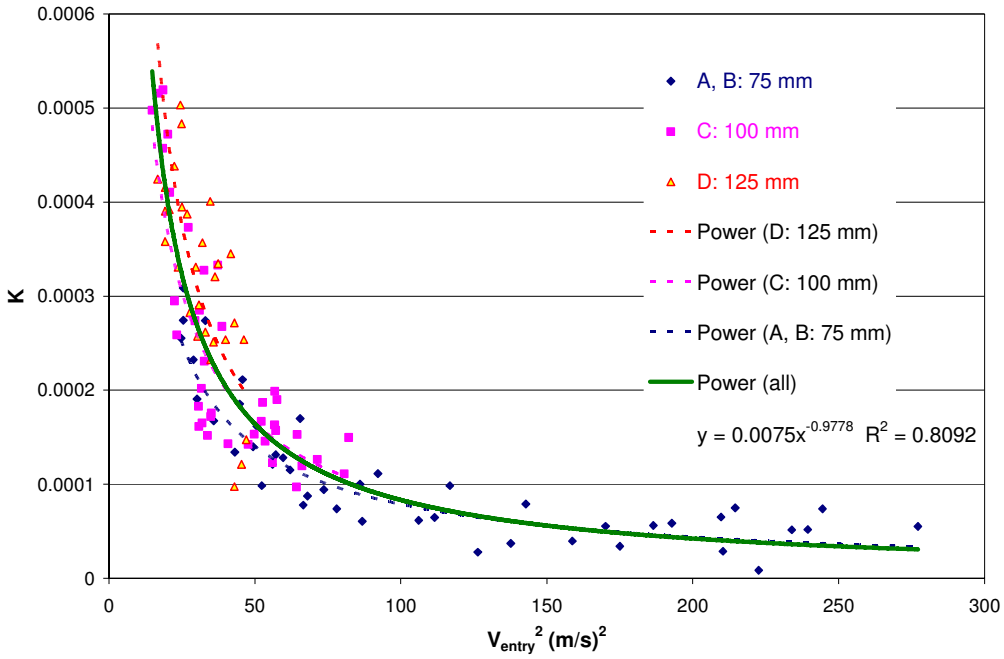

Figure 4-16: K vs. V_{entry}^{2} for straight pipe sections for barytes conveying in all (A, B, C and D) pipeline configurations.

The finding of overlapping of K curves for different pipe diameters was further substantiated by the results obtained for other materials as well. The combined K curves for the straight pipe section for cement and ilmenite conveying are presented in Figure 4-17 and Figure 4-18 respectively.

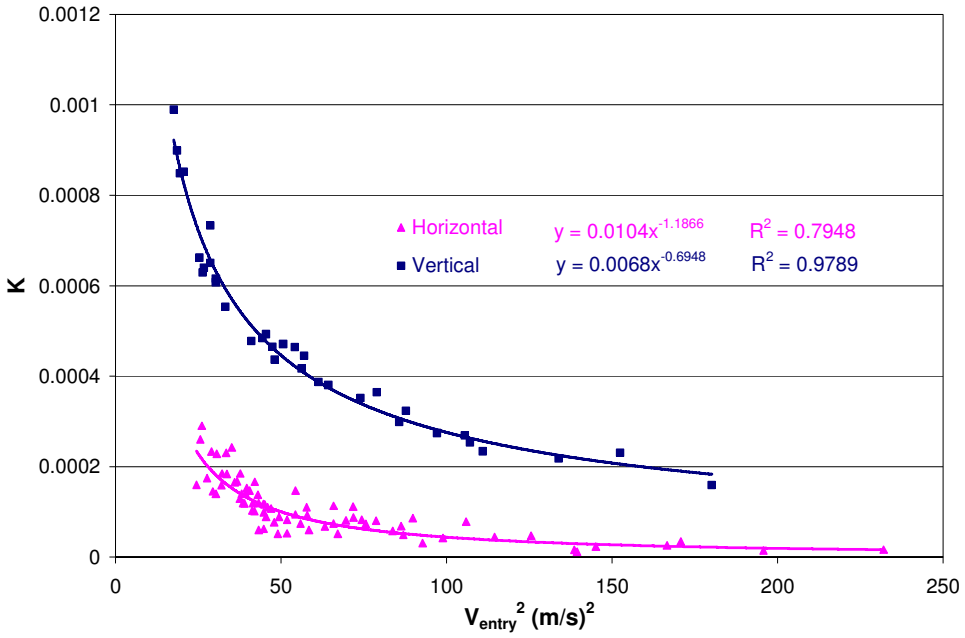

Figure 4-17: K vs. V_{entry}^2 for straight pipe sections for cement conveying in all (A, B, C and D) pipeline configurations

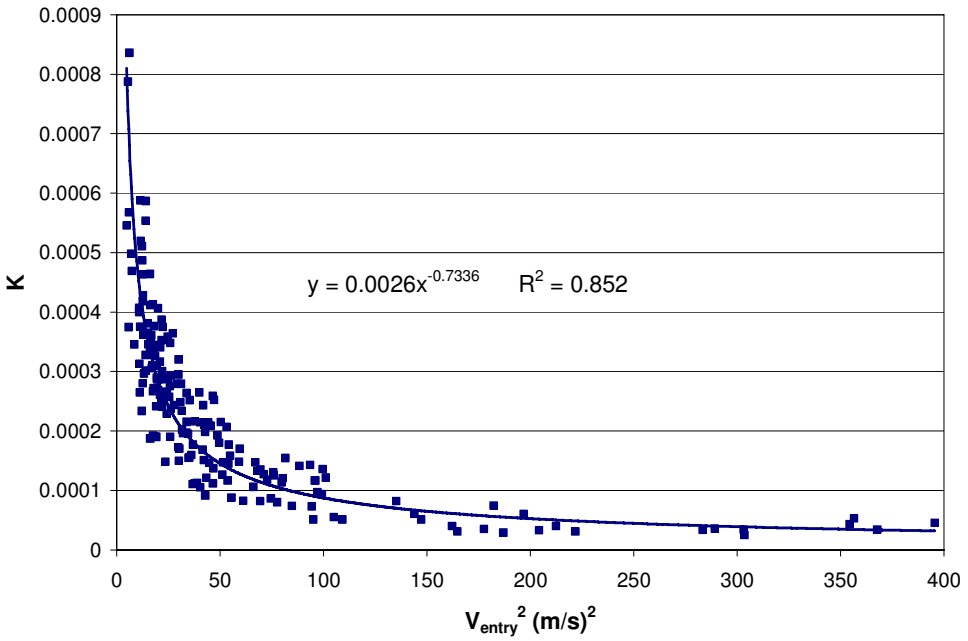

Figure 4-18: K vs. V_{entry}^2 for straight pipe sections for ilmenite conveying in all (B, C and D) pipeline configuration.

The Figure 4-17 and Figure 4-18 clearly proves that the functional relationship of '*K*' with V_{entry}^2 is independent of pipe diameter for straight pipe sections.

4.7.2.2 Bends and Valves

In the same line as with straight pipe sections, first the *K* curves were generated and plotted against the square value of their individual entry velocities. They also show the trend of power-law relationship of *K* with increasing entry velocity value similar to the case of straight pipe sections. When the attempts were made to put the *K* vs. V_{entry}^2 curves of a specific component for different pipe diameters within a same set of axes, it was found that they also overlapped each other nicely and made a single curve as in straight pipe sections. This could be clearly seen in the Figure 4-19 and Figure 4-20 that are given as two representative curves for all bends and valves for all conveying bulk materials.

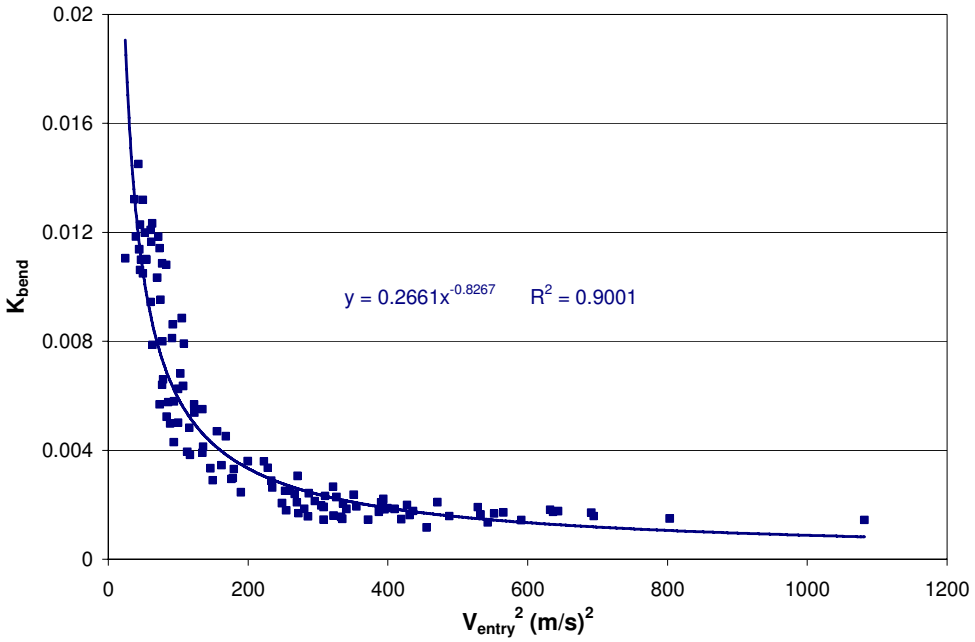

Figure 4-19: K_{bend} vs. V_{entry}^2 of 5D bend for cement conveying in all (B, C and D) pipeline configuration.

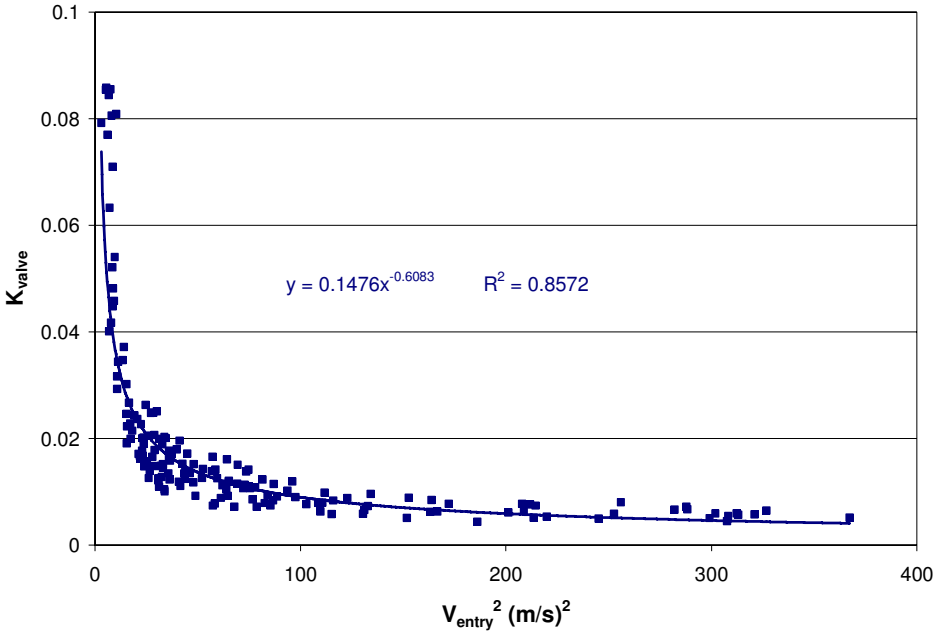

Figure 4-20: K_{valve} vs. V_{entry}^2 for butterfly valve for barytes conveying in all (B, C and D) pipeline configuration.

From the above figures, it could be seen that the behaviour of K_{valve} vs. V_{entry}^2 of all other pipe sections is also independent of pipe diameter for a particular conveying material as in the case of straight pipe sections.

4.7.3 The Effect of Particle Size on 'K'

The results, which have been discussed so far, were dealt with materials with one particular mean particle size. Among the test material, alumina possessed a special place, since it was in 5 different qualities in terms of mean particle size as shown in Table 4-1. Consequently, the experimental data of different alumina qualities could be used to determine the effect of mean particle size to the behaviour of *K* values. Under this section, the influence of mean particle size is discussed in terms of horizontal and vertical straight pipe sections in detail.

4.7.3.1 Horizontal Pipe Sections

For one particular alumina quality, the K_{valve} vs. V_{entry}^2 curve showed the similar trend as in other materials discussed under the Section 4.7.2. When 'K' values were plotted against V_{entry}^2 for the horizontal straight pipe section for all the five qualities of alumina within one set of axes, the curves for different qualities could be distinguished each other as shown Figure 4-21.

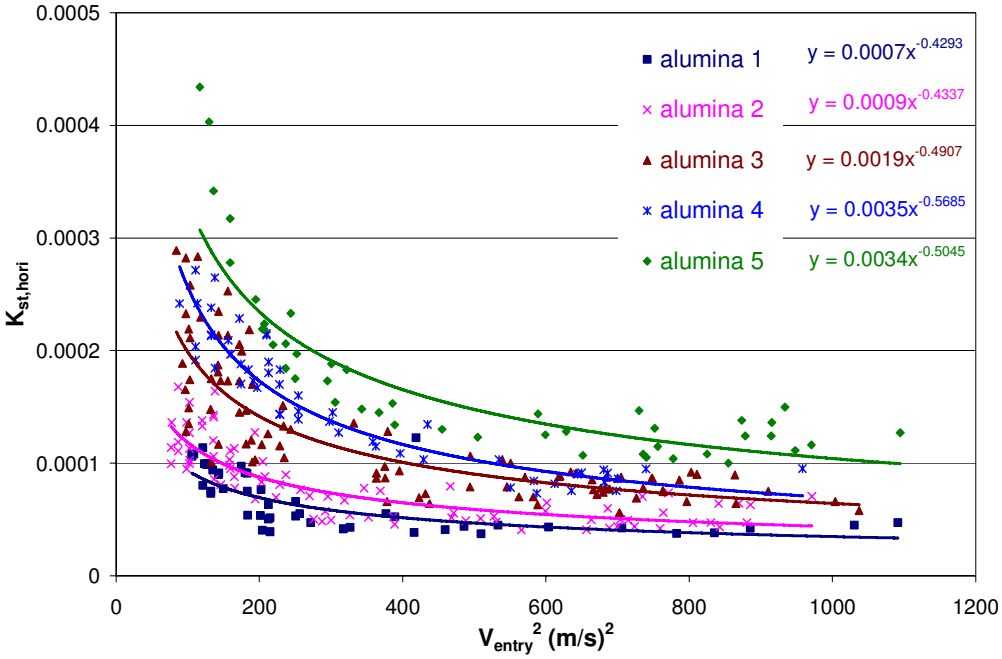

Figure 4-21: $K_{st,hori}$ vs. V_{entry}^2 for horizontal sections of all alumina qualities conveying in pipeline E.

It is evident that each almunina quality behaves as an individual quality of material as they all have separate identifiable 'K' curves. Further, it is also seen that for a given value of entry velocity, the value of 'K' increases with increase in the mean particle size (d_{50}). This behaviour is in agreement with the finding of Goder et al. [108] whose conclusion was that finer particles have higher transport capacity than the coarser counterparts for a particular pressure drop. Hyder et al. [100] also reported that particle size gets larger, the pressure losses along straight sections of pipeline increase.

4.7.3.2 Vertical pipe Section

In contrarily to the horizontal pipe sections, when the '*K*' values for all the five qualities of alumina were plotted against V_{entry}^2 for the vertical straight section, all the data overlapped on each other and resulted in a single '*K*' curve as shown in Figure 4-22.

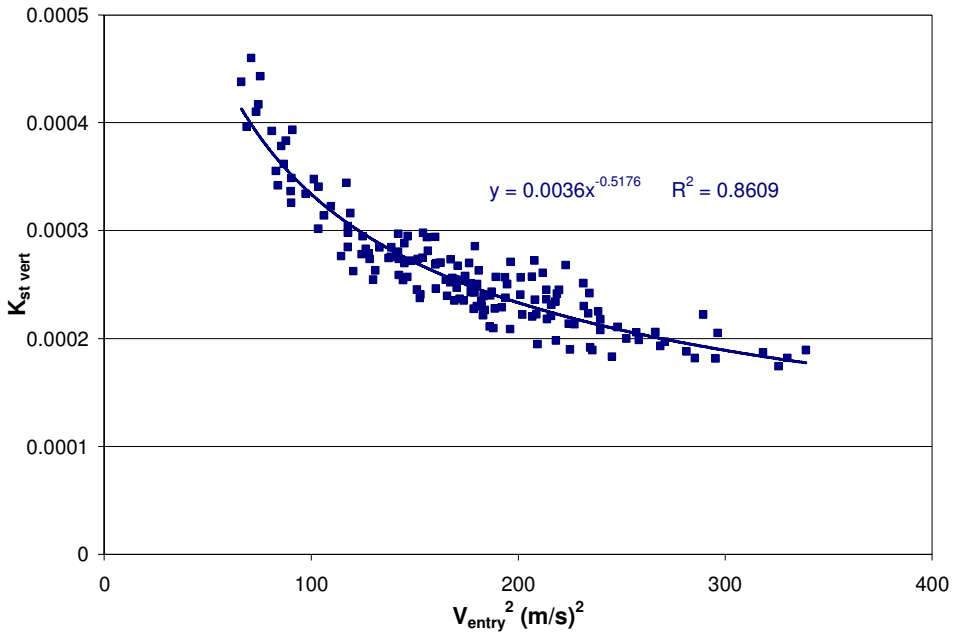

Figure 4-22: $K_{st,vert}$ vs. V_{entry}^2 for vertical sections of all alumina qualities conveying in pipeline E.

This indicates that the '*K*' curve for the vertical section is independent of the particle size distribution also for a given material having a given particle density. This is presumably due to the different conveying mechanism in vertical section as compared to that in the horizontal section.

4.7.4 Summary of Findings

- There is a strong relationship between *K* value, which can be calculated using Equation (4.5) for straight pipe sections and Equation (4.6) for other pipe sections like bends, valves, etc, and the entry velocity of the concerned section

- The behaviour of '*K*' vs. V_{entry}^2 curves for straight section and other pipe components shows a common trend of power-law relationship with increasing entry velocity for all conveying bulk materials tested. The *K* factor could be explained as a parameter, which is very sensitive to the entry section velocity in dense phase conveying. In dilute phase region, the gas-solid flow becomes an approximation to a single phase flow with less influence from solid particles, thus the K behaves like the friction factor for conveying gas.
- The relationship between *K* and V_{entry}^2 is independent of pipe diameter for all pipe sections.
- The behaviour of '*K*' vs. V_{entry}^2 for horizontal pipe sections is dependent on the mean particle size of the conveying material, while the same for vertical pipe sections is independent of particle size. This finding facilitates to avoid the elaborate tests for different qualities (in terms of mean particle size) of a given material with vertical sections.

4.8 Model Validation

Having thus established the functional relationship of *K* and $V_{entry,}$ the next stage was to validate the model with the help of available experimental data. For this purpose, the *K* vs. V_{entry}^2 curves generated by combining the results of all pipe sizes were used to define the relationship between *K* value and the entry velocity of the concerned component. Then, these relationships were used to calculate the pressure drop values across individual features. Finally the calculated pressure values were compared with the experimental values. Under this section, calculation procedure, results and comparison of validation are discussed in detail.

4.8.1 Calculation Procedure of Validation

In the calculation procedure, the whole pipeline was considered as a virtual combination of short horizontal and vertical pipe sections, individual bends and other pipe components like valves. As discussed under the theoretical consideration, the concept of suspension density is best suited for rather short pipe sections. Hence any

straight horizontal or vertical pipe section was considered to be made up of virtual small sections each of 1m length.

The calculation procedure began with the available experimental conditions at the starting point of conveying loop. At the starting point, the pressure available just outside the blow tank was taken as the reference point and calculation proceeded along the pipeline by calculating the pressure drop of each individual section of the conveying loop. The exit pressure condition of the concerned section is updated by adding the calculated pressure drop to the start pressure value. The pressure available at the exit of one section was used as the entry condition to the next section. However, the bends, valves etc were considered as individual units and pressure losses incurred with them were calculated individually. This procedure can briefly be represented as shown in Figure 4-23. This calculation procedure was continued by updating the pressure value of the entry section of the consecutive section, from starting point of the conveying line until the receiving tank.

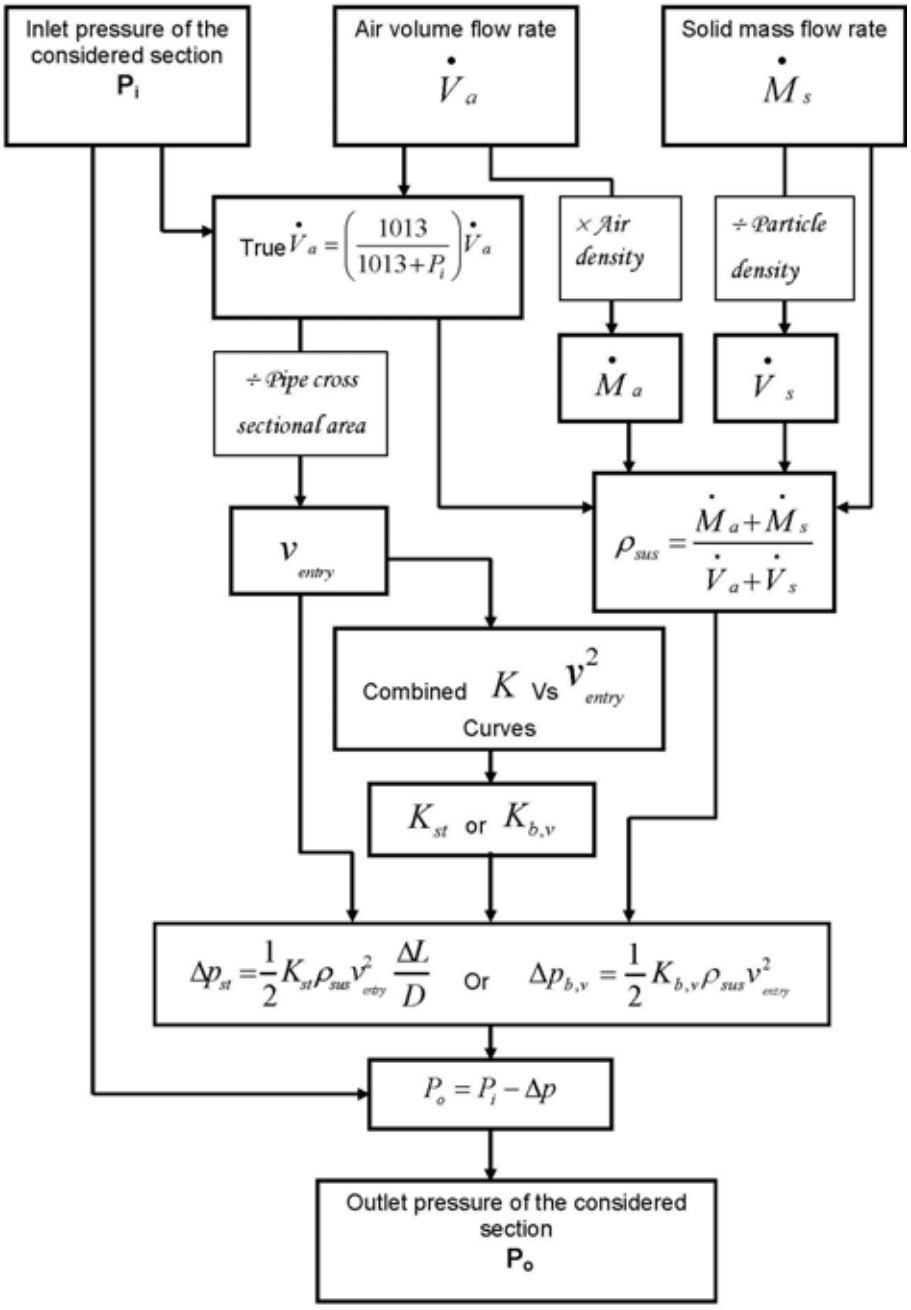

Figure 4-23: Flow chart diagram of the pressure drop calculation of a pipe section.

4.8.2 Validation Results

The procedure described in the above section naturally generated a large number of pressure values at different locations on the conveying loop for any given test condition. These calculated pressure values on the discrete positions were then

compared with the corresponding experimental pressure measurements at the corresponding locations on the conveying line. This was basically done in two modes; graphical comparison and analytical comparison.

4.8.2.1 Graphical Comparison

In this method, the calculated pressure values were plotted against the corresponding experimental measurements, to get a quantitative idea about the prediction capability of the proposed models. In this presentation, diagonal line that represents $y = x$ relationship, gives the perfect prediction, while the ordinate difference between the data point and $y = x$ line depicts the degree of under-estimation or over-estimation. In addition, the scatter of the data points around the ideal prediction line shows the biasness of the model towards to over- estimation or under-estimation of pressure drop value. Figure 4-24 and Figure 4-25 show such comparisons for bentonite and cement respectively.

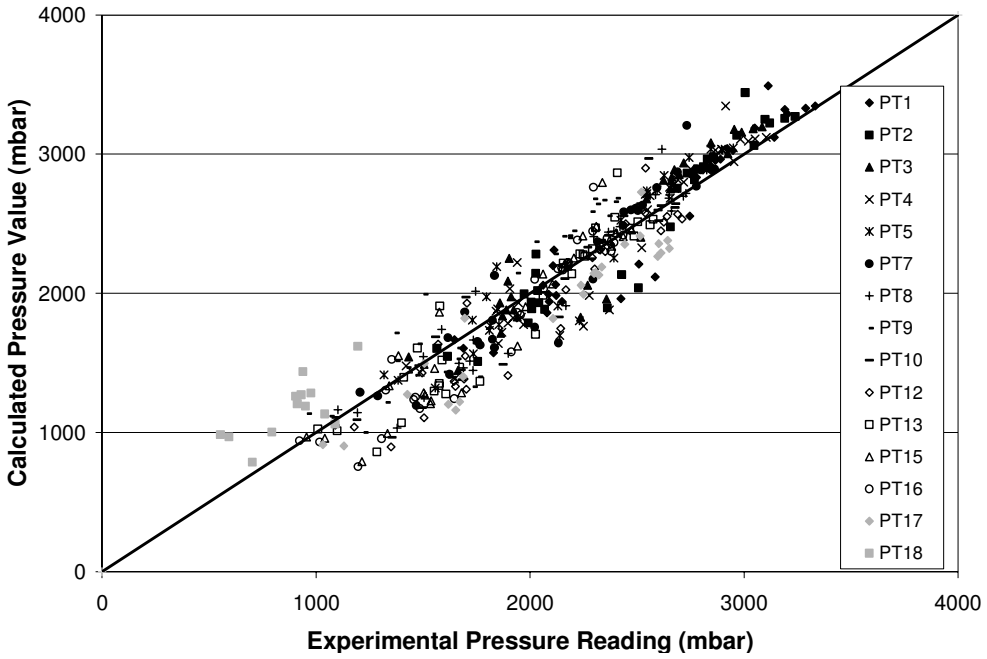

Figure 4-24: Experimental vs. calculated pressure readings values of bentonite conveying in pipeline A.

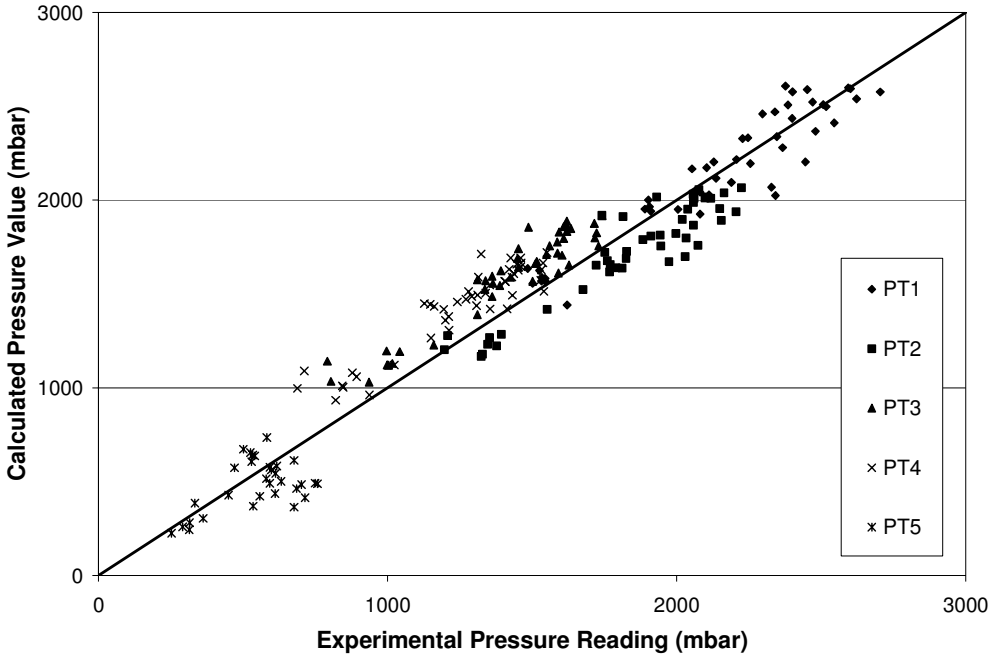

Figure 4-25: Experimental vs. calculated pressure readings values of cement conveying in pipeline D.

Other validation curves of different combinations of bulk materials and pipeline configuration are given under the Appendix C.

It was found that the calculated pressure values were in reasonably good agreement with the experimental pressure values. Further, the predicted values were always found to lie evenly distributed about the central line representing zero error condition. Even at the end sections of the pipeline where the deviation of predicted values has a natural tendency to be comparatively higher than the starting section, because of the error accumulation, the proposed model gave very promising results. This could be considered as a significant achievement, since the model answered the different flow conditions prevailing along the pipeline satisfactorily.

4.8.2.2 Analytical Comparison

In another approach, the results of model validation was analysed using some statistical tools. Generally, statistical parameters give a picture of cumulative performance of the models. Initially, the error of model prediction was determined

and its standard deviation was considered. In addition, an average absolute deviation of percentage error was also taken as another method for comparison. These terms are briefly described in the following section.

The Average Absolute Deviation

The percentage relative deviation of the experimental data points and those predicted by the proposed model could be defined as shown in Equation (4.8).

$$\%e_i = \left(\frac{P_{\exp} - P_{cal}}{P_{\exp}} \right) \times 100\% \tag{4.8}$$

where P_{exp} is the local pressure measured in experiments and P_{cal} is that of model calculation on the very same position of the pipeline. From the percentage relative deviation, the average absolute deviation of the percentage error could be defined as follows;

$$\left|\overline{e}\right| = \frac{1}{N} \sum_{1}^{N} \left|\%e_i\right| \tag{4.9}$$

Where, N is the number of data points in the particular set of data.

The Standard deviation

Generally, the error of model prediction could be defined as shown in equation

$$e_i = P_{\exp} - P_{cal} \tag{4.10}$$

In the usual way of defining the standard deviation of any population, the particular parameter for this comparison analysis could be presented as given below;

$$\sigma_e = \left[\frac{1}{N-1} \sum_{1}^{N} (e_i - \overline{e}_i)^2 \right]^{1/2} \tag{4.11}$$

where $\overline{e_i}$ is the average value of e_i.

The standard deviation yields essentially the same information as the average of the absolute deviation $\left|\overline{e}\right|$; however, the standard deviation is mostly biased by the very high relative deviations (because of the squaring operation), while $\left|\overline{e}\right|$ treats equally high or low relative deviations, thus the average absolute deviation is less affected by

extreme cases than the standard deviation. It is worth to rely on a low value of $|\overline{e}|$ than of σ in the model comparison, since it gives a quantitative measure of deviations of predicted values from the experimental measurements.

It must also be emphasized that a good prediction method is characterized by a value of average absolute deviation that is close to zero, i.e., no tendency towards over-predicting or under-predicting and low value of $|\overline{e}|$, which signifies that the absolute errors are not large. A low value of standard deviation will ensure that the spread of the deviations from their mean value is not high and this may account for the consistency of a correlation.

Table 4-4 shows the result of statistical comparison analysis of the model validation of different combinations of conveying bulk materials and pipeline configurations.

Table 4-4: Results of the statistical analysis.

Bulk Material	Pipeline	Error (mbar) : $e_i = P_{\exp} - P_{cal}$			Average Absolute Deviation of Percentage Error (%) $\left\|\overline{e}\right\| = \frac{1}{N}\sum_{1}^{N}\left\|\%e_i\right\|$
		Maximum (e_i)	Minimum (e_i)	Standard Deviation (σ_e)	
Barytes	A	487.2	-499.1	248.1	14.7
Bentonite	A	493.2	-498.8	202.0	9.1
Cement	A	353.0	-480.7	181.9	11.0
Barytes	C	494.6	-495.1	179.3	9.9
Cement	C	461.6	-482.0	166.7	10.5
Barytes	D	497.6	-498.9	279.4	19.9
Cement	D	330.6	-390.3	160.2	11.5
Ilmenite	B	499.9	-437.6	167.2	12.4
Alumina 1	A+B	497.4	-499.6	247.0	13.5
Alumina 3	A+B	489.1	-499.7	290.2	15.4

According to Table 4-4, the average absolute deviation of percentage error was always limited to 15% except only on one occasion when it was close to 20%, as shown in Table 4-4. The standard deviation of the error varies from 160 mbar to 290 mbar. It may be worthwhile to mention here that in that case of barytes transport in pipeline 'D' (diameter: 125mm and length: 68m), which has the highest value of average absolute percentage deviation, highly unstable flow situations were experienced during the experimentation and this will perhaps explain the high deviation.

4.9 Summary

The proposed model based on the piece-wise approach of scaling and well-known Darcy-Weisbach's equation was described with all conditions and applications. The series of tests carried out to establish and validate the proposed model were explained in detail including the information of test materials and test setup. Finally, the model validation procedure and comparison results were presented also in graphical and analytical forms.

5 COMPARISON ANALYSIS OF 'K' FACTOR METHOD WITH OTHER MODELS

5.1 Introduction

As explained in Chapters 4, the proposed scaling up model has shown good agreement with experimental measurements when it was tested with different bulk materials and pipeline configurations. In addition to validation of the model with the experimental observations, a comparison with other models was also done with the help of available test data. The objective of this work was to compare the performance of the proposed model with some other well-known scaling and pressure drop determination models with different materials and pipeline configurations.

Among the published scaling up techniques and pressure drop determination models, four methods have been selected for this investigation, as they are often referred in the literature. The chosen techniques are rather straightforward, as compared with the other techniques reported in the literature and are claimed to have better agreements with the experimental observations.

In order to examine the effect of pipeline diameter, length and the number of bends in the scaling method, different pipeline configurations have been selected. In the first stage, the models were tested with isolated straight pipe sections and the whole conveying circuit was addressed in the second stage of comparison. The experimental observations on a particular pipeline were used to predict the pressure drop values of other pipeline configuration, using different scaling models and then the calculated pressure drop values have been compared with the experimentally obtained pressure drop values. Some statistical tools have been used for the comparison. Calculation procedure, comparison methods, results and discussion are given in detail in this Chapter.

5.2 Outline of Scaling Techniques

As discussed in Chapter 2, there are basically two distinguished concepts used in empirical models of pressure drop determination of pneumatic conveying systems. One group considers the gas-solid flow as a mixture and defines the relevant parameters with respect to it. The other group splits the mixture into two different hypothetical components as gas flow and solid flow and characterizes the parameters like friction factor, etc, individually for them. As an alternative design method of pneumatic conveying systems, scaling up techniques also use two different approaches; namely global approach and piece wise approach.

Four different models, which represent all the different groups and approaches explained above, were selected, for this comparative analysis, with the aim of comparing the model proposed by author with all available methods of pressure drop determination in pneumatic conveying systems. The methods used are;

1. Weber's pressure drop determination method [43]
2. Pan's scaling up technique [22]
3. Keys and Chambers scaling model [95]
4. Molerus scaling method [91]

These models were described in detail in Section 2.9. In Weber method [43], the gas-solid flow is considered as a mixture and an empirical method is proposed to determine the friction factor of the whole mixture. The friction factor is considered to be a function of solids loading ratio and Froude number. The empirical coefficients are proposed to be the same for a particulate bulk material and independent of geometrical parameters of the pipeline. This method is claimed to be suitable for dilute phase transport.

Following the common approach of pressure drop determination where the gas-solid flow is considered as a combination of two distinguished hypothetical components of gas and solid, Pan and Wypych proposed a scaling up technique [22]. According to them, the pressure drop of the pneumatic transport of air-sold mixture is composed of component due to air only and of an additional component due to the solid part, which are independent from each other. They proposed [22, 46] two different

empirical models to determine the friction factors of each phases as a function of solids loading, Froude number and mean density of air, using dimensional analysis. Based on the experimental data of pressures across straight sections and bends, exponents of the empirical relationship are determined by minimising the sum of square errors of pressures. These exponents, as in the previous cases, are valid for the given product and independent of pipe geometry.

Keys and Chambers [95] preferred the global approach and proposed a method based on an empirical correlation. This method combines a number of non-dimensional flow parameters to predict the pressure loss in the pipeline system. The effects of conveying gas and bulk solid were considered separately, but, by addressing the whole pipeline together with the bends. Empirical correlations were obtained for gas and solid friction factors and used them to predict the pressure drop of another system that conveys the same bulk material.

Molerus [91] considered a unique relationship between two non-dimensional parameters; solid friction factor and Froude number of gas to define the gas-solid flow of given combination of gas and particulate material. He proposed to carry out pilot plant tests to get the data in terms of solid friction factor versus Froude number of gas and to use the resulting curve for the prediction of the pressure drop of the plant to be designed for conveying the same bulk material.

5.3 Method of Comparison

To evaluate the performances of different models, their predictions were compared with corresponding experimental data. This was done using both graphical method and statistical method. A brief description of these two methods was given in Section 4.8.2.

5.4 Test Setup and Conveying Materials

The test data generated by the main investigation were utilised for the comparative analysis. For the convenience of identification of pipe configurations and positions of

pressure transducers used for this section, a schematic diagram of test set-up is shown in Figure 5-1.

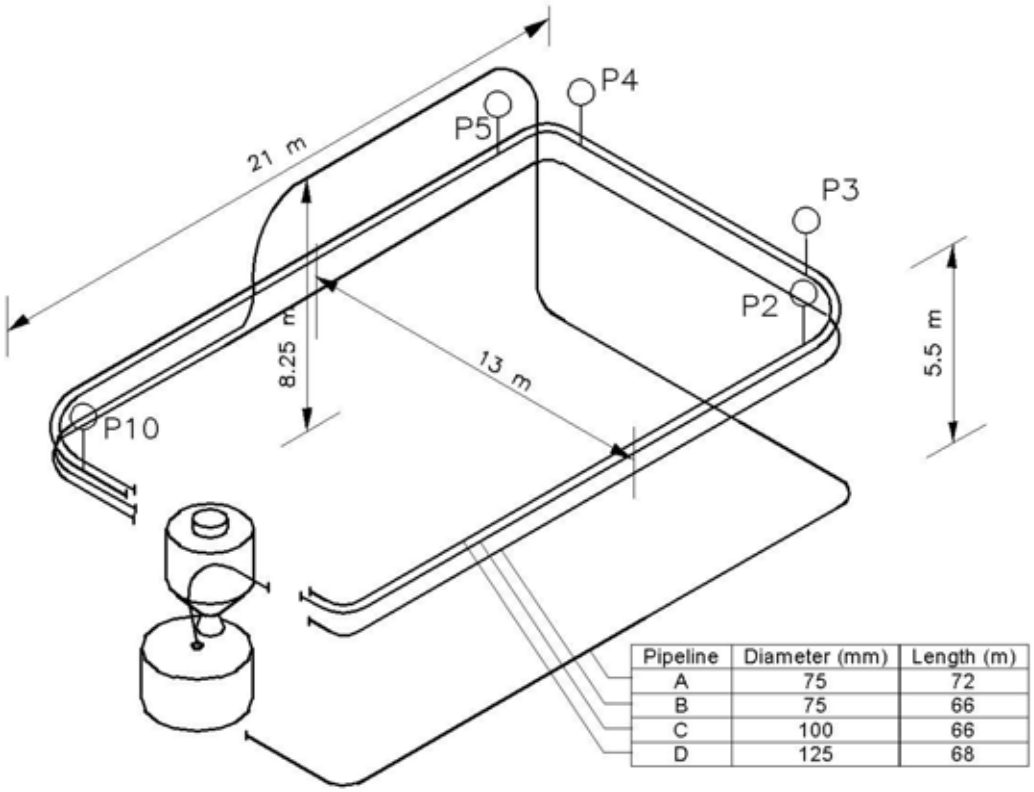

Figure 5-1: A line diagram of conveying loops.

Only barytes and cement were used for the comparative analysis.

5.5 Calculation Procedure

As discussed in Chapter 3, the experimental setup consists of basically four different pipeline configurations with three different pipe diameters. In order to compare the performances of selected models with the proposed model in this investigation, a kind of scaling up operations were carried out using the said models with the help of experimental data obtained during the pneumatic tests. One particular pipe configuration was selected and based on the experimental observation of that pipe configuration; the performances of the rest of the conveying configurations were

predicted. Finally, these predicted values were compared with actual measurements made during the experimentations. In the calculation procedure, first, experimental pressure drop data from 75 mm diameter pipeline was used to calculate the scaling factors and other relevant parameters and then those factors and parameters were used to determine the pressure drop value for 100 mm and 125 mm diameter pipe configurations. In the second part, the experimental data of 100 mm diameter pipeline were taken as the basis and the pressure drop of 125 mm diameter pipe conveying loop were calculated.

Basically, the calculations were carried out in two different approaches. Firstly, only the straight pipe sections were addressed and the calculated values of pressure drop in each straight section were compared with the experimentally observed values of the same. Two straight sections of 10 m and 20 m long were chosen in two different places. The experimentally measured parameters like pressure, solids mass flow rate, air volume flow rate, etc, of the inlet section were taken as the reference and the outlet conditions were calculated using the relevant scaling up and/or pressure drop determination method. Consequently, the calculated values were compared with the corresponding measured values at the outlet using the comparison techniques described in Section 5.3.

In the second approach, the whole conveying loop was considered. The experimentally measured parameters at the pipeline inlet were taken as the reference values and the different models were used to calculate the outlet parameters of the conveying line. The pressure values at discrete positions on pipeline were calculated and compared with the experimental observations. Since some of the works [43, 91] did not address the analysis of other components than the straight sections, the second approach could not be performed, with these models.

5.6 Results and Discussion

Under this section, the findings of this comparison analysis are presented. The abbreviations used to symbolize different models are given below;

- ‘Weber’ - the method proposed by M. Weber [43]

- ‘K&C’ – the scaling technique proposed by S. Keys and A.J. Chambers [95]
- ‘Molerus’ – the scaling technique proposed by O. Molerus [91]
- ‘Pan’ – the scaling technique proposed by R. Pan and P. W. Wypych [22]
- ‘*K* Method’ – the scaling technique proposed in the current investigation

5.6.1 Piecewise Consideration

5.6.1.1 Graphical Comparison

The results of piecewise consideration of graphical comparison analysis, for two different bulk materials in different pipeline configurations are shown in Figure 5-2 to Figure 5-3.

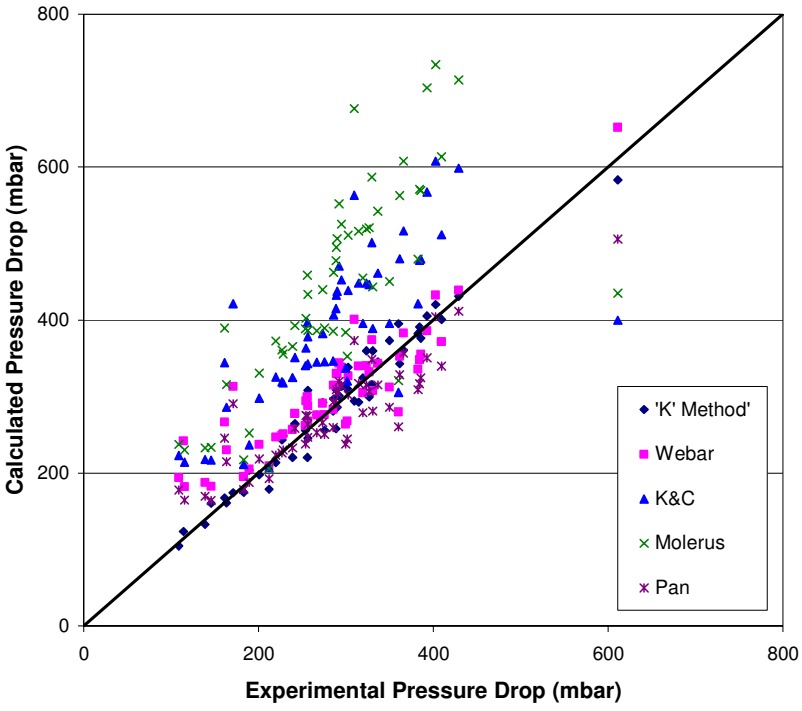

Figure 5-2: Calculated pressure drop vs. experimental pressure drop of 10 m length for barytes transport in 100 mm diameter pipeline scaled up from 75 mm diameter pipeline.

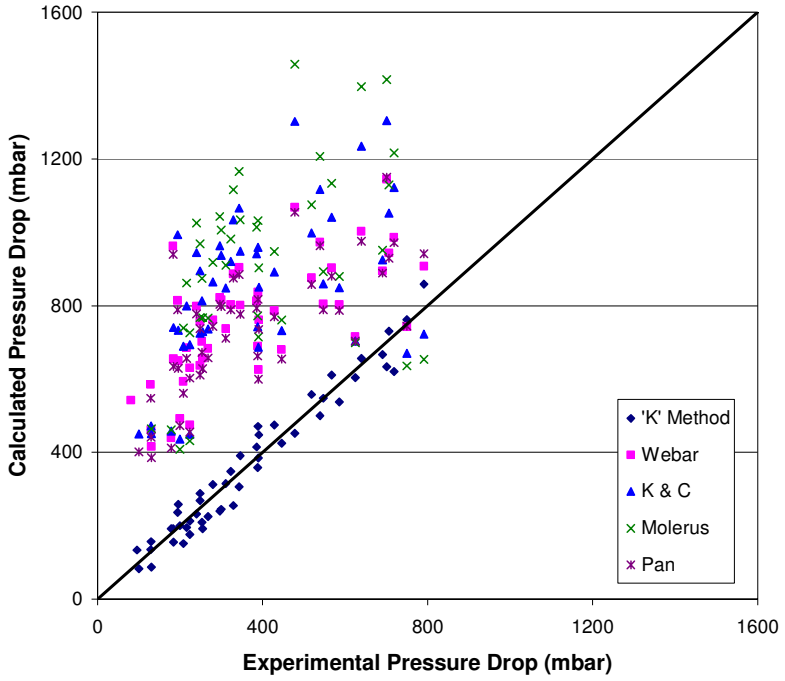

Figure 5-3: Calculated pressure drop vs. experimental pressure drop of 20 m length for barytes transport in 100 mm diameter pipeline scaled up from 75 mm diameter pipeline.

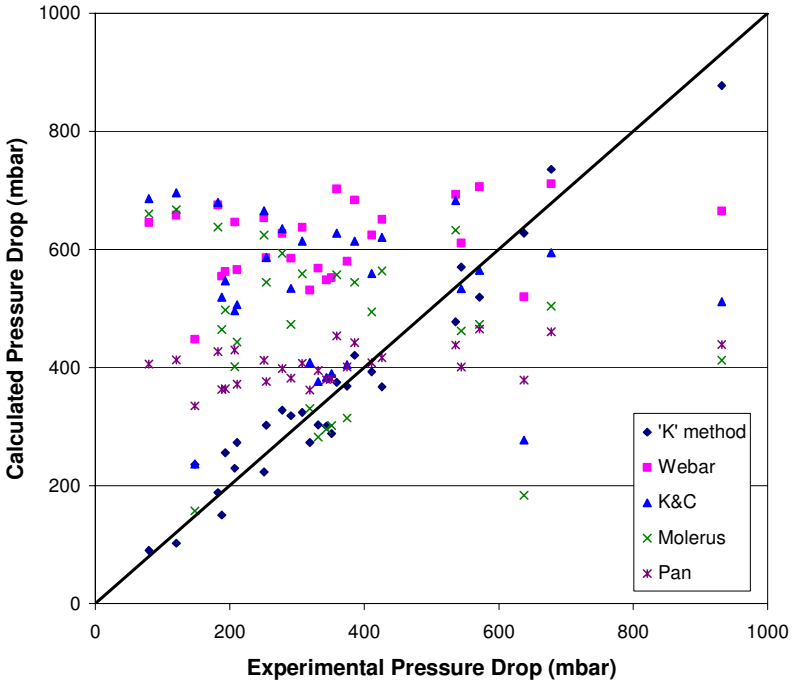

Figure 5-4: Calculated pressure drop vs. experimental pressure drop of 20 m length for barytes transport in 125 mm diameter pipeline scaled up from 75 mm diameter pipeline.

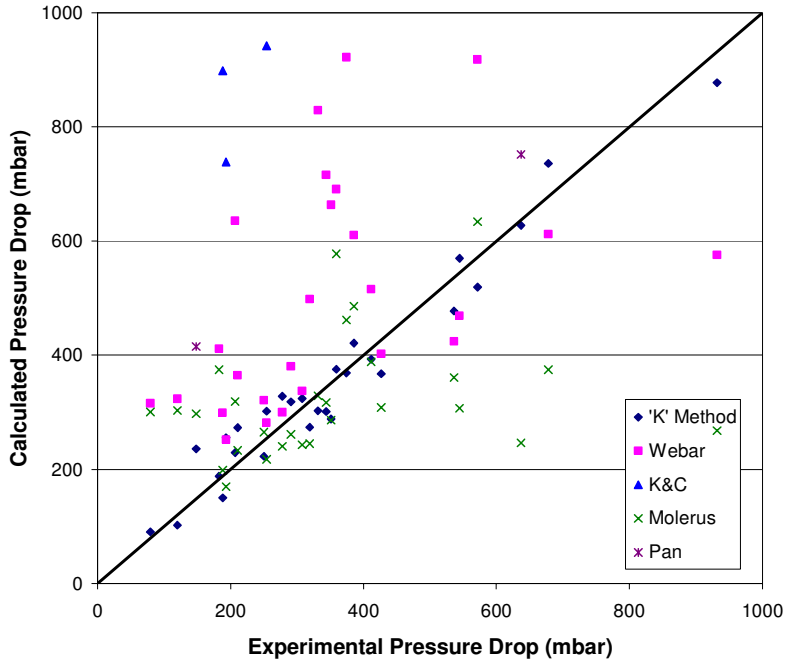

Figure 5-5: Calculated pressure drop vs. experimental pressure drop of 20 m length for barytes transport in 125 mm diameter pipeline scaled up from 100 mm diameter pipeline.

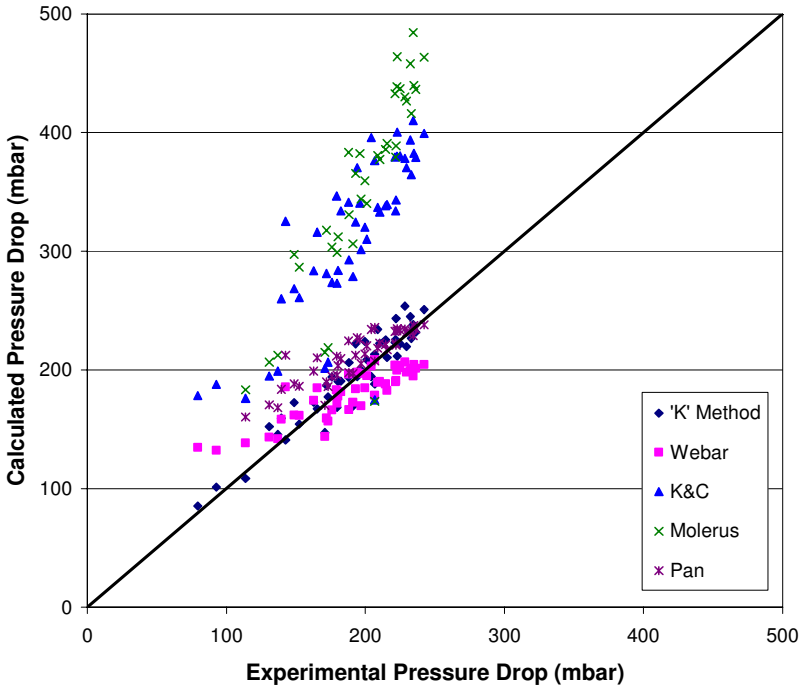

Figure 5-6: Calculated pressure drop vs. experimental pressure drop of 10 m length for cement transport in 100 mm diameter pipeline scaled up from 75 mm diameter pipeline.

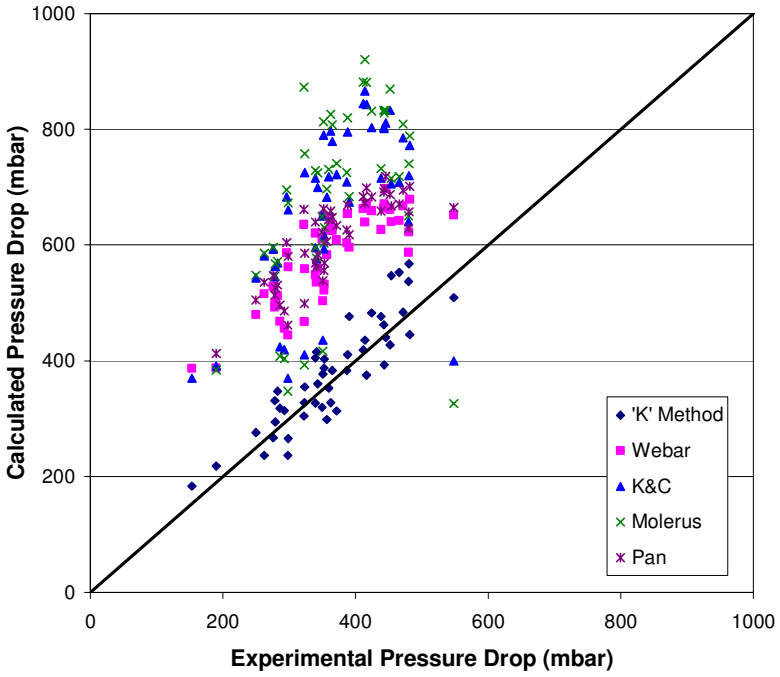

Figure 5-7: Calculated pressure drop vs. experimental pressure drop of 20 m length for cement transport in 100 mm diameter pipeline scaled up from 75 mm diameter pipeline.

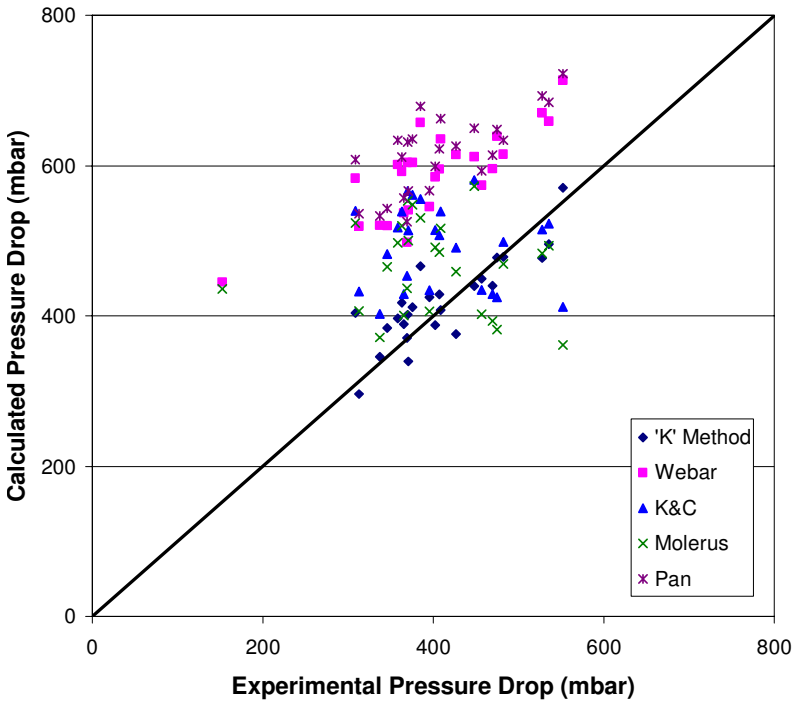

Figure 5-8: Calculated pressure drop vs. experimental pressure drop of 20 m length for cement transport in 125 mm diameter pipeline scaled up from 75 mm diameter pipeline.

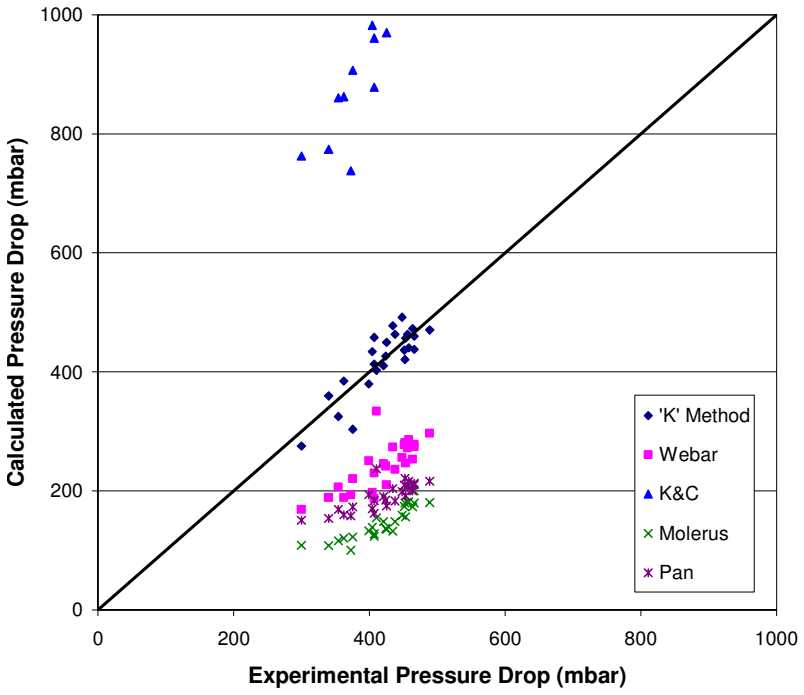

Figure 5-9: Calculated pressure drop vs. experimental pressure drop of 20 m length for cement transport in 125 mm diameter pipeline scaled up from 100 mm diameter pipeline.

The above graphs show the variations of the calculated pressure drop values and experimentally obtained pressure drop values for different materials transported in different pipeline diameters.

It was evident that the model proposed in this investigation, i.e. *K* method, predicted pressure drops which were in reasonably good agreement with the experimental values. All the data points could be seen lying close to central bold line ($y = x$) that represents the ideal prediction. On the other hand, a balanced distribution of data points around the central line could also be seen.

So far as the other models were concerned, it was clear that some models gave comparatively better predictions for 10 m long sections than that for 20 m long sections, although their absolute performances were worse than '*K*' method. The accumulation of errors as the calculation proceeded along the pipeline can be cited as the reason for this difference. For shorter pipe lengths, as shown in Figure 5-2 and Figure 5-6, Weber's as well as Pan's method could be seen better than Molerus' and Keys' methods. In most of other cases, the considered models except 'K method'

seemed to over-predict the pressure drop. An exception could be seen in Figure 5-9, where cement transportation in 100 mm pipeline was used to predict the pressure drop across 20 m of 125 mm line. The models proposed by Pan, Molerus and Weber under-predicted the pressure drop, while Key's technique over-predicted.

5.6.1.2 Analytical Comparison

As a first step of analytical analysis, the prediction errors of each model were calculated as a percentage of their experimental values and the worst case values of each method of prediction are presented in tabular form in Table 5-1.

Table 5-1: The worst case prediction errors of each method.

Material	Conveying line diameter/ Pilot line diameter (mm)	Pipe Length (m)	Worst Case Prediction Error (%)				
			Webar	K & C	Molerus	Pan	'K' Method
Barytes	100/75	10	-112.3	-146.5	-141.8	-70.2	-29.7
		20	-271.8	-210.6	-367.0	-212.0	-20.1
	125/75	20	-257.6	-183.0	-157.5	-134.1	-23.6
	125/100	20	-210.4	-200.6	-152.6	-237.2	-13.1
Cement	100/75	10	-69.4	-127.8	-179.1	-48.8	-23.0
		20	-152.6	-141.5	-309.8	-97.1	-16.5
	125/75	20	-191.7	-74.9	-185.8	-96.9	-30.8
	125/100	20	54.1	-265.9	-53.6	-18.0	19.0

From Table 5-1, it is clear that although all methods over-predict the pressure drop, the over-prediction is very small in case of K factor method.

The worst case error does not give a reasonable judgement about the overall performance of a model, since it deals with only the extreme cases. To have an overall assessment, some statistical tools were used. Table 5-2 and Table 5-3 show the overall deviations of the calculated values from the experimental observations in terms of average absolute deviation $|\bar{e}|$, and standard deviation σ.

Table 5-2: Average absolute deviations of each method.

Material	Conveying line diameter/ Pilot line diameter (mm)	Pipe Length (m)	Average Absolute Deviation of Error; $\|\bar{e}\|$ (mbar)				
			Webar	K & C	Molerus	Pan	'K' Method
Barytes	100/75	10	35.9	109.6	157.7	31.3	15.0
		20	344.4	398.1	744.8	324.7	32.2
	125/75	20	287.4	183.0	166.0	122.7	32.1
	125/100	20	235.7	518.9	122.3	589.7	38.8
Cement	100/75	10	20.0	124.2	657.4	17.7	10.5
		20	217.8	291.7	715.0	236.9	35.4
	125/75	20	187.4	100.1	105.0	197.0	28.2

Table 5-3: Standard deviations of each method.

Material	Conveying line diameter/ Pilot line diameter (mm)	Pipe Length (m)	Standard Deviation of Error (σ)				
			Webar	K & C	Molerus	Pan	'K' Method
Barytes	100/75	10	41.7	71.2	90.5	43.3	18.8
		20	144.7	198.8	317.5	141.2	41.9
	125/75	20	181.6	210.0	224.8	167.4	39.7
	125/100	20	254.5	506.9	189.6	432.5	43.9
Cement	100/75	10	22.1	43.2	342.0	16.8	12.3
		20	47.0	116.4	389.8	44.3	42.2
	125/75	20	49.7	91.4	107.7	47.8	37.2
	125/100	20	52.3	176.6	79.3	47.4	28.4

According to Table 5-2 and Table 5-3, K method gives the least value of average absolute deviation and standard deviation of for all combinations of pipe sizes, lengths and conveying materials. The average absolute deviation gives a quantitative measure of how the predictions differ with respect to experimental value. The 'K method' gives the lowest values of average absolute deviation and hence better than the other models considered here. Pan's and Weber's models also gave good results especially in short distance conveying cases. But for long pipe sections, their average absolute deviation went up to 200-300 mbar range. Keys' as well as Molerus' method showed a high average absolute deviation for all combinations of transportations.

5.6.2 Whole Conveying Line Consideration

As explained in Section 5.5, the second stage of comparative analysis addressed the whole conveying line. Only Pan's scaling technique and *K* method were used for this part. In this case also, the experimental data based on 75 mm diameter pipeline was used to calculated the pressure values of 100 mm and 125 mm diameter pipeline. The experimentally measured value of pressure just outside of the blow tank was taken as the initial point and the calculations were carried out in steps of 1m distance until the last pressure tapping point, using Pan's method and *K* method. Then, calculated and measured values of each pressure tapping were compared.

5.6.2.1 Graphical Comparison

The resulted graphs are shown in Figure 5-10 to Figure 5-13. Figure 5-1 gives the details of the configurations of conveying line and the positions of pressure transducers.

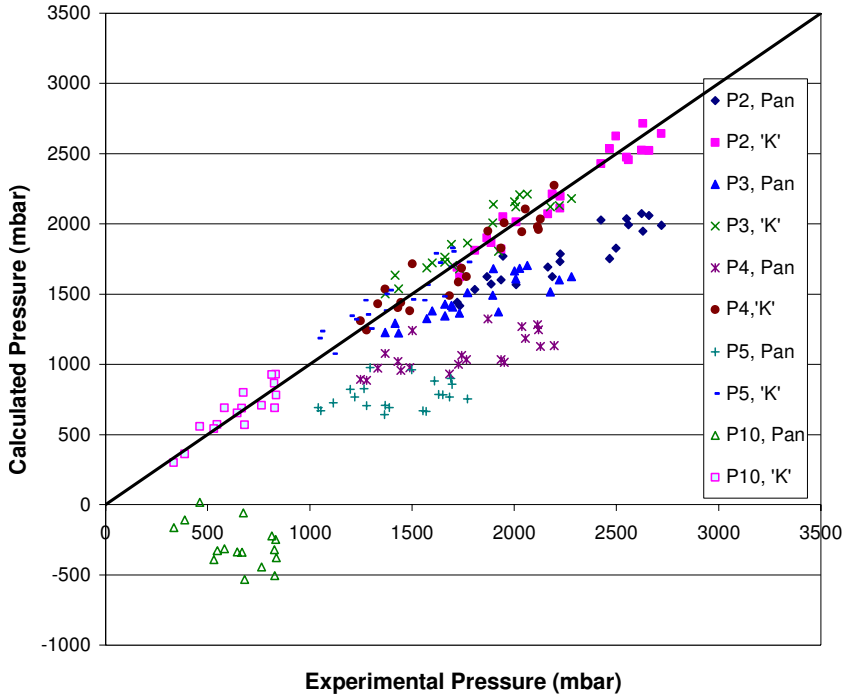

Figure 5-10: Calculated pressure values vs. experimental pressure values of barytes transport in 100 mm diameter pipeline.

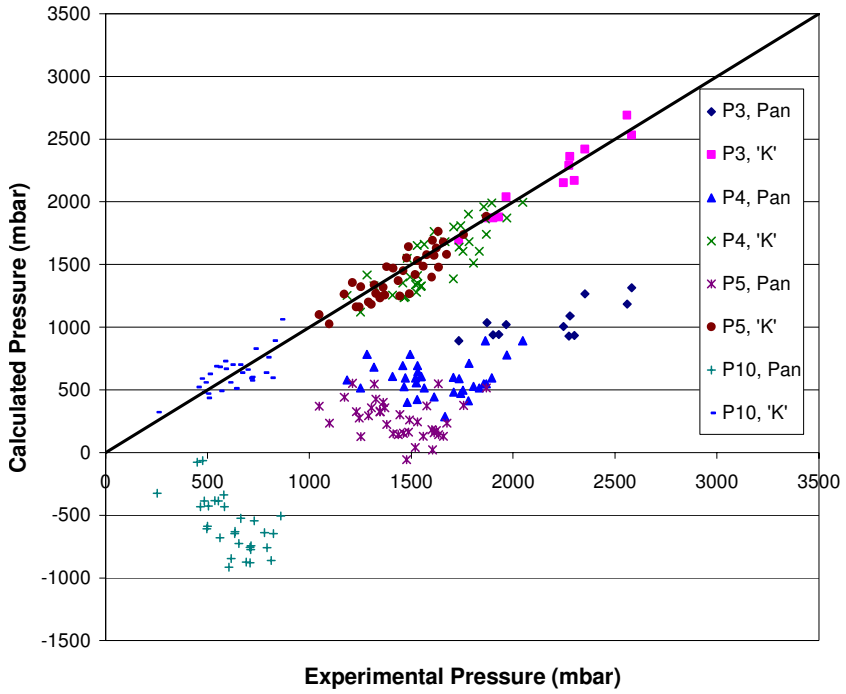

Figure 5-11: Calculated pressure values vs. experimental pressure values of barytes transport in 125 mm diameter pipeline.

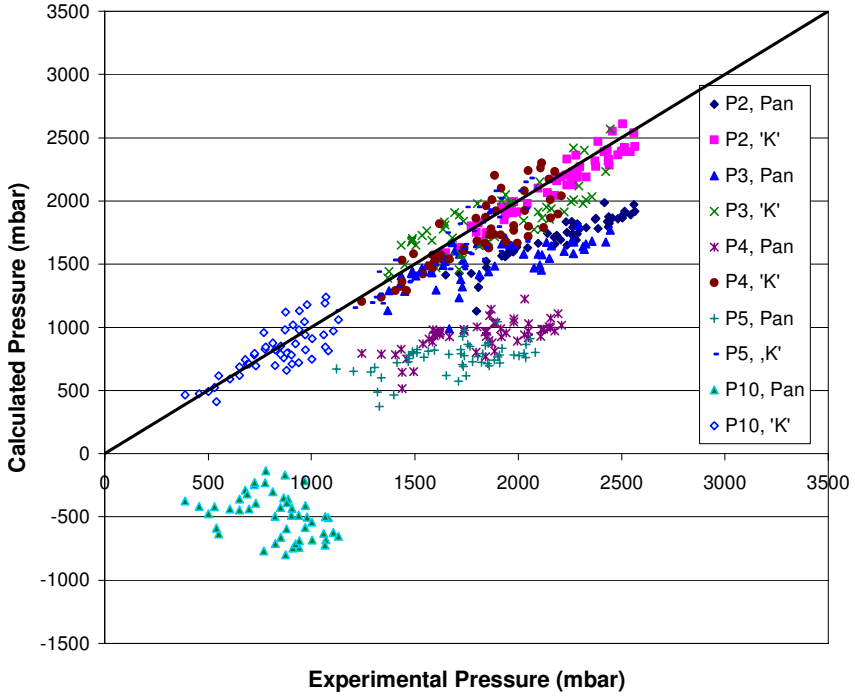

Figure 5-12: Calculated pressure values vs. experimental pressure values of cement transport in 100 mm diameter pipeline.

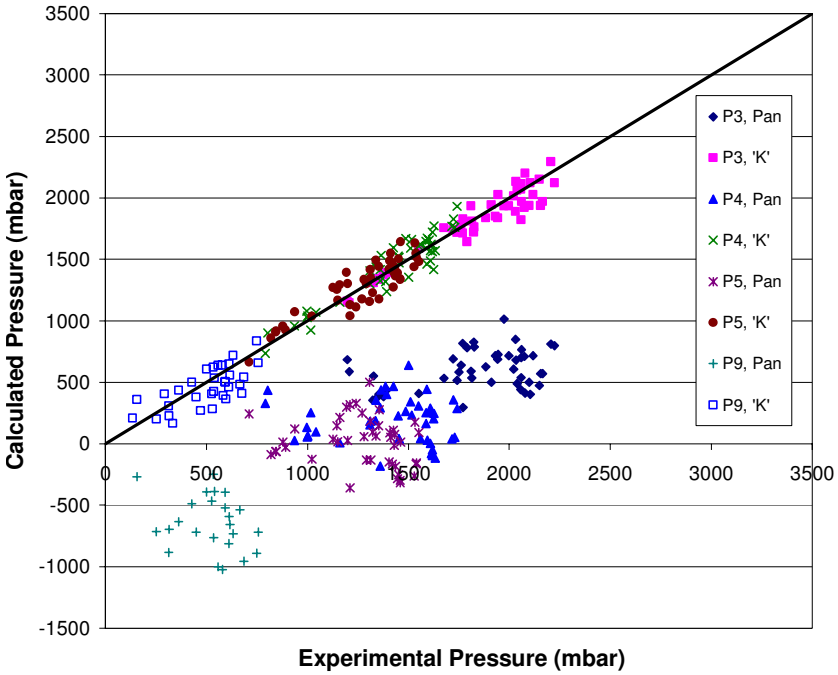

Figure 5-13: Calculated pressure values vs. experimental pressure values of cement transport in 125 mm diameter pipeline.

above Figures clearly show the difference of predictions of the considered models. According to these results, it is obvious that *K* method has the ability to predict the pressure values even at the end of the conveying loop with considerable accuracy. In few cases, it could be seen that Pan's scaling method predicted the pressure values relatively better at the initial pressure points of the conveying line as compared to the later sections. As the calculation proceeds along the conveying line, the pressure predictions at the end of the line deviated much from the experimental measurements as shown in Figure 5-10 to Figure 5-13. In most of the cases, Pan's method over-predicted the pressure drop, thus under-estimated the available pressure. The degree of over-prediction was so large that the calculated pressure values, in most cases, were negative at the end of the conveying line. However, *K* method predicted the pressure values much better where most of the data points lay along and closer to central line representing $y = x$. Even at the end of the line, i.e., the last pressure tapping point (P9 or P10), which is about 70m away and crossing 4 bends from the starting point, the results were rather good.

5.6.2.2 Analytical Comparison

Table 5-4 shows the minimum and maximum prediction errors as a percentage of their corresponding starting pressure for each method.

Table 5-4: The worst case percentage prediction errors of each method.

Conveying Material	Pipeline Diameter (mm)	Worst Case Percentage Prediction Error (%)			
		Pan		'K' Method	
		Max.	Min.	Max.	Min.
Barytes	100	-8.8	-178.4	20.7	-16.7
	125	-38.9	-251.2	28.3	-26.6
Cement	100	-0.7	-238.5	28.1	-25.4
	125	-42.9	-383.0	21.3	-27.8

As shown in Table 5-4, the minimum and maximum errors of Pan's predictions are always negative. This shows the high degree of over-prediction of the model. Conversely, a well balanced behaviour could be seen in *K* method's predictions with respect to the percentage of worst case errors. As discussed earlier, the average absolute errors were also calculated to verify the collective performances of the models' predictions and the results are shown in Table 5-5.

Table 5-5: Average absolute deviations of each method.

Material	Pipeline Diameter (mm)	Average Absolute Deviation; $\lvert\bar{e}\rvert$ (mbar)	
		Pan	K Method
Barytes	100	576.0	92.1
	125	1096.5	103.6
Cement	100	792.3	126.1
	125	1004.3	84.4

According to Table 5-5, the *K* method gives the least average deviation for all combination of conveying materials and pipe configuration, while predictions of Pan's scaling technique showed high degree of deviations.

5.7 Conclusion

Five different methods of pressure drop calculation including the model proposed in this investigation were used to calculate the pressure drop values for 100 mm and 125 mm diameter pneumatic transport pipelines based on 75 mm diameter pipeline data. To check the effect of conveying distance, two different pipe sections were employed for the analysis. In the first stage, two isolated horizontal pipe sections of 10 m and 20 m length were chosen for the analysis. When the experimentally measured pressure drops were compared with its corresponding values of predictions based on different models, it was clear that the 'K' factor method discussed in detailed in Chapters 4, gave the best predictions among the considered models and scaling up techniques. The results showed that, the pressure drop was over-predicted by the available techniques of scaling and pressure drop prediction, in most of the cases.

In the second stage, the complete conveying loop was addressed with Pan's and 'K' factor scaling up techniques. Taking the test results of 75 mm line as the basis, the available pressure values at discrete positions of 100 mm and 125 mm lines were calculated and compared with the actual pressures available at the same points. Confirming the results of first stage, the 'K' factor method was identified as the method, which gave the least percentage of error by analysing the results of second stage. Specially, when the whole conveying loop including bends and other pipeline accessories was considered, there was a risk of error accumulation of all other methods, which lead to high discrepancies at the end of the conveying line. But, 'K' factor scaling technique was seen as a method that dealt this situation, satisfactorily.

6 PREDICTION OF PRESSURE DROP AT THE ENTRY SECTION OF TOP DISCHARGE BLOW TANK

6.1 Introduction

As discussed in Chapter 2, in recent years, quite a lot of research papers have been published on the topic of scaling up [16, 25, 42, 95, 101, 153], basically in two distinguished categories; the global approach [16, 95, 153] and the piecewise approach [25, 42, 101]. But, unfortunately, none of these methods addressed the entry pressure loss i.e. the pressure drop across the feeding section of a top discharge blow tank system. In fact, the entry pressure loss contributes to the total pressure drop significantly. Especially, when the blow tank pressure has to be determined, this component plays a vital role. Under the current investigation, a special attempt was made to formulate a simple and straight forward scaling technique, which could be used to determine the entry loss using the experimental data generated with different bulk material. In this section, the back ground, model formulation and validation of proposed scaling technique for entry pressure are discussed in detail.

6.2 Background

It is known that a blow tank has the interesting mechanism of self-regulation to change the solid mass flow rate and mass loading ratio automatically, depending on the conveying distance and on air pressure available in the tank. Rivkin [154] explained this phenomena analogous to a closed-loop automatic control system, where the conveying distance serves as feed back for the entrance to the conveying line. He defined a threshold of the conveying distance, up to which this mechanism seems to be valid (approximately 100 m) and this critical length is said to be dependent upon the characteristics of the conveying bulk material such as particle size, density, fluidizeability, etc. Lohrmann and Marcus [155, 156] studied the performance of a bottom discharge blow tank with varying system parameters such

as line length, conveying velocity, etc. Jones et al. [33] compared the performance differences between top and bottom discharge blow tanks and found that there is no significant difference in the pressure, and thus the energy required to convey a product through a pipeline at a given mass flow rate and loading condition in both configurations. In a series of publications, Tomita et al. [157-162] explained the performance and feed rate characteristics of a high pressure blow tank. Marjanovic [163] formulated a model to predict the transient behaviour of a blow tank. But, none have provided with any model to calculate the pressure loss incurred in the entry section from a high pressure blow tank system.

With the aim of formulating a complete scaling up procedure, which can be applied from initial point to end point of conveying system, a special attempt was made to find a way of scaling up of the pressure loss at the entry section to pipeline (henceforth called entry pressure loss) with the help of the experimental data. The model has been formulated theoretically using dimensional analysis and later validated with experimental data.

Under the current topic, the model formulation and validation results are presented in details.

6.3 Test Setup

The details of the feeding section are shown in Figure 6-1.

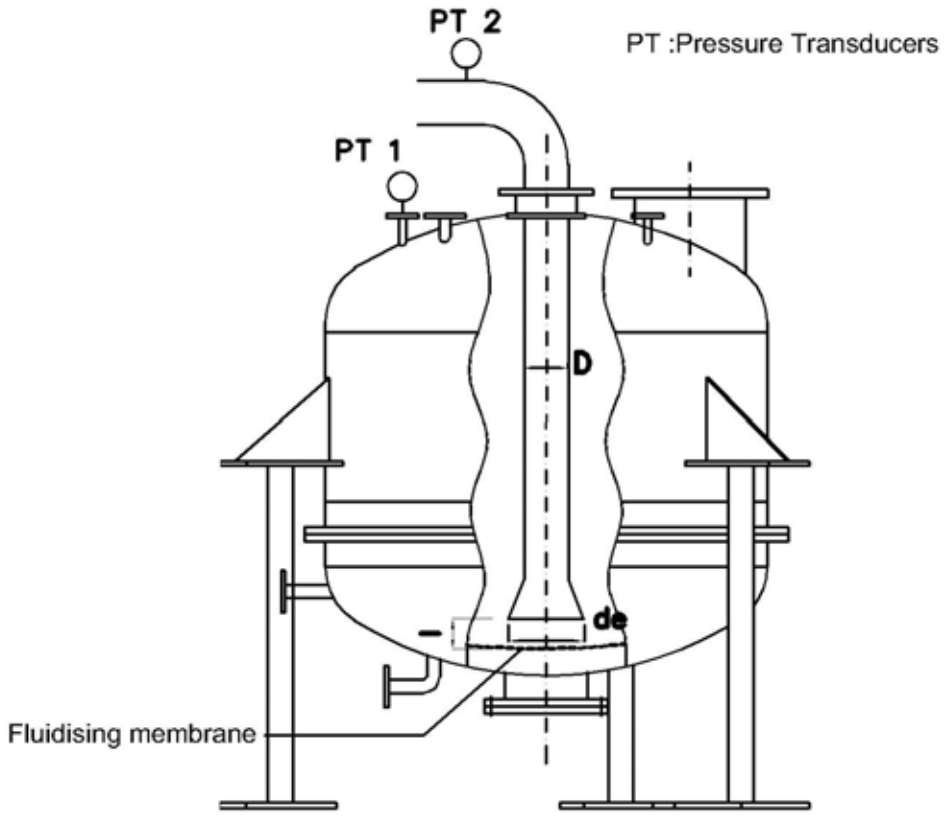

Figure 6-1: Schematic view of the blow tank and the entry section.

Table 6.1: Parameter of different pipeline configuration.

Pipeline Diameter (mm)	***D* (mm)**	***d_e* (mm)**	***l* (mm)**
75	80	100	150
100	102	128	192
125	130	160	240

As shown in Figure 6-1, a porous plate was used at the bottom of the blow tank to fluidise the bulk material before introducing the pipeline. In the top discharge configuration, a riser pipe with a nozzle at the end was used. The internal diameter of riser pipe, the opening diameter of nozzle and the nozzle inlet height (gap between

nozzle inlet and the porous plate) are labelled in Figure 6-1 as D, d_e and l respectively and their nominal values for different pipeline configurations are given in Table 6.1.

6.4 Details of Experiments

The data generated by the series of experiments described under the Section 4.5 were utilised for the current investigation as well. Among the test materials for the main investigation, only four bulk powders were selected for the current analysis. Barytes, cement, ilmenite and five different qualities of alumina were chosen as the conveying bulk materials. The properties and other relevant details of the test materials were given in Chapter 4.

Under this investigation, a special attention was made on the entry section and the pressure measurements and other readings relevant to entry section were taken into consideration together with common measurements such as solids mass flow rate and air volume flow rate.

6.5 Theoretical Approach

For this investigation, a well-known mathematical technique called dimensional analysis [44, 164] has been used to derive a relationship between entry pressure loss and the probable influencing parameters. The Buckingham π theorem, which is the key theorem in dimensional analysis, states that the functional dependence between a certain number (e.g.: n) of variables can be reduced by the number (e.g. m) of independent dimensions occurring in those variables to give a set of $p = n - m$ independent, dimensionless numbers. A detailed description about the dimensional analysis and the Buckingham π theorem is available in Ref.s [44, 164-166].

According to the standard procedure of dimensional analysis, the step wise approach of model formulation is simply described in the following section.

6.5.1 List of influential parameter

Generally, the influential variables could be identified by considering few main concepts, such as the geometry of the system, fluid properties involved with the system and influential external effects of the system. According to this categorization, the entry pressure loss can be considered as a function of a number of pertinent variables:

1. Set pressure in blow tank (P_s)
2. Entry pressure loss (ΔP_e)
3. Mass flow rate of solids (M_s)
4. Air volume flow rate (Q_a)
5. Diameter of the riser tube (D)
6. Nozzle inlet height (l)
7. Particle density (ρ_s)
8. Particle mean diameter (d_p)
9. Loading ratio (μ)
10. Entry diameter of the riser tube (d_e)
11. Air density (ρ_a)

Thus, the number of variables required to described the system could be found as 11 (n = 11; according to the usual notations).

6.5.2 Number of Dimensionless Groups Required

In the next step, the basic dimensions of the listed parameters were taken into account. After checking the basic dimensions of the above variables, it was revealed that all of them could be defined using three independent dimensions; e.i., M-mass, L-length and T-time.

Thus, number of reference dimensions; m = 3.

According to the Buckingham Π theorem, the number of dimensionless groups required to describe the system could be determined as;

$$p = n - m$$

Therefore, $p = 11 - 3 = 8$

Then, the functional relationship among the still unknown dimensionless groups could be presented as;

$$f\left(\Pi_1,.....,\Pi_8\right)=0 \qquad (6.1)$$

where, Π_i is a particular dimensionless combination of variables.

6.5.3 Determination of Repeating Variables

These repeating variables have to be selected from the original list of variables and can be combined with each of the remaining variables to form Π term. Few conditions have to be satisfied when the repeating variables are selected [164]:

- All of the required reference dimensions must be included within the group of repeating variables.
- The dimensions of one repeating variable cannot be reproduced by some combination of products of powers of the remaining repeating variables (i.e., all repeating variable must be dimensionally independent of each other).
- The repeating variables cannot themselves be combined to form a dimensionless product.

As its name implies, the repeating variables will generally appear in more than one Π term. Thus, from the above listed parameters, three parameters were selected as the basic variables to combine with the rest of variables to form the required number of dimensionless groups. Usually, the number of repeating variables required is equal to the number of reference dimensions.

In this model formulation, few different combinations of repeating variables were tried. According to the outcome of those different combinations, finally ΔP_e, M_s and D were selected as the repeating variables, since this combination of variables was the best to satisfy the conditions of selections of repeating variable as mentioned in Ref. [164].

6.5.4 Formation of Dimensionless Groups

The general procedure of formulation of a typical Π term can be presented in the following equation.

$$\Pi_i = u_i u_1^{a_i} u_2^{b_i} u_3^{c_i} \tag{6.2}$$

where; u_i is one of the non-repeating variables

u_1, u_2 and u_3 are the repeating variables

a_i, b_i and c_i are the exponents

These exponents to the repeating variables are determined so that the combination is dimensionless.

6.5.4.1 A Specimen Simplification

The following simplification presents the usual way of determination of a dimensionless group (or a Π term), as a specimen calculation.

The selected repeating variables: ΔP_e, M_s and D

Consider ρ_s as the non-repeating variable and term the dimensionless number as Π_1;

According to equation (6.2),

$$\Pi_1 = \rho_s \left(\Delta P_e\right)^{a_1} \left(M_s\right)^{b_1} \left(D\right)^{c_1} \tag{6.3}$$

Considering the basic dimensions of each term;

$$\left(M^0 L^0 T^0\right) \equiv \left(ML^{-3}\right)\left(ML^{-1}T^{-2}\right)^{a_1} \left(MT^{-1}\right)^{b_1} \left(L\right)^{c_1} \tag{6.4}$$

Equating the exponents of each of basic dimensions;

M: $\quad 1 + a_1 + b_1 = 0$ (6.5)

L: $\quad -3 - a_1 + c_1 = 0$ (6.6)

T: $\quad -2a_1 - b_1 = 0$ (6.7)

Simplifying equations (6.5), (6.6) and (6.7), the values of exponents could be determined as;

$$\begin{aligned} a_1 &= 1 \\ b_1 &= -2 \\ c_1 &= 4 \end{aligned} \tag{6.8}$$

Equation (6.3) could then be rewritten as;

$$\Pi_1 = \rho_s \left(\Delta P_e\right)\left(M_s\right)^{-2}\left(D\right)^4 \tag{6.9}$$

By rearranging the equation (6.9);

$$\Pi_1 = \frac{\Delta P_e \rho_s D^4}{M_s^2} \tag{6.10}$$

Following the same procedure, the rest of the *Π* groups could also be found and the list of all *Π* terms is given below.

$$\Pi_1 = \frac{\Delta P_e \rho_s D^4}{M_s^2} \tag{6.11}$$

$$\Pi_2 = \frac{P_s}{\Delta P_e} \tag{6.12}$$

$$\Pi_3 = \frac{M_s Q_a}{\Delta P_e D^4} \tag{6.13}$$

$$\Pi_4 = \frac{\Delta P_e \rho_a D^4}{M_s^2} \tag{6.14}$$

$$\Pi_5 = \frac{l}{D} \tag{6.15}$$

$$\Pi_6 = \frac{d_p}{D} \tag{6.16}$$

$$\Pi_7 = \frac{d_e}{D} \tag{6.17}$$

$$\Pi_8 = \mu \tag{6.18}$$

6.5.5 Final Form of Functional Relationship

Putting them all together, the final set of *Π* groups could be shown as below;

$$f\left[\frac{\Delta P_e \rho_s D^4}{M_s^2}, \frac{P_s}{\Delta P_e}, \frac{M_s Q_a}{\Delta P_e D^4}, \frac{\Delta P_e \rho_a D^4}{M_s^2}, \frac{l}{D}, \frac{d_p}{D}, \frac{d_e}{D}, \mu\right] = 0 \tag{6.19}$$

Equation (6.19) could be manipulated further to the following form.

$$f\left[\frac{\Delta P_e \rho_s d_p Q_a}{P_s M_s D}, \frac{P_s}{\Delta P_e}, \frac{\rho_s}{\rho_a}, \frac{l}{d_e}, \frac{l}{D}, \frac{d_p}{D}, \frac{d_e}{D}, \mu\right] = 0 \tag{6.20}$$

According to Ref.[167], the dimensionless groups, which comprise of only geometrical factors, are less important for the task of formulating a model. Similarly, the density ratio between particle and air can also be discarded, if only a particular bulk material is considered. The dimensionless parameter of the ratio between blow tank pressure and entry pressure loss shows the proportional relationship between them. Naturally, higher the blow tank pressure, higher the entry loss component.

Thus, only two terms are left among the dimensionless numbers available in equation (6.20) for further analysis. One can easily isolate those terms as shown in equation (6.21);

$$\frac{\Delta P_e}{P_s}\frac{\rho_s d_p Q_a}{M_s D} = f(\mu) \tag{6.21}$$

For the ease of presentation, the left hand side term of the equation (6.21) could be simply equated to a single parameter (η) as shown below.

$$\text{Let, } \eta \equiv \frac{\Delta P_e}{P_s}\frac{\rho_s d_p Q_a}{M_s D} \tag{6.22}$$

$$\text{Thus, } \eta = f(\mu) \tag{6.23}$$

As noted before, the dimensional analysis alone cannot provide a complete answer to the given problem, since the analysis only gives the dimensionless groups describing the phenomenon and not the specific relationship among them. To obtain the exact relationship, experimental measurements have to be utilised for obtaining an empirical relationship.

6.6 Model Formulation

The final outcome of the dimensional analysis process was some sort of functional relationship between few variables. The numerical constant and exponents could then be realized by fitting a curve to represent the functional relationship with the help of the experimental measurements.

Using the experimental data, the values of the dimensionless parameter η described by the equation (6.22) were calculated for different conveying conditions. These data were then plotted; η as *y*-axis and solids loading ratio as *x*-axis. When the results

were presented in graphical form, it was revealed that there is a strong relationship between the dimensionless group; η and the solids loading ratio, since the best fitted power curves showed high degrees of fitting (R^2). These curves were generated using MS Excel® software package.

After further analysis, it could be noted that the curves representing a particular conveying material, but different diameters of conveying pipes were overlapping on each other. This phenomenon could be clearly seen in the following Figures, which present the variation of η vs. loading ratio for different bulk material. The equations of best fitted curves are given in Table 6.1.

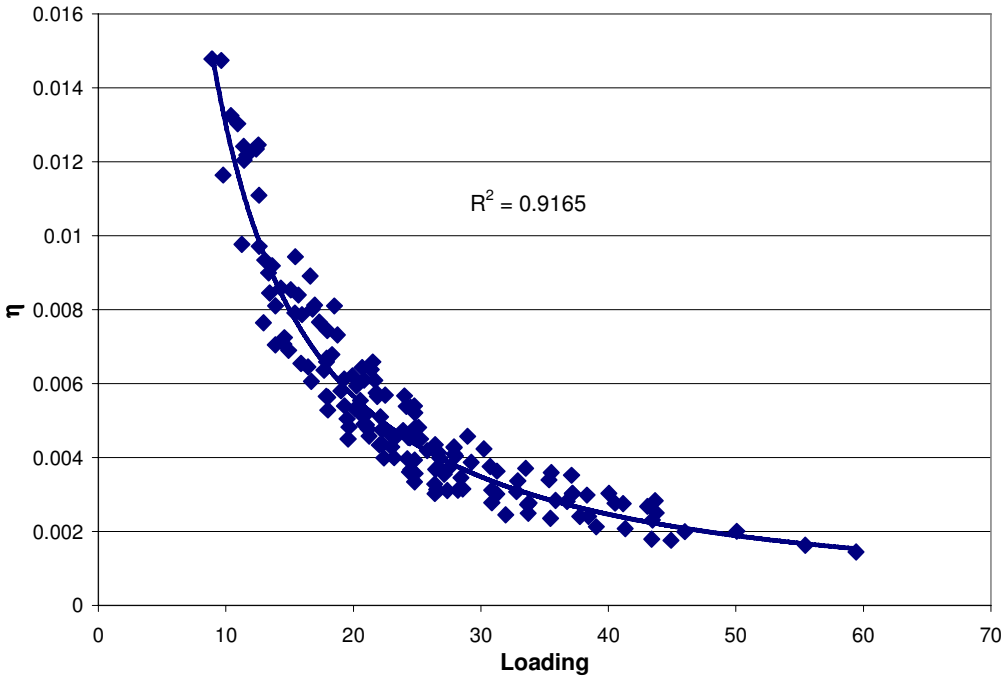

Figure 6-2: The Variation of η with loading ratio for alumina conveying for 75 mm pipe sizes.

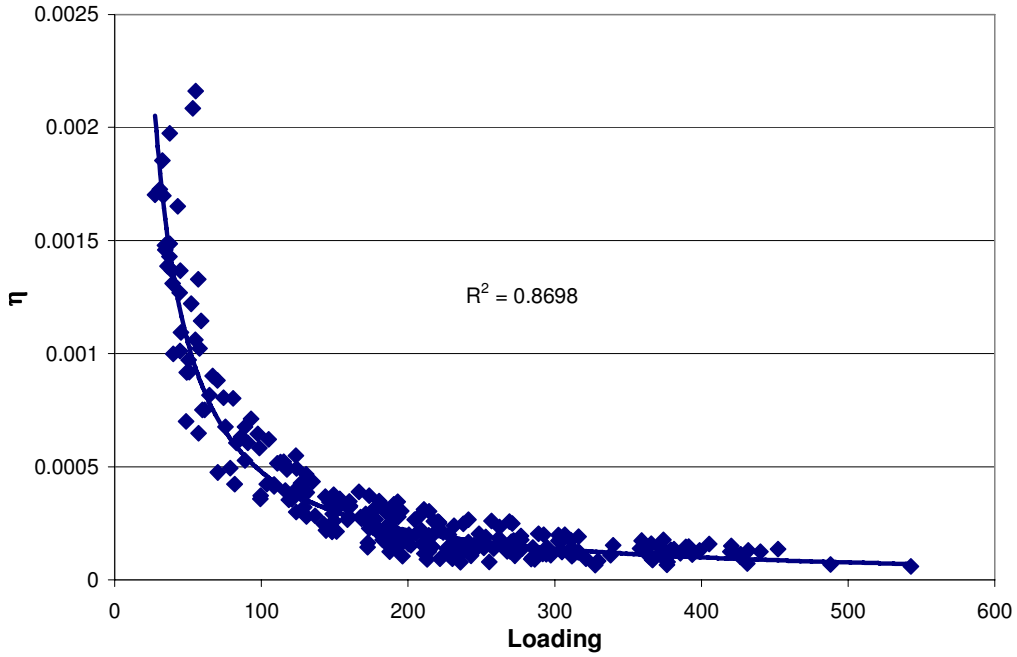

Figure 6-3: The Variation of η with loading ratio for barytes conveying for 75 mm, 100 mm and 125 mm pipe sizes.

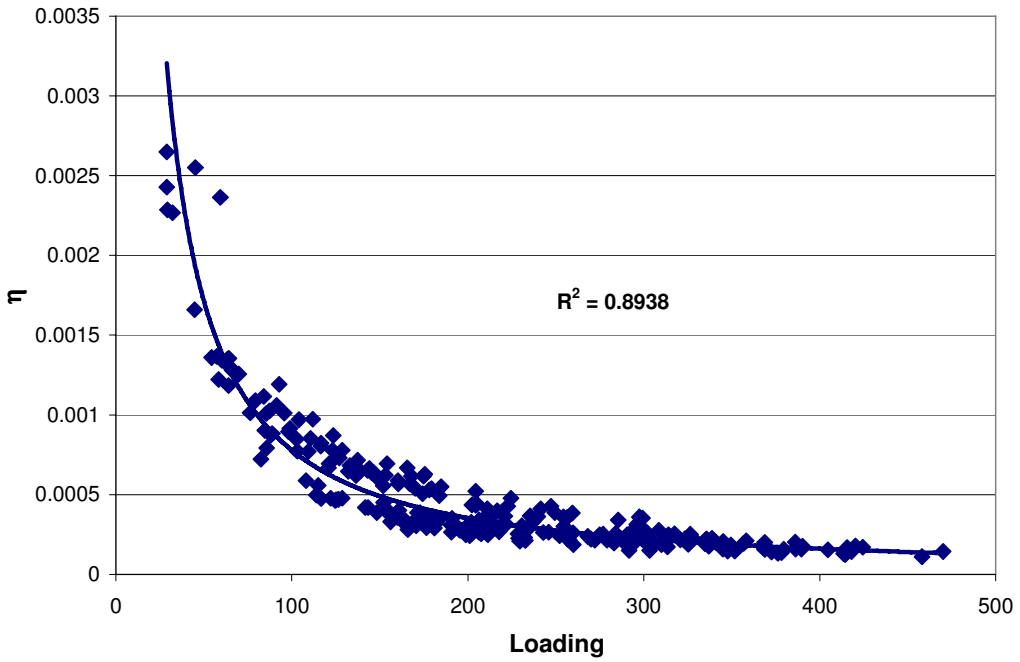

Figure 6-4: The Variation of η with loading ratio for cement conveying for 75 mm, 100 mm and 125 mm pipe sizes.

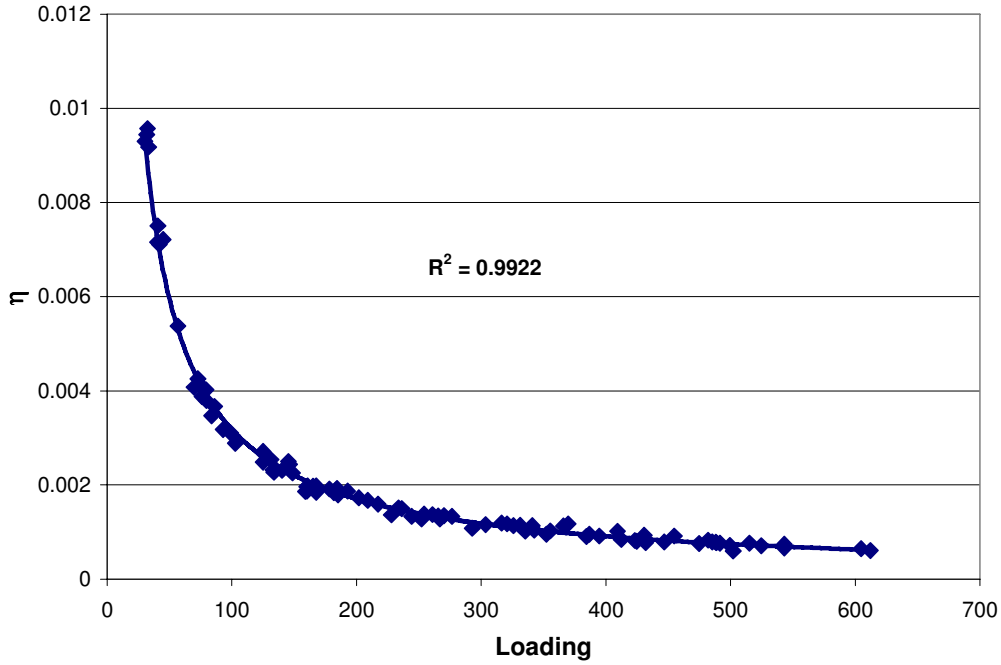

Figure 6-5: The Variation of η with loading ratio for ilmenite conveying for 75 mm, 100 mm and 125 mm pipe sizes.

As shown in Figure 6-2 to Figure 6-5, it was clear that all η vs. loading curves describe similar trends, which show a power-law relationship of η with solids loading ratio. On the other hand, the degree of fitting (R^2) of curves were rather good.

As one can see, all curves of η vs. loading are in the following form;

$$\eta = A\mu^B \qquad (6.24)$$

Table 6.2 shows the numerical values of the constants of equation for different bulk material.

Table 6.2: Experimentally found constants of the Equation (6.24).

Conveying Material	A	B
Alumina	0.2051	-1.1985
Barytes	0.0875	-1.1315
Cement	0.1481	-1.1399
Ilmenite	0.2039	-0.9033

According to Figure 6-2 to Figure 6-5, the relationship between the term η and the loading ratio was proven as independent of the conveying pipe diameter. This leads to a new concept of scaling up of entry pressure loss term, which is included in dimensionless number η. Once the curve of η vs. loading is established for a particular pipe diameter (in other words, relevant A and B is known for the particular conveying material), the relationship between them can be used to determine the entry pressure loss for any other pipe diameter, provided that the conveying material is same in both cases and the rest of the terms available in equation (6.22) are known. By following a simple back calculation procedure, entry pressure loss of other pipe diameters can easily be determined as given in equation

$$\Delta P_e = A' \left[\frac{P_s M_s D}{\rho_s d_p Q_a} \right] \mu^{B'} \tag{6.25}$$

where, A´ and B´ are material dependent constant.

6.7 Validation of Model

Since it is necessary to check how the proposed model deviates from the actual measurements once it is used in a practical situation, a simple validation technique is followed. Under this section, the procedure of validating the model along with graphical and analytical comparison of model prediction and real measurements are given.

To validate the proposed model, a technique termed as 'test set validation' was used. In this procedure, the data generated by the series of experiments described under the Section 4.5, were divided in to two parts. One half of the experimental data were used to get the equation of empirically fitted η vs. loading curves given as the equation (6.23). Then, the relationships revealed were used to calculate the entry pressure loss for the rest of the experimental condition. These calculated entry loss pressure values were then compared with the corresponding experimental pressure measurements. This comparison was done in two ways; graphical comparison and analytical comparison.

6.7.1 Graphical Comparison

In this method, the calculated entry loss values were plotted against the corresponding experimental measurements. A brief description about the graphical comparison is available under Section 4.8.2.1. The following figures show such comparisons for different bulk materials considered under this study.

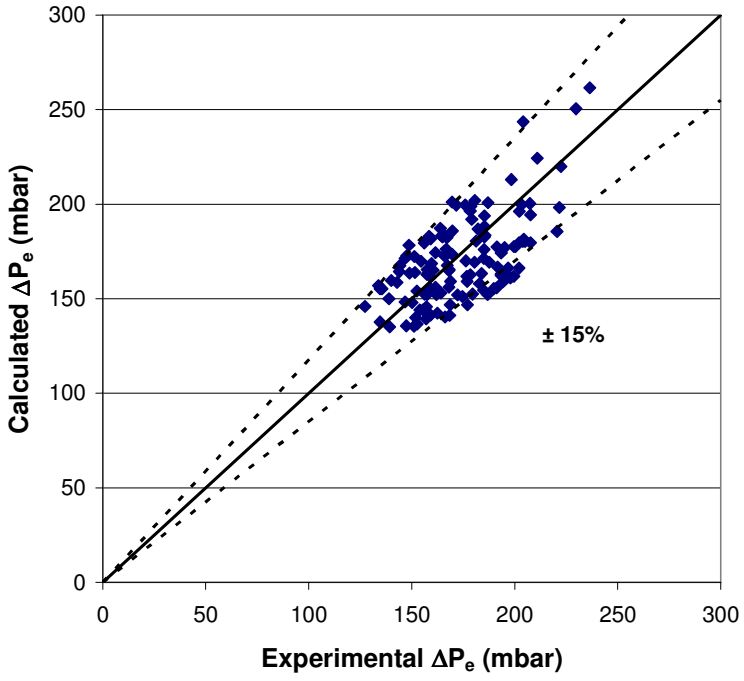

Figure 6-6: Calculated vs. experimental entry loss pressure drop values for alumina conveying.

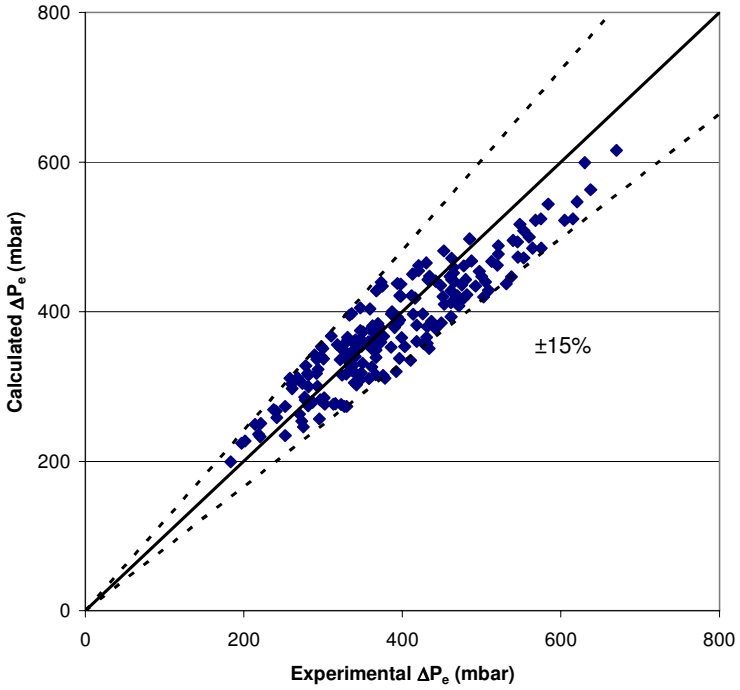

Figure 6-7: Calculated vs. experimental entry loss pressure drop values for barytes conveying.

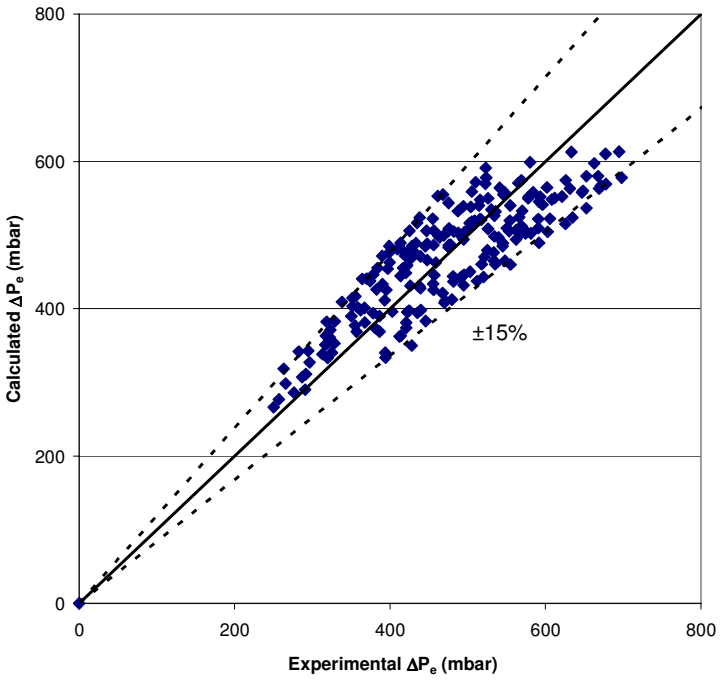

Figure 6-8: Calculated vs. experimental entry loss pressure drop values for cement conveying.

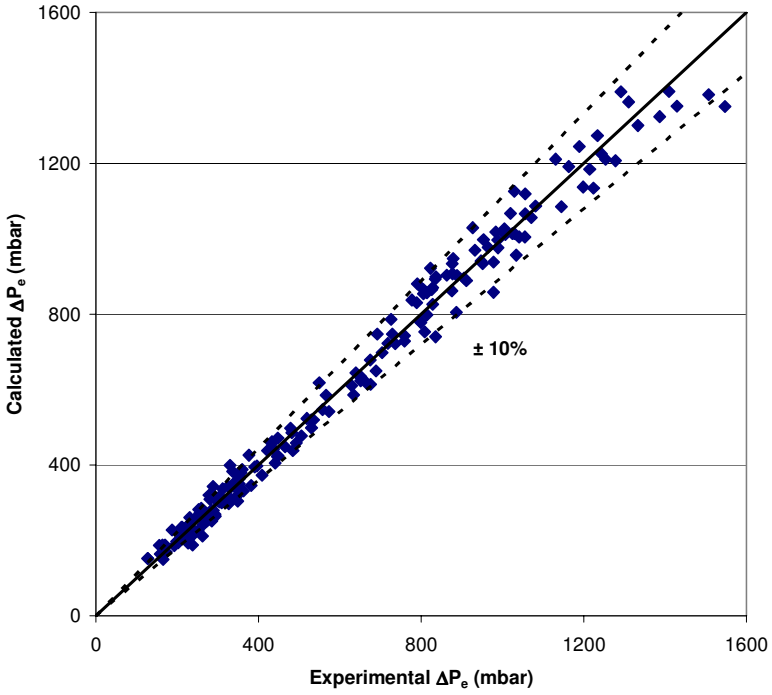

Figure 6-9: Calculated vs. experimental entry loss pressure drop values for ilmenite conveying.

As shown in Figure 6-6 to Figure 6-9, ± 15% accuracy level could be achieved with alumina, barytes and cement, while much better results of ± 10% was obtained for ilmenite. According to the validation curves, one can clearly see that the data points are equally distribute around the centre line. Since the experiments covered a large range of conveying conditions in terms of solids loading ratio, transport velocity, etc., this is a significant achievement, especially with a simple and straight forward method.

6.7.2 Analytical Comparison

In another approach, the results of model validation was analysed using some statistical tools. Generally, statistical parameters give the information of cumulative performance of the models. Under this analysis, the worst case error and the standard deviation of model prediction was considered. In addition, an average absolute deviation of percentage error was also used as another tool for comparison. The

definitions of these terms were briefly described under the Section 4.8.2.2. Table 6.3 shows the results of the statistical comparison.

Table 6.3: Results of the statistical analysis.

Material	**Error (mbar)** $e_i = P_{\exp} - P_{cal}$			**Average Absolute Deviation of Percentage Error (%)** $\lvert\overline{e}\rvert = \frac{1}{N}\sum_{1}^{N}\lvert\%e_i\rvert$
	Maximum e_i	**Minimum** e_i	**Standard Deviation** σ_e	
Alumina	37.7	-39.3	11.0	9.6
Barytes	93.9	-66.5	10.2	9.4
Cement	116.3	-91.6	10.6	9.3
Ilmenite	125.4	-102.9	7.0	5.5

According to Table 6.3, the worst case error of model prediction was comparatively low in cases of alumina and barytes conveying while the highest values of maximum error is related to ilmenite. During the experiments, it was noticed that the entry pressure loss values of ilmenite conveying were higher than that of the rest of the bulk materials. This may explain the highest worst case error in case of Ilmenite. But, as one can see in Table 6.3, the lowest values of standard deviation of error and average absolute deviation of percentage error are also applicable to ilmenite. The average absolute deviation of percentage error was always less than 10% while the standard deviation of the error was around 10-11 mbar. However, as an overall performance, the model prediction could be seen as quite promising.

6.8 Conclusion

The model for prediction of entry pressure loss in a top discharge blow tank situation, derived using dimensional analysis promises to be a very useful and reliable scaling up tool, which can be used in conjunction with the pressure drop prediction technique proposed in Chapter 4. The predicted values of entry pressure loss agree well with the experimental data. The model proposed here is very simple and needs only readily available experimental data without any complicated manipulation.

7 SCALING UP OF MINIMUM CONVEYING CONDITIONS IN A PNEUMATIC TRANSPORT SYSTEM

7.1 Introduction

The minimum conveying air velocity is one of the key parameters in the pneumatic transport of particulate bulk materials. An unnecessarily high conveying velocity will result in higher energy costs due to an increased pressure drop in the system, solids degradation, and pipe erosion that can result in an economically unattractive operation. On the other hand, systems designed with extremely low conveying velocities or extremely high solid flow rates are subject to erratic operation due to solids disposition or they may be completely inoperable because of blocking. Keeping gas velocity above minimum conveying velocity in all horizontal sections of a pipeline ensures no deposition of solids in the system and a continuous, safe and steady transport.

According to the description under Section 2, it was clear that many terms have been used to refer to minimum conveying velocity by researchers and designers of pneumatic conveying systems, over the years. Among them, minimum transport velocity [37, 168], saltation velocity [14, 34, 35, 89, 169], pickup velocity [34, 35, 89], critical velocity [170, 171], velocity at the pressure minimum point of the general state diagram [37, 39], stability limit [69], etc., are popular terminologies to define the lowest safe gas velocity to convey the particulate materials in a pipe system. Definitions of these terms are based on visual observations and pressure drop measurements, and they are often applied to indicate some transition in the way, in which the particles are moving or begin to move.

Although quite a few scaling up techniques [16, 25, 42, 95, 101] are available in the literature, there still remain some doubt whether they address the important issues of the minimum conveying velocity properly. Specially, after the findings of few researchers, like Yi et al. [172], it has been revealed that the existing models are not

good enough to address the conveying of fine bulk materials. In a review paper, Yi et al. [172] evaluated the influence of particle properties, pipeline configuration and conveying conditions on minimum conveying velocity by comparing 11 recommended correlations. They found that the predictions showed quite different trends for variations in particle diameter, particle density, gas density, gas viscosity and temperature. In case of fine bulk materials (<100 μm approximately), the scatter in the predicted values was so significant that they could not provide any reliable minimum conveying velocity for industrial application. Hence there exists a need for developing a technique for prediction of minimum conveying velocity for such bulk powders.

In the process of formulating a complete scaling technique, a special attention was paid to formulate a model to scale up the minimum conveying condition together with other important issues like conveying line pressure drop and entry section pressure drop discussed in earlier Chapters 4 and 6.

This chapter presents the results and findings of the investigation on minimum conveying velocity with respect to different bulk materials conveyed in different pipe configurations. In addition, the performance of the proposed model was compared with some other correlations, which could readily be used in scaling up and determination of minimum conveying velocities. Four materials including one with five different qualities have been tested in four different pipeline configurations with respect to pipe length and diameter.

7.2 Background

The literature survey described under the Chapter 2 revealed that numerous theoretical and empirical correlations [14, 34-38, 89, 90, 94, 146, 168-171, 173-183] have been developed for the prediction of minimum conveying velocity. Some of them [34, 35, 89, 180] require particular information about the single particle behaviours, which needs special experimental measurements. On the other hand, some correlations [14, 171] need graphically determined parameters. Similarly, some correlations [170, 171, 179, 181] are based on parameters, which do not have

properly accepted procedures of determination (e.g. solid friction factor etc,). Among the well accepted models, few correlations, which are rather simple and straightforward, have been selected for comparison with the model proposed under the current investigation.

7.2.1 Rizk method [38, 176]

In his investigation on horizontal pipe sections using pipelines of 50 mm, 100 mm, 200 mm and 400 mm diameter, Rizk proposed the following relationship between the minimum conveying velocity and solids loading ratio to determine the pressure minimum curve defined as the minimum conveying curve.

$$\mu = \frac{1}{10^{\delta}} Fr_{\min}^{\chi} \tag{7.1}$$

where, Fr_{min} is the Froude number related to the minimum transport velocity.

Here the values of exponents δ and χ should be determined by the following equations

$$\delta = 1.44 d_p + 1.96 \tag{7.2}$$

$$\chi = 1.1 d_p + 2.5 \tag{7.3}$$

where, 'd_p' is the particle diameter in millimetres.

7.2.2 Hilgraf method [175, 182, 183]

In an attempt to define the boundary limits of pneumatic conveying system, Hilgraf [175, 182, 183] found that the minimum conveying velocity depends on the pipeline diameter, the absolute value of conveying pressure and the qualities of conveying material. He formulated a relationship between these parameters, which can be presented as shown in equation (7.4).

$$v_{\min} = K^* \frac{D^k}{P^l} \tag{7.4}$$

where, K^*, k and l are defined as material dependent numerical constants and proposed to use minimising sum of square error method to determine those.

7.2.3 Wypych method [174]

Wypych and Reed [174] used an empirical method to find out the minimum transport velocity in the process of designing stepping pipelines. Specially for the purpose of scaling up of pneumatic conveying characteristics, they proposed the following equation for the minimum conveying velocity for a given product, by using dimensional analysis method.

$$u_{g,\min} = x_1 \mu^{x_2} \rho_g^{x_3} D^{x_4} \tag{7.5}$$

where, x_i are the coefficients to be determined by minimizing sum of square error method.

7.2.4 Matsumoto method [37]

Matsumoto et al. [37] tested three different granular materials (glass beads, copper beads and polystyrene) in two different pipe sizes (26 mm and 49 mm) with the aim of determining the mean air velocity required to prevent the settling of particles on the bottom of a horizontal pipe. Their correlation for the minimum conveying velocity can be shown in the following equation (7.6).

$$U_{sm} = 3.4\sqrt{gD}\left(\frac{\rho_a}{\rho_s}\right)^{0.294}\left(\frac{v_t}{\sqrt{gd}}\right)^{1.02}\mu^{0.277} \tag{7.6}$$

Where; U_{sm}: minimum superficial air velocity

7.2.5 Doig & Roper method [169]

By plotting the Froude number of the gas-solid mixture against solid loading ratio, they identified a relationship between these two parameters. Their correlation in dimensionless form is given in equation (7.7).

$$v_{\min} = (gD)^{0.5}\,\mu^{0.25}\,10^{\left(\frac{u_t - 0.61}{8.54}\right)} \tag{7.7}$$

7.2.6 Martinussen's model [36]

Martinussen [36] used experimental set-up of 15m long horizontal pipeline with 53 mm bore. The fluid analogy was applied to develop a model for the prediction of when blockage will occur in pipeline and a model was proposed to determine the minimum conveying velocity.

$$v_{\min}^2 = KDg\frac{\rho_b}{\rho_a}\left[1-\mu\frac{\rho_a}{\rho_b}\right]^3 \qquad (7.8)$$

where K; geometrical factor = $\pi/4$ at the filling level of $D/2$. This gives better predictions for fine materials since the effect of the permeability has not been included.

7.3 Test Setup and Material

As explained under the section 7.1, this investigation was carried out as a part of the main task to formulate a complete scaling technique for the pneumatic conveying system design.

7.4 Theoretical Consideration

The main objective of this work is to formulate a possible scaling up procedure for the minimum conveying boundary that can be graphically shown in typical pneumatic conveying characteristics as shown in Figure 7-1.

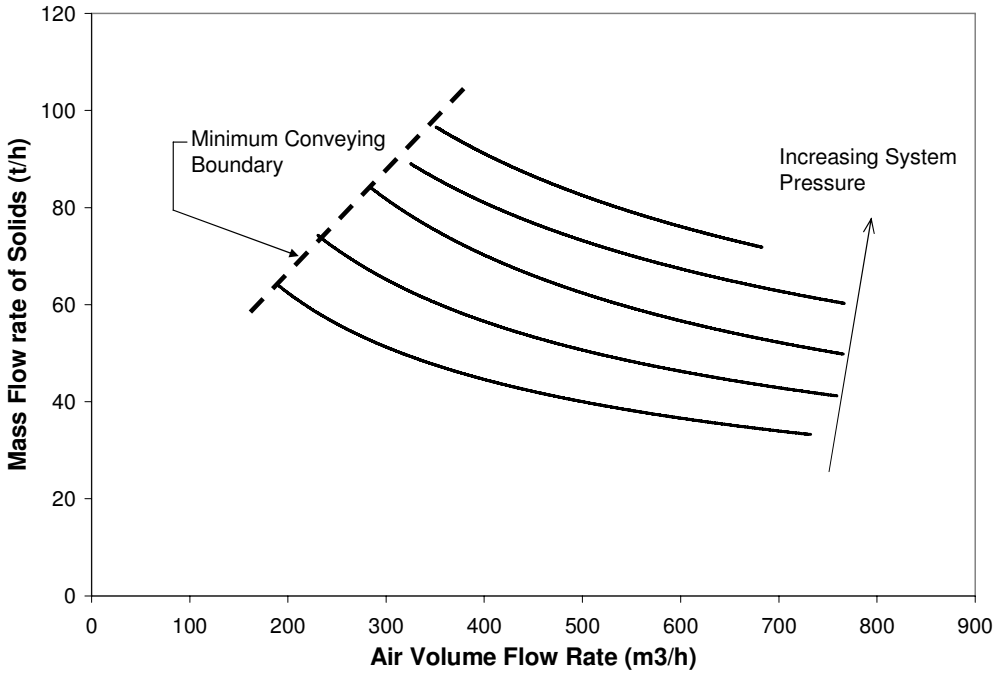

Figure 7-1: Typical pneumatic conveying characteristics of a particulate material.

In this investigation, the minimum conveying velocity is defined as the lowest possible air velocity that can be applied at the inlet to the conveying pipeline, for given conveying pressure. Hilgraf [175] and Wirth and Molerus [4, 171] also used the same concept for their investigations, but they have used different terminologies like limiting velocity, critical velocity, etc,.

7.4.1 The Influential Variables

Similar to the other problems pertinent to pneumatic conveying systems, the major challenge that the researchers and system design engineers face in modelling the minimum conveying velocity is the diversity of the influential parameters.

The list of variable that could be considered as relevant for the minimum conveying velocity under the present investigation is given below;

1. Pipe diameter (Dt)
2. Pipe length (L)
3. Mean particle diameter (ds)

4. Particle density (Rhos)
5. Solids mass flow rate (Ms)
6. Air volume flow rate (Ma)
7. Density of air (Rhoa)
8. Solids loading ratio (SLR)
9. Blow tank pressure (BTP)

For the convenience of referring the variables in later data analysis stages, the notations corresponding to each variable (given in parenthesis) will be used. In the model formulation, there are, basically, three major steps as listed below;

1. Screening of relevant physical characteristics, using a mathematical tool called 'Principal Component Analysis (PCA)' described in multivariate data analysis [184]
2. Use of the concept of dimensional analysis [164, 166] to formulate a functional relationship between the most important parameters.
3. Utilising the experimental measurements to establish the exact relationship.

7.4.2 Use of Multivariate Data Analysis

'Principal Component Analysis (PCA)' is a multivariate statistical procedure that transforms a number of correlated variables into a smaller number of uncorrelated new variables called 'Principal Components (PC)'. The concept of principal component is also used in regression methodology in same line as Multiple Linear Regression (MLR). This regression technique is generally termed as 'Partial Least Squares Regression (PLS-R)' or in popular terminology 'PLS', which has also been interpreted as 'Projection to Latent Structures'. These tools and concepts are described in Ref. [184], in details.

However, PLS technique facilitates to identify the 'Loading Weights' of independent variable in the process of building a regression relationship between dependent and independent variables. These loading weights could be graphically represented in terms of considered principal components. Each independent variable has a loading weight along each model component. All the data analysis operations in the present

investigation were carried out with the help of a software package called 'The Unscrabler®' [184].

The loading weights describe how much each variable contributes to explaining the response variation along each model component. Generally, they can be used to represent the relationship between independent and dependent variables. These loading weight plots could be easily used to identify the most important variables among all other assumed parameters at the starting of model formulation. A similar technique could be seen in Ref. [185] where these data analysis tools were effectively used for variable reduction in model formulation.

7.4.3 Data Analysis Trials

Few simple multivariate data analysis trials were carried out with the help of the Unscrabler® using experimental data. In this stage, the experimental observations relevant to a particular conveying material were chosen for the preliminary data analysis process.

Initially, the experimental measurements of the variables listed under section 7.4.1 were taken into account together with the corresponding velocity values. Special attention was paid to consider the data relevant to extreme conveying conditions, which correspond to minimum conveying air flow rate or the maximum solids loading conditions. It is reasonable to take these observations as the experimental data applicable to minimum conveying condition, since special care was taken during the tests to obtain the lowest possible conveying air flow rates, which were nearly the blocking limits of each conveying materials.

7.4.3.1 PCA

Initially, the experimental data were tested with PCA technique to find out the required number of PC to explain most of the information of the considered problem. It could be noticed that the data relevant to different materials behaved in almost similar way in PCA testing. For the convenience of presentation, the results of cement data are only given and described.

The classical PCA is vulnerable with respect to outlying observations. Even one massive outlier can heavily influence the parameter estimates of the method. It is thus important to identify and remove the outliers in all analysis methods involved with PCs. This can easily be carried out with the help of the software used, the Unscrabler®.

One typical variance curve is shown in Figure 7-2.

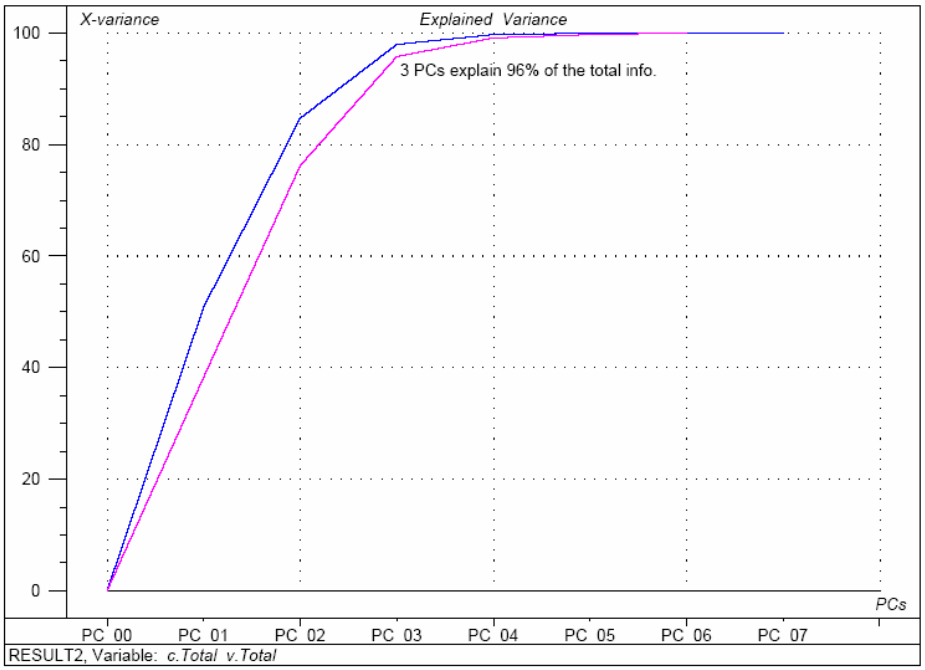

Figure 7-2: Variance plot of PCA relevant minimum conveying conditions of cement.

From Figure 7-2, it is clear that three PCs explain about 96% of the information considered in the analysis. Thus in later analysis, only the first three PCs were considered.

In the next step, the loading plot, which tells about the influence of different variables to the considered PCs was taken into account. The loading plot relevant to cement conveying is shown in Figure 7-3.

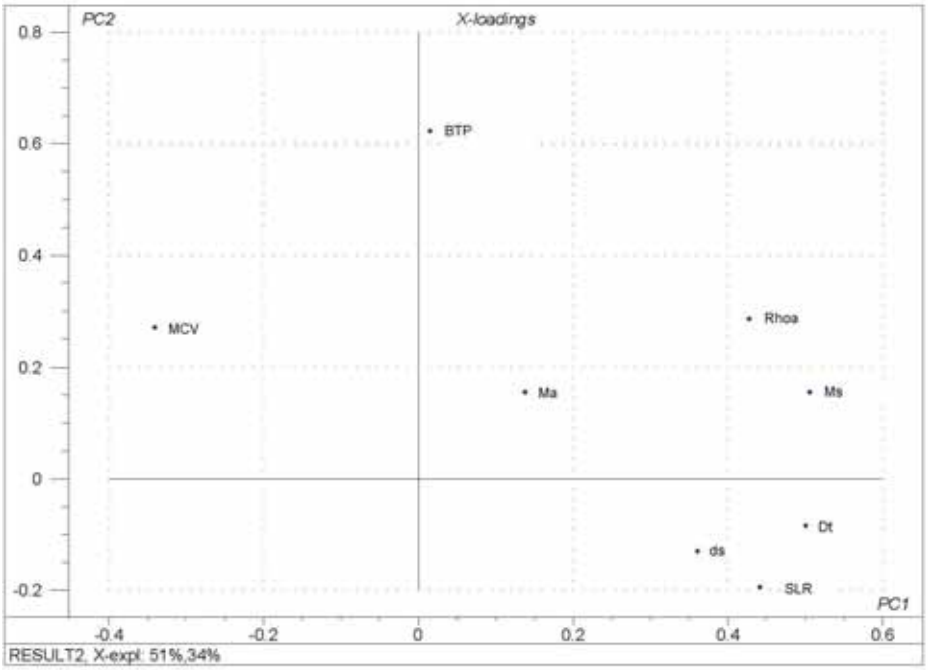

Figure 7-3: The loading plot from PCA for cement conveying data.

According to Figure 7-3, it could be assumed that the first PC (PC1) corresponds to the minimum conveying velocity and other variables close to horizontal axis have significant influence to PC1. Although some other information is also possible to reveal with respect to the other PCs, they are not very important in this course of analysis.

7.4.3.2 PLS Regression

In PLS regression, all variables given in section 7.4.1 were considered as the X-variables while minimum conveying velocity was taken as the dependent variable or Y. Considering three PCs, the PLS model was defined.

Usually, the loading weight plot tells, which variables are most important to predict the Y-variable. Here also, all bulk materials showed some approximately similar behaviour. Figure 7-4 shows the loading weight curve relevant to cement conveying.

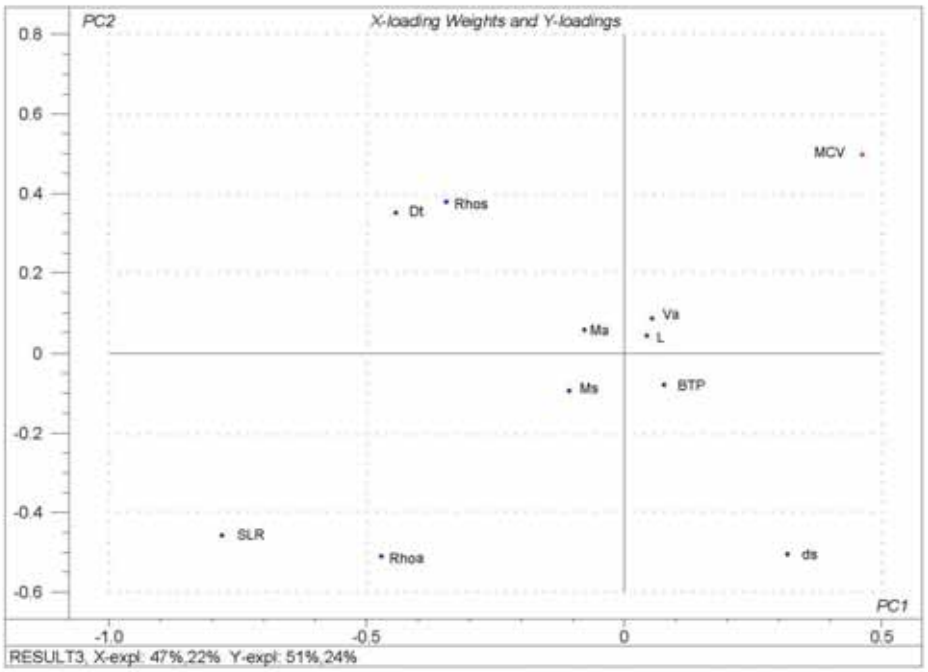

Figure 7-4: Loading weight plot of PLS regression for cement conveying data.

Since the loading weights show how much each X-variable contributes to dependent Y-variable, the variables, which lie close to the origin of loading weight plot could be considered as comparatively unimportant variable for the phenomenal description. According to Figure 7-4, it could easily be concluded that the most influential parameters of the minimum conveying velocity are; solids loading ratio, pipeline diameter, conveying air density and particle density.

7.4.4 Determination of Dimensionless Groups

After recognizing the most influential parameters to minimum conveying velocity, the next step is to put them together in a systematic way so that an effective functional relationship between them could be derived. As discussed under the chapter 4, dimensional analysis can play a vital role in such applications. Since at this stage, the number of parameters is comparatively less, it is convenient to form few dimensionless groups out of the relevant parameters.

As explained in Ref. [164], it is even possible to simply form the $\prod$ groups by inspection, without resorting to the more formal procedure. According to the basic

requirements of dimensional analysis, the following functional relationship could easily be formulated by simply manipulating the variables identified under the Section 7.4.3.2, in the correct way.

$$\frac{Fr_{start}}{Fr_T} = f(\mu) \tag{7.9}$$

where, Fr_{start} and Fr_T are the Froude numbers related to the minimum conveying velocity and terminal velocity respectively. They could mathematically be presented in following forms:

$$Fr_{start} = \frac{v_{start}}{(D_t g)^{0.5}} \tag{7.10}$$

$$Fr_T = \frac{v_T}{(d_p g)^{0.5}} \tag{7.11}$$

In equation (7.11), terminal velocity; v_T could be determined according to ref. [6].

7.5 Test Results

All materials except five qualities of alumina were tested in all different pipeline configurations. Only pipeline 'E' (see Figure 4-5) was used for the five different qualities of alumina. During the experimentations, special attempts were made to obtain the minimum conveying conditions for each material (material quality) using different pipeline configurations. The maximum loadings and minimum conveying velocities for different material conveying in different pipe sizes are presented under the Section 4.6.2.

The lowest velocity that could be achieved for transportation of barytes, cement and ilmenite was approximately in the range of 1.4-2.4 m/s. In case of different alumina qualities, this value was within the range of 5.8-8.8 m/s. For a particular material, experimental results relavant to extream conveying conditions were considered for this analysis. These points are graphically shown in Figure 7-1 by the conveying boundary and the minimum velocity values were calculated considering corresponding pressures and air volume flow rates. These data were then used for the verification described in next section.

7.6 Model Verification with Experimental Results

The experimental data were used to verify the model formulated under the section 7.4. The values of the dimensionless parameter in equation (7.9) were calculated for different conveying conditions and presented in graphical form as shown in Figure 7-5 to Figure 7-8. A strong relationship between the Froude number ratios and corresponding solids loadings could be seen. The fitted power curves for the relationship of equation (7.9) showed high degrees of fitting (R^2) and the coefficients of model curves are given in Table 7-1.

In further analysis, it could be noted that the curves of Froude number vs. solids loading ratio show a quite similar trend of power-law relationship (i.e., form of $y = C x^p$) for different bulk materials. In addition, the curves corresponding to different diameters of conveying pipes were overlapping each other in case of a particular conveying material. This phenomenon could be clearly seen in the following Figure 7-5 to Figure 7-8, which present the variation of Froude number ratio vs. solids loading ratio for different bulk material.

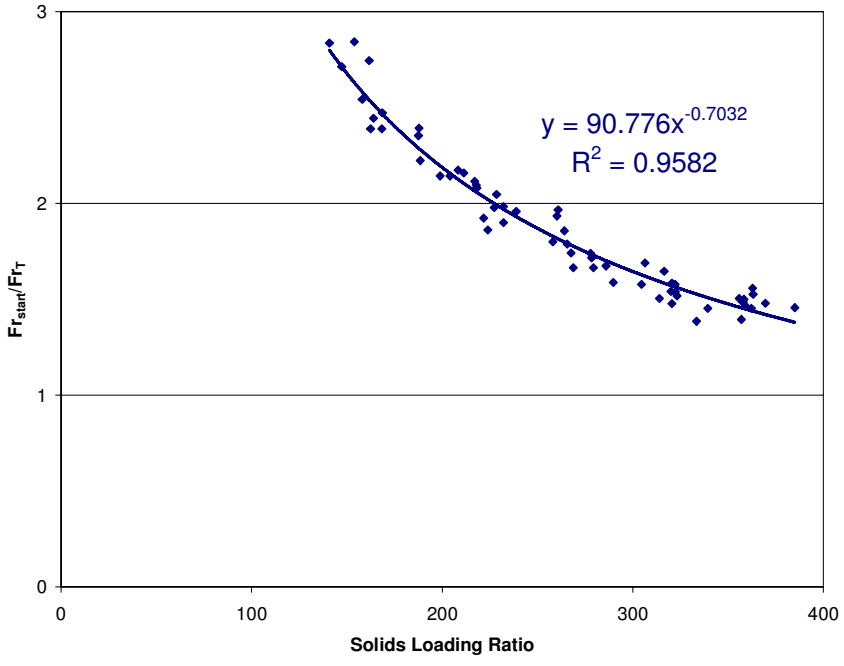

Figure 7-5: Variation of Froude number ratio vs. solids loading ratio for barytes conveying.

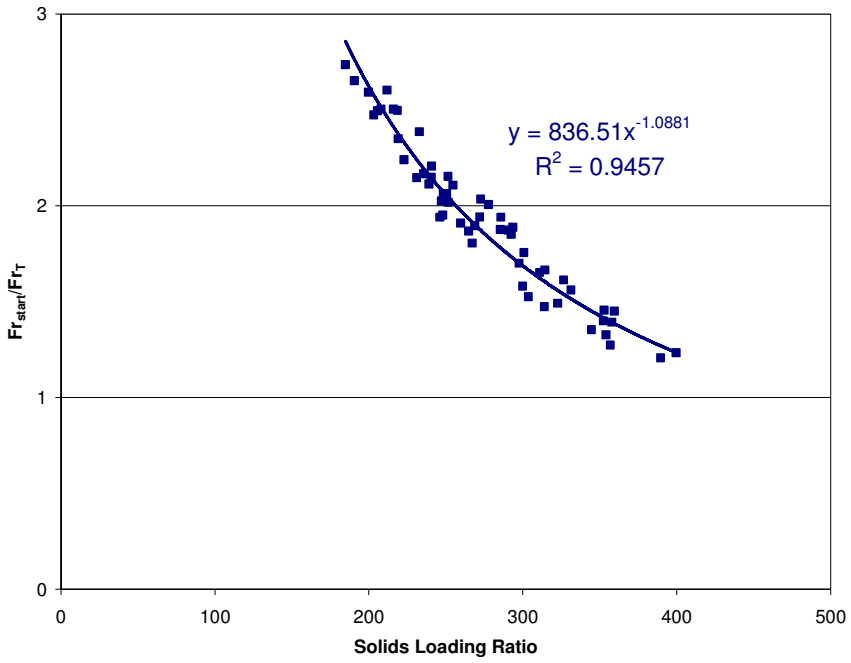

Figure 7-6: Variation of Froude number ratio vs. solids loading ratio for cement conveying.

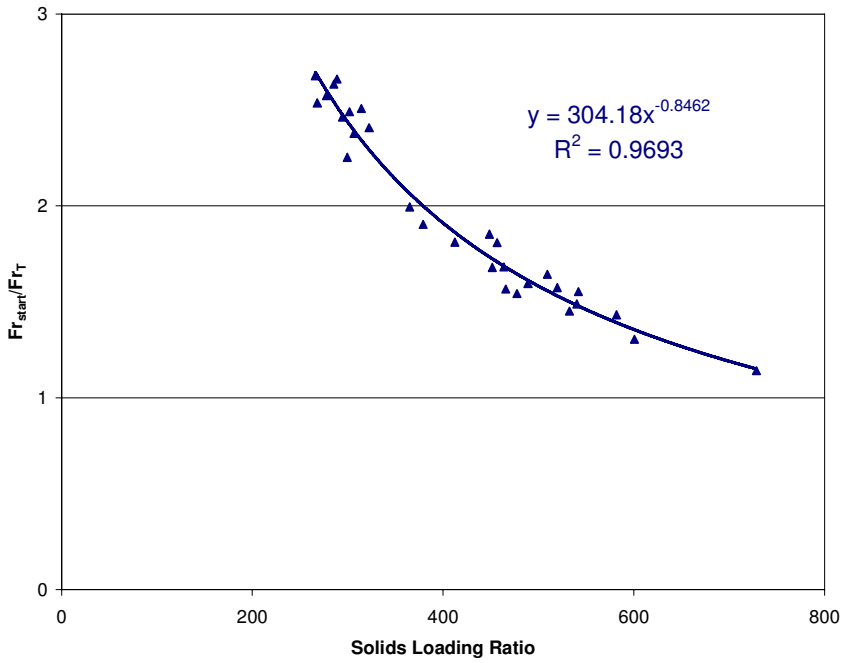

Figure 7-7: Variation of Froude number ratio vs. solids loading ratio for ilmenite conveying.

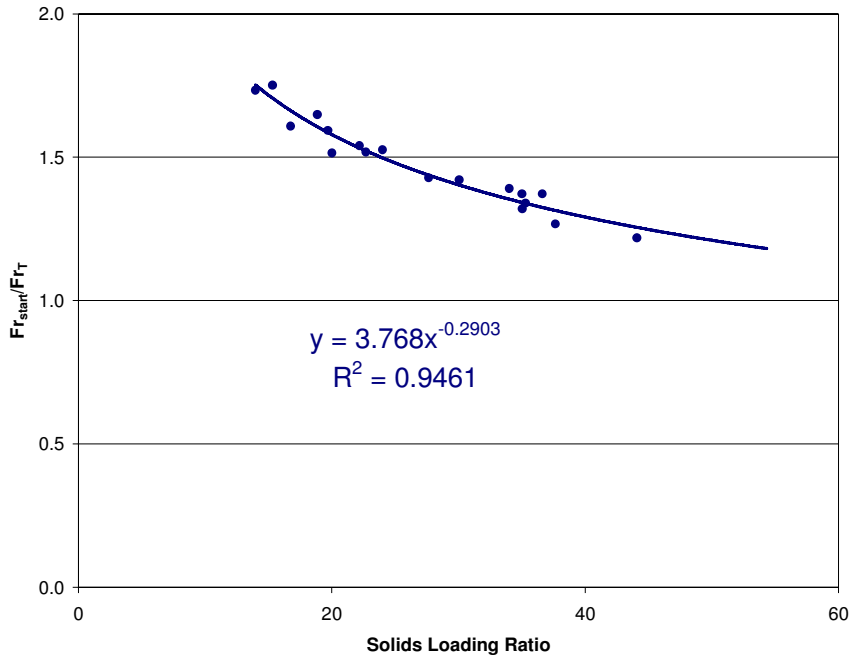

Figure 7-8: Variation of Froude number ratio vs. solids loading ratio for alumina conveying.

As one can see, the R^2 values of curves are around 0.95 for all different material. According to the best fitted curves shown in Figure 7-5 to Figure 7-8, the equation (7.9) could be re-written in the following form.

$$\frac{Fr_{start}}{Fr_T} = A(\mu)^B \qquad (7.12)$$

Table 7-1 shows the numerical values of the constants of the equation (7.12) for different bulk material.

Table 7-1: Experimentally found constants of the Equation (7.12).

Conveying Material	A	B
Barytes	90.776	-0.7032
Cement	836.51	-1.0881
Ilmenite	304.18	-0.8462
Alumina	3.768	-0.2903

This finding is possible to use as a tool for scaling up of minimum conveying velocity. When the relationship is fixed with the experimental results of a particular pipeline (diameter), the minimum conveying velocity can be determined for other pipe sizes for the same conveying material. The following equation shows the general form of the minimum conveying velocity determination formula.

$$v_{\min} = A' v_T \left(\frac{D_t}{d_p} \right)^{\frac{1}{2}} \mu^{B'} \qquad (7.13)$$

Where A´ and B´ are the material dependent constant that has to be determined using the pilot plant test.

7.7 Validation

To validate the proposed relationship, some of the experimental data points were selected and based on those data, the minimum conveying velocity relevant to the rest of the test conditions were predicted. Having conveyed in all pipe configurations, all materials except alumina generated quite a large number of data points. It was possible to consider the data relevant to one pipe size and based on that to predict the minimum conveying velocities for other pipe sizes. For barytes, cement and ilmenite, the data generated by 75mm pipe were scaled up to calculate the minimum conveying velocities relevant to the tests with 100mm and 125 mm pipe sizes. The data generated by one quality of alumina (alumina 2) were used to

calculate the lowest possible velocities of other alumina qualities. Finally, the calculated minimum conveying velocities were compared with the corresponding experimentally measured values. Since the minimum conveying velocities of alumina were little higher than the other materials, two graphs have been used to present the results so as to show them clearly. Figure 7-9 and Figure 7-10 show the calculated minimum conveying velocity vs. experimentally measured minimum velocity graphs for all materials. The predicted values were within the error band of ± 10% of the experimental measurement for barytes, cement and Ilmenite, while much better results of ±7% error margin were obtained in case of alumina.

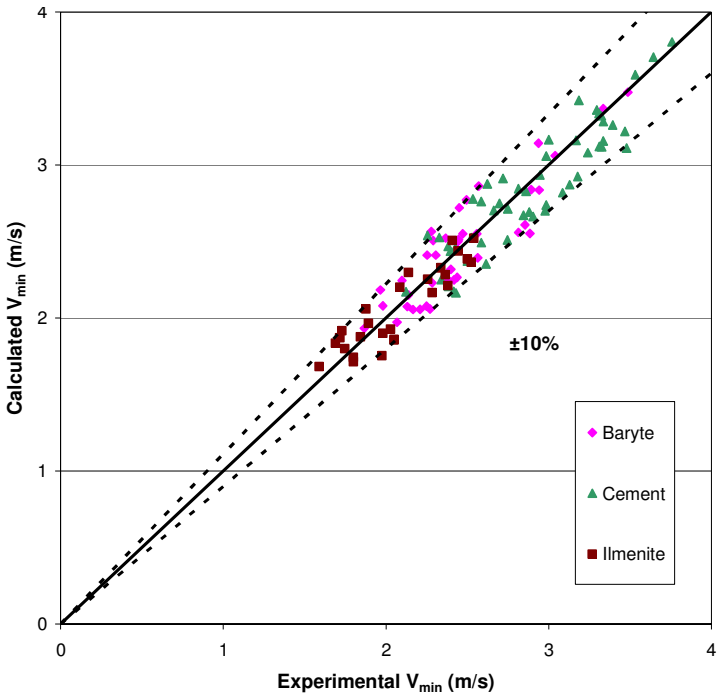

Figure 7-9: The graph of calculated vs. experimental minimum conveying velocity for conveying materials; barytes, cement and ilmenite.

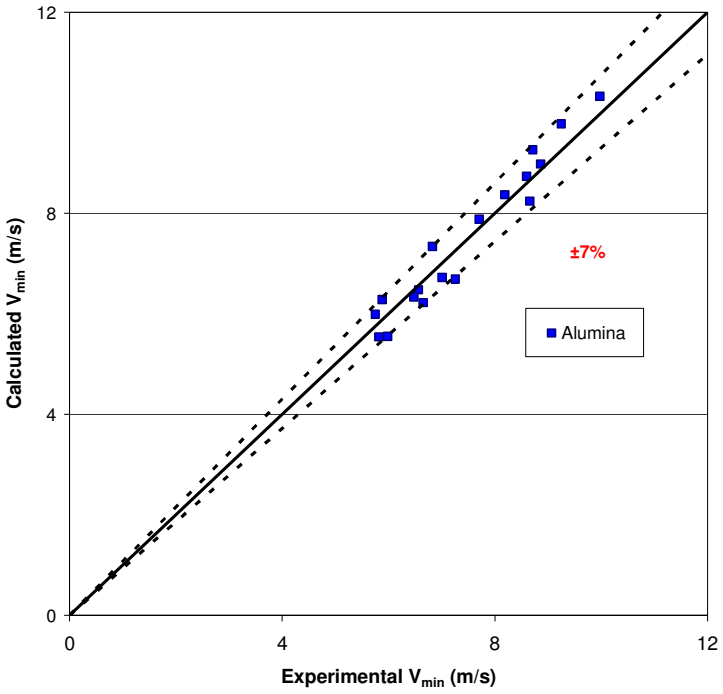

Figure 7-10: The graph of calculated vs. experimental minimum conveying velocity for alumina.

7.8 Comparison with Others Models

To compare the prediction of proposed model with the other correlations described under section 7.2, the same experimental data points were considered and the prediction were made with the help of different correlations. The calculated values of minimum conveying velocities were compared with the corresponding experimentally measured values. In this cause of comparison, basically three tools were used; worst case errors (maximum values of over-prediction and under-prediction denoted by e_{max} and e_{min} respectively), standard deviations of error (σ_e) and average absolute deviation of percentage error ($|\overline{e}|$). These statistical tools are described in details under the Section 4.8.2.2. The comparison results are shown in Table 7-2.

Table 7-2: The results of the comparison study.

Material	Parameter	Rizk	Hilgraf	Wypych	Matsumoto	Doig & Roper	SEM	New Model
Barytes	e_{max}	-2.19	0.86	0.96	1.26	1.33	-1.20	0.33
	e_{min}	-8.64	-0.36	-0.42	-1.98	-2.61	-19.01	-2.07
	σ_e	1.72	0.33	0.31	0.90	0.94	4.05	0.37
	$\lvert\overline{e}\rvert$	185.15	14.09	25.88	40.12	40.08	218.50	4.95
Cement	e_{max}	-2.35	1.22	0.84	0.56	0.93	0.47	0.37
	e_{min}	-8.31	-0.47	0.18	-2.66	-2.53	-12.12	-0.28
	σ_e	1.35	0.34	0.16	0.81	0.82	2.73	0.17
	$\lvert\overline{e}\rvert$	151.53	13.23	20.48	35.14	21.32	102.84	4.99
Ilmenite	e_{max}	-3.91	0.47	0.24	0.47	-0.43	-4.49	0.22
	e_{min}	-6.96	-0.27	-0.26	-1.09	-2.49	-14.90	-0.19
	σ_e	1.18	0.23	0.14	0.56	0.75	3.44	0.13
	$\lvert\overline{e}\rvert$	243.53	11.56	9.24	28.55	65.58	288.10	5.14
Alumina	e_{max}	6.38	2.66	2.69	2.12	8.48	2.33	0.57
	e_{min}	-4.68	-1.06	-1.04	-5.21	3.78	-2.08	-0.55
	σ_e	3.40	1.22	1.23	2.16	1.32	1.00	0.37
	$\lvert\overline{e}\rvert$	42.95	12.05	12.09	24.08	63.94	9.94	4.45

From Table 7-2, it is clear that most of the available models are not producing reliable predictions of minimum conveying velocity. When the predictions of available models are compared with each other, one can see that Rizk's model gives over predicted results in most of the cases. With reference to Rizk's publications [38, 176], this correlation can be used to predict the velocity corresponding to the pressure minimum condition, which he termed as saltation velocity. This terminology totally contradicts the definition of minimum conveying velocity of this publication. But, in quite a few research publications [172, 179, 180, 186], this model have been used to predict the minimum conveying velocity. This may be due to the controversy on how to define the minimum conveying velocity, as explained in Section 2.8. Wirth [171] discussed the difference between the pressure minimum velocity given by Rizk's equation and the critical velocity (that is how he defines the minimum conveying velocity) and claimed that the critical velocity is slightly smaller than the pressure minimum velocity.

Although Martinussen [36] claimed that his model is expected to give better predictions for fine materials than for coarse ones, his model gives the maximum over prediction among the all other models considered here. The model by Doig and Roper [169] gives all most similar results as Martinussen's, although the degree of over prediction is little less. The correlations of Matsumoto [175, 182, 183], Wypych [174] and Hilgraf [175, 182, 183] are performing in equal degree of accuracy. Although their models are claimed to be good for the scale up purposes, the calculated values are deviated much from the experimental measurements.

The proposed model in the present investigation gives the best results among the models considered. It gives ±10% error margin for barytes, cement and alumina while the accuracy level for alumina becomes ±91%. From Figure 7-9 and Figure 7-10, it is clear that the model performs well balanced without biasing to over prediction or under prediction. This is a considerably good achievement among the other discrepancies reported in the current investigation and some other publications [172] as well.

7.9 Prediction of Minimum Conveying Boundary in Experimental PCC

Using the proposed correlation, an attempt was made to predict the minimum conveying boundaries for different bulk materials and different pipeline configurations. For barytes, cement and ilmenite, the data generated by 75mm pipe were scaled up to calculate the minimum conveying boundaries relevant to the tests with 100mm and 125 mm pipe sizes. In similar way, experimental data of alumina 2 was used to determine the minimum conveying boundaries of other alumina qualities. The results were much compatible with the experimental measurements. The predicted minimum conveying boundaries have been super-imposed on the experimental pneumatic conveying characteristics of various combinations of conveying bulk materials and pipeline configurations and few of the resulted graphs are shown in Figure 7-11 to Figure 7-14, representing all tested materials and different pipeline configurations used in the present investigation. The rest of the conveying characteristic curves for other different combinations of conveying material and pipe configuration together with their minimum conveying boundaries determined by the proposed model are presented under Appendix B.

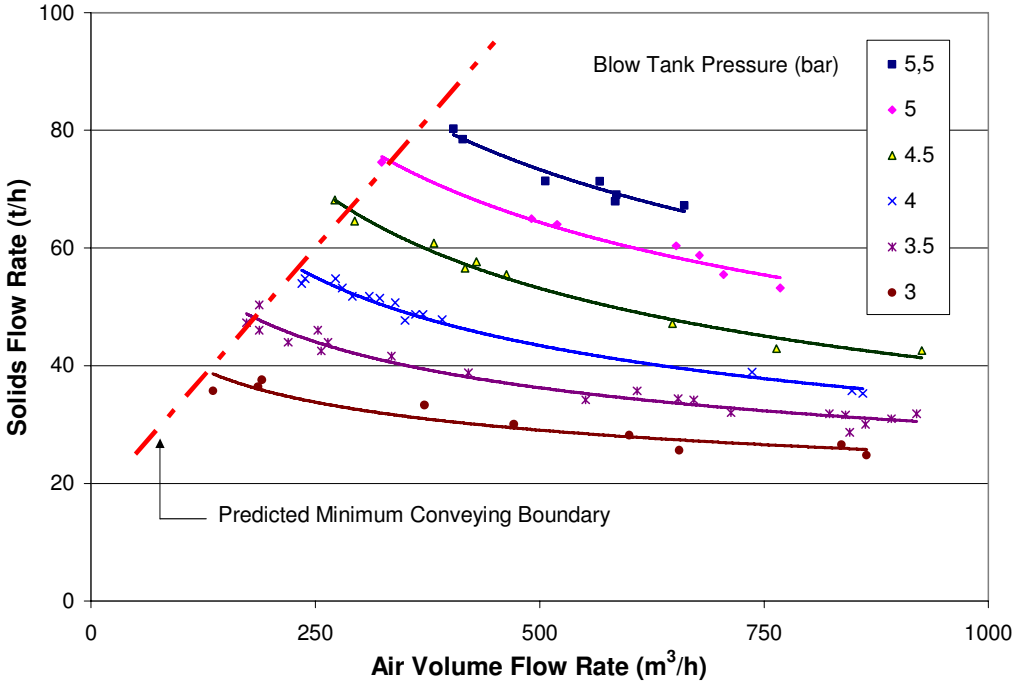

Figure 7-11: Pneumatic conveying characteristics of barytes in pipeline B with predicted minimum conveying boundary superimposed.

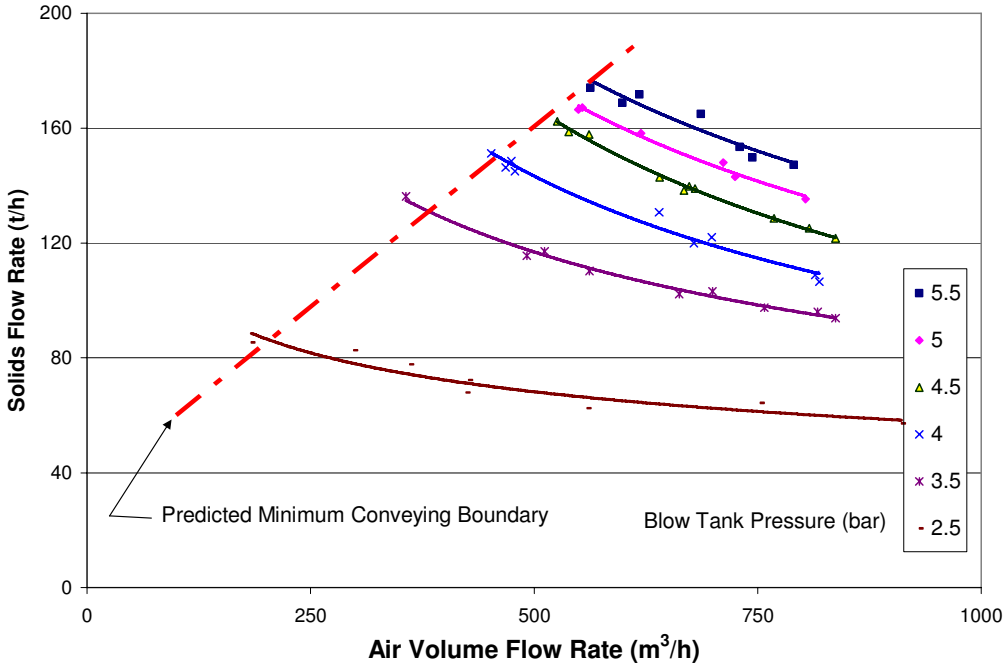

Figure 7-12: Pneumatic conveying characteristics of cement in pipeline C with predicted minimum conveying boundary superimposed.

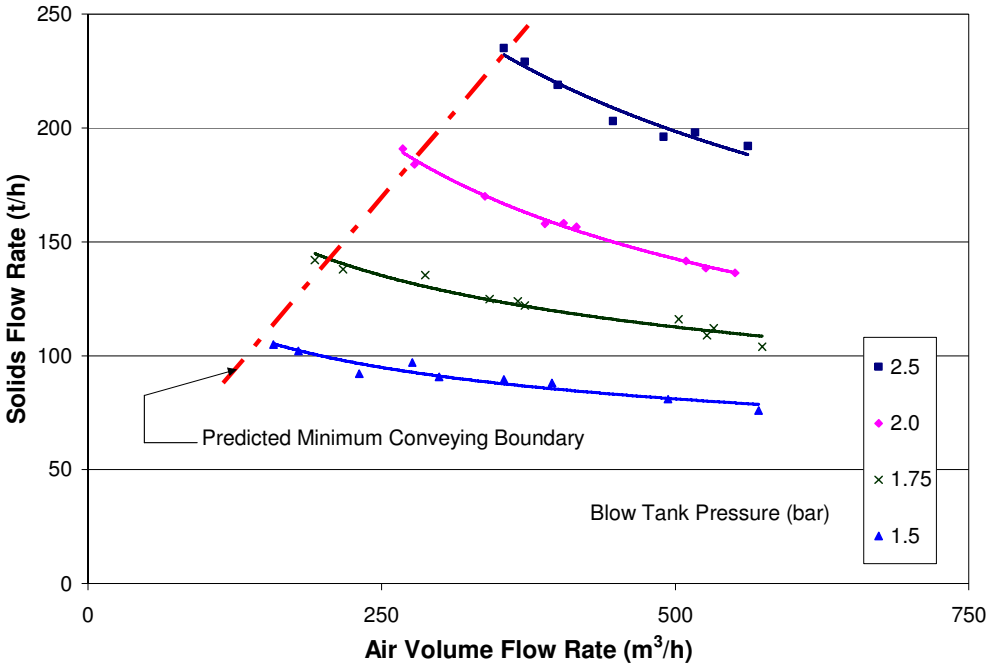

Figure 7-13: Pneumatic conveying characteristics of ilmenite in pipeline D with predicted minimum conveying boundary superimposed.

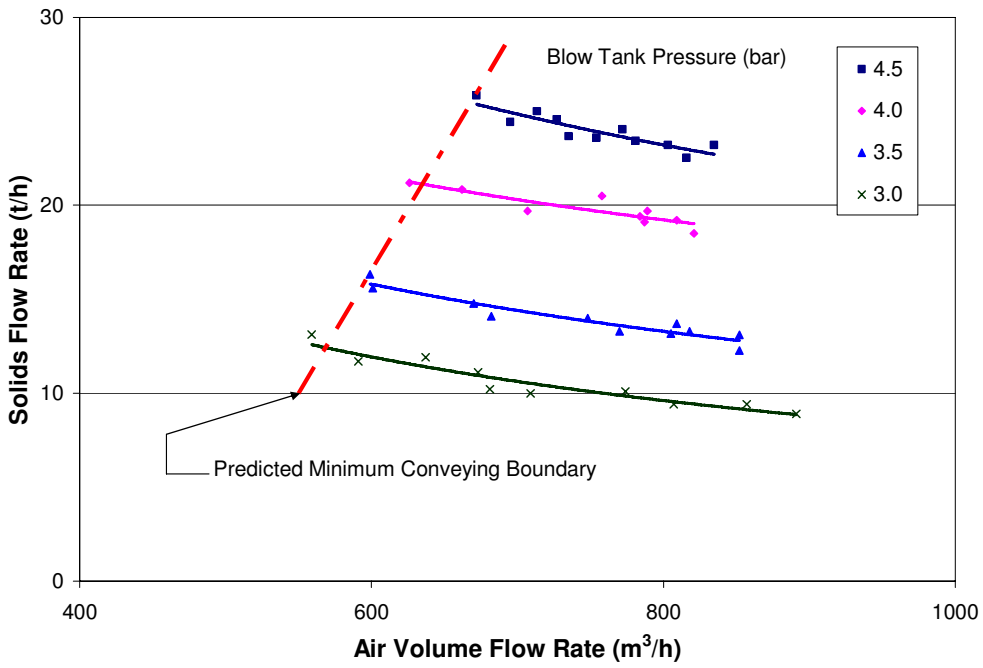

Figure 7-14: Pneumatic conveying characteristics of alumina 4 in pipeline E with predicted minimum conveying boundary superimposed.

One can clearly see that the minimum conveying boundary predicted by the proposed scaling model correctly shows the experimental limit of conveying.

7.10 Conclusion

According to Figure 7-9 and Figure 7-10, it is clear that using the proposed method, the minimum conveying velocity can be predicted with an accuracy of approximately ± 90%. This is a significant achievement amidst the large discrepancies reported [172] in the available correlations, specially, in case of fine powders (< 100 μm). As revealed during the comparison above, the proposed model is much superior to the other models considered under this study. Further, since the prediction matches fairly well with the experimental findings, this method seems to have a good potential for use as a reliable scaling tool in pneumatic conveying system designs, especially conjunction with the proposed scaling up technique under the Section 4.

8 PUTTING IT ALL TOGETHER AND A CASE STUDY

The scaling up model of line pressure drop and line entry pressure loss were combined together with the scaling up model of minimum conveying velocity to form a complete scaling up technique for pneumatic conveying system. With the aim of using them in designing of industrial scale pneumatic conveying systems, all these models were put together with the help of a computer programme to form a general calculation programme. The following sections are describing the structure of the software programme, calculation procedure adopted, etc, in detail. At the end of the chapter, the results of an investigation where the newly formulated calculation programme was used to determine the pressure drop and velocity of an industrial scale pneumatic conveying plant are given in a form of a case study.

8.1 Introduction

Since the calculation procedure consists of some sort of repetitive calculations, it was decided to set-up a computer based calculation programme that can be used as general software in pneumatic conveying system designs. As an initial step, Microsoft Excel® was used to formulate the general calculation programme.

The basic necessity of the calculation programme is that the results of preliminary conveying tests conducted in a laboratory scale pilot plant, are available for the conveying bulk material and all the relationships relevant to different scaling models proposed under the current investigation are known for at least one pipe diameter. The calculation software is programmed so that it easily calculates the pressure drop across each and individual pipe sections. In addition, the conveying velocity is also calculated.

To check the validity of the software programme, it was used in a design procedure of an industrial scale conveying system. The comparison of calculated and experimental results is presented at the end of the chapter.

8.2 General Calculation Programme

This calculation programme basically consists of four main sections;

1. Implementation of the model relationships formulated from the pilot plant tests for different pipe elements.
2. Introduction of design inputs together with provisional parameters
3. Pressure drop and velocity calculations
4. Presentation of output results

Each of the above stages is briefly described in following sections.

8.2.1 Implementation of Model Relationships

According to the conclusions made in relevant sections, it was clear that the relationships derived in Chapters 4, 6 and 7, were independent of conveying pipe sizes and the predictions could be made for different pipe sizes by just conducting a series of tests with conveying bulk material in one particular pipe diameter. Consequently, the calculation programme is based on the findings of the pilot plant tests and the experimentally found functional relationships of different parameters for individual pipe elements, as mentioned earlier. In cases of entry pressure loss and minimum conveying velocity, the numerical values of the functional relationships that are shown in equations (6.21) and (7.9) could be used in the calculation programme. In case of the scaling model for line pressure drop described in Chapter 4, the numerical constants of the functional relationship between the K and V^2_{entry} have to be introduced. In addition, the asymptotic constant value of K for high entry velocity values (see Figure 4-15 to Figure 4-20) and corresponding lowest velocities have to be used in the calculation programme.

All those parameters in numerical form are put in one sheet and it is named as 'Pilot Plant Test Results'. One screen shot of it is shown in Figure 8-1.

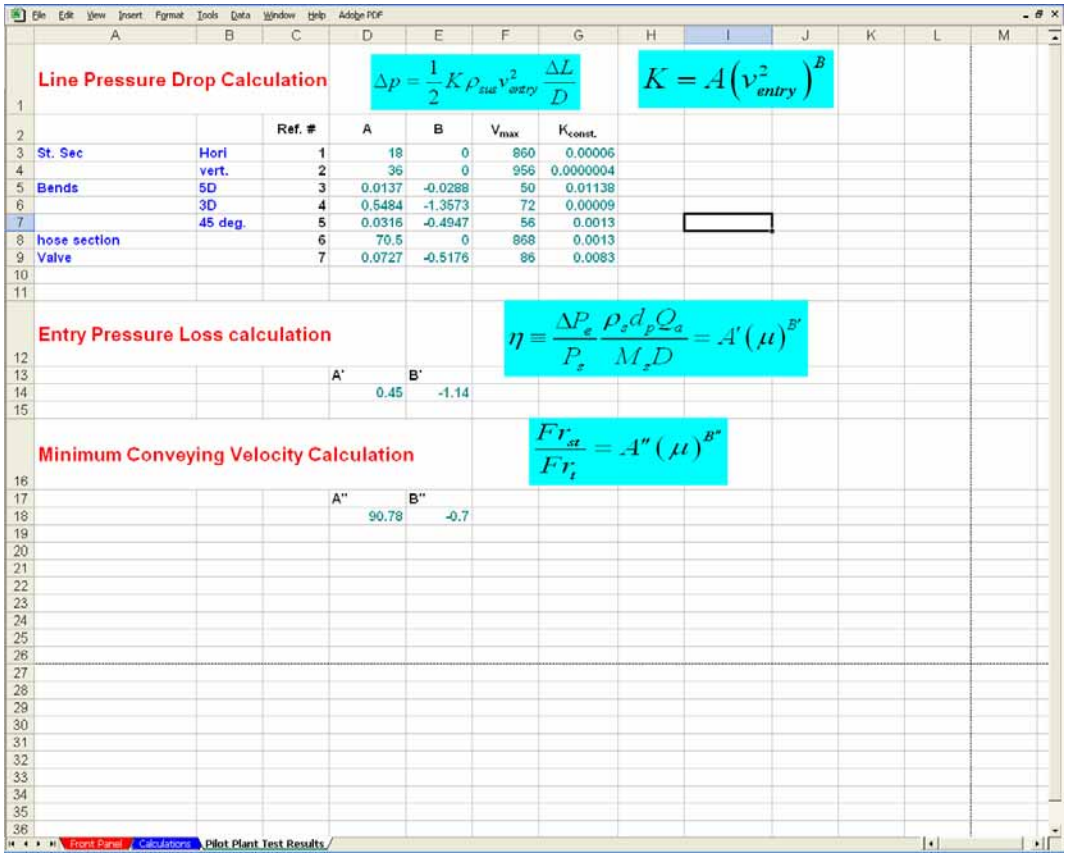

Figure 8-1: A screen shot of sheet where the pilot plants test results are given.

As shown in Figure 8-1, all the experimentally determined constants for conveying material are given in the sheet 'Pilot Plant Test Results'. Generally, this sheet is not needed, after the numerical constants from the pilot plant tests are fed to programme

8.2.2 Introduction of Design Input

The parameters required for the calculations are fed to the programme through the front panel. The user has to introduce, basically, three main groups of design information that can be categorised as below;

- Main design inputs
- Conveying material data
- Geometrical parameters of the conveying line

8.2.2.1 Main Inputs

The basic design parameters are considered under this category. The required capacity (mass flow rate of solids) of the plant, the supply air volume capacity of the available prime mover (compressor or so) and the suggested value of start blow tank pressure should be given by the user.

8.2.2.2 Material Data

The mean particle diameter and the particle density of the conveying bulk material have to be provided under this category.

8.2.2.3 Geometrical Parameters

The whole conveying line is considered as a combination of small components in this process of calculation. The straight pipe sections, pipe bends and other pipeline accessories like valves and flexible hose sections are considered as individual sections. The user has to determine the number of such sections in the pipeline layout. To identify the different sections, a special numbering system is used for identifying each section. Simultaneously, another numbering system is used to define the pipe diameter of the concerned section. All instructions about how to select the section and diameter identification numbers are provided in the front panel. When the user click the cell to assign a section identification number or a diameter identification number, the relevant number format is displayed as a special comment. A screen shot of front panel is shown in Figure 8-2.

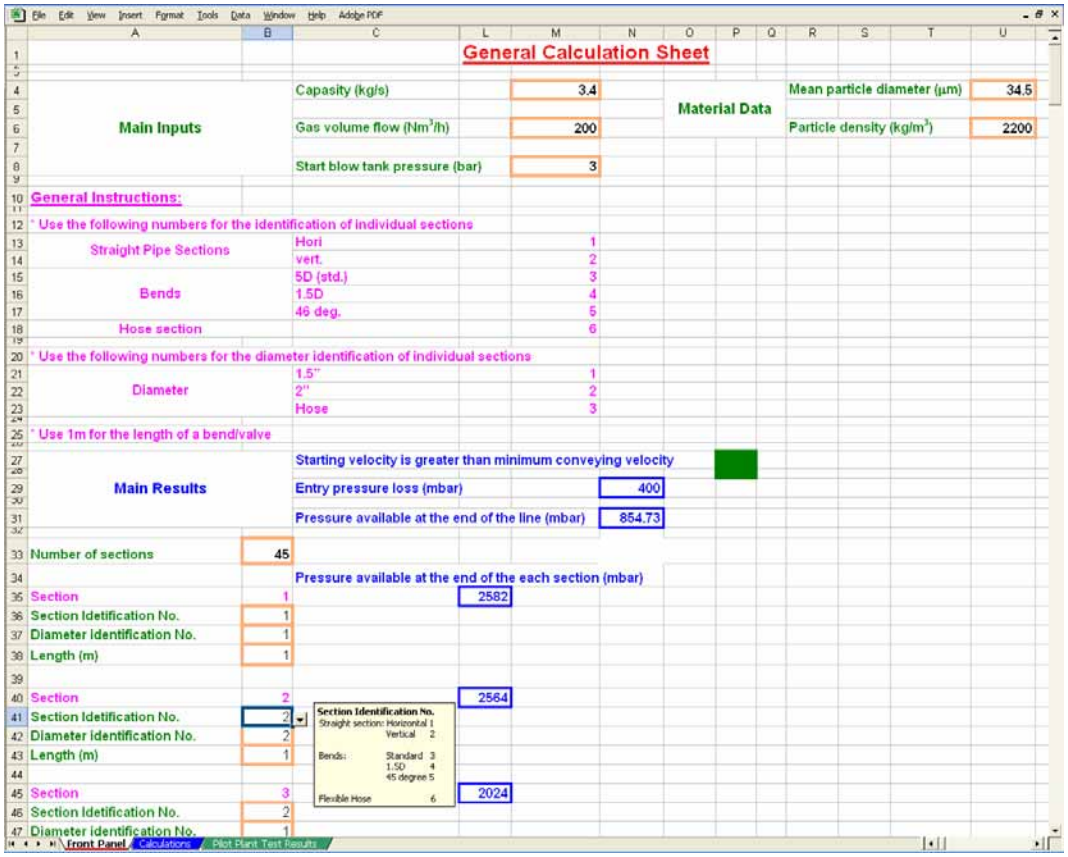

Figure 8-2: A screen shot of front panel of the calculation programme.

As shown in Figure 8-2, the cells framed with light double lines are the input cells and the user has to fill them properly according to the instructions given.

8.2.3 Pressure Drop and Velocity Calculation

There is a separate sheet to do the necessary calculations required to determine the pressure drops and relevant velocities. In the calculation procedure, the straight pipe sections are considered as combinations of short pipe sections of 1 m length. Bends and other pipe components are considered as individual elements.

The calculation procedure begins with the available pressure at the blow tank or the set pressure of blow tank. The entry section pressure drop is then calculated with the help of proposed model under Chapter 6 and according to the input data provided in the front panel. After calculating the pressure drop incurred in the entry section, the pressure available at the inlet of the consequent section is calculated by deducting the

entry loss from the available pressure in the blow tank. In next sections, pertinent pressure drops for each pipe sections are calculated according to the models proposed under Chapter 4. A kind of cell reference technique is used to take the appropriate data from front panel and required model constants from 'Pilot Plant Test Results' sheet. In the calculation process, the pressure values are updated after each and every pipe sections and the same calculation procedure continues until the end of the line.

In addition to the above described pressure drop calculation, the minimum conveying velocity is calculated with the help of the model proposed in Chapter 7, using the material constants given in 'Pilot Plant Test Results' sheet. The velocity at the starting point of the conveying line can also be calculated using the given inputs in front panel. These two velocity values are compared and result is shown in front panel.

Usually the calculation sheet is also kept hidden, since the user has no need interaction there.

8.2.4 Presentation of Output Results

The entry pressure loss together with the pressure drop values encountered in each and every section is presented as results. Also, the pressure available at the end of the conveying line is given. In addition, the indication is given by comparing the calculated start velocity at the entry section and the scaled up minimum conveying velocity from the pilot plant test. When the start velocity is lower than the minimum conveying velocity, the phrase 'Starting velocity is less than the minimum conveying velocity' is appeared with a red blinking. Otherwise, the phrase 'Starting velocity is greater than minimum conveying velocity' will be displayed with green button.

For the ease of presentation, the output results are also shown in front panel. This can be clearly seen in Figure 8-2. The results are shown in cells framed with thick lines.

8.3 Use of Calculation Programme

Once the pneumatic conveying tests are concluded in a laboratory scale pilot plant at least with one pipe size, the required relationships among the interesting parameters can be established easily for the particular bulk material. On the other hand, the relationships and models formulated during the present investigation have been proven to be valid for both dilute and dense phase conveying modes. Consequently, the both of these conveying modes can be dealt with the calculation programme without any trouble.

The advantage of the calculation program is that once the relevant parameters are fed, it can be used to predict the performance of different pipeline configurations together with different combinations of design inputs such as plant capacity, blow tank pressure values, etc. This kind of trials can be easily performed by just changing one or more of the considered parameters and checking the cell output called 'Pressure available at the end of the line'. If the value is negative, it means the assign values are not suitable for the particular pipeline configuration. Otherwise, the user can optimise the design inputs so that the pressure available at the end of the line is minimised.

Simultaneously, the user has to check the status of the conveying velocity at the starting point of the pipeline. As mentioned under section 8.2.4, the displayed phrase is changing automatically according to the comparison status of the start velocity with the minimum conveying velocity for the particular material and pipe configuration. This can also be recognised without any trouble by the colour status of the indication cell just beside the main results.

Since the input parameters and output results are displayed in a common sheet, the above mentioned trial procedure can easily be performed. If the user is concerned about the available pressures at particular point or points on the conveying line, the relevant section has to be checked by scrolling down in the front panel.

In addition to the above explained tasks, this calculation programme can straightforwardly be used to obtain the pneumatic conveying characteristics of the considered bulk material in the considered pipeline configuration, by just changing

the values of capacity, air volume flow and start pressure to obtain the optimised performance of the conveying system.

8.4 An Application: A Case Study

The calculation programme was used to predict the performance of a pneumatic conveying loop, which was rather complicated than the configurations that were used to validate the proposed models during the main investigation. The conveying bulk material and pipe diameters used were also different from those used in the main study. This case study was performed for one industry where the pneumatic conveying systems are extensively used for the fire fighting systems on ships. The results and findings of the case study are briefly explained in following sections.

8.4.1 Background

This case study was mainly based on an industrial project on pneumatic conveying. The key objective was to assess the capabilities of fire fighting equipments, which are operating with the principles of pneumatic conveying. The bulk powder used was called as BC dry chemical, which are suitable for use as a recharge agent in fire extinguishers that utilize sodium bicarbonate based dry chemical powder. Its name implies its suitability for using on fires involving flammable liquids (Class B), and energized electrical equipments (Class C). BC powder is typically white in colour and has mean particle size of 34.5 μm and particle density of 2200 kg/m^3. The concerned bulk powder conveying systems consist of metal pipelines and flexible hose sections.

8.4.2 Experimental Test Set-up

Three different closed loop test pipe layouts were used for the testing;

a) 70 m, 38.5 mm pipe with both 45° and 90° bend (Figure 8-3)
b) 70 m, 38.5 mm pipeline with 45° bends and 70 m 50.8 mm pipe with 45° bend (Figure 8-4)

c) 70 m, 38.5 mm pipeline with 90° bends and 70 m 50.8 mm pipe with 90° bend (Figure 8-5)

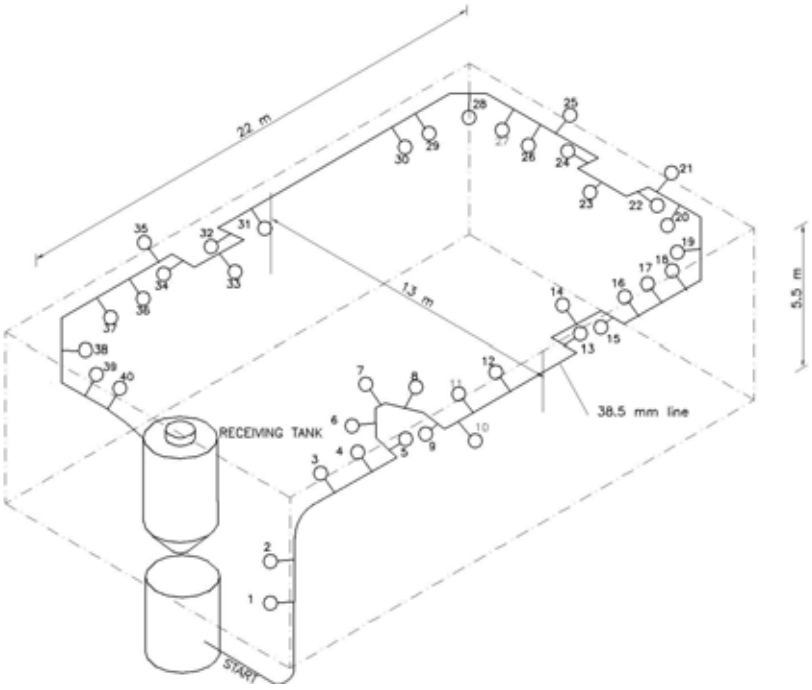

Figure 8-3: Schematic view of the test set-up (a).

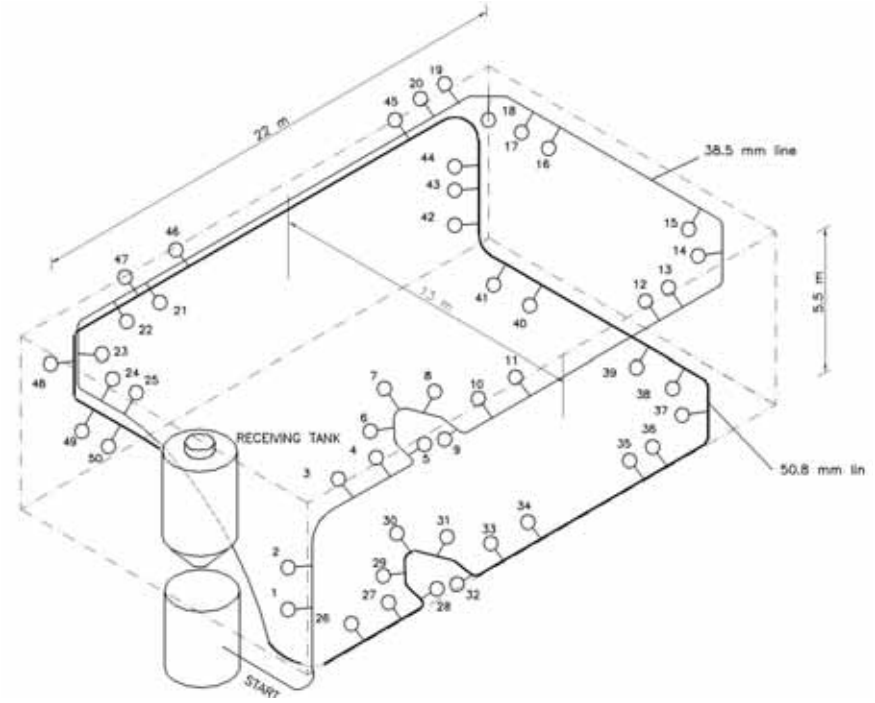

Figure 8-4: Schematic view of the test set-up (b).

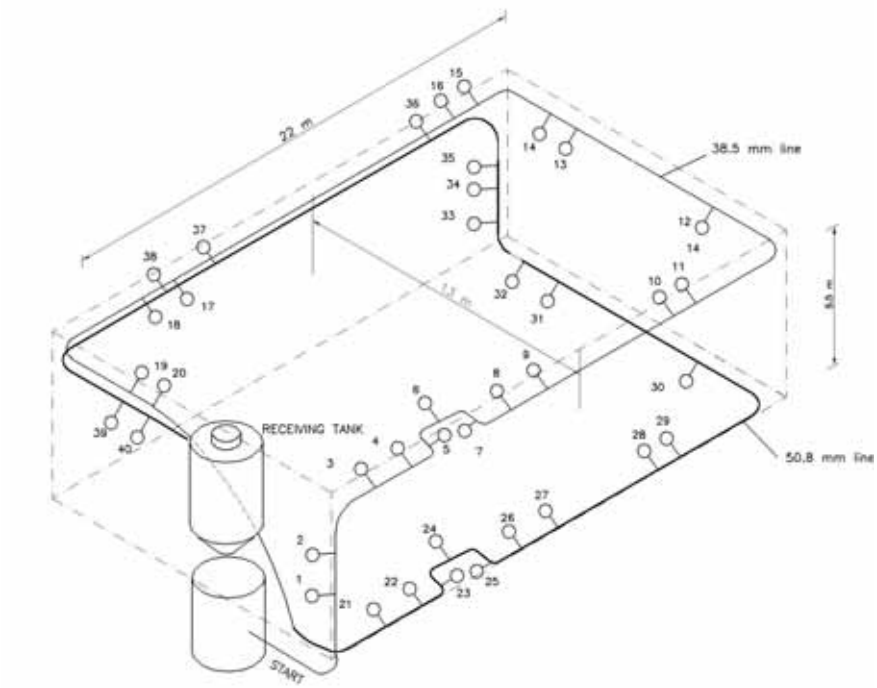

Figure 8-5: Schematic view of the test set-up (c).

A large number of pressure transducers were located on the pipeline so as to isolate the pressure drop components of each concerned sections. In case of bends, two pressure transducers were fixed before and after each bend. Similarly, two pressure transducers were used for each straight (both vertical and horizontal) pipe sections with an approximate distance of 2 m, as explained in Chapter 4.

8.4.3 Usage of the Calculation Programme

The set up shown in Figure 8-3 (test set-up (a)) was selected as the base for the calculation programme (i.e., it was considered as the pilot plant), since it consisted of all types of bends that were used in other pipeline configurations. The K vs. v^2_{entry} curves generated from the data relevant to the said set-up was fed to the calculation programme. Then, the calculation programme was used to predict the performances of the other pipeline configurations. The pressure values calculated using the calculation programme were compared with corresponding experimental measurements at the different points on the pipe layouts. The comparison curves correspond to test set-ups (b) and (c) are shown in Figure 8-6 and Figure 8-7 respectively. The different curves were plotted for different release pressure (blow tank set pressure) values.

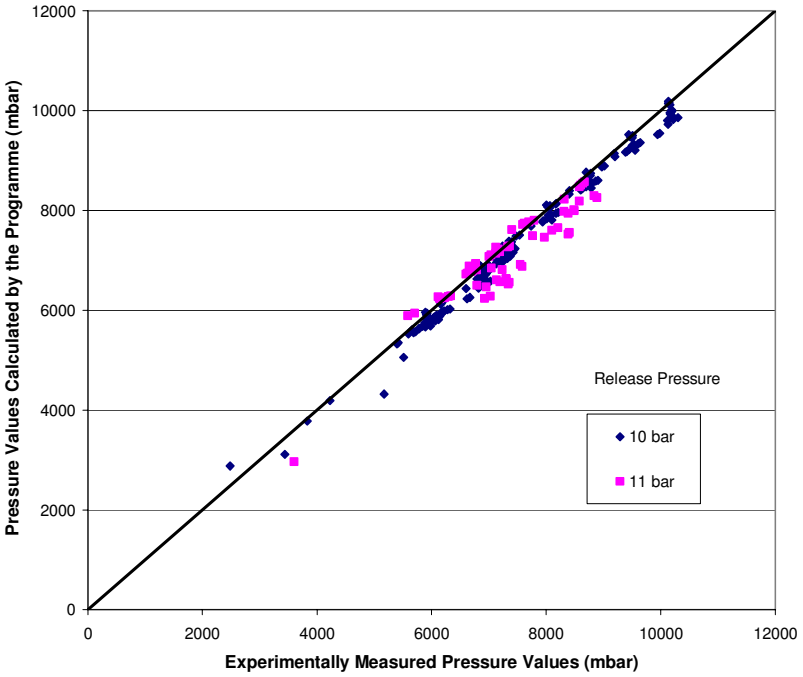

Figure 8-6: The comparison graph for the test set-up (b).

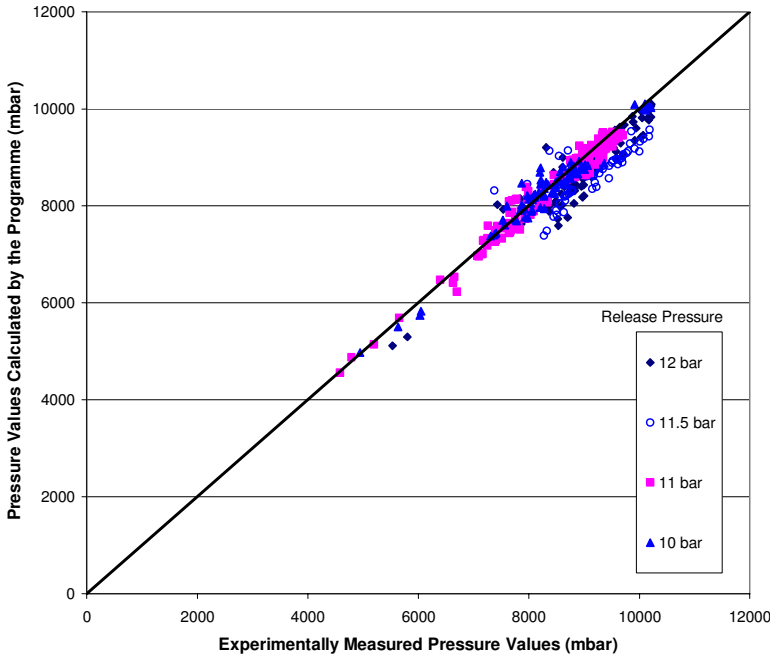

Figure 8-7: The comparison graph for the test set-up (c).

In fact, one particular data set consists of the pressure values at different locations on the pipeline. Being all the data points on and around the diagonal line, which represents the ideal prediction, it can be concluded that the calculation programme was able to predict the pressure drops all along the conveying loop rather accurately.

8.5 Conclusion

Putting all the models and techniques together, the computer based calculation programme was designed for pneumatic conveying system designs and optimisations. Being rather simple software, programmed calculation sheet can easily be used as an effective tool.

The above mentioned example clearly shows that the predictions made by the calculation programme are in good agreement with the experimental measurements. Specially, its ability to deal with rather complex pipe configurations, smaller pipe sizes and higher system pressures than the cases where the individual scaling models were validated is to be emphasized.

In next stages, this calculation programme will be developed with the help of a computer programming language as a user friendly, self-executable software package, in which the test data of different bulk materials can be stored as a data base for the purpose of pneumatic conveying system designing and upgrading.

Including the findings of case study using the calculation programme, the proposed models on line pressure drop, entry loss and minimum conveying velocity have been tested with six different bulk materials including one with five different qualities, in seven different pipeline configurations of five different pipe diameters varying from 35 mm to 125 mm. In all cases, the models predictions have shown rather good agreements with experimental observations in different occasions.

9 COMPUTATIONAL FLUID DYNAMICS AS A PRESSURE DROP PREDICTION TOOL IN DENSE PHASE PNEUMATIC CONVEYING SYSTEMS

9.1 Introduction

As an alternative approach to the classical methods of analysing gas-solid flows, computational techniques have been a well-accepted tool, throughout the last two decades. Specially, Computational Fluid Dynamics (CFD) technique, which means a computational technology that enables one to study the dynamics of single and multi-phase flows, has been becoming popular in scientific research field and industry of two-phase flow systems. In fact, CFD is increasingly used in all branches of engineering. Originally applied to aerodynamic problems in the aerospace industry, with advances in computer processing power and more powerful numerical methods, it can now be applied to more complex situations. With the invention of high- speed high-capacity desk top personal computers, scientists and researches have extensively been using several large scale commercial computer codes to predict the flow phenomena in pneumatic conveying systems, which are very complicate to deal with only first principle based prediction methods.

As discussed under Section 2.11.2, although a number of numerical simulations have been carried out to model the flow phenomena of pneumatic conveying systems, those relevant to dense phase systems could rarely be seen among them. On the other hand, only few attempts could be found where the CFD techniques have been used to predict the line pressure drop of a pneumatic conveying system.

As a part of the present research, a CFD simulation was included to investigate the pressure drop prediction capabilities of CFD techniques in the dense phase flow conditions of a pneumatic conveying system. The main objective of this work was to investigate how good the predictions of a commercial CFD code when it is compared with the experimental observations of a dense phase pneumatic conveying system.

Rather than developing a research purpose code to carry out two-phase flow simulations from the very beginning, it might be more advantageous to use commercially distributed and widely spread software. A well-known CFD software code; Fluent® was used for the simulation and basically, two major parts of a conveying line were addressed; a short straight pipe section and a standard 90° bend. With a numerous number of experimental data generated by different conveying materials and pipeline configurations, it could be possible to compare the simulation results with the real experimental measurements with respect to different combinations of those. The determination of pressure drop across the considered pipe sections was the main focal point, while few other parameters like variation of solid volume fraction, variation of velocity profiles, etc, were also investigated.

9.2 Background

In Section 2.11, the applications of CFD in gas-solid flow systems were briefly discussed together with their historical evolutions. The following paragraphs will give a brief summery of the current status of CFD applications in pneumatic conveying.

Among the two basic approaches of CFD; Eulerian and Lagrangian approaches, the Lagrangian method has been found to be more suited for dilute flows, since it has limited applicability to dense flows because it may be necessary to include an enormous number of particles. On the other hand, the Euler-Euler granular model is suitable for dense gas-solids flows. Some investigations, which tried to predict the gas-solid system behaviours using Eulerian approach, came with interesting results [113, 130, 187, 188].

In recent years, a break through could be achieved, specially in the CFD applications of dense phase gas-solid flow systems when some research works [189-193] discussed the dynamics of inter-particle collisions. Based on this concept, Gidaspow [194] explained the kinetic theory approach, which uses one equation model to determine the turbulent kinetic energy of the particles in terms of the granular temperature.

According to the literature survey carried out to investigate the status of CFD techniques in the field of pneumatic conveying, it was clear that although a considerable number of research publications on dilute phase pneumatic transport [117, 119-121, 195] and fluidised bed systems [113, 196-198] could be seen in open literature, the applications on dense phase conveying is comparatively less. Even if some commercial CFD codes claim better performances in case of dense phase pneumatic conveying applications, their usability in real situations is very limited. On the other hand, only a few cases [81, 196, 198, 199] could be found where some attempts were made to use CFD codes to predict the pressure drops across the parts of gas-solid systems. They also concerned either very dilute phase conveying [81, 199] or fluidised bed applications [196, 198].

9.3 Test Sections

The experimental setup was described in details under Chapter 3 and the data generated by the procedure mentioned in Section 4.5 were used for the simulation work. To highlight the test sections that were considered for the CFD modeling, a schematic view of the considered transport line is shown in Figure 9-1 and individual dimensions of bends of different pipe sizes are given in Table 9-1.

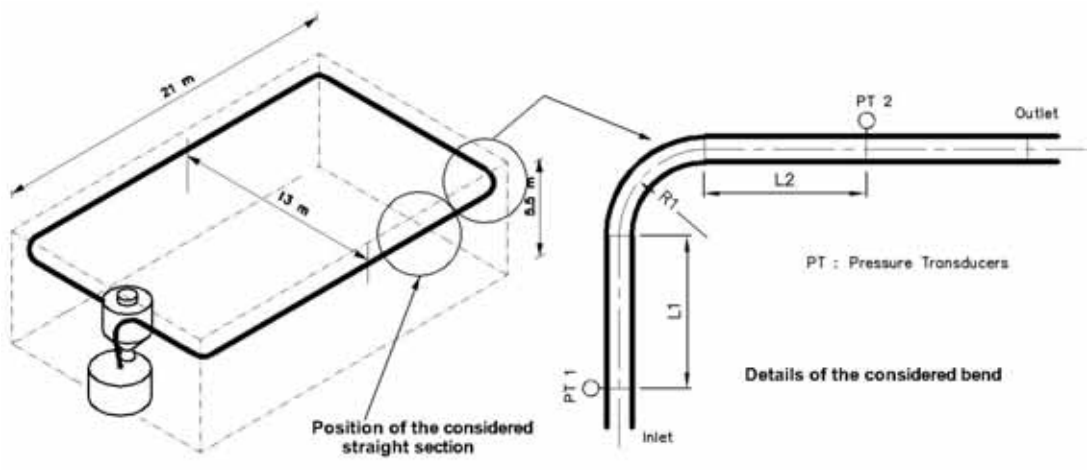

Figure 9-1: The schematic view of the experimental setup.

Table 9-1: The dimensions of different bends (nomenclatures in Figure 9-1).

Pipe Diameter (mm)	L1 (mm)	L2 (mm)	R1 (mm)
78	475	500	267
102	515	600	343
128	515	550	424

9.4 Theoretical Consideration

In CFD analysis technique, a single set of conservation equations for momentum and continuity is usually solved for a single-phase system. But, for multi-phase flow applications, obtaining accurate solutions is much more challenging, not just because each of the phases must be treated separately, but, in addition, a number of new and difficult factors come into play. Some of these additional factors due to accommodate the inter-phase reactions in a multiphase system, can be listed as follows;

- Drag and lift forces
- ‘‘Slip’’, i.e. relative motion, between the phases
- Electrostatic and/or electrophoretic forces
- Particles sizes, size distribution and shapes
- Inter-particle forces, e.g. due to van der Waals forces
- Inter-particle collisions
- Collisions/interactions of particles with the wall of the containing vessel.

As a result of such factors, the CFD models for dense multiphase systems have adopted a wide range of different approaches; Eulerian, Lagrangian or combinations of the two; interpenetrating two-fluid approach or discrete particles; two-dimensional or three dimensional codes; solution via finite difference, finite element or finite

volume approaches, etc. In the process of introducing additional sets of conservation equations, the original set must also be modified. The introduction of the volume fractions of gas and solid phases and the exchange mechanism for the momentum between the phases are the main modifications for a multi-phase CFD model.

9.4.1 CFD Model

As mentioned earlier, Fluent® (version 6.1) was used to simulate the flow across the considered sections. The Euler-Euler granular multiphase model, which considers the solid and gas phases as interpenetrating continuum that share the space, has been used for this simulation. Generally, Fluent® uses a control-volume based technique to convert the governing differential equations of the flow system to algebraic equations, which can be solved numerically. The volume averaged dicretization approach consists of integrating the governing equations about each and every control volume, generating separate equations that conserve each quality on a control-volume basis. The discretized equations, along with the initial and boundary conditions, were solved to obtain a numerical solution. Conservation equations of mass and momentum were developed using the Eulerian approach, and solved simultaneously by considering the phases separately but linking them through the drag forces in the momentum equation. In the Fluent® software code, the Phase Coupled SIMPLE (PC-SIMPLE) algorithm that is an extension of the SIMPLE algorithm [111] to multiphase flows is used for the pressure-velocity coupling. The velocities are solved coupled by phases, but in a segregated fashion. A pressure correction equation is built based on total volume continuity rather than mass continuity. Pressure and velocities are then corrected so as to satisfy the continuity constraint. To model the turbulence, the k-ε (k: turbulent kinetic energy, ε: turbulent kinetic energy dissipation) model has been used.

9.4.2 Model Equations

The full details of the model and the solution procedure are given in detail in the Fluent® user's guide [112], while the following few sections give an overview of the basic model equations.

9.4.2.1 Continuity equations

The conservation of mass for the gas phase can be presented as shown in Equation (9.1).

$$\frac{\partial}{\partial t}\left(\alpha_g \rho_g\right)+\frac{\partial}{\partial x_j}\left(\alpha_g \rho_g u_{j,g}\right)=0 \tag{9.1}$$

The same for the solid particulate phase appears as in Equation (9.2).

$$\frac{\partial}{\partial t}\left(\alpha_s \rho_s\right)+\frac{\partial}{\partial x_j}\left(\alpha_s \rho_s u_{j,s}\right)=0 \tag{9.2}$$

9.4.2.2 Momentum equations

The conservation of momentum for the gas phase is given in Equation (9.3).

$$\frac{\partial}{\partial t}\left(\alpha_g \rho_g u_{j,g}\right)+\frac{\partial}{\partial x_j}\left(\alpha_g \rho_g u_{j,g} u_{i,g}\right)=-\alpha_g \frac{\partial P}{\partial x_i}+\frac{\partial \tau_{ij,g}}{\partial x_j}+\alpha_g \rho_g g_i+K_{gs}\left(u_{i,s}-u_{i,g}\right) \tag{9.3}$$

Although there should be an additional term to account for the external forces (e.g. lift force, virtual mass force, etc.) besides drag and gravity forces, those are insignificant compared to the drag force and not included in momentum conservation equations. Equation (9.4) shows how the stress-strain tensor of the gas phase, $\tau_{ij,g}$ is related to the gradient of velocity components.

$$\tau_{ij,g}=-\frac{2}{3}\alpha_g \rho_g k_g \delta_{ij}+\alpha_g \mu_{eff,g}\left[\left(\frac{\partial u_{i,g}}{\partial x_j}+\frac{\partial u_{j,g}}{\partial x_i}\right)-\frac{2}{3}\delta_{ij}\frac{\partial u_{k,g}}{\partial x_k}\right] \tag{9.4}$$

The conservation of momentum for solids phase can be presented as in Equation (9.5).

$$\frac{\partial}{\partial t}\left(\alpha_s \rho_s u_{j.s}\right)+\frac{\partial}{\partial x_j}\left(\alpha_s \rho_s u_{j,s} u_{i,s}\right)=-\alpha_s \frac{\partial P}{\partial x_i}-\frac{\partial P_s}{\partial x_i}+\frac{\partial \tau_{ij,s}}{\partial x_j}+\alpha_s \rho_s g_i+K_{sg}\left(u_{i,g}-u_{i,s}\right) \tag{9.5}$$

The total stress tensor for the solid phase is given by Equation (9.6).

$$\tau_{ij,s} = \alpha_s \mu_s \left(\frac{\partial u_{i,s}}{\partial x_j} + \frac{\partial u_{j,s}}{\partial x_i} \right) + \left(\alpha_s \upsilon_s - \frac{2}{3} \alpha_s \mu_s \right) \delta_{ij} \frac{\partial u_{k,s}}{\partial x_k} \tag{9.6}$$

The term υ_s and μ_s in Equation (9.6) imply the solids bulk and solids shear viscosities described in Equations (9.16) and (9.13) respectively. The term '*P*' in Equations (9.3) and (9.5) represents the gas phase pressure.

9.4.2.3 Solids phase pressure

Combining kinetic and collisional pressures, the solids phase pressure, P_s can be presented as in Equation (9.7).

$$P_s = \alpha_s \rho_s \left[1 + 2(1 + e_{ss}) \alpha_s g_{0,ss} \right] \theta_s \tag{9.7}$$

where, e_{ss} is the coefficient of restitution for the particle collisions, which is set at 0.9 and $g_{0,ss}$ is the radial distribution function given in Equation (9.8).

$$g_{0,ss} = \left[1 - \left(\frac{\alpha_s}{\alpha_{s,\max}} \right)^{\frac{1}{3}} \right]^{-1} \tag{9.8}$$

The maximum packing limit, $\alpha_{s,max}$ is set to 0.7 in the simulation. The radial distribution function can be defined as a correction factor for dense phase flow. The magnitude of $g_{0,ss}$ increases with decreasing void fraction, from one, which represents the dilute phase flow to infinity as the system reaches a state of particles packed so close that no mutual motion is possible. θ_s is the granular temperature presented in Equation (9.33).

9.4.2.4 Gas-solid particle exchange coefficient

The K_{sg} and K_{gs} are the gas-solid exchange coefficients, which account for the momentum exchange between the phases. These terms can be inter-related as shown in Equation (9.9).

$$K_{sg} = K_{gs} \tag{9.9}$$

It can be further expanded as shown in Equation (9.10), according to Wen and Yu [200].

$$K_{sg} = \frac{3}{4} C_D \frac{\alpha_s \alpha_g \rho_g \left| u_{i,s} - u_{i,g} \right|}{d_p} \alpha_g^{-2.65} \tag{9.10}$$

where C_D is the drag coefficient defined in terms of relative Reynolds number, Re_s, as presented in Equation (9.11).

$$C_D = \frac{24}{\alpha_g \psi_s \mathrm{Re}_s} \left[1 + 0.15 \left(\alpha_g \mathrm{Re}_s \right)^{0.687} \right] \qquad \text{for } \mathrm{Re}_s = \frac{\rho_g d_p \left| u_{i,s} - u_{i,g} \right|}{\mu_g} \leq 1000$$

$$C_D = 0.44 \qquad \text{for } \mathrm{Re_s} > 1000 \tag{9.11}$$

where Ψ_s is the shape factor, which becomes unity for spherical particles and between zero and one for particles of other shapes. That can simply be defined as in Equation (9.12).

$$\Psi_s = \frac{s}{S} \tag{9.12}$$

where, s is the surface area of a sphere having the same volume as the considered particle while S is the actual surface area of the particle.

9.4.2.5 Solids Viscosity

As shown in Equation (9.13), the collisional and kinetic parts are combined to get the shear viscosity of the particles, which accounts for the particle momentum exchange.

$$\mu_s = \mu_{col,s} + \mu_{kin,s} \tag{9.13}$$

The components due to collisions and translation can be defined according to Gidaspow et al. [201] and Syamlal et al. [202] as presented in Equations (9.14) and (9.15) respectively.

$$\mu_{col,s} = \frac{4}{5} \alpha_s \rho_s d_p g_{0,ss} \left(1 + e_{ss} \right) \left(\frac{\theta_s}{\pi} \right)^{0.5} \tag{9.14}$$

$$\mu_{kin,s} = \frac{\alpha_s \rho_s d_p \sqrt{\theta_s \pi}}{6 \left(3 - e_{ss} \right)} \left[1 + \frac{2}{5} \left(1 + e_{ss} \right) \left(3 e_{ss} - 1 \right) \alpha_s g_{0,ss} \right] \tag{9.15}$$

The solid bulk viscosity (υ_s) accounts for the resistance of the granular particles to compression and expansion. It can be expressed in Equation (9.16), according Lun et al. [190].

$$\upsilon_s = \frac{3}{4}\alpha_s \rho_s d_p g_{oss}\left(1+e_{ss}\right)\left(\frac{\theta_s}{\pi}\right)^{0.5} \tag{9.16}$$

9.4.2.6 Turbulent kinetic energy equation

As explained early, the number of terms to be modelled in the momentum equations of multiphase flows is larger than that of the single-phase flow, and in turn the modelling of turbulence in this case becomes extremely complex. Fluent® gives three methods for turbulence modelling in multiphase flows within the context of the *k*-ε models, which can be listed as; Mixture turbulence model, Dispersed turbulence model and Per phase turbulence model (considering each individual phase). For this work, per phase turbulence model was used.

In this approach, a set of *k* and ε (*k*: turbulent kinetic energy and ε: dissipation of *k*) transport equations for each phase is solved. The per-phase turbulence model is more computationally intensive than the other multiphase turbulence models. The model also accounts for the inter-phase turbulence transfer. Additional transport equations for the turbulence and its effects on the respective phases are presented with the model. For each phase, two additional transport equations are solved.

The turbulent kinetic energy equation for gas phase is obtained with the Equation (9.17).

$$\begin{aligned}&\frac{\partial}{\partial t}\left(\alpha_g \rho_g k_g\right)+\frac{\partial}{\partial x_j}\left(\alpha_g \rho_g u_{j,g} k_g\right)=\frac{\partial}{\partial x_j}\left[\alpha_g \frac{\mu_{t,g}}{\sigma_{k,g}}\frac{\partial k_g}{\partial x_j}\right]+\alpha_g \rho_g\left(G_g-\varepsilon_g\right)\\&+K_{sg}\left(C_{sg}k_s-C_{gs}k_g\right)-K_{sg}\left(u_{j,s}-u_{j,g}\right)\frac{\mu_{t,s}}{\alpha_s\sigma_{k,s}}\frac{\partial \alpha_s}{\partial x_j}+K_{sg}\left(u_{j,s}-u_{j,g}\right)\frac{\mu_{t,g}}{\alpha_g\sigma_{k,g}}\frac{\partial \alpha_g}{\partial x_j}\end{aligned} \tag{9.17}$$

The same for solid particulate phase is shown in Equation (9.18).

$$\frac{\partial}{\partial t}\left(\alpha_s\rho_s k_s\right)+\frac{\partial}{\partial x_j}\left(\alpha_s\rho_s u_{j,s}k_s\right)=\frac{\partial}{\partial x_j}\left[\alpha_s\frac{\mu_{t,s}}{\sigma_{k,s}}\frac{\partial k_s}{\partial x_j}\right]+\alpha_s\rho_s\left(G_s-\varepsilon_s\right)$$
$$+K_{gs}\left(C_{gs}k_g-C_{sg}k_s\right)-K_{gs}\left(u_{j,g}-u_{j,s}\right)\frac{\mu_{t,g}}{\alpha_g\sigma_{k,g}}\frac{\partial\alpha_g}{\partial x_j}+K_{gs}\left(u_{j,g}-u_{j,s}\right)\frac{\mu_{t,s}}{\alpha_s\sigma_{k,s}}\frac{\partial\alpha_s}{\partial x_j} \quad (9.18)$$

The dissipation of turbulent kinetic energy for gas phase is given in Equation (9.19).

$$\frac{\partial}{\partial t}\left(\alpha_g\rho_g\varepsilon_g\right)+\frac{\partial}{\partial x_j}\left(\alpha_g\rho_g u_{j,g}\varepsilon_g\right)=\frac{\partial}{\partial x_j}\left[\alpha_g\frac{\mu_{t,g}}{\sigma_{\varepsilon,g}}\frac{\partial\varepsilon_g}{\partial x_j}\right]+\alpha_g\rho_g\frac{\varepsilon_g}{k_g}\left(C_{1\varepsilon}G_g-C_{2\varepsilon}\varepsilon_g\right)$$
$$+C_{3\varepsilon}\frac{\varepsilon_g}{k_g}\left(C_{sg}k_s-C_{gs}k_g\right)-C_{3\varepsilon}\frac{\varepsilon_g}{k_g}K_{sg}\left(u_{j,s}-u_{j,g}\right)\frac{\mu_{t,s}}{\alpha_s\sigma_{\varepsilon,s}}\frac{\partial\alpha_s}{\partial x_j} \quad (9.19)$$
$$+C_{3\varepsilon}\frac{\varepsilon_g}{k_g}K_{sg}\left(u_{j,s}-u_{j,g}\right)\frac{\mu_{t,g}}{\alpha_g\sigma_{\varepsilon,g}}\frac{\partial\alpha_g}{\partial x_j}$$

Similarly for the solid phase, Equation (9.20) shows the relationship for dissipation of turbulent kinetic energy.

$$\frac{\partial}{\partial t}\left(\alpha_s\rho_s\varepsilon_s\right)+\frac{\partial}{\partial x_j}\left(\alpha_s\rho_s u_{j,s}\varepsilon_s\right)=\frac{\partial}{\partial x_j}\left[\alpha_s\frac{\mu_{t,s}}{\sigma_{\varepsilon,s}}\frac{\partial\varepsilon_s}{\partial x_j}\right]+\alpha_s\rho_s\frac{\varepsilon_s}{k_s}\left(C_{1\varepsilon}G_s-C_{2\varepsilon}\varepsilon_s\right)$$
$$+C_{3\varepsilon}\frac{\varepsilon_s}{k_s}\left(C_{gs}k_g-C_{sg}k_s\right)-C_{3\varepsilon}\frac{\varepsilon_s}{k_s}K_{gs}\left(u_{j,g}-u_{j,s}\right)\frac{\mu_{t,g}}{\alpha_g\sigma_{\varepsilon,g}}\frac{\partial\alpha_g}{\partial x_j} \quad (9.20)$$
$$+C_{3\varepsilon}\frac{\varepsilon_s}{k_s}K_{gs}\left(u_{j,g}-u_{j,s}\right)\frac{\mu_{t,s}}{\alpha_s\sigma_{\varepsilon,s}}\frac{\partial\alpha_s}{\partial x_j}$$

The turbulent viscosity is written in terms of the turbulent kinetic energy and its dissipation of each phase, as shown in Equations (9.21) and (9.22);

$$\mu_{t,s}=\rho_s C_\mu\frac{k_s^2}{\varepsilon_s} \quad (9.21)$$

$$\mu_{t,g}=\rho_g C_\mu\frac{k_g^2}{\varepsilon_g} \quad (9.22)$$

In Equations (9.17)-(9.20), G_s and G_g are the generation of turbulence kinetic energy of the solid particle and gas phases respectively. The relationship of these parameters are given in Equations (9.23) and (9.24).

$$G_g = \mu_{t,g}\left(\frac{\partial u_{j,g}}{\partial x_i}+\frac{\partial u_{i,g}}{\partial x_j}\right)\frac{\partial u_{j,g}}{\partial x_i} \tag{9.23}$$

$$G_s = \mu_{t,s}\left(\frac{\partial u_{j,s}}{\partial x_i}+\frac{\partial u_{i,s}}{\partial x_j}\right)\frac{\partial u_{j,s}}{\partial x_i} \tag{9.24}$$

The terms C_{sg} and C_{gs} are approximated as in Equations

$$C_{sg} = 2 \tag{9.25}$$

$$C_{gs} = 2\left(\frac{\eta_{sg}}{1+\eta_{sg}}\right) \tag{9.26}$$

where;

$$\eta_{sg} = \frac{0.135 K_{sg} k_g}{\alpha_s \rho_s \varepsilon_g \left(\frac{\rho_s}{\rho_g}+0.5\right)\sqrt{1+\xi^2\left(1.8-1.35\cos^2\theta\right)}} \tag{9.27}$$

and

$$\xi = \sqrt{\frac{2}{3}}\frac{0.135\left|u_{i,s}-u_{i,g}\right|}{k_s^{0.5}} \tag{9.28}$$

The term θ in the Equation (9.27) means the angle between the mean particle velocity and the mean relative velocity.

For the inter-phase turbulent momentum transfer, the momentum transfer term in Equations (9.3) and (9.5) can be modified as a turbulent drag term.

$$K_{sg}\left(u_{i,s}-u_{i,g}\right) = K_{sg}\left(V_{i,s}-V_{i,g}\right)+K_{sg}\left(\frac{D_s}{\sigma_{sg}\alpha_s}\frac{\partial \alpha_s}{\partial x_j}-\frac{D_g}{\sigma_{sg}\alpha_g}\frac{\partial \alpha_g}{\partial x_j}\right) \tag{9.29}$$

Where, V values are phase-weighted velocities. σ_{sg} is defined as the dispersion Prandtl number and sets in the default value of the Fluent®, 0.75. The diffusivities, D_g is modeled from the expression in Equation (9.30).

$$D_g = \frac{2}{3}\tau_{F,gs}\left(\left(\frac{b+\eta_{gs}}{1+\eta_{gs}}\right)k_s\eta_{gs}+\left(k_g-bk_s\left(\frac{b+\eta_{gs}}{1+\eta_{gs}}\right)\right)\right) \tag{9.30}$$

where,

$$b = 1.5\left(\frac{\rho_g}{\rho_s} + 0.5\right)^{-1} \tag{9.31}$$

$$\tau_{F,gs} = \alpha_g \rho_g \frac{\left(\frac{\rho_g}{\rho_s} + 0.5\right)}{K_{gs}} \tag{9.32}$$

The term D_s can be presented as Equation (9.29) with the terms whose subscripts are interchanged accordingly.

The set of constants for the turbulent model is shown in Table 9-2.

Table 9-2: Turbulent model constants.

Notation	$C_{1\varepsilon}$	$C_{2\varepsilon}$	$C_{3\varepsilon}$	C_{μ}	$\sigma_{k,g}$	$\sigma_{k,s}$	$\sigma_{\varepsilon,g}$	$\sigma_{\varepsilon,s}$
Value	1.42	1.68	1.2	0.09	1.0	1.0	1.3	1.3

9.4.2.7 Granular Temperature Equation

Ding and Gidaspow [193] derived the transport equation for granular temperature, θ_s as shown in Equation (9.33).

$$\frac{3}{2}\left[\frac{\partial}{\partial t}\left(\alpha_s \rho_s \theta_s\right) + \frac{\partial}{\partial x_j}\left(\alpha_s \rho_s u_{j,s} \theta_s\right)\right] = \left(-P_s \delta_{ij} + \tau_{ij,s}\right)\frac{\partial u_{i,s}}{\partial x_j} + \frac{\partial}{\partial x_j}\left(\kappa_{\theta_s}\frac{\partial \theta_s}{\partial x_j}\right) - \gamma_{\theta_s} + \phi_{gs} \tag{9.33}$$

where,

$\left(-P_s \delta_{ij} + \tau_{ij,s}\right)\frac{\partial u_{i,s}}{\partial x_j}$ is the energy generated by the solid stress tensor

$\gamma_{\theta s}$ is the collisional dissipation of energy

Φ_{gs} is the energy exchange between the fluid and solid phase

$\kappa_{\theta s}$ is the diffusion coefficient for granular energy

$\kappa_{\theta s}$ is given by Syamlal et al. [190] as in Equation (9.34).

$$\kappa_{\theta_s} = \frac{15 d_s \rho_s \alpha_s \sqrt{\theta_s \pi}}{4(41-33\eta)}\left[1 + \frac{12}{5}\eta^2(4\eta - 3)\alpha_s g_{oss} + \frac{16}{15\pi}(41-33\eta)\eta\alpha_s g_{oss}\right] \tag{9.34}$$

where,

$$\eta = \frac{1}{2}\left(1 + e_{ss}\right) \tag{9.35}$$

According to Lun et al. [190], the collisional dissipation of energy; $\gamma_{\theta s}$ can be presented as in Equation (9.36).

$$\gamma_{\theta_s} = \frac{12\left(1 - e_{ss}^2\right) g_o}{d_s \sqrt{\pi}} \rho_s \alpha_s^2 \theta_s^{\frac{3}{2}} \tag{9.36}$$

and $\phi_{gs} = -3K_{gs}\theta_s$ (9.37)

9.5 Grid Generation

The body-fitted coordinate technique was used with the help of the Gambit® software package to generate three-dimensional grids for bend and straight sections, according to the actual dimensions of the individual components.

9.5.1 Bend

In case of bend, the main focus was on the pipe bend and the short straight pipe sections at the upstream and down stream of bend. At the inlet, the calculation domain starts exactly with the position of inlet pressure transducer. To ensure the uniform and steady flow conditions at the outlet of calculation domain, the grid was extended about 0.5 m after the outlet pressure transducer (refer Figure 9-1). A typical grid of the calculation domain relevant to 78 mm diameter pipe is shown in Figure 9-2.

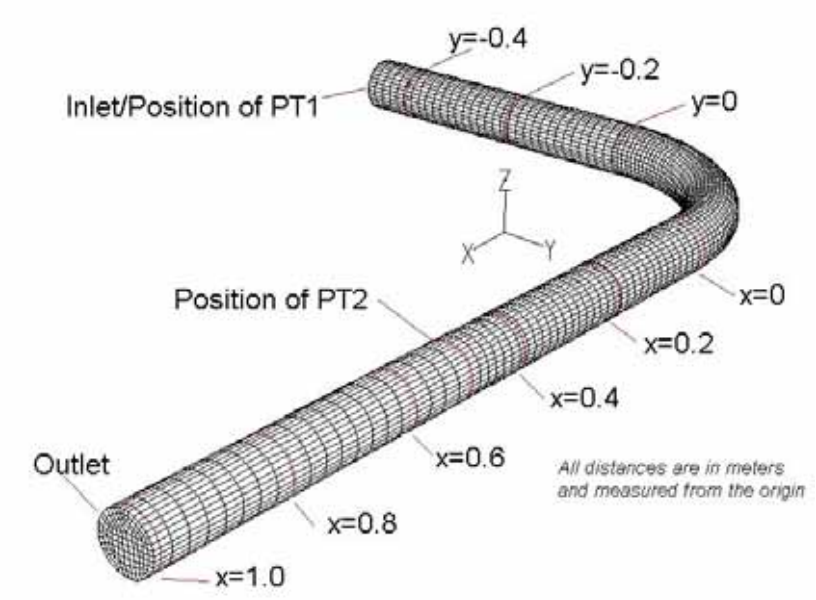

Figure 9-2: A typical grid of the calculation domain of 75mm diameter bend.

The grid statistics relevant to Figure 9-2 could be presented as below;

Volume statistics:

Minimum volume: 1.57×10^{-07} m^3

Maximum volume: 1.45×10^{-06} m^3

Total volume: 8.98×10^{-03} m^3

Face area statistics:

Minimum face area: 1.56×10^{-05} m^2

Maximum face area: 2.00×10^{-04} m^2

As shown in Figure 9-2, few hypothetical surfaces were generated within the pre-bend and the post-bend pipe sections for the purpose of using them in post processing stage as reference planes, to check the solid concentration and phase velocities.

9.5.2 Straight Section

A typical grid of the straight section, which is relevant to 75 mm diameter pipeline, is shown in Figure 9-3.

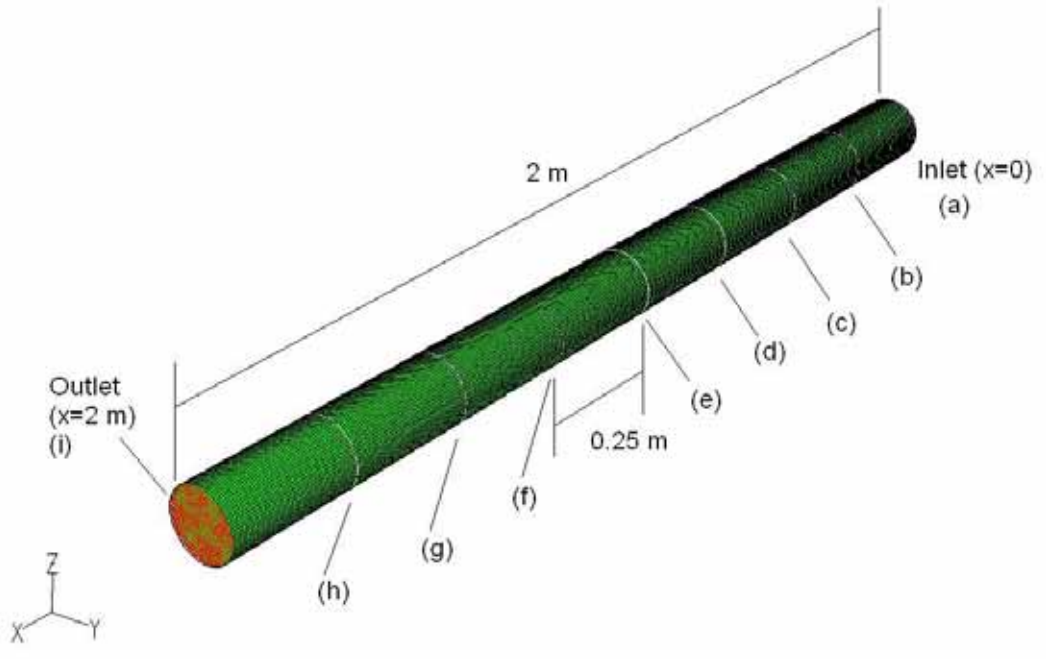

Figure 9-3: A typical grid of the calculation domain of 125mm diameter straight section.

The length of the computational domain was fixed to 2 m according to the dimensions of the test section. Few surfaces were generated in the grid domain as shown in Figure 9-3, to use as the reference planes for the post-simulation analysis. The statistical details of the grids shown in Figure 9-3 are given below;

Volume statistics:

Minimum volume: 5.378167×10^{-08} m^3

Maximum volume: 1.613413×10^{-07} m^3

Total volume: 9.507167×10^{-03} m^3

Face area statistics:

Minimum face area: 1.132038×10^{-05} m^2

Maximum face area: 3.298256×10^{-05} m^2

9.6 Numerical Simulation

The grid files generated by Gambit® were used for the simulation in Fluent®. The different model parameters have been defined as close as possible to the actual experimental conditions and Table 9-3 shows the selection of model parameters.

Table 9-3: Selection of different simulation parameters.

Parameter	Selection
Solver	segregated
Formulation	implicit
Time	unsteady
Space	3D
Velocity formulation	absolute
Unsteady formulation	1st order implicit
Gradient option	Cell-based
Porous formulation	Superficial velocity
Multiphase	Eulerian
Turbulent model	Standard k-ε (2-equation)
Near-wall treatment	Standard wall function
k-ε multiphase model	Per phase

In the problem specification, the discretization method called 'Phase Coupled SIMPLE' was selected for the pressure-velocity coupling while 'First Order Upwind' discretization method was used for other scalar parameters like momentum, volume fraction, turbulent kinetic energy etc. The simulations have been carried out for different test conditions in terms of air flow rate, material mass flow rate and total pressure drop value. Inlet boundary conditions such as inlet pressure, volume fraction of solid etc, have been defined according to the experimental inlet pressure of the considered sections. Since the considered bend is located after a straight horizontal

pipe of about 20 m from its predecessor (please refer Figure 9-1), distribution of cross sectional velocity is reasonable to assume as uniform at the bend inlet. As explained earlier, the outlet of the calculation domain is placed 500 mm down stream of the physical outlet of the bend. At wall, no slip condition is assumed and the wall roughness constant was taken as 0.5. For the convenience of the simulations, spherical mono sized particles were assumed for all bulk materials. With this assumption, particle mean diameters (d_{50}) were used for the simulations. To define the boundary conditions at the inlet, the velocities of both phases have to be given. The air velocity was determined according to the experimental measurements, while the concept of slip velocity had to be considered to calculate the solid phase velocity. Although a considerable number of models to calculate the slip velocity in dilute phase could be seen in open literature [203-207], very few models [178, 208] are available for the same in dense phase. To estimate the solid velocity, a graphical presentation of slip velocity curves [27] based on the model proposed by Arastoopour et al. [47] was used. The volume fraction of the bend inlet was calculated according to the experimental condition.

The process of solving a multiphase system is inherently difficult, and usually one may encounter some stability or convergence problems. The current algorithm in the new version of Fluent® (Fluent® 6.1) is clamed to be more stable than that used in Fluent® 4 [112]. Initially, a few iterations were performed with a small time step, at least an order of magnitude smaller than the characteristic time of the flow. The size of the time step could be increased after performing a few time steps. Generally, the size of a time step is selected as 0.002s. Almost in all the cases, the convergence condition was reached within first 1000 iterations. A typical residual plot is shown in Figure 9-4.

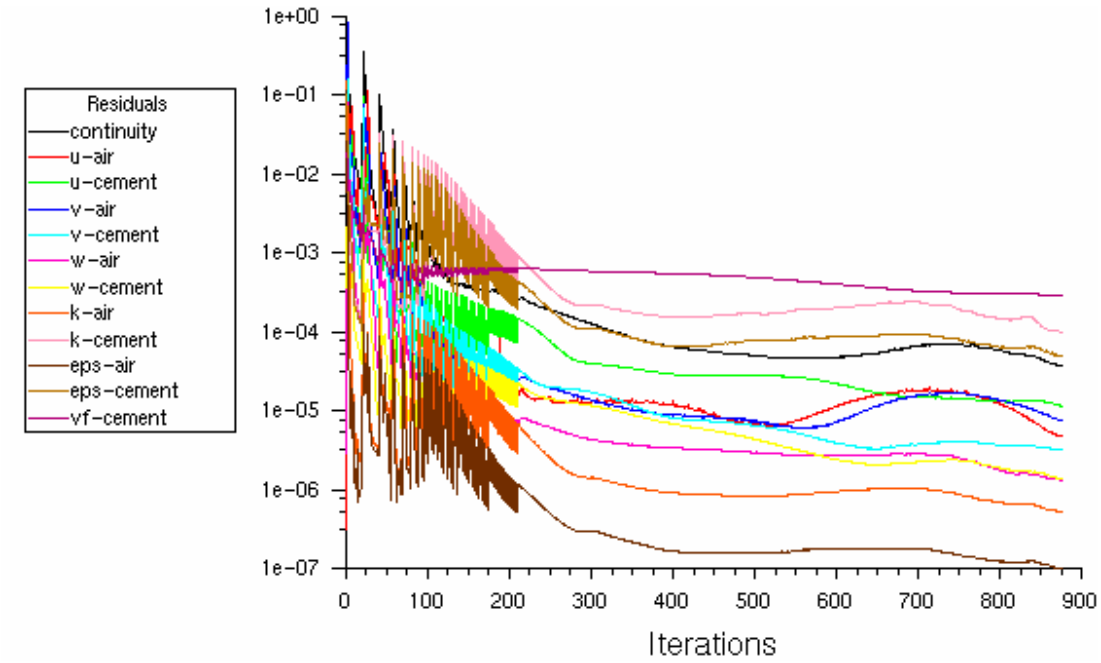

Figure 9-4: A typical residual plot for bend simulation (Material: cement, Diameter: 75mm).

After each simulation, the velocity and pressure profiles and distribution of volume fractions of each phase were inspected. The variations of the above variables with the time development were also examined according to the simulation results. Finally, the pressure drops across the considered sections for different test conditions were calculated using simulation results and then compared with the experimental observations made during the actual pneumatic conveying tests.

9.7 Results and Discussion

The Fluent® provides with the facilities to post-process the data and display the necessary contour, vector and profile plots of pressures, velocities, volume fractions, etc, of individual phases. After achieving the convergence condition, contour plots of solid phase were examined for each simulation. Using these plots, the characteristics of the flow across the pipe bend could be understood. In particular, the plots of contours of volume fraction are showing the flow behaviour of each phase, which is very difficult to observe during the experimentations. On the other hand, profiles of

velocities of each phase give a better understanding of their individual variations in addition to the slip velocity between them, which has been a much discussed topic in past investigations.

The results are categorised into three groups and presented here. Firstly, the variation of solid volume fraction was observed within the calculation domain. In the second stage, propagations of velocity profiles of each phase are discussed while the pressure drop determination and comparison with experimental data are given at last.

9.7.1 Variation of Volume Fraction

The volume fraction of a particular phase in a mixture is defined as the ratio between the volume of the considered phase and the total volume. Generally, the sum of the volume fractions of constituents of a mixture equals to unity.

In simulation works related pneumatic conveying systems, the volume fraction of solid phase plays a vital role. Under the current simulation, a special attempt was made to realize the variation of solid phase volume fraction across a bend and a straight pipe section.

9.7.1.1 Bend

After reviewing the contour plots of volume fractions of gas and solid phases, it could be noticed that all the plots showed a quite similar behaviour, especially in case of their propagation across the bend, independent from conveying bulk materials and pipe diameters. One such contour plot of variation of cement volume fraction across the 75 mm bend is shown in Figure 9-5.

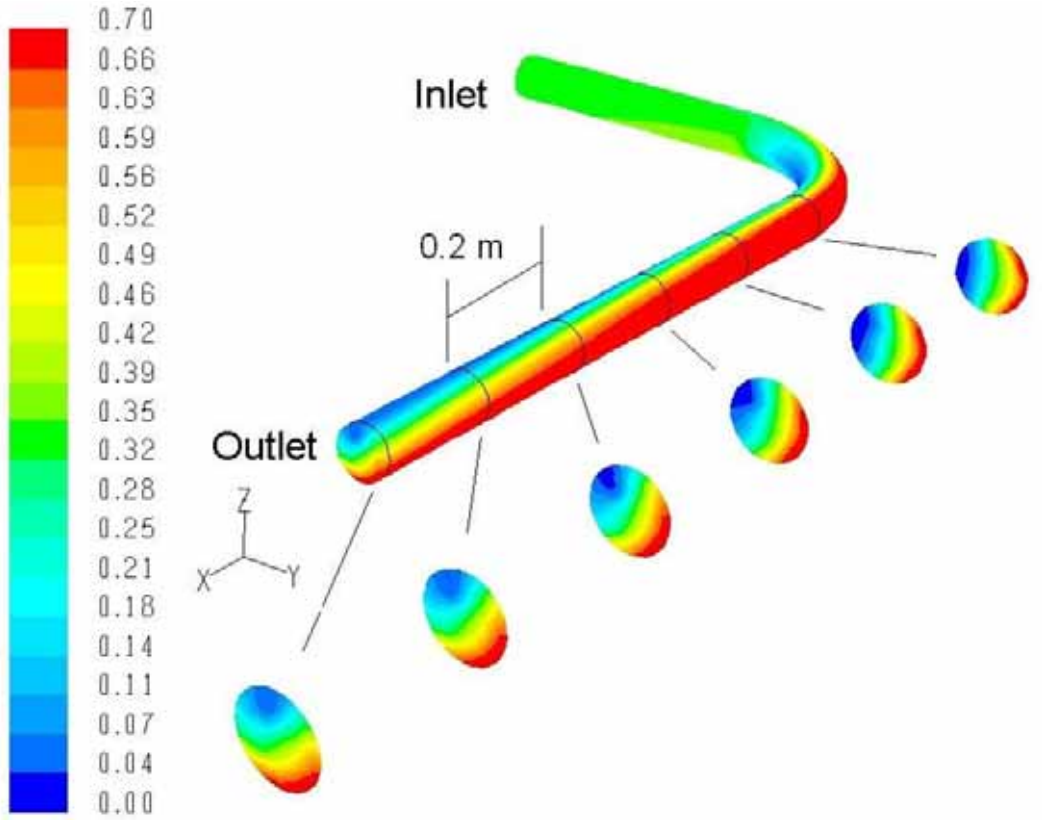

Figure 9-5: Contours of volume fraction (Material: cement, Diameter: 75mm).

Figure 9-5 depicts the contour plot of solid phase volume fraction of bend as a whole in two different view points and few cross sections along the axis of the pipe at 200 mm intervals in down stream of the bend. Figure 9-2 shows the exact positions of the surfaces. The contour plots clearly show a high particle concentration at the long radius wall of the bend. In the vicinity of outlet, similar high particle concentration could be seen at the bottom area of the conveying pipe. With the help of cross sectional contour plots, one can obviously see the area of high particle concentration slides gradually from the long radius side wall to the lower half of the pipe along the pipeline as the gas-solid mixture is heading out of the bend. This explains the behaviour of the solid particle inside the bend, specially, at the middle section of the bend where the solid particles are subjected to centrifugal forces and thrown towards the pipe wall. After fading away the centrifugal action, then, the particles are under

the gravitational effect and tend to concentrate at the pipe bottom giving high solid volume fraction in the lower half of the pipe cross-section.

9.7.1.2 Straight Section

Similar analysis explained in the last section was carried out for the straight sections as well. The contour plots of solids volume fraction relevant to the hypothetical planes whose exact positions were shown in Figure 9-3 were investigated. Figure 9-6 shows the variation of solids phase volume fractions together with colour legend, along the downstream of straight section. The lower case letters given with the contour plot denote the particular reference plane.

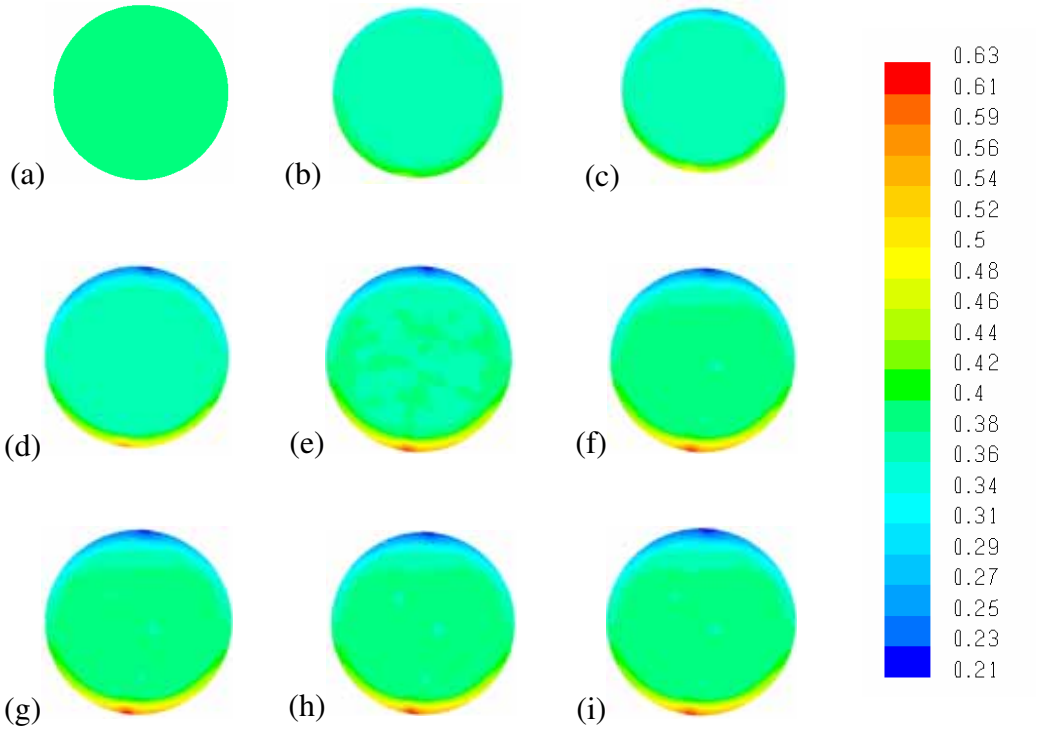

Figure 9-6: Contour plots of volume fraction of solids of few cross sectional planes of straight pipe section (Material: cement, Diameter: 75mm, exact positions of planes are shown in Figure 9-3).

According to the series of contour plots, it is clear that when the flow negotiates the downstream of the straight section, the solid concentration in the bottom region gradually grows. Specially, a clear difference can be seen in the solid volume fractions of the bottom and top region of the cross-section of the outlet region of the straight section.

The similar phenomenon was reported in many other investigations [209-214] as well. Most of them explained the presence of high solid fraction at the bottom of the horizontal pipe wall as a result of gravitational settling of solids. Huber and Sommerfeld [211] described it as a result of high loss of solids momentum at the bottom of the pipe due to more intense particle-particle and particle-wall collisions as compared to the upper portion of the pipe. They also found inelastic particle collisions and viscous dissipation of the gas phase as the reasons for high momentum loss. Some researchers [199, 209, 213, 215] have observed a characteristics of a rope of solid particles inside and/or just downstream of a bend. Some of them also reported a secondary flow pattern of a double vortex at the downstream of the bend. However, these phenomena are quite common in dilute phase conveying where the solid particles have more freedom to move. But, the flow modes under the consideration of this investigation were completely in dense phase (the solid loading ratio ranging from 29 to 257) according to the experimental observations discussed in details in Section 4.6.2. Consequently, the solid particles have less freedom to move around the conveying domain, thus the roping phenomenon may not be applicable here.

9.7.2 Velocity profiles of gas and solid phase

In this stage, different aspects of velocities were examined using the post processing facilities available in Fluent®. To understand the variations of gas and solid velocities, the *x-y* plots of theses variables were examined along the pipeline. In spite of conveying material and pipeline configuration, some common trends of velocity distribution could be observed similar to the case of volume fractions. Figure 9-7 shows a typical graph of the variation of air and solid phase axial velocity profiles in

the pre-bend pipe section. The reference planes are defined according to Figure 9-2 and scale of *x*-axis is adjusted so that the details of peak velocities can be clearly visible.

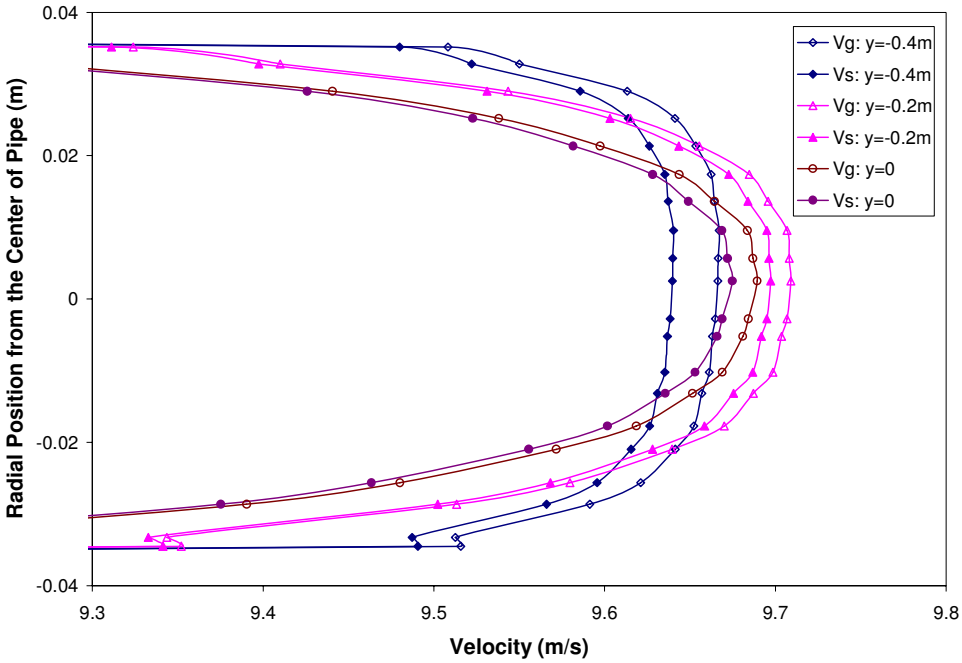

Figure 9-7: Variation of axial velocities of gas and solid phase in the pre-bend straight pipe section (Material: cement, Pipe Diameter: 75mm).

According to Figure 9-7, more uniform axial velocity profile could be detected in early cross sections than the cross sections close to the bend in the straight part of the pre-bend pipe section. This is because the flow inside the pipe was developed while flowing along the straight tube. It was also visible that the difference between solid and gas phase velocities that is usually termed as 'slip velocity' was reducing along the pipe length. As the flow reached to the bend, the slip velocity seemed to be very small compared to that of the inlet section of the calculation domain. The characteristics of these velocity profiles seemed to be in accordance with findings of other researchers [115, 117, 121, 127-129, 211], qualitatively.

The axial air velocity profiles of post-bend pipe sections were also examined. The corresponding graph to the above discussed case (Material: cement, Pipe Diameter:

75mm) is shown in Figure 9-8. To detect the true shape of the whole velocity profile, *x*-axis has been set to the auto-scale status.

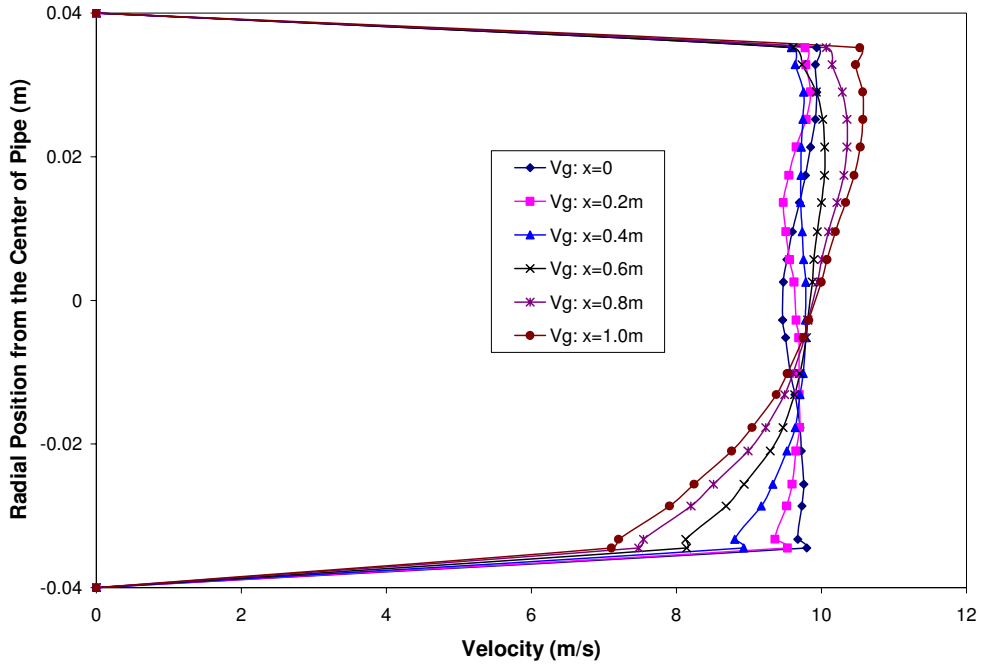

Figure 9-8: Variation of axial velocities of air in the post-bend straight pipe section (Material: cement, Pipe Diameter: 75mm).

Figure 9-8 clearly shows how the axial velocity profiles of gas-phase changes after the gas-solid flow leaves the bend. As the flow propagates through the pipeline, the gas-phase velocity profile, which has been approximately uniform in pre-bend region, as shown in Figure 9-7, is getting distorted and the maximum velocity value tends to the top region of the pipe cross section. Close to the outlet of the considered pipe section, this phenomenon could be seen clearly. One reason, which could be emphasized here, is the high particle concentration close to the bottom of the pipe than the top half of the pipe. Due to high frequent particle collisions in the bottom region, comparatively high loss of momentum of gas-phase can be expected in the lower part of the pipe circumference than the upper portion. This higher collision frequency, as discussed earlier, is a result of gravitational settling of solid particle in the lower half of the pipe cross-section. Since the momentum is required from the air flow to transport and accelerate the solid particles, the axial component of gas

velocity is also reduced leading to the distortion of velocity profile in the lower half of the pipe cross-section.

The asymmetric profiles detected in this investigation were similar to those found in many other research studies [209, 211-214, 216]. Some of them [209, 212, 213] used numerical simulation methods based on CFD principles while others [211, 214, 216] utilised various methods of velocity measurement like phase-Doppler anemometry (PDA), electrical capacitance tomography (ECT), etc, to detect the velocity profiles of gas-solid flows in pipeline systems. In most of their studies, this phenomenon was verified with help of experimental measuring methods.

To detect change in the slip velocity in post-bend region, two cross sections; one just after the bend (x = 0) and one close to the outlet (x = 1.0) were chosen as the reference planes and the axial solid velocity profiles of gas-phase in these two cross sectional surfaces were plotted against the radial distance, along with solid-phase velocity profiles. Figure 9-9 shows the detailed differences of the gas and solid phase velocity changes.

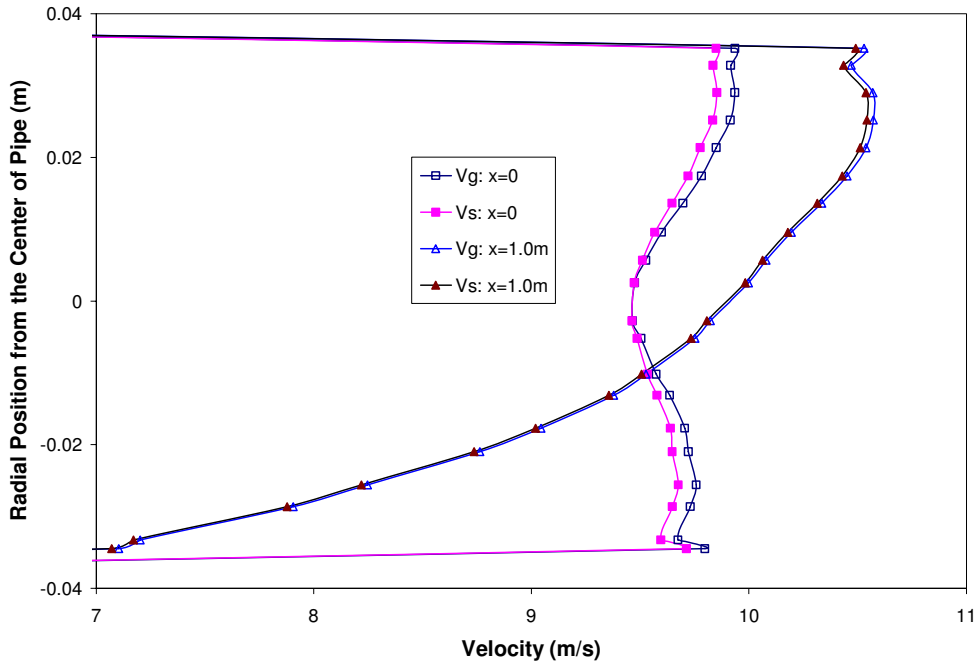

Figure 9-9: Variation of axial velocities of gas and solid phase in the post-bend straight pipe section (Material: cement, Pipe Diameter: 75mm).

According to Figure 9-9, a clear difference could be seen between the gas and solid velocity profiles corresponding to the cross section, which is just after the bend curvature (x = 0), while the two profiles approximately coincide each other in the cross section at further down stream (x = 1.0). Consequently, it is clear that the slip velocity becomes less as the gas-solid mixture flows along the down-stream of the bend. Similar features could be seen in pre-bend region as well. As the flow approaches to the bend, the slip velocity becomes less as shown in Figure 9-7. This demonstrates that the particle velocity is not very different from the gas velocity in the developed flow. On the other hand, since the particles used for this investigation is rather small, the possibility of experiencing a significant slip between two phases is very less. However, the slip velocity is comparatively less, particularly, in dense phase conveying conditions [6].

The concept of slip velocity or the velocity difference between phases has drawn a special attention in research field of pneumatic conveying and considerable number of publications could be found on this topic. Among them, some studies [47, 178, 203-208, 211] reported similar results to the current investigation.

9.7.3 Pressure drop determination

During the post processing of simulation data, it could be able to determine the pressure drop across the considered bend. The pressure drops across the bend, mainly in between the locations of two pressure transducers, were calculated with the help of the simulation outcomes and compared with the experimental observations. Figure 9-10 shows the graph of experimental pressure drop values vs. calculated pressure drop results for all three conveying materials in three different pipe sizes.

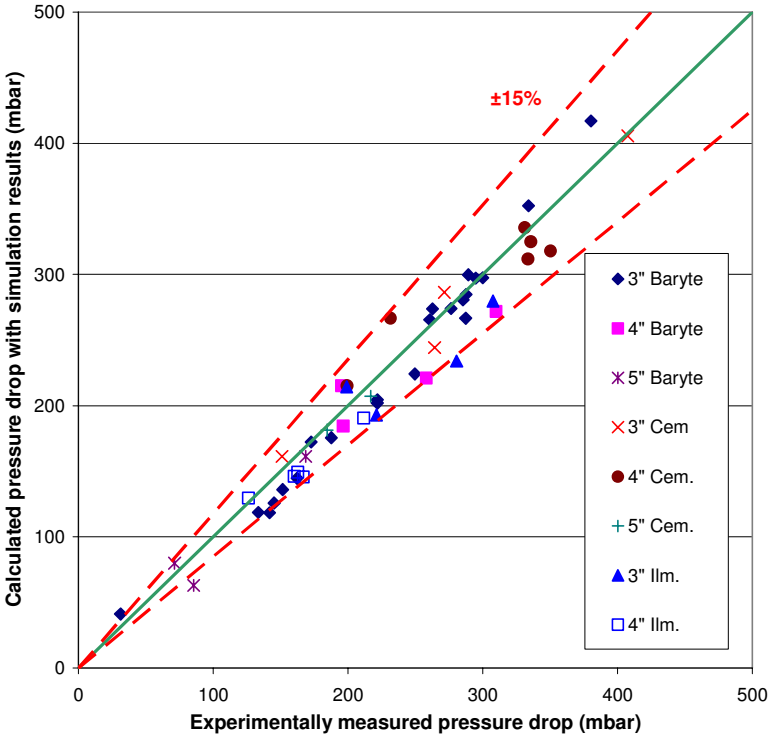

Figure 9-10: Simulation vs. experimental results of pressure drop across the bend.

According to Figure 9-10, it is clear that the simulation results are in considerable good agreement with the experimental observation, with ±15% deviation in general. The same procedure was followed for the straight section analysis. The relevant graph showing the comparison between the simulation results and experimental measurements is given in Figure 9-11.

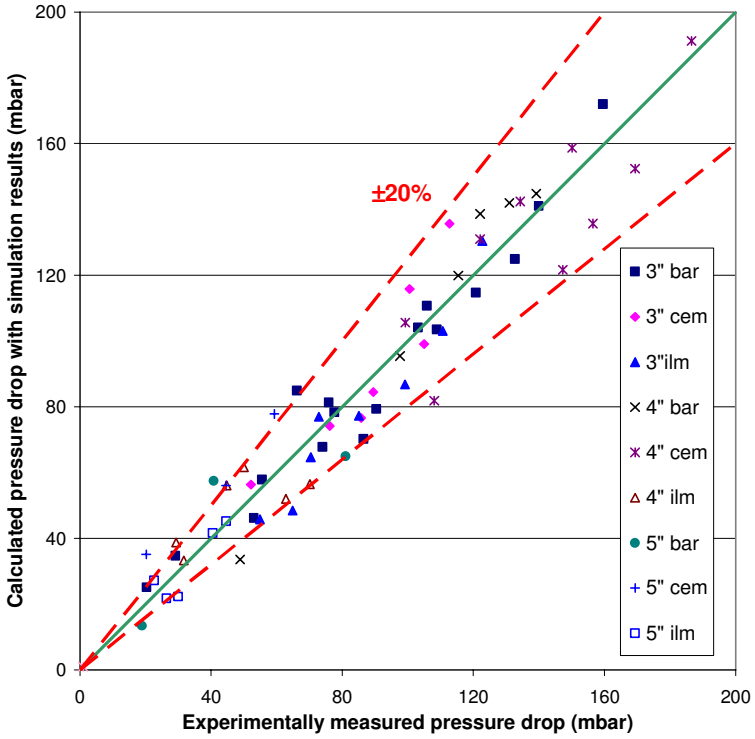

Figure 9-11: Simulation vs. experimental results of pressure drop across the straight section.

This is a quite interesting result, particularly without using any user defined subroutines or any such additional tuning to the basic model available in Fluent® 6, except the carefull selection of boundary conditions.

As mentioned earlier, it was assumed the solid particles are of mono-size and spherical in shape. This assumption deviates from the real situation where barytes, cement and Ilmenite are roughly of uneven fractural (prismatic), cubical and conchoidal shapes respectively, as described in Chapter 4. Similarly, the assumption of mono-sized particles is also not compatible with the real situation. Even with these assumptions, the pressure drop calculations were within acceptable range with basic model formulation available in the Fluent® software package. With this observation, it is clear that the Fluent® software code can reliably be used to calculate and predict the flow phenomena in dense phase pneumatic transport.

9.8 Conclusion

The Euler-Euler granular approach with the kinetic theory for the multiphase flow has been used to simulate the gas-solid particle flow in a standard 90º horizontal to horizontal bend and a straight pipe section of 2m long of a pneumatic transport system with dense phase flow condition, using a commercial CFD software package; Fluent® in three-dimensional space. To simulate the turbulence for the gas and solid phases, the k-ε model has been used. Pneumatic conveying tests were carried out using three different materials and three different pipeline configurations with respect to the pipe diameter.

The results on variations of volume fraction of solid particle, gas and solid phase velocity profiles and pressure drop determination across the bend were analysed using the post-processing facilities available with the software. Although no experimental measurement was made on solid particle concentrations and phase velocities, a good qualitative agreement of the simulation results could be detected with the published results by other research workers. In case of pressure drop determination, considerably good agreement could be found between the experimental measurements and simulation results with error margins of ± 15% for the bends and ± 20% for the straight sections for all conveying conditions and combinations under the consideration of this investigation.

From the simulation results, it is clear that Fluent® CFD software has a good potential to model the gas-sold flow across a bend in dense phase pneumatic conveying satisfactorily. In fact, this investigation and the simulation work have been carried out as an initial step towards a reliable modelling technique of dense phase pneumatic conveying.

10 CONCLUSIONS AND SUGGESTIONS FOR FUTURE WORK

10.1 Introduction

As discussed in details under Chapter 1, the main aim of the present investigation was to formulate a comprehensive scaling up technique for pneumatic conveying system designs. The investigation was conducted in few steps addressing different important issues separately and formulating the models to explain the behaviour of gas-solid flow in various sections of conveying line. In the final stage, all proposed models were put together in the form of a computer based software programme. In addition, a detailed investigation was carried out to check the ability of a commercial software; Fluent® based on computational fluid dynamics principles, to use as a tool for pressure drop prediction across different pipeline components.

Under this chapter, the general conclusions based on the findings of the present investigation are discussed followed by the conclusions drawn in respect of;

- Scaling up of line pressure drop
- Scaling up of entry loss
- Scaling up of minimum conveying conditions
- Numerical simulations

At the end, suggestions are made for the continuation of this scientific investigation leading to a better understanding and control of pneumatic conveying systems.

10.2 General Conclusions

As mentioned under Chapter 1, this investigation was planned on the basis of the findings of a preliminary investigation [29], where the capabilities of available scaling up and pressure drop prediction models of pneumatic conveying systems were discussed. According to the said investigation, the available scaling up techniques were found to over-estimate the pressure drop, in most of the cases. This, in other words, implies that the material transport capacity of the system is

underestimated for a particular available pressure head. The literature survey carried out with the aim of exploring the current status of pneumatic conveying field in the light of modern scientific studies, also revealed the lack of scaling up and pressure drop predicting techniques, which are simple, straight forward, complete and reliable in their applications of both dilute and dense phase conveying. The above described findings indicated a need for a scientific study to investigate the possibilities of formulating a comprehensive scaling up technique.

The research investigation presented in this thesis is believed to be an important contribution to the knowledge in the field of pneumatic conveying. This is the first time that all the aspects and components of conveying line together with the minimum conveying conditions are addressed in scaling up standpoint. A number of important conclusions, as described in individual sections, have been drawn from the pneumatic conveying tests and the model formulations for scaling up methods.

10.2.1 Scaling up of Line Pressure Drop

This section basically addressed the conveying line starting from the outlet section of the blow tank to the inlet section of receiving tank including all types of bends, together with all pipeline accessories like valves, hose sections, etc,. The pneumatic conveying test runs were carried out with five different bulk materials including one with five different qualities in terms of mean particle diameter and particle size distribution. Five different configurations of conveying pipelines were used during the tests. Attempt was made to cover the whole range of conveying conditions, i.e., from dilute phase to dense phase for all the materials tested.

A model was proposed based on the well-known piece wise approach of scaling. The piece wise approach, as understood by many other researchers as well, gives comparatively better results than in the case of global approach, where the whole conveying line is considered as a single unit with all bends and other accessories on it, since the positions of individual features of pipeline are taken into account together with their inlet velocities. One can easily understand the importance of the inlet velocities of different sections, since it varies along the pipeline and the

behaviour of gas-solid flow is greatly influenced by the inlet velocity of the concerned section.

The proposed model is a modified version of the well-known Darcy-Weisbach's equation for single phase flows. The friction factor is replaced with a newly introduced factor called 'pressure drop coefficient' or *K* factor and the density term is also replaced by suspension density as defined in Section 4.2.2.

The properties of *K* factor and the relevant conclusions could be listed as follows.

- After plotting the *K* factors against few different parameters, it was revealed that there is a strong relationship between *K* value of straight pipe sections and other pipe accessories like bends, valves, etc, and the square value of entry velocity of the concerned section.
- The behaviour of *K* vs. V_{entry}^2 curves shows a common trend of power-law relationship with increasing entry velocity for all conveying bulk materials. This leads to a conclusion that the value of *K* factor decreases rapidly with increase in conveying velocity for dense phase conditions, where the conveying velocity is low and attains more or less a constant value for the dilute phase conveying condition.
- The relationship between *K* and V_{entry}^2 is found to be independent of pipe diameter for all pipe sections and all conveying materials tested in this study.
- The behaviour of *K* vs. V_{entry}^2 for horizontal pipe sections was found to be dependent on the mean particle size of the conveying material, while the same for vertical pipe sections was found to be independent of particle size.
- In the validation analysis using graphical and statistical tools, all possible combinations of pipeline configurations, bulk materials and flow conditions were used and it showed a reasonably good agreement between predicted and experimentally measured pressure values along the conveying pipeline. This is considered to be a significant achievement.
- The predictions of proposed model were compared with some popular scaling up and pressure drop determination techniques available the literature. The scaling up technique proposed in this thesis gave the least error in all flow conditions considered.

10.2.2 Scaling up of Entry Loss

During the conveying tests with different materials and pipeline configurations, it was noticed that the pressure loss incurred at the entry section of the conveying line is significant, especially in case of top discharge blow tank systems. Under the present investigation, a model was derived using dimensional analysis for scaling up of entry pressure loss in a top discharge blow tank. The model developed was found to be independent of pipe size and hence could be used as a very useful tool for scaling up. The proposed model is very simple and needs only readily available experimental data without any complicated manipulation. The validation analysis showed very promising results for different conveying materials, pipeline configurations and flow conditions tested.

10.2.3 Scaling up of Minimum Conveying Velocity

The determination of minimum conveying velocity is crucial for the successful operation of a pneumatic conveying system. It was found that the available models did not give reliable predictions, especially for fine powders.

The major problem for formulating a general model for minimum conveying velocity has been identified as the availability of numerous influential parameters such as, particle size and size distribution, particle density, particle shape, gas density, etc. During the present investigation, the mathematical techniques called principal component analysis and dimensional analysis were successfully used to screen out the influential parameters and formulate a relationship between the most important physical parameters of the minimum conveying velocity. The validation and comparison analysis showed a good agreement between the predictions of proposed model and experimentally observed minimum conveying conditions.

10.2.4 Computer Based Calculation Programme

Having developed all the models, i.e., conveying line pressure drop for straight sections, bends, valves, etc, entry pressure drop, minimum conveying velocity

prediction, an attempt was made to develop a general computer based calculation programme. The calculation in the programme is done in steps of 1 m pipe sections for straight pipe sections. However, valves bends and other pipe components are considered as individual sections in calculation programme.

Using the test plant results for each material, one can have a general system design programme for that material for any variations of pipe size, transport capacity, air pressure and air flow rate. The calculation programme has been tested for all the materials under this study.

10.2.5 CFD Simulation on Pipe Bends and Straight Sections

As an alternative approach to the classical methods of pressure drop determination using various models, the numerical simulation technique using computational fluid dynamics (CFD) principles has also been tried in this study. The basic objective of the inclusion of numerical simulation component to this experimental study was to find out whether the commercially available CFD software codes are good enough to predict the pressure drop of a pneumatic transport system reliably.

The Euler-Euler granular approach with the kinetic theory for the multiphase flow was used to simulate the gas-solid particle flow in a standard 90º horizontal to horizontal bend and a straight section of 2m long of a pneumatic transport system with dense phase flow condition, using a commercial CFD software package, called Fluent®, in three-dimensional space. The turbulence of gas and solid phases was modelled using the k-ε model. The results produced by three different conveying materials and three different pipeline configurations were used for the simulation work.

With the help of the post-processing facilities of considered software, the results on variations of volume fraction of solids particle, gas and solid phase velocity profiles and pressure drop determination across the bend were analysed. During the experimentations, measurements were not made on solid particle concentrations and phase velocities. But, the results of numerical simulations were seen in a good

qualitative agreement with the published results by other research workers. In case of pressure drop determination, a good agreement could be found between the experimental measurements and simulation results with error margins of ± 15% for the bends and ± 20% for the straight sections for all conveying conditions and for all combinations of conveying materials and pipe configurations considered. This is a considerable achievement amidst the divergent disagreements reported in literatures.

10.3 Suggestion for Future Works

Although the models proposed under the present investigation have been remarkably successful for the different materials and pipeline configurations tested, it has been understood that there are still many aspects that have not been fully addressed. There are some areas where further scientific studies and investigations would further improve our general understanding of the complex flow phenomenon of pneumatic conveying. The followings are some suggestions for future studies.

- Although the scaling up models produce very good results for conveying materials selected for the current investigation, more experiments need to be undertaken to cover an even wider range of bulk materials. Since the selected materials are mostly representing the group 'A' and 'C' materials of Geldart classification, the testing of bulk materials of other groups are recommended.
- One shortcoming of the measurement procedure adopted during the current investigation was that the re-acceleration pressure drops related to bends and other pipe components did not taken into account. The modifications are recommended for the measurement procedure and the effect of re-acceleration of flow has to be determined.
- The inclusion of vertical sections of 125 mm pipe diameter is also recommended.
- The pressure drop coefficient or K factor has been found to be dependent on the material quality. It will be interesting to investigate if it is possible to predict the K factor based on material characteristics.

- In the proposed models, the mean particle diameter or d_{50} has been used instead of particle size distribution. Attempt should be made to incorporate the effects of particle side distribution in the proposed models.
- The effect of particle shape on pressure drop will also be interesting to investigate.
- It is suggested that further studies should be made for the applicability of CFD simulation technique for various other types of bends, pipe components and vertical sections.

11 BIBLIOGRAPHY

1. Purutyan, H., T.G. Troxel, and F. Cabrejos, *Propel your pneumatic conveying system to higher efficiency.* Chemical Engineering Progress, 2001. **97**(4): p. 42-55.
2. Woodcroft, B. *The pneumatics of hero of Alexandria*. 1851 [cited 2005; Available from: http://www.history.rochester.edu/steam/hero/.
3. Wypych, P.W., *Introduction to Pneumatic Conveying.* Transport of Particulate Materials, An Intensive Short Course, Porsgruun, Norway, 1999.
4. Molerus, O., *Overview: Pneumatic Transport of Solids.* Powder technology, 1996. **88**(3): p. 309-321.
5. Huggett, M.R. *The Evalution of the Practice of Pneumatic Conveying*. in *Pneumatech 3, Third International Conference on Pneumatic Conveying Technology*. 1987. The Grand Hotel, Jersey, Channel Islands.
6. Klinzing, G.E., Marcus, R.D., Rizk, F. and Leung, L.S., *Pneumatic Conveying of Solids -A Theoretical and Practical Approach*. 1997: Chapman & Hall.
7. Soo, S.L., *Long Distance Pneumatic Transportation.* Journal of Pipelines, 1984. **4**: p. 79-85.
8. Link, W.H., 1998, *Investigation of the Efficacy of the Flow Enhancer and the Indentification of the Beginning of the Unstable Zone in Pneumatic Conveying Systems*, Graduate Faculty, School of Engineering, University of Pittsburgh, Pittsburgh, USA.
9. *AIR-TEC System: Official Website*, http://www.air-tec.it/index_materialitrasp_uk.html
10. Zapato, L., *The Inteli-Tube Pneumatic Transportation System.*
11. Liu, H. *Pneumatic Casule Pipeline- Basic Concept, practical Considerations, and Current Research*. in *Mid-Continent Transportation Symposium*. 2000. Iowa State University, Ames, Iowa, USA.

12. De Silva, S.R. and B.K. Datta, *Transport of Particulate Materials- Dilute Phase Pneumatic Transport*, in *Lecture Notes on Powder Technology, Telemark University College, Porsgruun, Norway*. 2000.
13. *The Basics of Pneumatic Conveying*, 2004, http://www.dynamicair.comsystems.html
14. Zenz, F.A., *Conveyability of Materials of Mixed Particle Size.* Industrial and Engineering Chemistry, American Chemical Society, 1964. **3**(1): p. 65-75.
15. Zenz, F.A. and D.F. Othmer, *Fluidization and fluid particle systems*. 1960: Reinhold, New York.
16. Mills, D., *Pneumatic Conveying Design Guide*. 1990: Butterworth.
17. Mills, D., *Optimizing pneumatic conveying.* Chemical Engineering, 2000. **107**(13): p. 74-80.
18. Mills, D., *A review of the research work of Professor Predrag Marjanovic.* Chemical Engineering and Processing, 2005. **44**(2): p. 141-151.
19. Mills, D. and J.S. Mason, *The Uprating of Pneumatic Conveying Systems.* Journal of Pipelines, 1982. **2**(2-4): p. 199-210.
20. Mills, D. and J.S. Mason. *The influence of conveying distance on the performance and air requiremnts of pneumatic conveying system pipelines*. in *Reliable Flow of Particulate Soilds*. 1985. Bergen, Norway.
21. Behera, S. and S. Das, *Desirable conveying characteristics for pneumatic transportation of fly-ash, sand, cement and crushed bath.* Powder Handling & Processing, 2000. **12**(1): p. 23-25.
22. Pan, R. and P.W. Wypych, *Scale-up Procedures for Pneumatic Conveying Design.* Powder Handling and Processing, 1992. **4**(2): p. 167-172.
23. Pan, R. and P.W. Wypych, *Pressure Drop and Slug Velocity in Low-Velocity Pneumatic Conveying of Bulk Solids.* Powder Technology, 1997. **94**(2): p. 123-132.
24. Wypych, P.W., *Prediction and Scaling up of Steady-State Operating Condition.* Transport of Particulate Materials, An Intensive Short Course, Porsgruun, Norway, 1999.

25. Wypych, P.W. and P.C. Arnold, *On Improving Scale-up Procedures for Pneumatic Conveying Design.* Powder Technology, 1987. **50**(3): p. 281-294.
26. Klinzing, G.E., N.D. Rohatgi, A. Zaltash, and C.A. Myler, *Pneumatic Transport - a Review (Generalized Phase-Diagram Approach to Pneumatic Transport).* Powder Technology, 1987. **51**(2): p. 135-149.
27. Woodcock, C.R. and J.S. Mason, *Bulk Solids Handling - An Introduction to the Practice and Technology*. 1987: Leonard Hill.
28. Meyers, S., R.D. Marcus, and F. Rizk, *The state diagrame for fine-particle gas/solids suspensions.* Bulk Solids Handling, 1985. **5**(4): p. 779-782.
29. Ratnayake, C., 2000, *An Experimental Investigation of Scaling Up Techniques in Pneumatic Conveying*, MSc, Dept. of Powder Science and Technology, Telemark University College, Porsgrunn, Norway.
30. De Silva, S.R., *Transport of Particulate Material- Dilute Phase Pneumatic Transport.* Lecture Notes on Powder Technology, Telemark University College, Porsgruun, Norway, 1995.
31. Mills, D., *Troubleshooting Pneumatic Conveying.2. Major Systems and Their Key Components.* Chemical Engineering, 1990. **97**(7): p. 101-107.
32. Marcus, R.D., C. Wiggill, and F. Rizk, *Parameters Influencing Long-Distance Pneumatic Conveying Systems.* The Best of Powder Handling & Processing Bulk Solids Handling, 1985. **D/86**: p. 17-24.
33. Jones, M.G., D. Mills, and J.S. Mason, *A Comparison of the Performance of Top and Bottom Discharge Blow Tank Systems.* Bulk Solids Handling, 1987. **7**(5): p. 701 - 706.
34. Cabrejos, F.J. and G.E. Klinzing, *Incipient Motion of Solid Particles in Horizontal Pneumatic Conveying.* Powder Technology, 1992. **72**(1): p. 51-61.
35. Cabrejos, F.J. and G.E. Klinzing, *Pickup and saltation mechanisms of solid particles in horizontal pneumatic transport.* Powder technology, 1994. **79**(2): p. 173-186.
36. Martinussen, S.E., 1996, *The Influence of the Physical Characteristics of Particulate Materials on their Conveyability in Pneumatic Transport*

Systems, PhD, Technological Department, Telemark University College, Porsgruun, Norway.

37. Matsumoto, S., Hara, M., Saito, S., Maeda, S., *Minimum Transport Velocity for Horizontal Pneumatic Conveyimg.* Journal of Chemical Engineering, Japan, 1974. **7**(6): p. 425-430.
38. Rizk, F., *Pneumatic Conveying at Optimal Conditions and a Solution of Barth's Equation.* Pneumotransport 3, Third International Conference on the Pneumatic Transport of Solids in Pipes, 1976. **Paper D4**: p. 43-58.
39. Rizk, F., *Pneumatic Transport in Dilute and Dense Phase.* Bulk Solids Handling, 1982. **2**(2): p. 9-15.
40. Woodcock, C.R., *Review of Latest Theoretical Studies.* Course on Advanced Pneumatic Conveying, Copenhagen, Denmark.
41. Weber, M., *Correlation Analyses in the Design of Pneumatic Transport Plant.* Bulk Solids Handling, 1982. **2**(2): p. 231-233.
42. Pan, R. and J. Chambers, *Pneumatic Conveying of Iron Ore in a High Pressure System -Part B: Details of Test Runs and Scale-up Procedures.* Bulk Solids Handling, 1999. **19**(3): p. 321-327.
43. Weber, M., *Friction of the Air and Air/Solid Mixture in Pneumatic Conveying.* Bulk Solids Handling 2, 1991. **11**(1): p. 99-102.
44. Massey, B.S., *Mechanics of Fluids*. 6th Edition ed. 1989: Van Nostrand Reinhold.
45. Streeter, V.L. and E.B. Wylie, *Fluid Mechanics*, ed. s. metric: McGraw Hill.
46. Wypych, P.W. and R. Pan, *Determination of Air-only pressure Drop in Pneumatic Conveying Systems.* Powder Handling and Processing, 1991. **3**(4).
47. Arastoopour, H., M.V. Modi, D.V. Punwani, and A.T. Talwalkar. *A Review of Design Equations for the Dilute-Phase Gas-Solids Horizonntal Conveying Systems for Coal and Related Materials*. in *Proc. of International Powder and Bulk Solids Handling and Processing Conference*. 1979. Philadelphia.
48. Rose, H.E. and H.E. Barnacle, *Flow of Suspensions of Non-cohesive Spherical Particles in Pipes.* The Engineer, 1957. **203**: p. 898-901.

49. Hinkle, B.L., *Acceleration of Particle and Pressure Drop Encountered in Horizontal Pneumatic Conveying.* PhD Thesis, Georgia Institute of Technology, 1953.
50. Richardson, J.F. and M. McLeman, *Pneumatic Conveying: Part II; Solids Velocities and Pressure Gradients in a One-inch Horizontal Pipe.* Transactions of Institution of Chemical Engineers, 1960. **38**: p. 257-266.
51. Boothroyd, R.G., *Flowing Gas-Solids Suspensions*. 1971: Chapman and Hall, London.
52. Yang, W.C., *Correlations of Solid Friction Factors in Vertical and Horizontal Pneumatic Conveying.* AiChE Journal, 1974. **20**(3): p. 605-607.
53. Szikszay, G., *Friction factor for Dilute Phase Pneumatic Conveying.* Bulk Solids Handling 2, 1988. **8**(4): p. 395-399.
54. Pan, R. and P.W. Wypych, *Pressure Drop Due to Solids-Air Flow in Horizontal and Vertical Pipes.* Proc. of International Conference on Bulk Material Handling &Transportation; Symposium on Freight Pipelines, Wollongong, Australia, 1992.
55. Duckworth, R.A., *Empirical Correlations for the Dilute Phase.* Lecture Notes, C.S.I.R.O. mineral Engineering, Dept. Of Chemical Engineering, Univ. of Queensland.
56. Stermerding, S., *The Pneumatic Transport of Cracking Catalist in Vertical risers.* Chemical Engineering Science, 1962. **17**(8): p. 599-608.
57. Reddy, K.V.S. and D.C.T. Pei, *Particle Dynamics in Solids-Gas Flow in a vertical Pipe.* Industrial Engineering Chemical Fundamental, 1969(8): p. 490.
58. Capes, C.E. and K. Nakamura, *Vertical Pneumatic Conveying: An Experimental Study with Particles in Intermediate and Turbulent Flow Regimes.* Canadian Journal of Chemical Engineering, 1973. **51**: p. 31.
59. Konno, H. and S. Saito, *Pneumatic Conveying of Soilds through Straight Pipes.* Journal of Chemical Engineering, Japan, 1969. **2**(2): p. 211.
60. Klinzing, G.E., C.A. Myler, A. Zaltash, and S. Dhodapkar, *A Simplified Correlation for Solids Friction Factor in Horizontal Conveying Systems*

Based on Yang's Unified Theory. Powder Technology, 1989. **58**(3): p. 187-193.

61. Molerus, O. and U. Heucke, *Pneumatic Transport of Coarse Grained Particles in Horizontal Pipes.* Powder Technology, 1999. **102**(2): p. 16.
62. Mills, D., D.J. Mason, and V.K. Agarwal, *An Accesment of Acceleration Length through Erosive Measurements.* Proc. of 10th Annual Conference on Powder & Bulk Solids Handling and Processing, Rosemont, Illinois, 1985: p. 215-228.
63. Marcus, R.D., *Pneumatic Conveying of Bulk Solids.* Notes of Short Courses on Pneumatic Conveying, The Univ. of Newcastle, NSW, Australia, 1983.
64. Konrad, K., D. Harrison, R.M. Neddermann, and J.F. Davidson, *Prediction of the Pressure Drop for Horizontal Dense Phase Conveying of Particles.* Pneumotransport 5, Proc. of 5th International Conference on the Pneumatic Transport of Solids in Pipes, London, UK., 1980: p. 225-244.
65. Konrad, K., *Dense-Phase Pneumatic Conveying through Long Pipelines: Effect of Significantly Compressible Air Flow on Pressure Drop.* Powder Technology, 1986. **48**(3): p. 193-203.
66. Legel, D. and J. Schwedes, *Investigation of Pneumatic Conveying of Plugs of Cohesionless Bulk Solids in horizontal Pipes.* Bulk Solids Handling, 1984. **4**(2): p. 399-405.
67. Mi, B. and P.W. Wypch, *Pressure-Drop Prediction in Low-Velocity Pneumatic Conveying.* Powder Technology, 1994. **81**(2): p. 125-137.
68. Mi, B. and P.W. Wypych, *Investigations into Wall Pressure during Slug-Flow Pneumatic Conveying.* Powder Technology, 1995. **84**(1): p. 91-98.
69. Pan, R., B. Mi, and P.W. Wypych, *Pneumatic Conveying Characteristics of Fine and Granular Bulk Solids.* KONA, 1994. **12**: p. 77-85.
70. Matsuda, M., N. Sugita, S. Nihimori, N. Sugimoto, and Y. Morikawa, *Dense Phase Flow of Powder in Horizontal and Inclined Pneumatic Conveying by a Nemo Pump.* Powder Handling and Processing, 2000. **12**(1): p. 17-21.

71. Hong, J., Y.S. Shen, and S.L. Liu, *A Model for Gas-Solid Stratified Flow in Horizontal Dense-Phase Pneumatic Conveying.* Powder Technology, 1993. **77**(2): p. 107-114.
72. Woodcock, C.R., Mason, J.S., *Bulk Solids Handling - An Introduction to the Practice and Technology*. 1987: Leonard Hill.
73. Werner, D., *Influence of Particle Size Distribution during Pneumatic Dense Phase Conveying in Vertical and Horizontal Pipes.* Bulk Solids Handling, 1983. **3**(2): p. 351-359.
74. Plumpe, J.G., C. Zhu, and S.L. Soo, *Measurements of Fluctuations in Motion of Particles in a dense phase gas/solid suspension in vertical pipe flow.* Powder Technology, 1993. **77**(2): p. 209-214.
75. Rautiainen, A., G. Stewart, V. Poikolainen, and P. Sarkomaa, *An Experimental Study of Vertical Pneumatic Conveying.* Powder Technology, 1999. **104**(2): p. 139-150.
76. Tsuji, Y. and R. Asano, *Fundamental investigation of plug conveying of cohesionless particles in a vertical pipe (pressure drop and friction of a stationary plug).* The Canadian Journal of Chemical Engineering, 1990. **68**: p. 758/767.
77. Yang, W.C., *Correlation for Solid Friction Factor in Vertical Pneumatic Conveying Lines.* AIChE Journal, 1978. **24**(3): p. 548-552.
78. Carpinlioglu, M.O., T.A. Ozbelge, and V. Oruc, *Flow frictional resistance in pneumatic conveying of solid particles through inclined lines.* Powder Technology, 2002. **125**(2-3): p. 292-297.
79. Ginestet, A., P. Guigon, J.F. Large, and J.M. Beeckmans, *Further-Studies on Flowing Gas-Solids Suspensions in a Tube at High Angles of Inclination.* Canadian Journal of Chemical Engineering, 1994. **72**(4): p. 582-587.
80. Hirota, M., Y. Sogo, T. Marutani, and M. Suzuki, *Effect of mechanical properties of powder on pneumatic conveying in inclined pipe.* Powder Technology, 2002. **122**(2-3): p. 150-155.
81. Levy, A., T. Mooney, P. Marjanovic, and D.J. Mason, *A Comparison of Analytical and Numerical Models with Experimental Data for Gas-Solid*

Flow through a Straight Pipe at Different Inclinations. Powder Technology, 1997. **93**(3): p. 253-260.

82. Aziz, Z.B. and G.E. Klinzing, *Dense Phase Plug Flow Transfer:The 1-inch Horizontal Flow.* Powder Technology, 1990. **62**: p. 41-49.
83. Ito, H., *Pressure losses in smooth pipe bends.* Journal of Basic Engineering, 1960(March): p. 131-143.
84. Mills, D. and M.J. Mason, *The Influence of Bend geometry on Pressure Drop in Pneumatic Conveying System Pipelines.* Proceedings of 10th Annual Conference on Powder and Bulk Solids Handling and Processing. Rosemont. Illinois., 1985: p. 203-214.
85. Klinzing, G.E., *A comparison of pressure losses in bends between recent data and model for gas-solid flow.* The Canadian journal of chemical engineering, 1980. **58**: p. 670-672.
86. Pan, R., P.W. Wypych, and P.C. Arnold, *Pressure Drop due to different Radius Bends connected by Short Straight Pipes.* Proceedings of International Symposium 'RELPOWFLO II'. Oslo. Norway, 1993: p. 1022-1029.
87. Westman, M.A., E.E. Michaelides, and F.M. Thomson, *Pressure Losses Due to Bends in Pneumatic Conveying.* Journal of Pipelines, 1987. **7**(1): p. 15-20.
88. Marcus, R.D., J.D. Hilbert, and G.E. Klinzing, *The Flow through Bends in Pneumatic Conveying Systems.* Journal of Pipelines, 1984. **4**(2): p. 103-112.
89. Cabrejos, F.J. and G.E. Klinzing, *Minimum Conveying Velocity in Horizontal Pneumatic Transport and the Pickup and Saltation Mechanisms of Solid Particles.* Bulk Solids Handling, 1994. **14**(3): p. 541.
90. Hayden, K.S., K. Park, and J.S. Curtis, *Effect of Particle Characteristics on Particle Pickup Velocity.* Powder Technology, 2003. **131**: p. 7-14.
91. Molerus, O., *Principles of flow in disperse systems*. 1993: Chapman & Hall.
92. Weber, M., *Principles of Hydraulic and Pneumatic Conveying in Pipes.* The Best of the Bulk Solids handling 1981-85, Pneumatic Conveying of bulk & Powder., 1981. **D86**: p. 1- 7.

93. Xu, G.W., K. Nomura, S. Gao, and K. Kato, *More fundamentals of dilute suspension collapse and choking for vertical conveying systems.* Aiche Journal, 2001. **47**(10): p. 2177-2196.

94. Yang, W.C., *A Mathematical Definition of Choking Phenomenon and a Mathematical Model for Predicting Choking Velocity and Choking Voidage.* AIChE Journal, 1975. **21**(5): p. 1013 - 1015.

95. Keys, S. and A.J. Chambers. *Scaling Pneumatic Conveying Characteristics for Pipeline Pressure*. in *International Symposium: Reliable Flow of Particulate Solids II*. 1993. Oslo, Norway.

96. Bradley, M.S.A., *pressure Losses Caused by Bends in Pneumatic Conveying Pipelines -Effects of Bend Geometry and Fittings.* Powder Handling and Processing, 1990. **2**(4): p. 315-321.

97. Bradley, M.S.A. and A. Reed, *An Improved Method of Predicting Pressure Drop Along Pneumatic Conveying Pipelines.* Powder Handling & Processing, 1990. **2**(3): p. 223-227.

98. Hettiaratchi, K., M.S.A. Bradley, R.J. Farnish, I. Bridle, L.M. Hyder, and A.R. Reed, *An investigation into the effect of product type when scaling for diameter in vertical pipelines.* Powder Technology, 2000. **112**(3): p. 229-234.

99. Hettiaratchi, K., M.S.A. Bradley, A.R. Reed, and M.J. Smith, *Pressure drop in pneumtic conveying through vertical pipelines.* BULK MAT. HANDL. & TRANSP., 1992(July 6, - 8.): p. 73 - 77.

100. Hyder, L.M., M.S.A. Bradley, A.R. Reed, and K. Hettiaratchi, *An investigation into the effect of particle size on straight-pipe pressure gradients in lean-phase conveying.* Powder Technology, 2000. **112**(3): p. 235-243.

101. Reed, A. and M.S.A. Bradley, *Advances in the Design of Pneumatic Conveying Systems - A United Kingdom Perspective.* Bulk Solids Handling, 1991. **11**(1): p. 93-97.

102. Geldart, D., *Types of Gas Fluidization.* Powder Technology, 1973. **7**: p. 285 - 292.

103. Dixon, G., *How do different powders behave?* Bulk Storage Movement Control, 1979. **5**(5): p. 81 - 88.
104. Dixon, G. *Fluidisation theory throws light on dense phase conveying practice*. in *Pneumatech 4, 4th International Conference on Pneumatic Conveying Technology*. 1990. Glasgow, Scotland.
105. Mainwaring, N.J., *Characterization of Materials for Pneumatic Conveying.* American Ceramic Society Bulletin, 1993. **72**(8): p. 63-&.
106. Mainwaring, N.J. and A.R. Reed, *Permeability and air retention charadteristics of bulk solid materials in relation to modes of dense phase pneumatic conveying.* Bulk Solids Handling, 1987. **7**(June No. 3): p. 415 - 425.
107. Jones, M.G. and D. Mills, *Product classification for pneumatic conveying.* Powder Handling and Processing, 1990. **2**(June No. 2): p. 117 - 122.
108. Goder, D., H. Kalman, G. Ben-Dor, and M. Rivkin, *Experimental Investigation of the Effect of Moisture Content and Particle Size on the Pneumatic Transportability in a Dense Phase.* Powder Handling and Processing, 1994. **6**(3): p. 295-299.
109. Pan, R., *Material properties and flow modes in pneumatic conveying.* Powder Technology, 1999. **104**(2): p. 157-163.
110. Versteeg, H.K. and W. Malalasekera, *An Introduction to Computational Fluid Dynamics- The Finite Volume Method*. 1995: Prentice Hall.
111. Patankar, S.V., *Numerical Heat Transfer and Fluid Flow*. 1980: Hemisphere Publication Corp., Washington.
112. *Fluent 6.1 User's Guide*. Vol. 1, 2 & 3. 2003: Fluent Inc., Lebanon.
113. Mathiesen, V., 1997, *An Experimental and Computational Study of Multiphase Flow Behaviour in Circulating Fluidizing Beds*, PhD, Process Technology, Telemark University College. Norway,
114. Frank, T., K.P. Schade, and D. Petrak, *Numerical simulation and experimental investigation of a gas-sold two-phase flow in a horizontal channel.* International Journal of Multiphase Flow, 1993. **19**(1): p. 187-198.

115. Sommerfeld, M. and C.A. Ho, *Numerical calculation of particle transport in turbulent wall bounded flows.* Powder Technology, 2003. **131**(1): p. 1-6.
116. Watano, S., S. Saito, and T. Suzuki, *Numerical simulation of electrostatic charge in powder pneumatic conveying process.* Powder Technology, 2003. **135**: p. 112-117.
117. Li, H. and Y. Tomita, *A numerical simulation of swirling flow pneumatic conveying in a horizontal pipeline.* Particulate Science and Technology, 2000. **18**(4): p. 275-291.
118. Mathiesen, V., T. Solberg, and B.H. Hjertager, *Predictions of gas/particle flow with an Eulerian model including a realistic particle size distribution.* Powder Technology, 2000. **112**(1-2): p. 34-45.
119. Yasuna, J.A., H.R. Moyer, S. Elliott, and J.L. Sinclair, *Quantitative predictions of gas-particle flow in a vertical pipe with particle-particle interactions.* Powder Technology, 1995. **84**(1): p. 23-34.
120. Srivastava, A. and S. Sundaresan, *Analysis of a frictional-kinetic model for gas-particle flow.* Powder technology, 2003. **129**(1): p. 72-85.
121. Sommerfeld, M., S. Lain, and J. Kussin. *Analysis of Transport Effects of Turbulent Gas-Particle Flow in a Horizontal Channel*. in *Proc. of 4th International Conference on Multiphase Flow*. 2001. New Orleans, ICMF.
122. Tsuji, Y., *Activities in discrete particle simulation in Japan.* Powder Technology, 2000. **113**(3): p. 278-286.
123. Adewumi, M.A. and H. Arastoopour, *Two-Dimensional Steady-State Hydrodynamic Analysis of Gas Solids Flow in Vertical Pneumatic Conveying Systems.* Powder Technology, 1986. **48**(1): p. 67-74.
124. Pelegrina, A.H., *Analysis of pneumatic conveying of particles.* Latin American Applied Research, 2002. **32**(1): p. 91-96.
125. Levy, A., *Two-fluid approach for plug flow simulations in horizontal pneumatic conveying.* Powder Technology, 2000. **112**(3): p. 263-272.
126. Mason, D.J. and A. Levy, *A model for non-suspension gas-solids flow of fine powders in pipes.* International Journal of Multiphase Flow, 2001. **27**(3): p. 415-435.

127. Bilirgen, H., E. Levy, and A. Yilmaz, *Prediction of pneumatic conveying flow phenomena using commercial CFD software.* Powder Technology, 1998. **95**(1): p. 37-41.
128. Balzer, G., *Gas-solid flow modelling based on the kinetic theory of granular media: validation, applications and limitations.* Powder Technology, 2000. **113**(3): p. 299-309.
129. Arastoopour, H., *Numerical simulation and experimental analysis of gas/solid flow systems: 1999 Fluor-Daniel Plenary lecture.* Powder Technology, 2001. **119**(2-3): p. 59-67.
130. Manger, E., 1996, *Modelling and Simulation of Gas/Solids Flow in Curvilinear Coordinates*, Ph.D., Process Technology, Telemark University College, Norway,
131. Tsuji, Y., T. Kawaguchi, and T. Tanaka, *Discrete particle simulation of two-dimensional fluidized bed.* Powder Technology, 1993. **77**(1): p. 79-87.
132. Tsuji, Y., Y. Morikawa, T. Tanaka, N. Nakatsukasa, and M. Nakatani, *Numerical simulation of gas-solid two-phase flow in a two-dimensional horizontal channel.* International Journal of Multiphase Flow, 1987. **13**: p. 671-684.
133. Tsuji, Y., T. Oshima, and Y. Morikawa, *Numerical simulation of pneumatic conveying in a horizontal pipe.* KONA, 1985. **3**: p. 38-51.
134. Tsuji, Y., N.Y. Shen, and Y. Morikawa, *Lagrangian simulation of dilute gas-solid flows in a horizontal pipe.* Advanced Powder Technology, 1991. **2**: p. 63-81.
135. Sommerfeld, M., *Analysis of collision effects for turbulent gas-particle flow in a horizontal channel: Part 1. Particle transport.* International Journal of Multiphase Flow, 2003. **29**(4): p. 675-699.
136. Arastoopour, H., S.C. Lin, and S.A. Weil, *Analysis of Vertical Pneumatic Conveying of Solids Using Multiphase Flow Models.* Aiche Journal, 1982. **28**(3): p. 467-473.

137. Arastoopour, H., C.-H. Wang, and S.A. Weil, *Particle--particle interaction force in a dilute gas--solid system.* Chemical Engineering Science, 1982. **37**(9): p. 1379-1386.
138. *The Official Website of Atlas Copco*, 2004, http://www.atlascopco.com/ac/ac.nsf/CTpages?readform
139. *Pressure Transmitter Cerabar S, User Guide*, E.H. Company, Editor. 2001.
140. *Instruction Manual, YEWFLOW Votex Flowmeter*. 1999.
141. *Operating Manual, Load Cells and Force Transducers*, H.H.B. Messtechnik, Editor. 1998.
142. Butter, G., *Plastics pneumatic conveying and bulk storage.* APPL. SCI. PUB., 1993: p. 56 - 66.
143. *User Manual; PCLD-780/880/8115 Screw Terminal Boards.* 1997.
144. *User's Manual of Helos Particle Size Analyser*. 2001.
145. Hilgraf, P., *Design of Pneumatic Dense-Phase Transport Systems Trials - Investigations into Scale-up.* ZKG (Zement-Kalk-Gips) International, 1989. **11**(42): p. 558-566.
146. Wypych, P.W. and J. Yi, *Minimum transport boundary for horizontal dense-phase pneumatic conveying of granular materials.* Powder Technology, 2003. **129**(1-3): p. 111-121.
147. Brown, G.O. *The History of the Darcy-Weisbach Equation for Pipe Flow Resistance*. in *the 150th Anniversary Conference of ASCE*. 2002. Washington, D.C., USA: American Society of Civil Engineers, Reston, VA.
148. Brown, G.O. (2002) *The History of the Darcy-Weisbach Equation*. http://biosystems.okstate.edu/darcy/DarcyWeisbach/Darcy-WeisbachHistory.htm
149. Carpinlioglu, M.O. and M.Y. Gundogdu, *Correlations for Development Length of Fully-suspended Flows in Horizontal Pneumatic Conveying.* Powder Handling & Processing, 2000. **12**(2): p. 145-150.
150. *Official Website of Mineral Information Institute (MII).* 2005 [cited; Available from: http://www.mii.org/.

151. *The Mineral Ilmenite*, 1995, http://mineral.galleries.com/minerals/oxides/ilmenite/ilmenite.htm

152. *Official Website of Institute of Plasma Physics*, 1997, http://www.ipp.cas.cz/Mi/i/at5s

153. Chambers, J.A. and R.D. Marcus, *Pneumatic Conveying Calculations.* Proc. of Second International Conference on Bulk Material Storage and Transportation, Wollongong, NSW, Australia, 1986: p. 49-52.

154. Rivkin, M., *Study of Air-Solid Two Phase Interaction in High Pressure Tank.* Pneumotransport 5, Proc. of 5th International Conference on the Pneumatic Transport of Solids in Pipes, London, UK., 1980. **Paper E2**: p. 245-256.

155. Marcus, R.D. and P.C. Lohrmann, *The Performance of a Bottom Discharge Blow Vessel Pneumatically Conveying Three Group A Materials.* Bulk Solids Handling, 1984. **4**(2): p. 73-76.

156. Lohrmann, P.C. and R.D. Marcus, *The Influence of Velocity, Pressure and Line Length on the Performance of a Blow Vessel.* Pneumatech 1, Proc. of International Conference on Pneumatic Conveying Technology, Stratford, UK., 1982: p. 1-21.

157. Jotaki, T. and Y. Tomita, *Characteristics of a Blow Tank Solids Conveyor and its Operating Points Working on Pipe Lines.* Pneumotrasport 4, 4th International conference on the pneumatic transport of solids in pipes, Paper D4, 1978. **4**: p. 1357-1363.

158. Jotaki, T. and Y. Tomita, *Performance Characteristics of a Blow-tank Conveying System.* Pneumotrasport 2, 2nd International conference on the pneumatic transport of solids in pipes, Paper F3, 1973. **2**: p. 21-30.

159. Tomita, Y., Y. Jotaki, T. Jotaki, and Y. Tsukida, *Pneumatic Transport of Solids by a Blow Tank System.* Bulletin of the JSME-Japan Society of Mechanical Engineers, 1978. **21**(159): p. 1357-1363.

160. Tomita, Y., T. Jotaki, and K. Fukushima, *Feed Rate Characteristics of a Blow Tank Solids Conveyor in Transport of Granular Material.* Powder Technology, 1980. **26**: p. 29-33.

161. Tomita, Y., *Feed Rate of a Blow Tank Solids Conveyor in which the Particles are Non-fluidized.* Journal of Pipelines, 1987. **6**: p. 147-154.
162. Tomita, Y., T. Jotaki, S. Makimoto, and K. Fukushima, *Similarity of Granular Flow in a Blow tank Solids Conveyor.* Powder Technology, 1982. **32**: p. 1-8.
163. Marjanovic, P., *Modelling of the Transient Behaviour of the Blow Tank Pneumatic Conveying System.* Powder handling & processing, 1993. **5**(3): p. 219-226.
164. Munson, B.R., D.F. Young, and T.H. Okiishi, *Fundamentals of Fluid Mechanics*. 4th ed. 2002, Ames, US: Wiley & Sons. 816.
165. Brown, R.C., J. Ahrens, and N. Christofides, *The contributions of attrition and fragmentation to char elutriation from fluidized beds.* Combustion and Flame, 1992. **89**(1): p. 95-102.
166. Kreith, F., *Mechanical Engineering Handbook*. (In electronic form). 1999: CRC Press LLC.
167. Churchill, S.W., *Similitude: Dimensional Analysis and Data Correlation*, in *Mechanical Engineering Handbook*, F. Kreith, Editor. 1999, CRC Press LLC. p. 3.28-3.43.
168. Thomas, D.G., *Transport Characteristics of Suspensions: Part VI. Minimum Transport Velocity for Large Particle Size Suspensions in Round Horizontal Pipes.* AiChE Journal, 1962. **8**(3): p. 373-378.
169. Doig, I.D. and G.H. Roper, *The Minimum Gas Rate for Dilute Phase Solids Transportation in a Gas Stream.* Australian Chemical Engineering, 1963. **1**: p. 9-19.
170. Wirth, K.-E., *Critical Velocity of Solids Transport through Horizontal Circular Pipelines.* Ger. Chem. Eng., 1983. **6**: p. 45-52.
171. Wirth, K.-E. and O. Molerus, *Critical Solids Transport Velocity with Horizontal Pneumatic Conveying.* Journal of Powder & Bulk Solids Technology, 1985. **9**(1): p. 17-24.

172. Yi, J., P.W. Wypych, and R. Pan, *Minimum Conveying Velocity in Dilute-Phase Pneumatic Conveying.* Powder Handling and Processing, 1998. **10**(3): p. 255-261.
173. Wypych, P.W., J. Yi, and D.B. Hastie, *Minimum transport for dense-phase conveying of granules.* Particulate Science and Technology, 2003. **21**(1): p. 75-82.
174. Wypych, P.W. and A.R. Reed, *The Advantages of Stepping Pipelines for the Pneumatic Transport of Bulk Solids.* Powder handling & processing, 1990. **2**(3): p. 217.
175. Hilgraf, P., *Minimum Conveying Gas Velocities in the Pneumatic Transport of Solids.* ZKG (Zement-Kalk-Gips) International, 1987. **40**(12): p. 610-616.
176. Rizk, F., *Pneumatic Conveying Developments in the Last Century.* Proc. of International Conference on Bulk Material Handling &Transportation; Symposium on Freight Pipelines, Wollongong, Australia, 1992: p. 5-11.
177. Chong, Y.O. and L.S. Leung, *Comparison of Choking Velocity Correlations in Vertical Pneumatic Conveying.* Powder Technology, 1986. **47**(1): p. 43-50.
178. Hong, J. and Y. Shen. *Characteristics in Horizontal Pneumatic Conveying at High Solids Loading and Low Gas Velocity*. in *International Symposium on reliable Flow of Particulate Solids II*. 1993. Oslo, Norway: POSTEC A/S.
179. Hong, J., Y. Shen, and Y. Tomita, *Phase-Diagrams in Dense Phase Pneumatic Transport.* Powder Technology, 1995. **84**(3): p. 213-219.
180. Hubert, M. and H. Kalman, *Experimental determination of length-dependent saltation velocity in dilute flows.* Powder Technology, 2003. **134**(1-2): p. 156-166.
181. Wirth, K.E. and O. Molerus, *The Influence of Pipe Geometry on the Critical Velocity of Horizontal Pneumatic Conveying of Coarse Particles.* Powder Technology, 1985. **42**(1): p. 27-34.
182. Hilgraf, P., *The Step-wise Enlargement of Pneumatic Conveying Lines with Particular Regard to Dense-phass Conveying.* ZKG (Zement-Kalk-Gips) International, 1991. **4**(44): p. 161-168.

183. Hilgraf, P., *Influencing Variables in the Energy Optimization of Dense-phase Pneumatic Conveying Systems.* ZKG (Zement-Kalk-Gips) International, 1988. **8**(41): p. 374-380.

184. Esbensen, K.H., *Multivariate Data Analysis: in Practice*. 4 ed. 2000: CAMO ASA.

185. Lia, P.E., 1996, *Modellerring av pneumatisk transport i uttynna tilstand ved hjelp av multivariabe dataanalyse- prediksjon av minimum transportluftmengde (in Norwegian)*, M.Sc., Process Technology, Telemark University College, Porsgrunn.

186. Geldart, D. and S.J. Ling, *Saltation Velocities in High Pressure Conveying of Fine Coal.* Powder Technology, 1992. **69**: p. 157-162.

187. Scott, A.M., *Pneumatic Transport of Granules.* Chemical Engineer-London, 1978(330): p. 189-190.

188. Wang, Q., 2001, *An Experimental and Computational Study of Gas/Particle Multiphase Flow in Process Equipment*, Ph.D., Process Technology, Telemark University College, Porsgrunn, Norway.

189. Jenkins, J.T. and S.B. Savage, *A Theory for the rapid flow of identical, smooth, nearly elastic spherical particles.* Journal of Fluid Mechanics, 1983. **176**: p. 67-93.

190. Lun, C.K.K., S.B. Savage, D.J. Jeffrey, and N. Chepurniy, *Kinetic Theories for Granular Flow: Inelastic Particles in Couette Flow and Slightly Inelastic Particles in a General Flow Field.* Journal of fluid mechanics, 1984. **140**: p. 223-256.

191. Johanson, P.C. and R. Jackson, *Frictional-collision constitutive relation for granular materials, with application to plane shearing.* Journal of Fluid Mechanics, 1987. **176**: p. 67-93.

192. Sinclair, J.L. and R. Jackson, *Gas-particle flow in a verticle pipe with particle-particle interactions.* AIChE Journal, 1989. **36**(4): p. 523-538.

193. Ding, J. and D. Gidaspow, *A Bubbling Fluidization model using kinetic theory of granular flow.* Aiche Journal, 1990. **36**: p. 523-538.

194. Gidaspow, D., *Multiphase Flow and Fluidization: Cotinuum and Kinetic Theory Description*. 1994: Academic Press.
195. Mason, D.J., P. Marjanovic, and A. Levy, *A simulation system for pneumatic conveying systems.* Powder Technology, 1998. **95**(1): p. 7-14.
196. Ye, M., M.A. van der Hoef, and J.A.M. Kuipers, *A Numerical Study of Fluidization Behaviour of Geldart A Particle using a Discrete Particle Model.* Powder Technology, 2004. **139**: p. 129-139.
197. Mathiesen, V. and T. Solberg, *Laser-Based Flow Measurements of Dilute Vertical Pneumatic Transport.* Chemical Engineering Communications, 2004. **191**(3): p. 414-433.
198. Benyahia, S., H. Arastoopour, T.M. Knowlton, and H. Massah, *Simulation of particles and gas flow behavior in the riser section of a circulating fluidized bed using the kinetic theory approach for the particulate phase.* Powder Technology, 2000. **112**(1-2): p. 24-33.
199. Giddings, D., A. Aroussi, S.J. Pickering, and E. Mozaffari, *A 1/4 scale test facility for PF transport in power station pipelines.* Fuel, 2004. **83**(16): p. 2195-2204.
200. Wen, C.Y. and Y.H. Yu, *Mechanics of Fluidization.* Chemical Engineering Prog. Symp., 1966. **62**: p. 100-111.
201. Gidaspow, D., R. Bezburuah, and J. Ding. *Hydrodynamics of circulating fluidized beds kinetic thoery approach*. in *Fluidization VII, Proceedings of 7th Engineering Foundation Conference on Fluidization*. 1992.
202. Syamlal, M., W. Rogers, and T.J. O'Brien, *MFIX Documentation: Volume 1. Theory Guide.* National Technical Information Service. Springfield. VA., 1993 (DOE/METC 9411004. NTIS/DE 940087).
203. Sankar, S.R. and T.N. Smith, *Slip Velocities in Pneumatic Transport.1.* Powder Technology, 1986. **47**(2): p. 167-177.
204. Sankar, S.R. and T.N. Smith, *Slip Velocities in Pneumatic Transport.2.* Powder Technology, 1986. **47**(2): p. 179-194.

205. Li, H. and Y. Tomita, *Measurements of particle velocity and concentration for dilute swirling gas-solid flow in a vertical pipe.* Particulate Science and Technology, 2002. **20**(1): p. 1-13.
206. Lodes, A. and O. Mierka, *particle velocities in two-phase solid-gas flow.* Powder Technology, 1989. **58**: p. 163-168.
207. Raheman, H. and V.K. Jindal, *Slip velocity in pneumatic conveying of agricultural grains.* Powder handling & processing, 1993. **5**(1): p. 15-20.
208. Midttveit, Ø. and S.R. de Silva. *Slip Velocity in Pneumatic Conveying*. in *4th International Conference on Pneumatic Conveying Technology*. 1990. Glasgow, Scotland: powder Advisory Centre, UK.
209. Bilirgen, H. and E.K. Levy, *Mixing and dispersion of particle ropes in lean phase pneumatic conveying.* Powder Technology, 2001. **119**(2-3): p. 134-152.
210. Venkatasubramanian, S., H. Tashiro, G.E. Klinzing, and K. Mykelbust, *Solids Flow Behaviour in Bends: Assessing Fine Solids Buildup.* Powder Technology, 2000. **113**: p. 124-131.
211. Huber, N. and M. Sommerfeld, *Characterization of the Cross-Sectional Particle Concentration Distribution in Pneumatic Conveying Systems.* Powder Technology, 1994. **79**(3): p. 191-210.
212. Huber, N. and M. Sommerfeld, *Modelling and numerical calculation of dilute-phase pneumatic conveying in pipe systems.* Powder Technology, 1998. **99**(1): p. 90-101.
213. Levy, A. and D.J. Mason, *The effect of a bend on the particle cross-section concentration and segregation in pneumatic conveying systems.* Powder Technology, 1998. **98**(2): p. 95-103.
214. Zhu, K., S. Madhusudana Rao, C.-H. Wang, and S. Sundaresan, *Electrical capacitance tomography measurements on vertical and inclined pneumatic conveying of granular solids.* Chemical Engineering Science, 2003. **58**(18): p. 4225-4245.
215. Yilmaz, A. and E.K. Levy, *Roping phenomena in pulverized coal conveying lines.* Powder Technology, 1998. **95**(1): p. 43-48.

216. Tsuji, Y. and Y. Morikawa, *LDV measurements of an air-solid two-phase flow in a horizontal pipe.* Journal of Fluid Mechanics, 1982. **120**: p. 385-409.

12 APPENDICES

A Particle Size Distributions

The size distribution curves for bulk materials tested under the experimental study are given below.

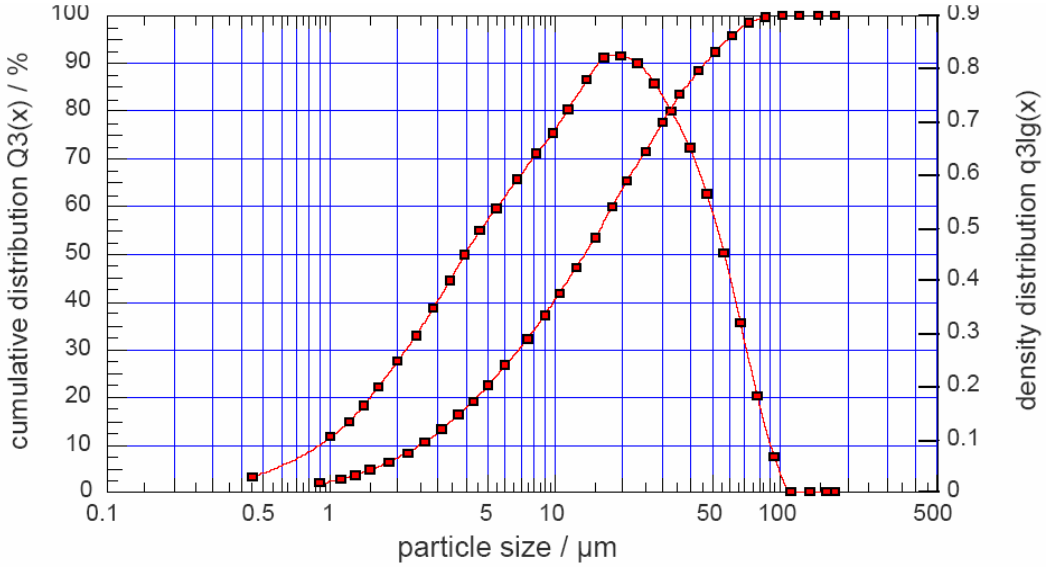

Figure 12-1: Particle size distribution for barytes.

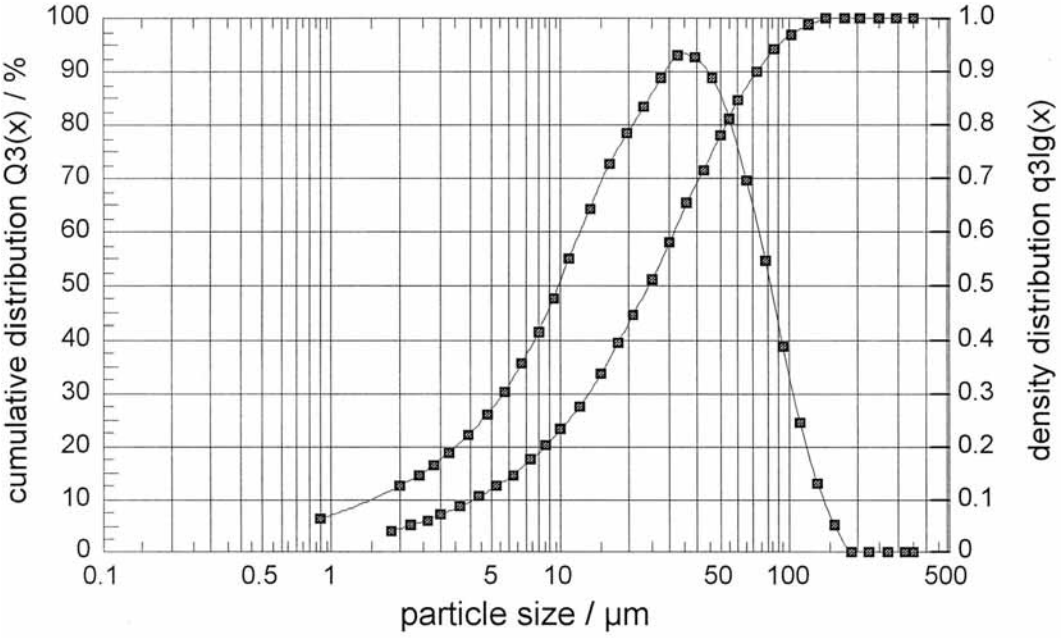

Figure 12-2: Particle size distribution for bentonite.

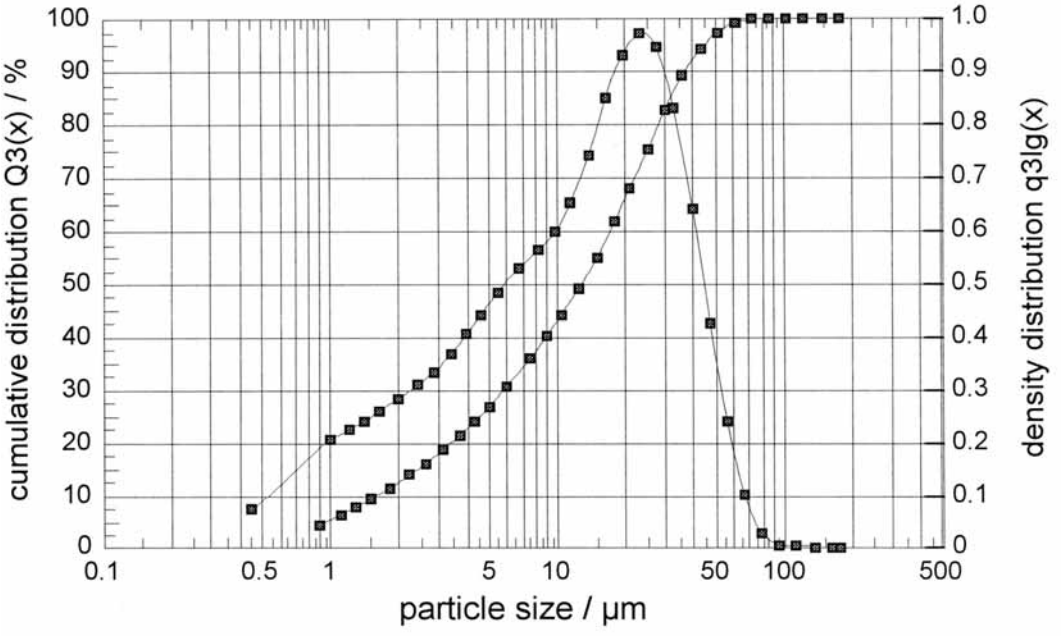

Figure 12-3: Particle size distribution for cement.

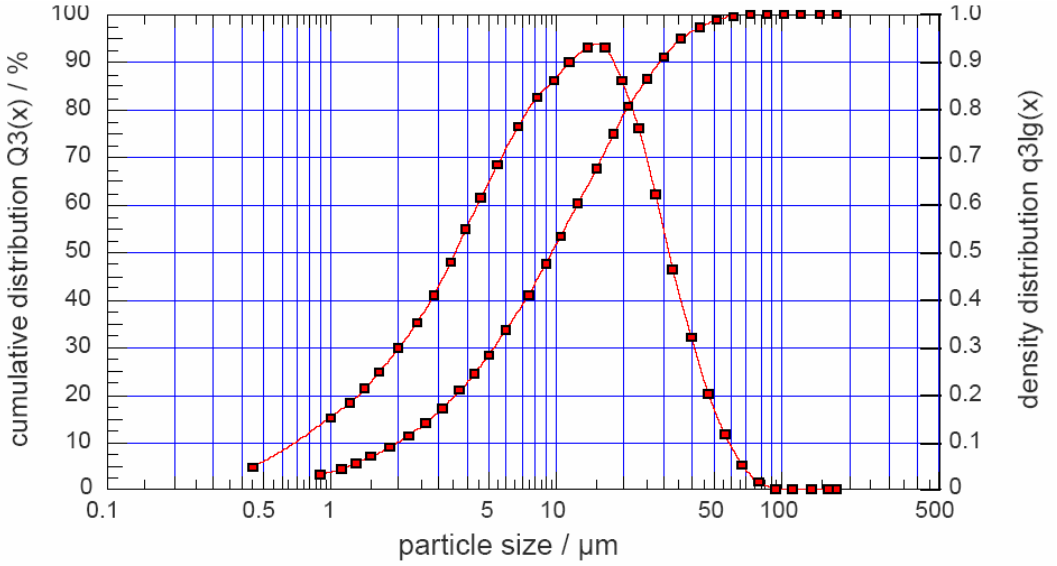

Figure 12-4: Particle size distribution for Ilmenite.

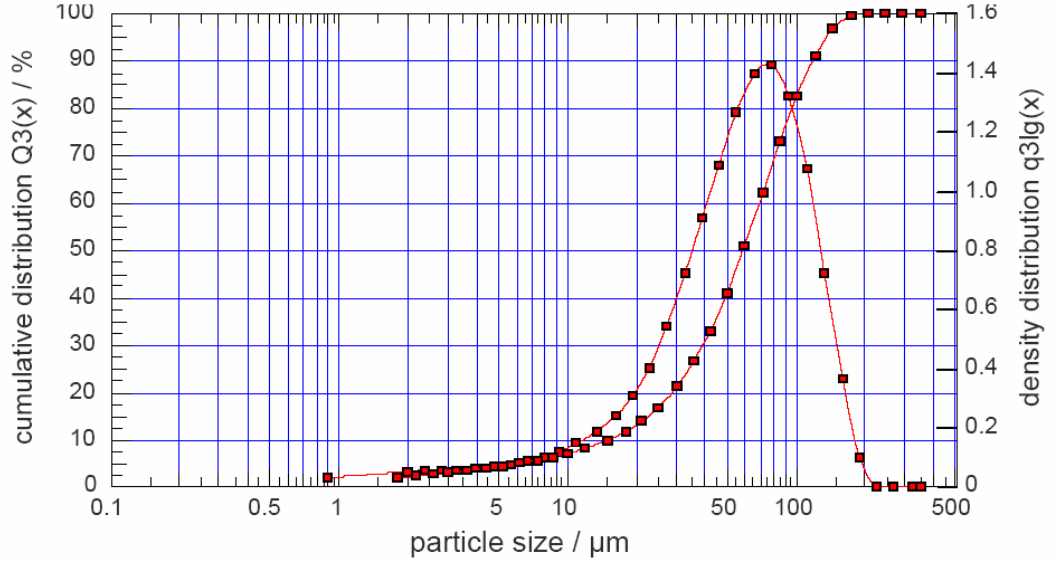

Figure 12-5: Particle size distribution for alumina 1.

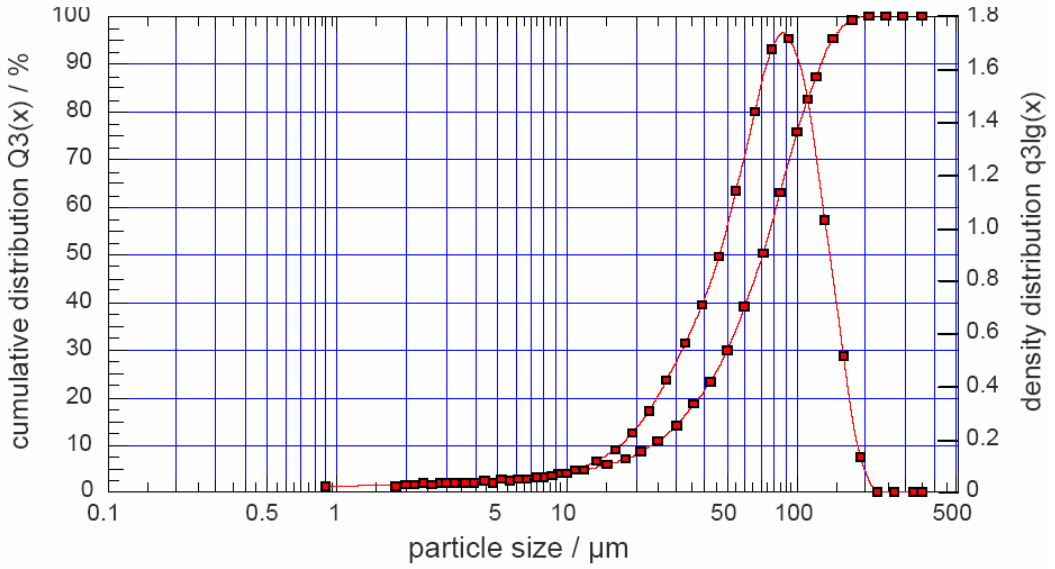

Figure 12-6: Particle size distribution for alumina 2.

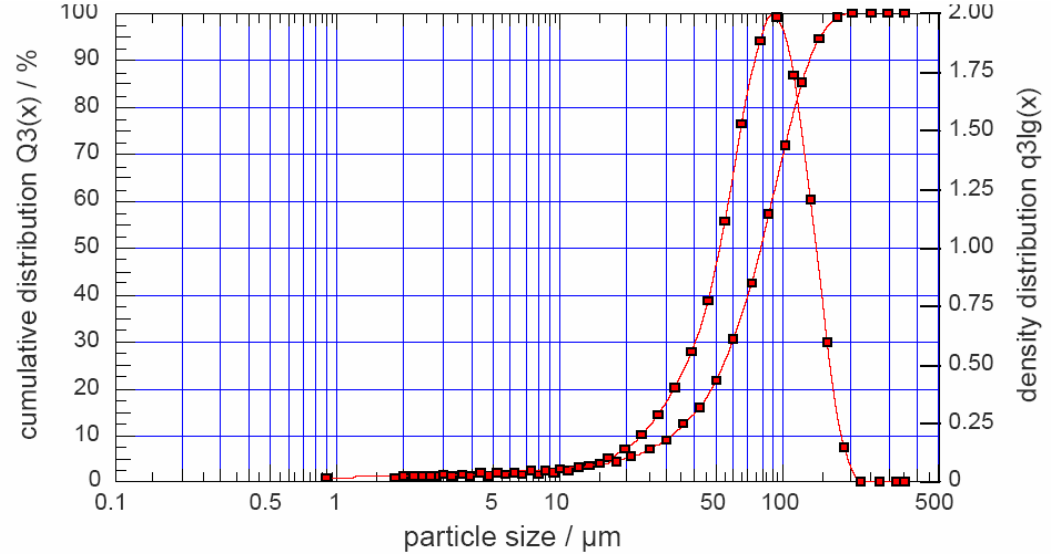

Figure 12-7: Particle size distribution for alumina 3.

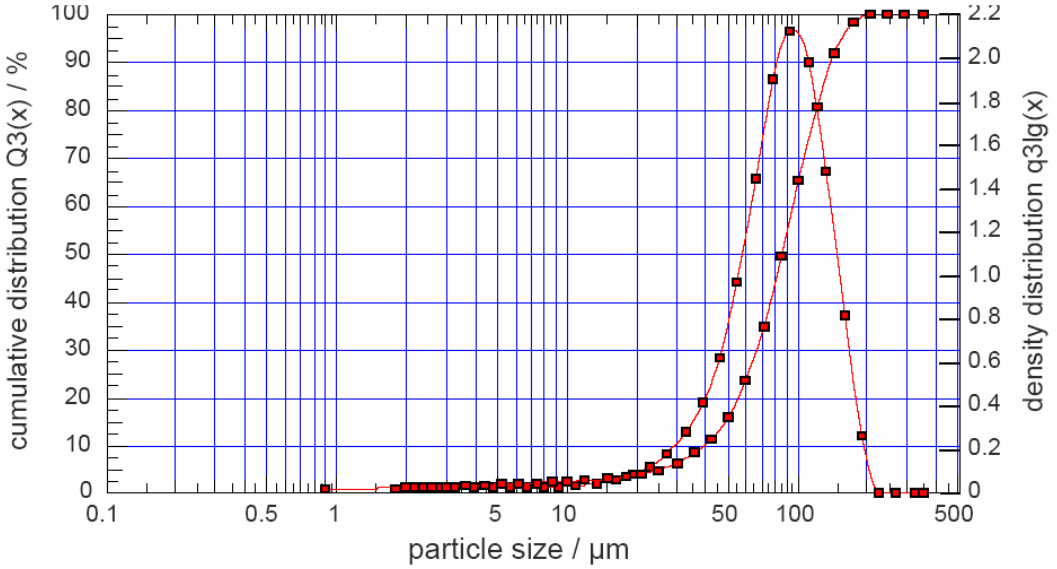

Figure 12-8: Particle size distribution for alumina 4.

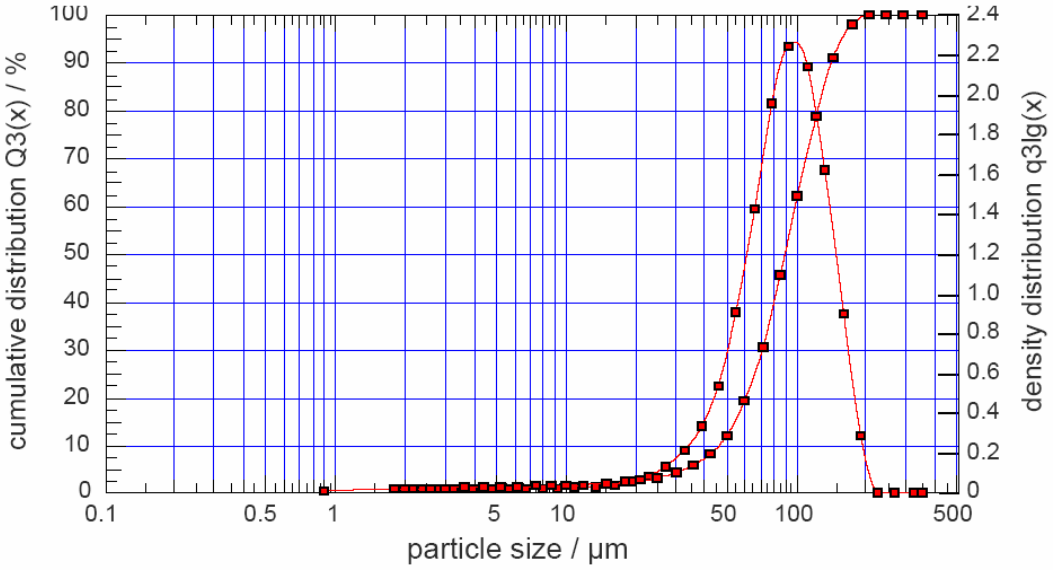

Figure 12-9: Particle size distribution for alumina 5.

B Pneumatic conveying characteristics curves

In this section, pneumatic conveying characteristics (PCC) curves generated during the tests are presented. The nomenclatures indicated in the Figures are shown in Figure 3-6.

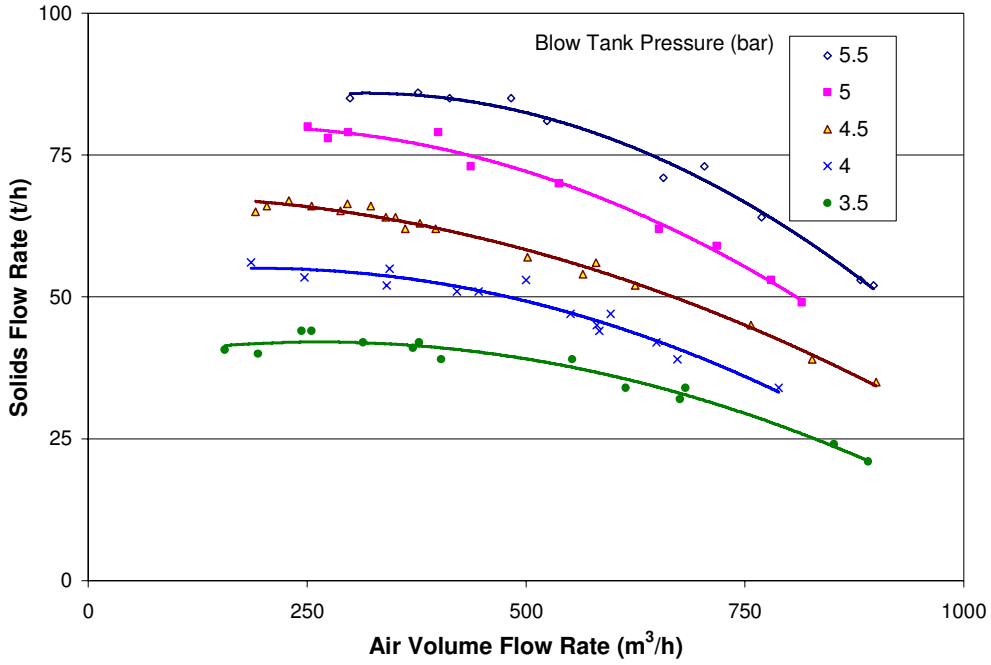

Figure 12-10: Pneumatic conveying characteristics for barytes conveying in pipeline A.

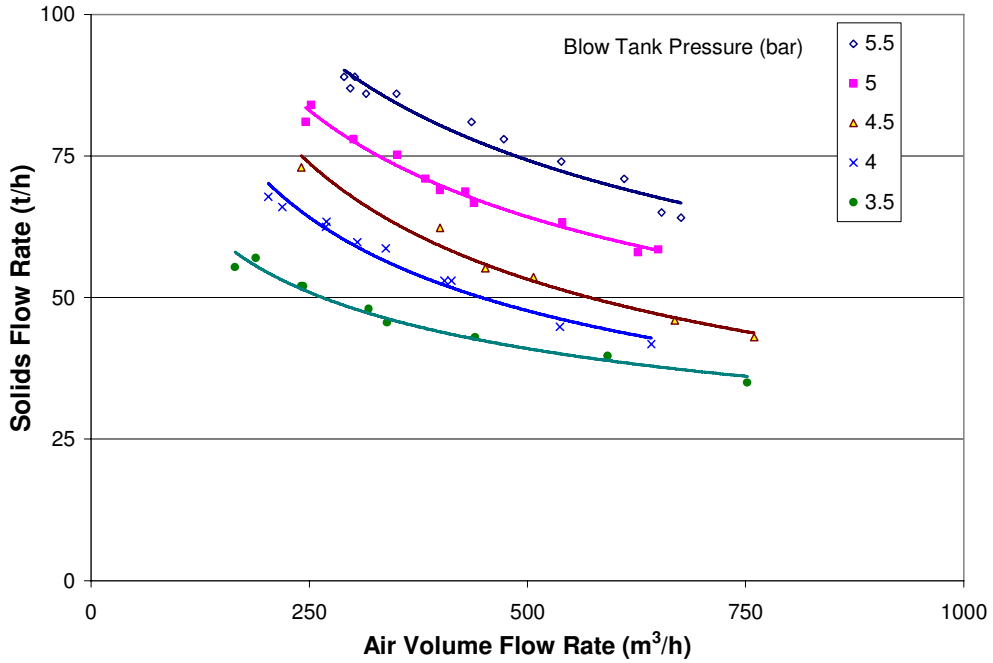

Figure 12-11: Pneumatic conveying characteristics for cement conveying in pipeline A.

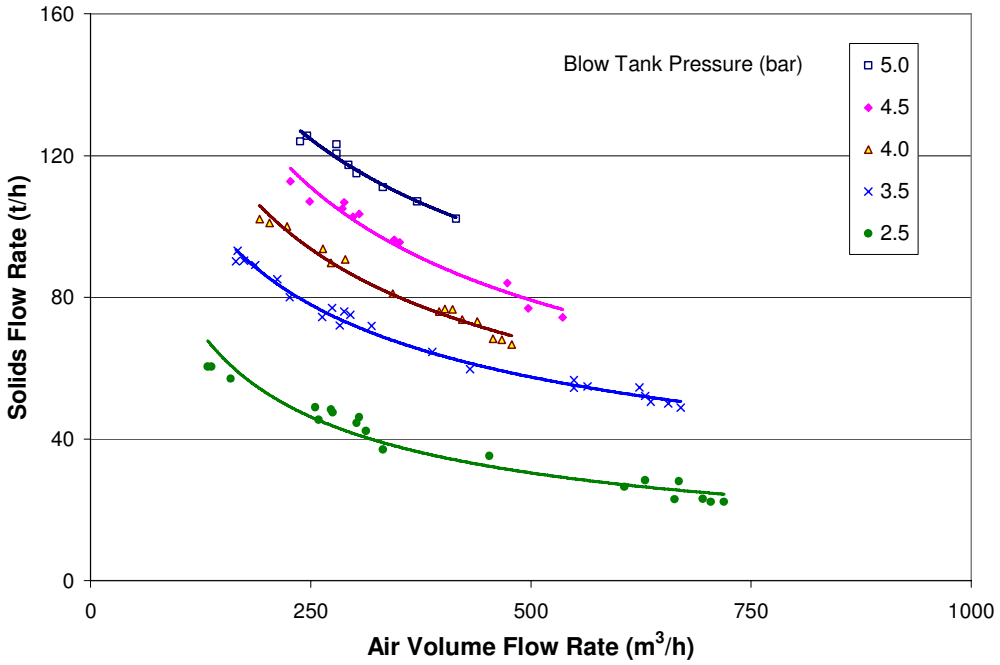

Figure 12-12: Pneumatic conveying characteristics for ilmenite conveying in pipeline B.

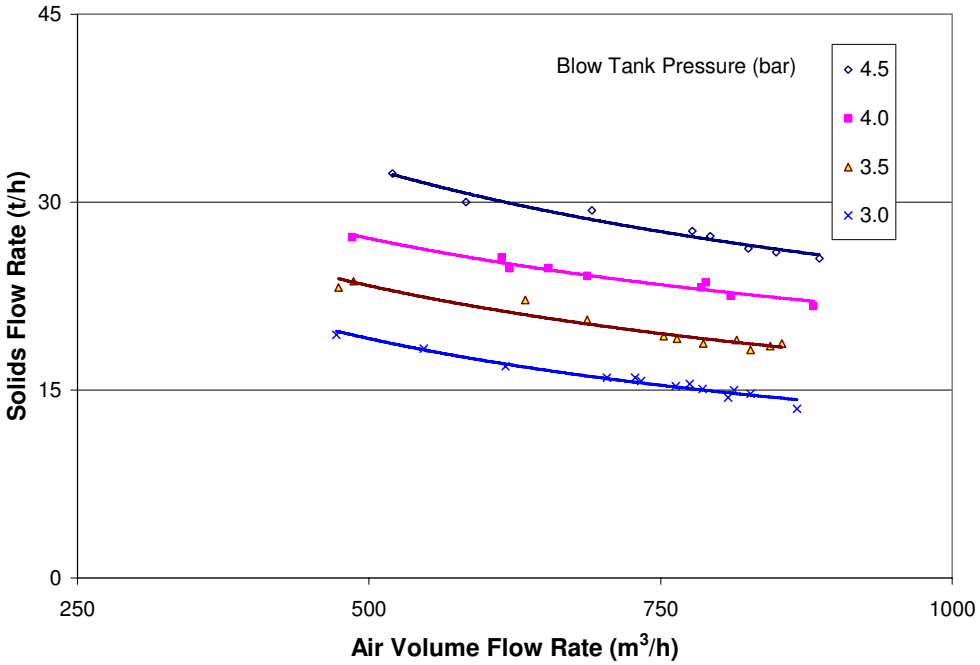

Figure 12-13: Pneumatic conveying characteristics for alumina 2 conveying in pipeline E.

PCC Curves with Predicted Minimum Conveying Boundaries

In PCC curves shown below, the predicted conveying boundaries, as described under the Chapter 7, are also superimposed on experimental curves.

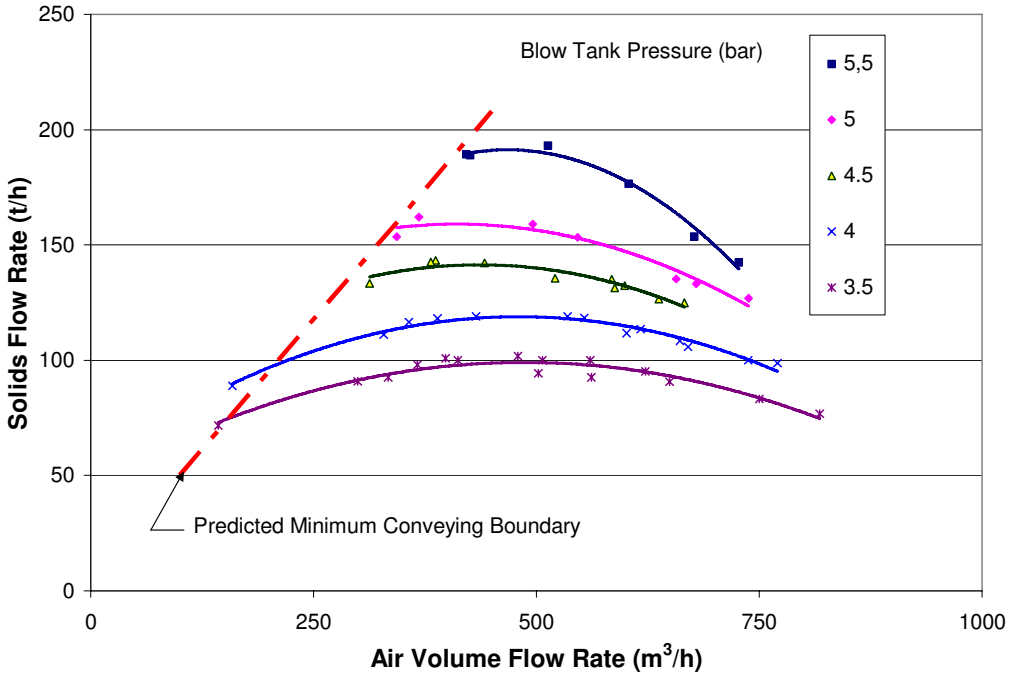

Figure 12-14: Pneumatic conveying characteristics of barytes in pipeline C with predicted minimum conveying boundary superimposed.

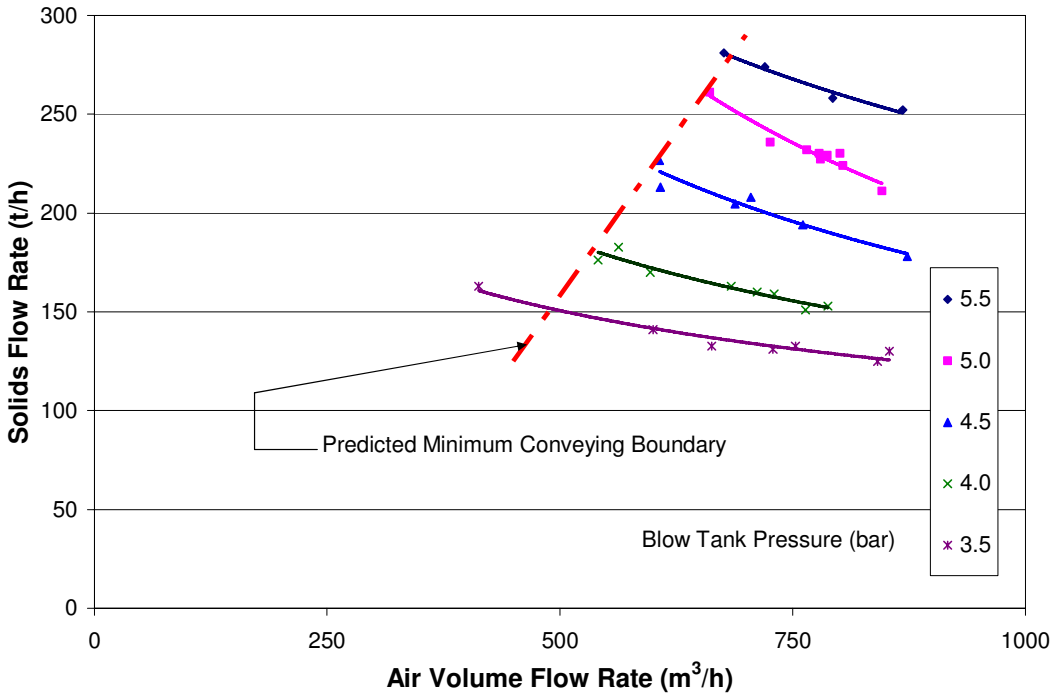

Figure 12-15: Pneumatic conveying characteristics of barytes in pipeline D with predicted minimum conveying boundary superimposed.

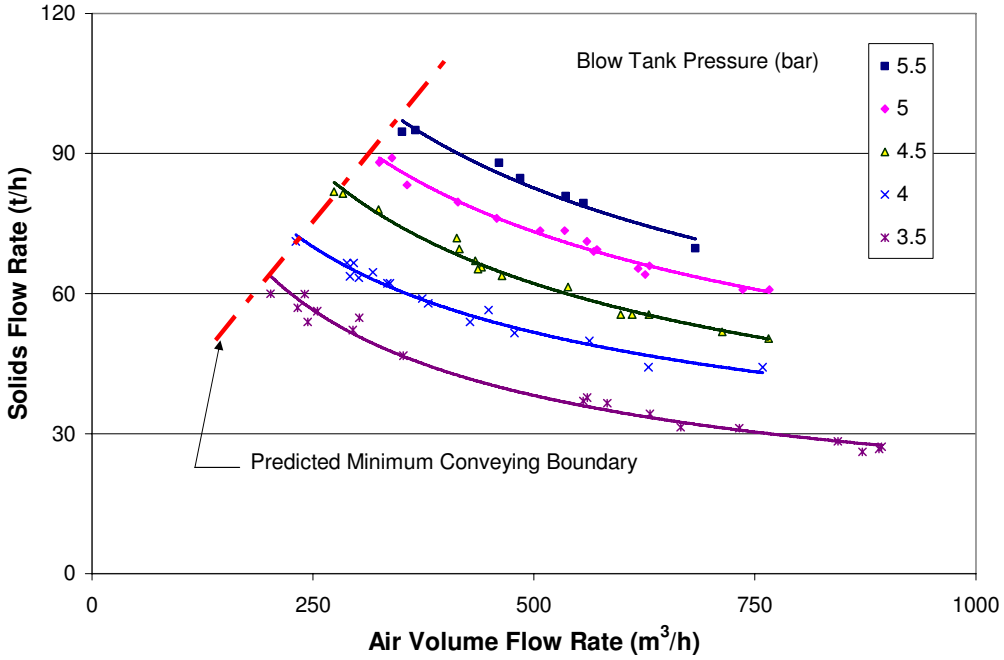

Figure 12-16: Pneumatic conveying characteristics of cement in pipeline B with predicted minimum conveying boundary superimposed.

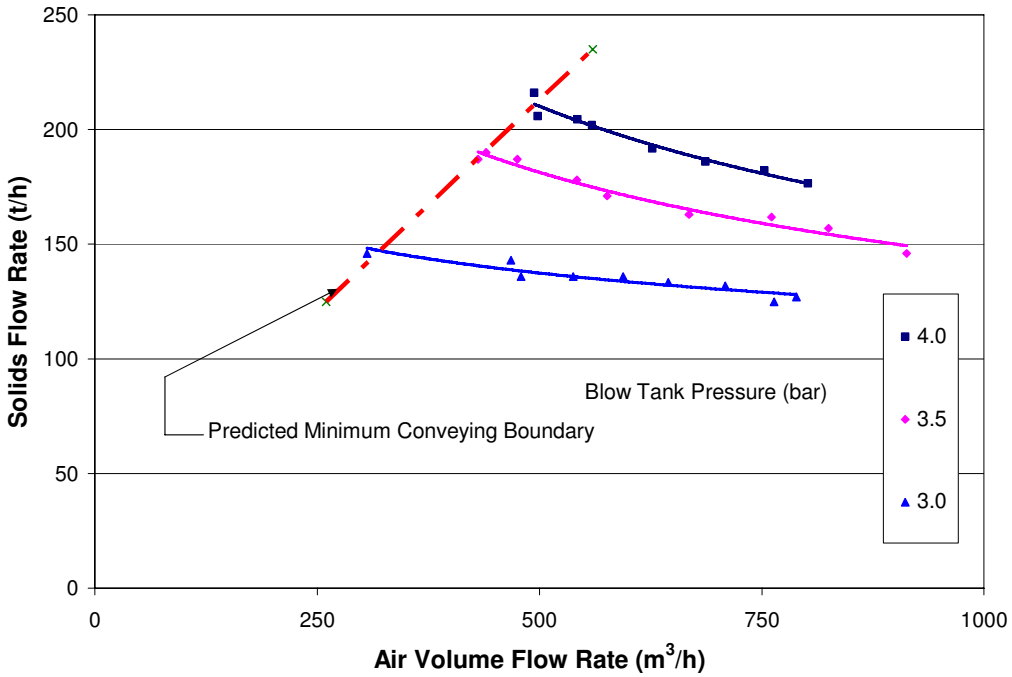

Figure 12-17: Pneumatic conveying characteristics of cement in pipeline D with predicted minimum conveying boundary superimposed.

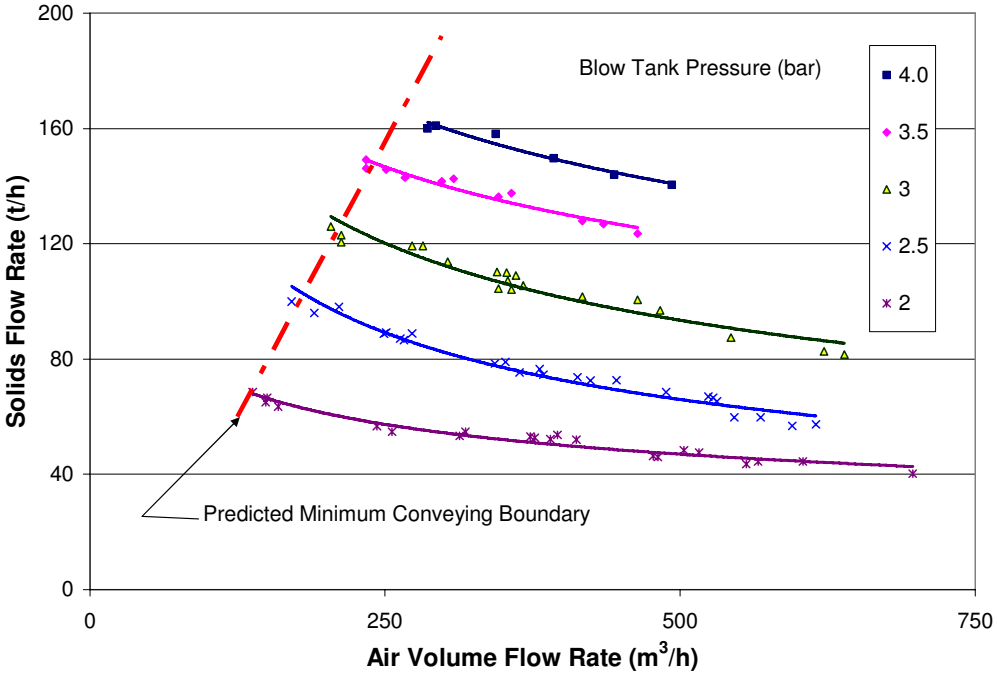

Figure 12-18: Pneumatic conveying characteristics of ilmenite in pipeline C with predicted minimum conveying boundary superimposed.

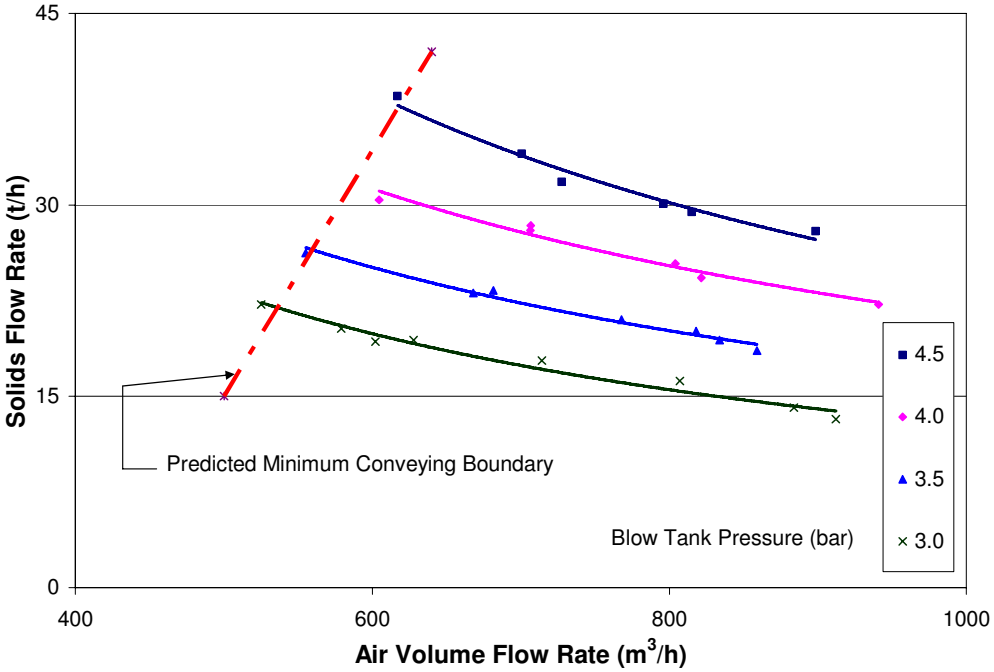

Figure 12-19: Pneumatic conveying characteristics of alumina 1 in pipeline E with predicted minimum conveying boundary superimposed.

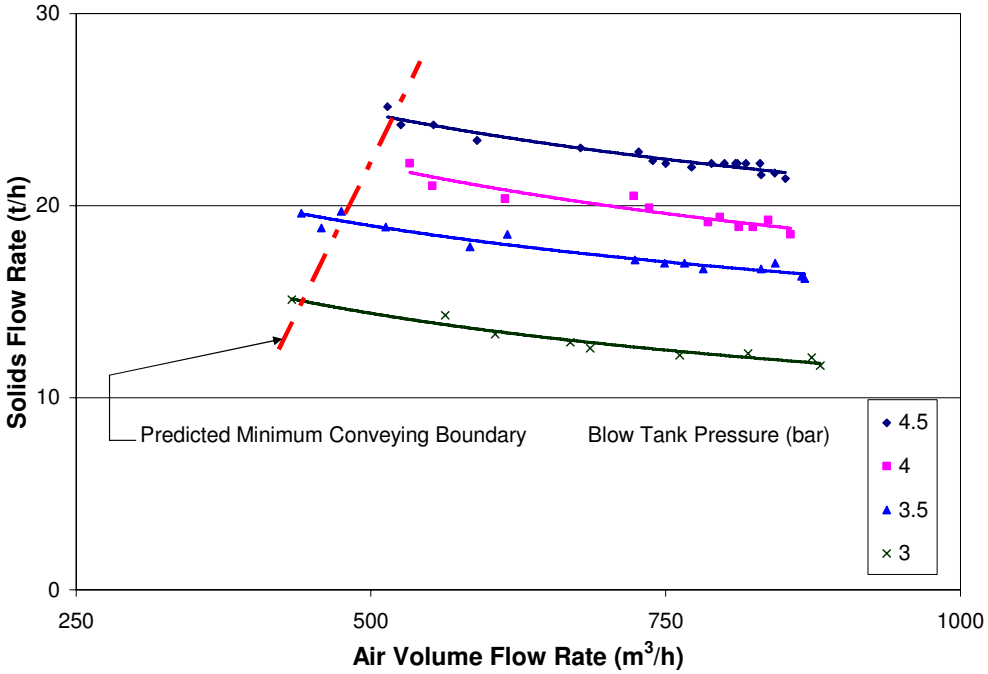

Figure 12-20: Pneumatic conveying characteristics of alumina 3 in pipeline E with predicted minimum conveying boundary superimposed.

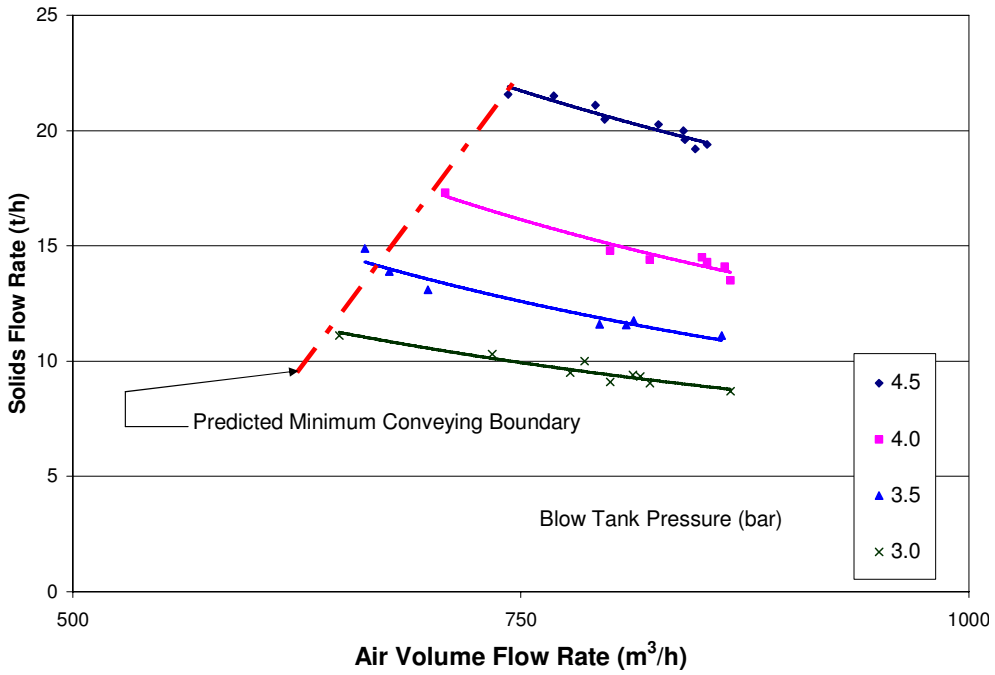

Figure 12-21: Pneumatic conveying characteristics of alumina 5 in pipeline E with predicted minimum conveying boundary superimposed.

ℂ Validation Curves

The validation curves for the tested materials are presented in this section.

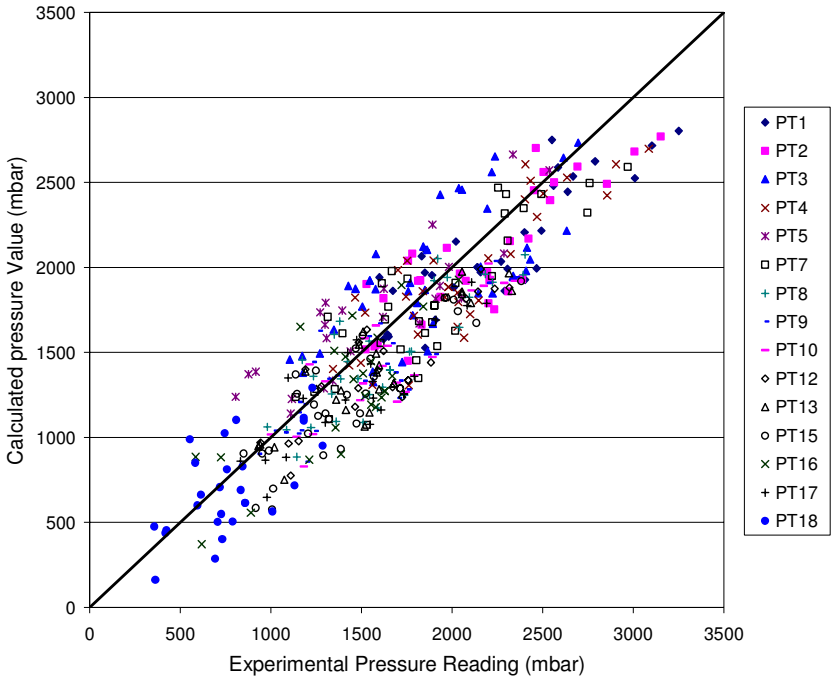

Figure 12-22: Experimental vs. calculated pressure readings values of barytes conveying on pipeline A.

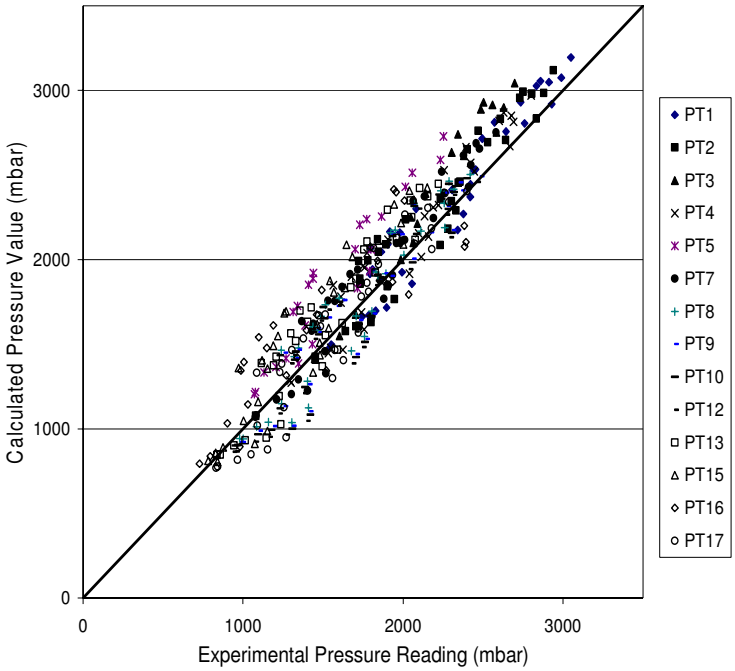

Figure 12-23: Experimental vs. calculated pressure readings values of cement conveying on pipeline A.

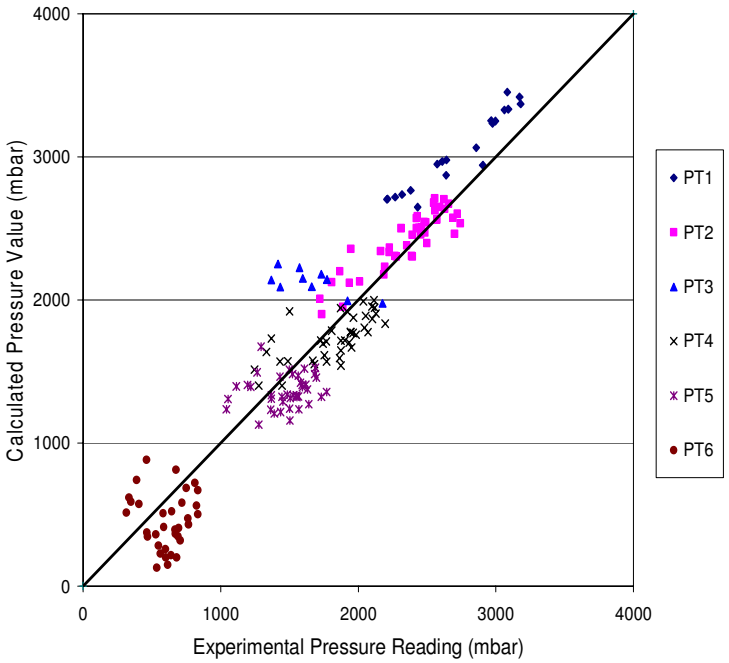

Figure 12-24: Experimental vs. calculated pressure readings values of barytes conveying on pipeline C.

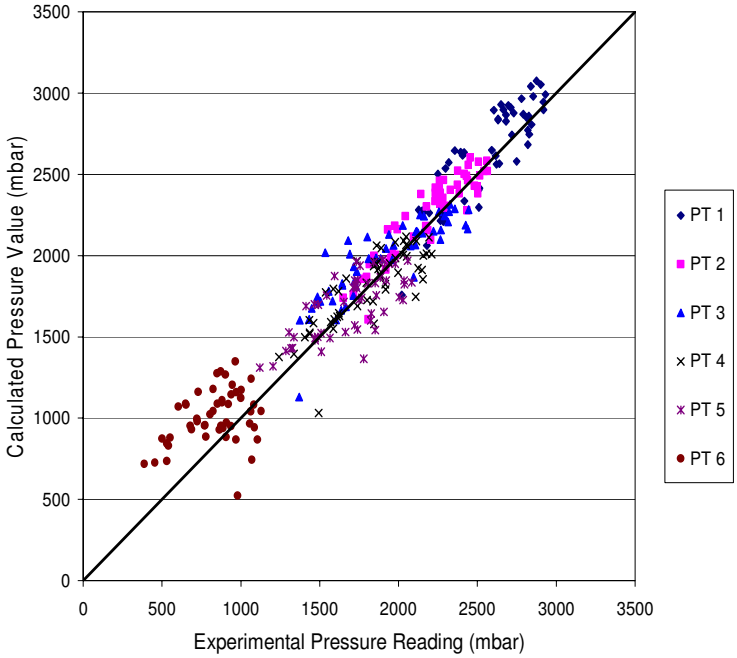

Figure 12-25: Experimental vs. calculated pressure readings values of cement conveying on pipeline C.

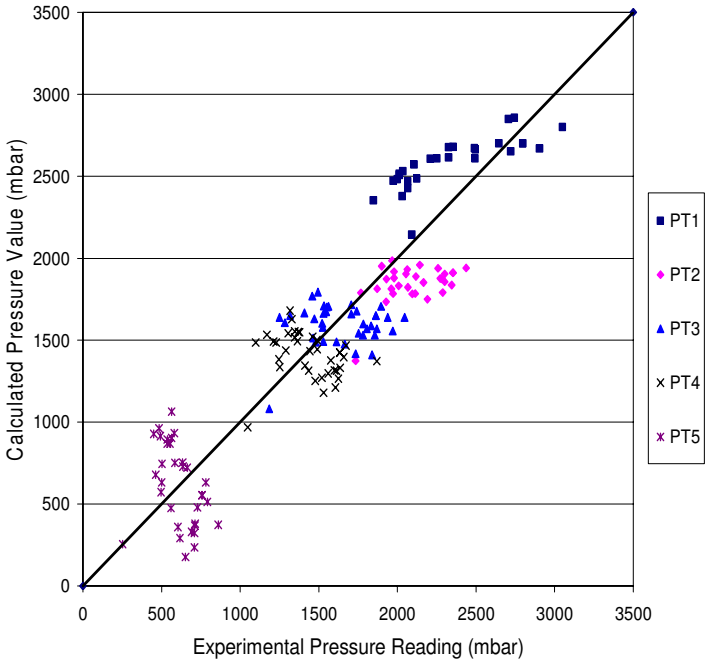

Figure 12-26: Experimental vs. calculated pressure readings values of barytes conveying on pipeline D**.**

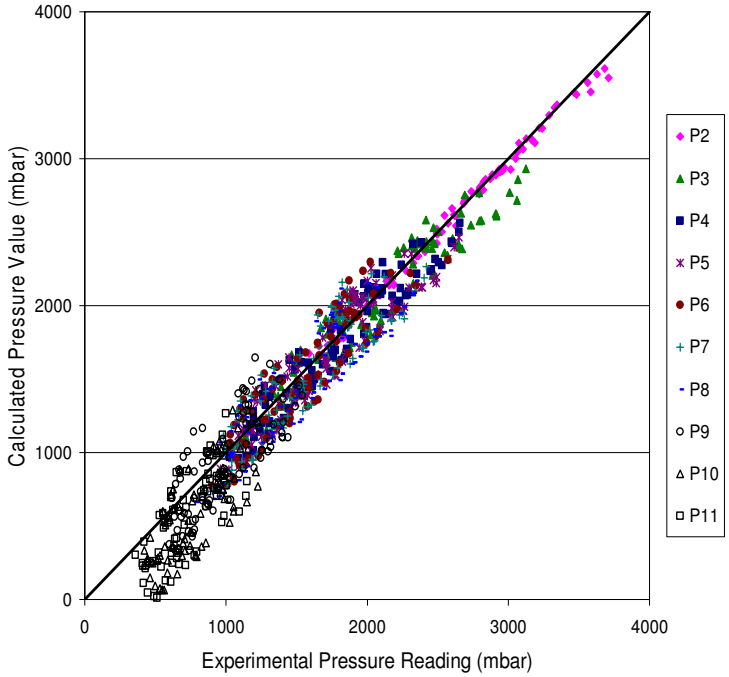

Figure 12-27: Experimental vs. calculated pressure readings values of ilmenite conveying on pipeline B.

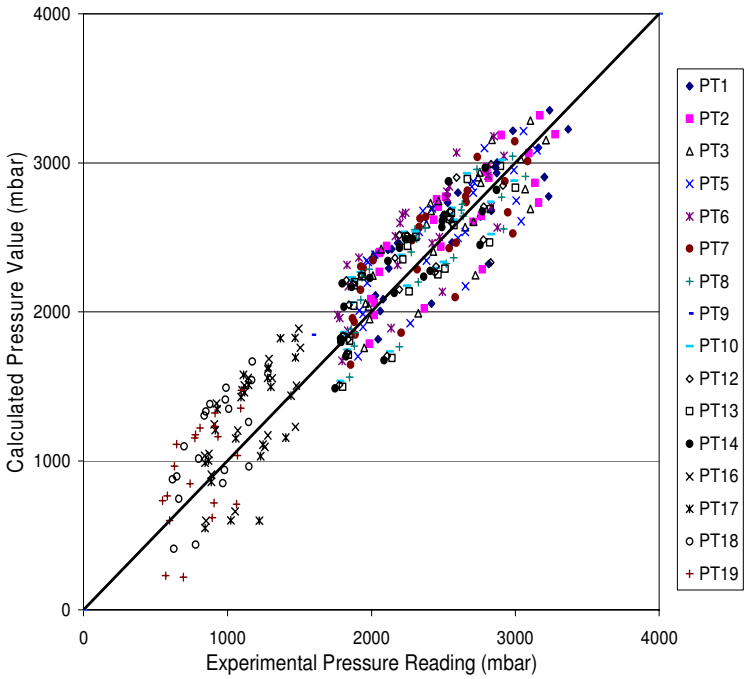

Figure 12-28: Experimental vs. calculated pressure readings values of alumina 1 conveying on pipeline E.

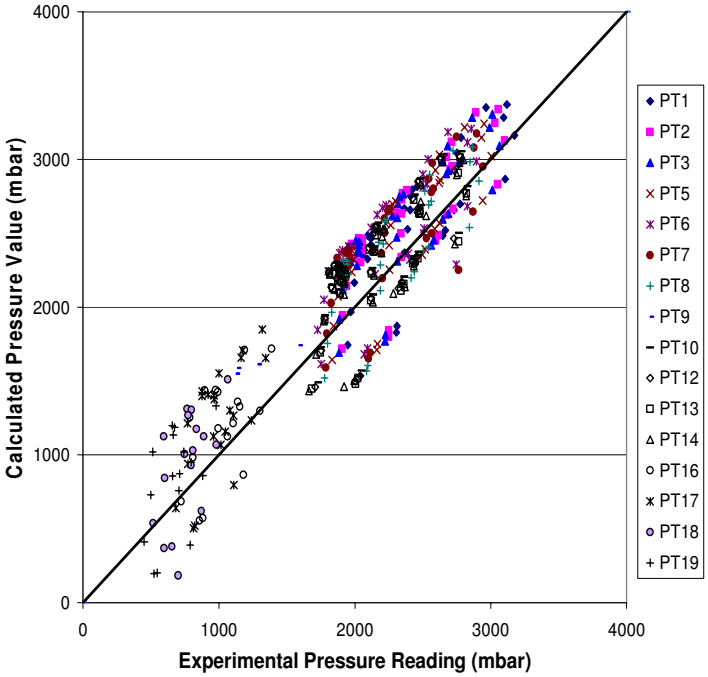

Figure 12-29: Experimental vs. calculated pressure readings values of alumina 2 conveying on pipeline E.

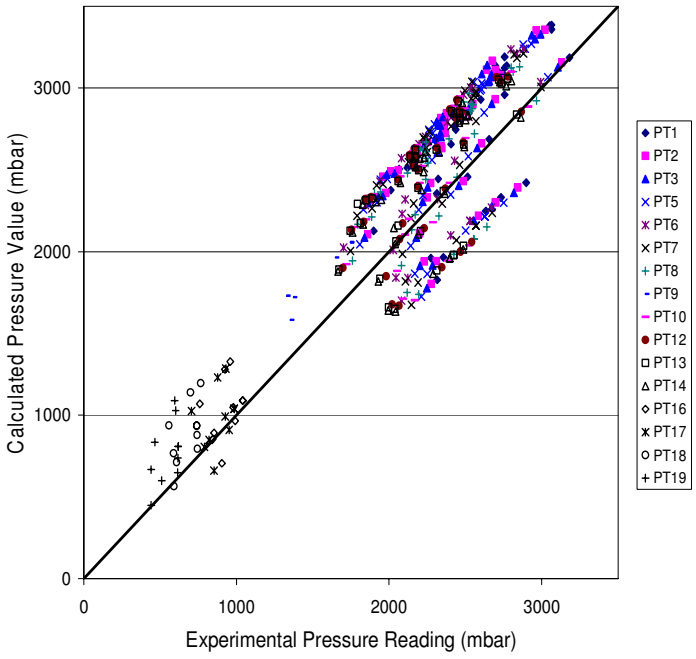

Figure 12-30: Experimental vs. calculated pressure readings values of alumina 3 conveying on pipeline E.

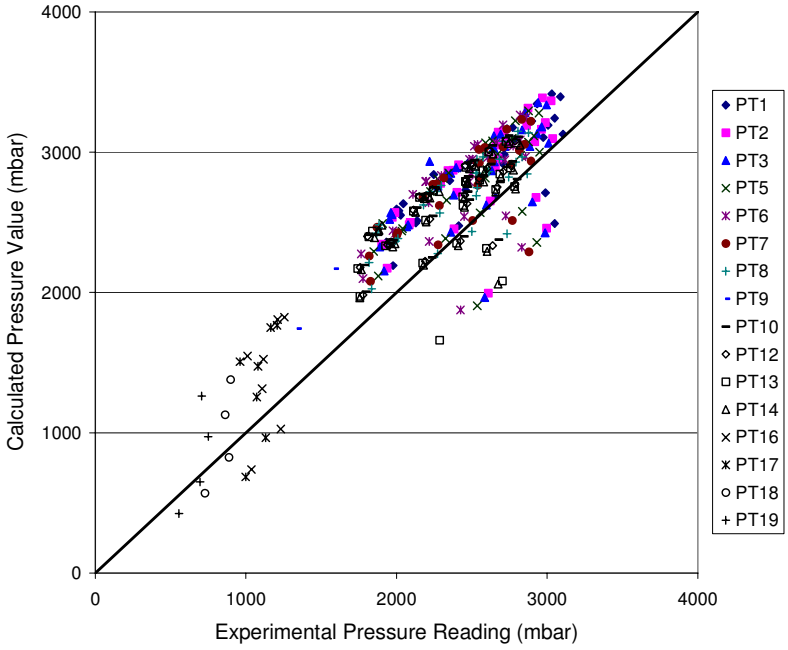

Figure 12-31: Experimental vs. calculated pressure readings values of alumina 4 conveying on pipeline E.

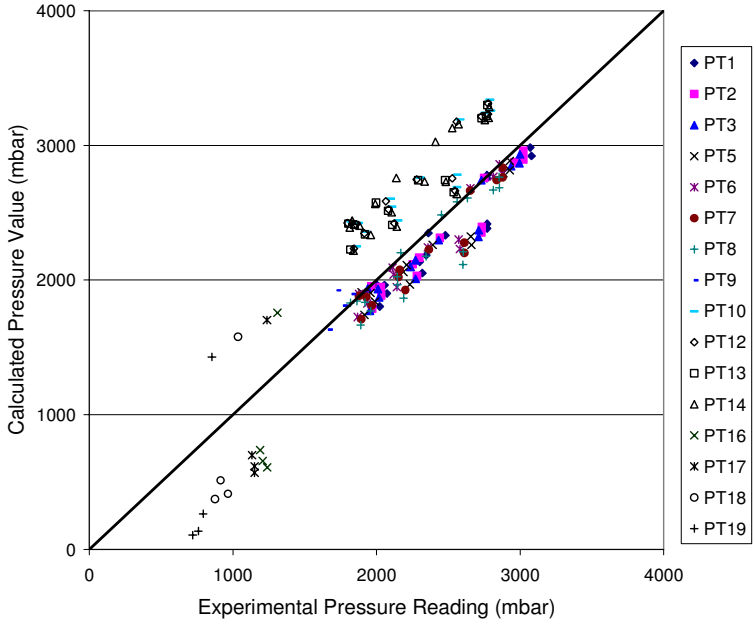

Figure 12-32: Experimental vs. calculated pressure readings values of alumina 5 conveying on pipeline E.

Ð List of Publications

International Journal Articles

1. B. K. Datta and **C. Ratnayake**, A Simple Technique for Scaling Up Pneumatic Conveying Systems, *Particulate Science and Technology*, Taylor & Francis Inc., Vol. 21, No. 3, ISSN: 0272-6351, DOI: 10.1080102726350390223240, pp. 227-236, 2003.
2. B. K. Datta and **C. Ratnayake**, A. Saasen and Y. Bastesen, A New Design Approach for Pneumatic Conveying, *Annual Transactions of the Nordic Rheology Society*, Vol. 11, 2003, ISSN 1601-4057, pp. 57-62.
3. B. K. Datta, A. Dyroy, **C. Ratnayake** and M. Karlsen, Influence of Fines Concentration on Pneumatic Transport Capacity of Alumina, *Particulate Science and Technology*, Taylor & Francis Inc., Vol. 21, No. 3, ISSN: 0272-6351, DOI: 10.1080/02726350390223259, pp. 283-291, 2003.
4. B. K. Datta and **C. Ratnayake**, A. Saasen and T.H. Omland, Hole Cleaning and Pressure Loss Prediction from a Bulk Transport Perspective, *SPE International*, Society of Petroleum Engineers, SPE 96315, 2005.
5. B.K. Datta and **C. Ratnayake**, A possible scaling-up technique for dense phase pneumatic conveying, *Particulate Science and Technology*, Taylor & Francis Inc., Vol. 23, No. 2, 2005.

Conference Papers

6. B. K. Datta and **C. Ratnayake**, A Possible Scaling Up Technique for Dense Phase Pneumatic Conveying, Proceedings of *the 4th International Conference for Conveying and Handling of Particulate Solids*, Budapest, Hungary, May 2003, Vol. 2, pp. 11.74-11.79
7. B. K. Datta and **C. Ratnayake**, Variation of Pneumatic Transport Characteristics of Alumina with Change in Size Distribution, *Bulk India 2003 - The International Conference and Exhibition for Handling, Processing,*

Storing and Transporting Bulk Materials, Renaissance Hotel, Mumbai, India, 9 -11 Dec. 2003 (in the electronic format – CD).

8. **C. Ratnayake**, B. K. Datta, A. Saasen and Y. Bastesen, An Experimental Study on Entry Pressure Loss in High Pressure Pneumatic Conveying Systems, Proceedings of *8th International Conference on Bulk Materials Storage, Handling and Transportation*, 2004, Wollongong, Australia, pp. 415-419.
9. **C. Ratnayake**, M.C. Melaaen and B. K. Datta, An Experimental Investigation and a CFD Modelling of Gas-solid Flow across a Bend in a Dense Phase Pneumatic Conveying System, Proceedings of *8th International Conference on Bulk Materials Storage, Handling and Transportation*, 2004, Wollongong, Australia, pp. 388-393.
10. **C. Ratnayake** and B.K. Datta, Scaling up of Minimum Conveying Conditions in a Pneumatic Transport System, Proceedings of *12th International Conference on Transport & Sedimentation of Solid Particles*, September 2004, Prague, Czech Republic, pp. 565-572.
11. **C. Ratnayake**, M.C. Melaaen and B. K. Datta, Pressure drop prediction in dense phase pneumatic conveying using CFD, *CFD 2005: 4th International Conference on CFD in the Oil and Gas, Metallurgical & process industries*, Trondheim, Norway, 6-8 June 2005 (in the electronic format – CD).

Papers Published in Periodicals

12. **C. Ratnayake**, Experimental Investigation of Scaling Techniques in Pneumatic Transportation, *The POSTEC Newsletter*, No. 19, Oct. 2000, http://www.tel-tek.no/site/content/download/117/446/file/newsletter19.pdf, pp. 12-13.
13. B. K. Datta and **C. Ratnayake,** A Step Towards Scaling up Pneumatic Conveying Systems, *The POSTEC Newsletter*, No. 21, 2002/2003, http://www.tel-tek.no/site/content/download/119/452/file/newsletter21.pdf, pp. 9-11.

14. **C. Ratnayake**, B. K. Datta and M.C. Melaaen, Models for the Scale-up of Pneumatic Conveying Tests, *The POSTEC Newsletter*, No. 22, 2004, http://www.tel-tek.no/site/content/download/634/4969/file/newsletter22.pdf, pp. 9-10.
15. **C. Ratnayake**, M.C. Melaaen and B. K. Datta , Pressure Drop Determination Across a Bend Using CFD, *The POSTEC Newsletter*, No. 22, 2004, http://www.tel-tek.no/site/content/download/634/4969/file/newsletter22.pdf, pp. 11-12.

Papers Communicated for Publication

16. B. K. Datta and **C. Ratnayake**, An Experimental Study on Degradation of Maize Starch during Pneumatic Transportation, Communicated to publish in *Particulate Science and Technology*, Taylor & Francis Inc.
17. **C. Ratnayake**, B.K. Datta and M.C. Melaaen, Scale up Technique of Entry Pressure Loss in Pneumatic Conveying Systems, Communicated to publish in *Particulate Science and Technology*, Taylor & Francis Inc.
18. **C. Ratnayake,** B. K. Datta and M.C. Melaaen, A Unified Scaling-Up Technique for Pneumatic Conveying Systems, Communicated to publish in *Particulate Science and Technology*, Taylor & Francis Inc.
19. **C. Ratnayake** and B.K. Datta, A Complete Scaling-Up technique for Designing of Pneumatic Conveying Systems, Accepted for *Bulk Days 2005*, Nuremberg, German.

Papers under Preparation

20. **C. Ratnayake,** B.K. Datta and M.C. Melaaen, An Evaluation of Models Used for the Pressure Drop Prediction in Pneumatic Conveying
21. **C. Ratnayake**, M.C. Melaaen and B. K. Datta, A CFD Modelling of Gas-Solid Flow across a Bend in a Dense Phase Pneumatic Conveying System.
22. **C. Ratnayake** B.K. Datta and M.C. Melaaen, Comparison Study on Available Correlations of Minimum Conveying Velocity.

23. **C. Ratnayake**, M.C. Melaaen and B. K. Datta, A CFD Modelling of Gas-solid Flow across a Straight Section in a Dense Phase Pneumatic Conveying System.
24. **C. Ratnayake**, M.C. Melaaen and B. K. Datta, CFD as a Pressure Drop Prediciton Tool in a Dense Phase Pneumatic Conveying System.